NATIONAL TECHNICAL UNIVERSITY OF ATHENS

SCHOOL OF CIVIL ENGINEER

Master Thesis

RESPONSE OF 8-STOREY REINFORCED CONCRETE BUILDING FOR NEAR-FAULT EARTHQUAKES

Evdokia Christou

Athens 2014

NATIONAL TECHNICAL UNIVERSITY OF ATHENS

SCHOOL OF CIVIL ENGINEER

RESPONSE OF 8-STOREY REINFORCED CONCRETE BUILDING FOR NEAR-FAULT EARTHQUAKES

of

Evdokia Christou

Athens 2014

APPROVAL FORM

Master thesis

Response of 8-storey reinforced concrete building for near-fault earthquakes

It presented by

Evdokia Christou

Supervisor ____

Commissioner ____

Commissioner ____

National Technical University of Athens

April, 2014

Copyrights

First of all, I would like to thank Professor I. Psycharis for giving me the possibility to work on this project. Deepest thanks to Dr. I. Taflampas, Civil Engineer for his valuable guidance and advices that gave me for the completion of this master thesis. I would also like to thank my friends for their encouraged in all my steps. Finally I am as ever, especially indebted to my parents. Thank you for your unconditional support and encourage throughout my studies.

ABSTRACT

Anticipating the response of a structure to near fault earthquakes, is an object of great concern to scientists worldwide and have proposed various methods of assessment of this response.

The main aim of this master thesis was to assess the vulnerability of an 8-storey reinforced concrete building that subjected to near-field earthquakes, based on the HAZUS methodology and to establish the reliability of the results according to SAP2000 program.

Moreover, comparing the maximum top displacement of the building through the sample of near field earthquakes we can conclude the important factors that give larger displacements and larger damages.The HAZUS methodology is a set of components that attempt to estimate losses, operational (probabilistic estimation) and economic, due to an earthquake scenario.

Firstly, the building subjected in modal analysis that generated the natural frequencies of it (T1 = 1.165 sec, T2 = 1.113 sec). Then it subjected in pushover analysis with load distribution according to the first Eigenmode in order to construct the pushover curve (base shear- top-floor displacement).The aim was to construct the fragility curves that defining by HAZUS. These curves classify the structure at four levels of damage (Slight, Moderate, Extensive, Collapse) and describe the possibility to have a certain level of damage to the building.

Depending on the type of building and the vulnerability curve we wanted to build was necessary to calculate standard deviations (vds) that take into account uncertainties on the curve pushover, with levels of performativity, with the features of construction, with the pulse of directivity and territorial motion. Eventually the curves defined by following lognormal distribution.

To determine the vulnerability of the building, it used an existing sample of near field earthquakes, with range of seismic magnitudes of 6.4 to 7.6, and larger maximum spectral displacement. Earthquakes applied through accelerograms (using SAP2000) in the building and after inelastic time-history analyses, resulted the maximum displacement for each record.

Comparing the records in each earthquake we are taking the following fragility curves and conclusions separate for each earthquake. The straight lines on the fragility curves are the maximum top-floor displacement for each record.

Table 25 presents the structural damage levels for all earthquake records, which have been obtained using the "HAZUS-Umax" and "Observation" methods, respectively, as those have been described in previous. A general observation is that all seismic motions result in structural damage, while, in the majority of the cases, the damage level is either "moderate" or "extensive", indicating the detrimental effects of near-fault ground-motions on the seismic performance of the 8-storey reinforced concrete building. Nevertheless, none of the two methods showed that the building will undergo complete damage or collapse during any of the selected seismic actions.

Moreover, it seems that the magnitude of the earthquake is not the primary factor that determines the severity of the damage of the analysed structure. It is observed that earthquakes of higher magnitude, such as the Izmit (Mw = 7.4) and Duzce (Mw = 7.1) result in lower damage levels than seismic events of lower magnitude, such as the Kobe (Mw = 6.8) and Northridge (Mw = 6.7) earthquakes. That means that other important factors and characteristics of the ground motion, in combination with the structural properties, determine the overall seismic performance of the building during an earthquake. For example, it is observed that a significant role on the severity of the damage plays the epicentral distance of the seismic recording. In particular, when observing the results in Table 25, we can see that in the case of the Chi-Chi earthquake, the ground-motions with relatively small epicentral distance (TCU065, TCU068 and TCU102) result in "extensive" damage, while the rest of the records from the same event with larger epicentral distances result in "moderate" and "slight" damage.

The ultimate goal was to understand how the magnitude of the earthquake, the directivity and the distance of the fault from the recording station affecting the results that have been obtained. Comparing the max$|U_{x,Top}$ results that analysis gave we can conclude the following:

1. **Forward directivity**: All the earthquakes that reach the extensive damage limit had forward directivity. Earthquakes with Neutral Directivity gave moderate damage limit even if they had larger magnitudes than others with forward directivity. This gives the result that earthquakes with forward directivity can give larger displacements and bigger damages.
2. **Closest distance from fault:** For the same earthquake and stations with the same directivity the displacements increase as the distance of the station from the fault. As

we can see from Chi-Chi Taiwan earthquake that gave the larger displacement, the records with smaller distance from the fault gave larger displacements.

3. **Magnitude of the earthquake:** Comparing the results of Tabas (Iran), Izmit (Turkey), Chi-Chi (Taiwan) and Duzce (Turkey) with magnitude 7.1, 7.6, 7.4 and 7.1 respectively we can see that only the Chi-Chi Taiwan earthquake occurs extensive damages. It is known that as the magnitude of the earthquake is increasing the building suffers from larger top displacements and therefore stronger levels of damage. From these records we can conclude that the magnitude is not the most important factor to occur larger displacements. This may be due to the saturation of the ground motion observed in large earthquakes, ie the size grows, but does not increase ground motion. However, larger magnitude with the factors that are written above can be catastrophic.

Conclusion of all seismic excitations can conclude that the forward directivity and the closest distance from the fault resulted in large displacements in the building and larger damages. However the displacements are increasing more when seismic magnitude is increasing.
We can note that the building did not reach a complete damage despite that it was suffered by very strong earthquakes. The record that occurred largest displacement (0.51 m) was TAK-000 Hanshin Kobe), Japan with magnitude 6.8 and classified the building damages as extensive and gave the larger possibility 40% for complete damage.

Knowing the consequences that will appear due to an earthquake, appropriate measures can take in order to reduce them. The proper design of structures and measures can reduce the damages of the structures and the number of casualties.

TABLE OF CONTENTS

LIST OF TABLES

LIST OF FIGURES

ABBREVIATIONS

FEMA:	Federal Emergency Management Agency
NIBS:	National Institute of Building Sciences
HAZUS:	HAZards U.S.
MH:	Multi-Hazards
NEHRP:	National Earthquake Hazards Reduction Program
AEBM:	Advanced Engineering Building Module

INTRODUCTION

The earthquake is a very common phenomenon that occurs in almost the entire planet Earth. There are daily earthquakes, most of which are small and more often they are not perceived by citizens, only by seismographs. Many times there have been large earthquakes without causing major damage and medium-sized earthquakes occurring large damage. The purpose of this master-thesis is to assess the response of 8-storey reinforced concrete building for near-fault earthquakes with aim to identifying the factors that play an important role in causing damage to specific building and generally. The assessment was made by using the HAZUS methodology and SAP2000 program.

The first chapter deals with Seismic Risk Assessment Methodology (HAZUS), overview of HAZUS Methodology, Building Classification, Structural and Nonstructural Systems and Contents, Damage States, Building Capacity Curves, Building Response Calculation and Building Fragility Curves. It is presents the Development of Capacity Curves and Response Parameters, Building Model and Pushover criteria, Development of Capacity Curve Control Points and Development of Response Parameters. Additionally, it is presents the Development of Fragility Curves, Building Response and Performance criteria, Development of Damage-State Medians and Development of Damage-State Variability.

The second chapter presents the features of territorial movement in near-fault seismic simulation, the effect of directionality, the customization of near-fault ground motions, the simulation models for near-field earthquakes and the effects of Fling Step.

The third chapter gives presentation and description of the building.

The fourth chapter focuses on the Eigen periods, Push-Over Curve, Capacity Curve and Fragility Curves.

The fifth chapter presents the selected near-fault ground motions, the displacement response spectra and spectral displacements, the method for assessing the seismic damage (HAZUS), the time-history analysis and the results from time-history analyses.

In the sixth chapter is comparison and discussion of the results.

Concluding in my work is given the findings for the factors that play an important role in causing damage to the specific building.

1 Seismic Risk Assessment Methodology (HAZUS)

1.1 Introduction

Many seismologists have said that "earthquakes do not kill people but the buildings". This is due to the fact that most deaths that occurring during earthquakes, are caused by buildings or other man-made structures, which collapsed during an earthquake. Earthquakes which happen in remote areas where there are no humans can not cause human casualties. The seismic risk depends on population density, seismic building codes and emergency plans.

The above factors justified with examples of earthquakes that took place in the past as the earthquake of magnitude 7.8 on the Richter scale that occurred in China in the province T'ang Shan, 1976 at 3:42 am and killed 240,000 people. Deaths caused due to the collapse of masonry buildings.

At 2010, Haiti earthquake magnitude 7.0 on the Richter scale caused the death of 316,000 people according to the government. Most buildings were made of poor quality reinforced concrete and were not designed with appropriate seismic design codes and this caused the collapse and the death of many people.

In contrast, in California to reduce seismic risk required by the design and construction of all structures stringent specifications to withstand a major earthquake. The design of structures using the appropriate Seismic Codes specific to each region, which are adapted depending on the circumstances and requirements of the region, is effective. This is justified by the magnitude 6.9 earthquake in San Francisco, California in 1989 that killed 63 people. Unlike ten months before an earthquake of magnitude 6.8 in Armenia caused the deaths of 25,000 people due to collapse of structures, which were not designed with Seismic Codes.

Seismic Risk is defined as the expected seismic consequences suffered by an area, which can be deaths and injuries to people, damage to structures and generally the overall impact on human activities in the area concerned.

The Seismic Risk can be expressed as the convolution of Seismic Hazard and Vulnerability. From this relationship, we conclude that if we reduce one of the two or both factors, then Seismic Risk is reduced. The Seismic Hazard cannot be influenced by human, because determined solely by physical factors. In contrast, the vulnerability can be reduced, because regards constructs in which man can intervene and check. This has the effect of reducing Seismic Risk of the region.

The relationship of Seismic Risk, Seismic Hazard and Vulnerability are shown graphically in Figure 1.

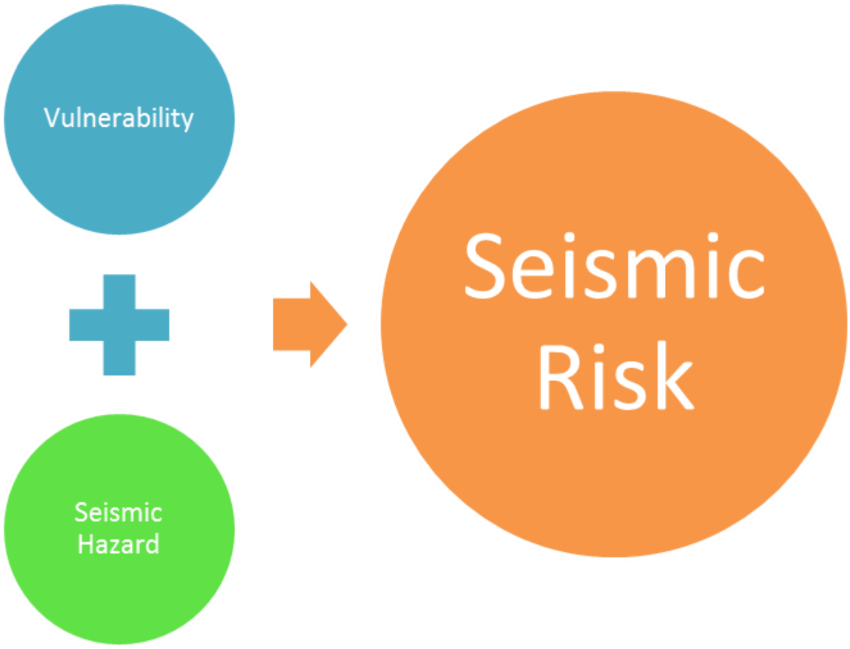

Figure 1: Schematic representation of the equation of Seismic Risk, R = H.V

Analytically, Seismic Hazard is defined as the probability of any particular region and given time to happen earthquake equal to or larger than expected size and depends on the expected deformations and soil movements in this region. They have used various methods of assessing the seismic hazard for specific areas, which are used by engineers in order to take the movements of the soil of this region and be able to use them in the calculation of the design of earthquake.

Additional, Vulnerability is the characteristic of every construction and expresses the expected response in the event of an earthquake. It is linked to Eigen period, the depreciation rate, regularity, quality of construction and other factors.

In this master thesis we are concerned the proposed method by Federal Emergency Management Agency (FEMA), which adopts the methodology of National Institute of Building Sciences (NIBS) U.S. . The FEMA / NIBS damage assessment methodology known as HAZUS is a complex collection of data designed to assess the functional losses and economic impact in a region due to an earthquake scenario.

Further, it is analyzed the methodology and software HAZUS-MH as are presented in Hazus-MH MR1 technical and user’s manual.

1.2 Hazus Methodology

HAZUS® (HAZards U.S.), developed for the Federal Emergency Management Agency (FEMA) by the National Institute of Building Sciences (NIBS), is geographic information system (GIS) based, standardized, nationally applicable multi-hazard loss estimation methodology and software to estimate physical, economic, and social impacts of disasters. Hazus is used for mitigation and recovery as well as preparedness and response. Local, state and federal government officials use HAZUS®MH for preparedness, emergency response, mitigation planning, and to determine losses and the most beneficial mitigation approaches to take to minimize them. Furthermore, Hazus can be used in the assessment step in the mitigation planning process, which is the foundation for a community's long-term strategy to reduce disaster losses and break the cycle of disaster damage, reconstruction, and repeated damage. Being ready will aid in recovery after a natural disaster, being ready will aid in recovery after a natural disaster.

HAZUS-MH is the most recent evolution of a family of natural hazards loss estimation software whose development began in the early 1990s. The purpose of HAZUS and natural hazards loss estimation software in general is to quantify the human, property, financial and social impacts of natural hazards such as earthquake, wind and flood, under existing conditions and given any of numerous possible mitigation measures. Quantification of losses under existing conditions is valuable for understanding and communicating the relative importance of natural hazards risks and the various factors (such as location, land use zoning, construction quality, etc.) contributing to that risk. Similarly, analysis of the beneficial impacts of mitigation measures (such as relocation, improved land use and planning, structural modifications, warnings, etc.) permits informed decision making and efficient allocation of scarce resources. The first release of HAZUS, in 1997, was for analysis of earthquake effects.

The FEMA/NIBS earthquake loss estimation methodology, commonly known as HAZUS, is a complex collection of components that work together to estimate casualties, loss of function and economic impacts on a region due to a scenario earthquake. The methodology is documented in the HAZUS-MH Technical Manual. One of the main components of the methodology estimates the probability of various states of structural and nonstructural damage to buildings. Damage state probabilities are used by other components of the methodology to estimate various types of building-related loss. Typically, buildings are grouped by model building type and evaluated on a census tract basis.

Currently, HAZUS includes building damage functions for 36 model building types and for various combinations of seismic design level and performance. Each model building type represents a "generic" group of buildings that share a common type of construction and a common seismic design level. Damage and loss functions for generic building types are considered to be reliable predictors of earthquake effects for large groups of buildings that include both above median and below median cases. They may not, however, be very good predictors for a specific building or a particular type of building that is known to have a weakness or earthquake vulnerability (e.g., W1 buildings with weak cripple walls would be expected to perform much worse than typical wood-frame buildings). Although the theory is applicable to an individual building, building- specific damage and loss functions are not provided and would need to be developed by the user. The complexity of the methods and underlying seismological and engineering phenomena makes development of building-specific functions challenging unless the user is an engineer experienced in nonlinear seismic analysis.

FEMA/NIBS projects in the area of earthquake hazard mitigation also include the Building Seismic Safety Council's (BSSC's) development of the NEHRP Guidelines for Seismic Rehabilitation of Buildings [FEMA, 1997], referred to simply as the NEHRP Guidelines. Like HAZUS, the NEHRP Guidelines represent a major, multi-year effort. Also like HAZUS, the NEHRP Guidelines use similar earth science theory and engineering techniques. For the first time, earthquake loss estimation and building seismic analysis are based on common concepts. The similarity of these fundamental concepts permits interfacing the methods of the NEHRP Guidelines with those of HAZUS for development of building-specific damage and loss models.

In conclusion the main purpose of HAZUS methodology is to provide for specific buildings the necessary tools assessing damages from earthquakes that are used by engineers specializing in the subject of earthquakes.

To produce accurate results, the engineers should be able to make a relatively complicated pushover analysis - a process described below. The other main approach of the methodology is to produce a combination between the nonlinear static analysis (pushover) and methods of assessment of losses. The engineers now presenting a detailed pushover analysis that may be take useful conclusions and more understandable results for the possible models failure of building, for total response of the structure-both structural and non-structural systems, and the costs and the time required for the repair of damaged building elements.

1.2.1 Overview of Hazus Methodology

The FEMA/NIBS earthquake loss estimation methodology, commonly known as *HAZUS*, has many components, or modules, as described in the *HAZUS-MH User's Manual* and *HAZUS-MH Technical Manual*.

The flow of the *HAZUS* methodology between those modules related to building damage and loss is illustrated in Figure 2.

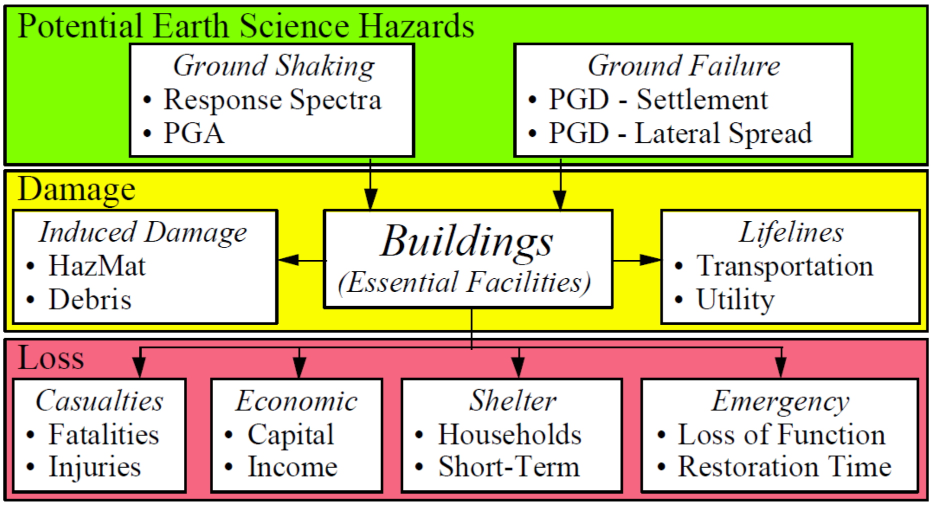

Figure 2: Building-Related Modules of the FEMA/NIBS Methodology (FEMA 2003)

Due to the above figure the most important components to estimate the building damage are the ground shaking and the ground failure.

Estimates of building damage are used as inputs to other damage modules, including hazardous materials facilities and debris generation, and as inputs to transportation and utility lifelines that have buildings as a part of the system (e.g., airport control tower).

Most importantly, building damage is used as an input to a number of loss modules, including the estimation of casualties, direct economic losses, displaced households and short-term shelter needs, and loss of emergency facility function and the time required to restore functionality.

HAZUS damage functions for ground shaking have two basic components:

(1) capacity curves and

(2) fragility curves.

The capacity curves are based on engineering parameters (e.g., yield and ultimate strength) that characterize the nonlinear (pushover) behavior of 36 different model building types. For each of these building types, capacity parameters distinguish between different levels of seismic design and anticipated seismic performance.

The fragility curves describe the probability of damage to the structural system, to the nonstructural components that are sensitive to drift and to the nonstructural components and contents that are sensitive to acceleration of the building. The fragility curves describe the probability of damage to the building's: (1) structural system, (2) nonstructural components sensitive to drift and (3) nonstructural components (and contents) sensitive to acceleration.

For a given level of building response, fragility curves distribute damage between four physical damage states: Slight, Moderate, Extensive and Complete. Earthquake loss due to building damage is based on the physical damage states that are deemed to be the most appropriate and significant contributors to that particular type of loss. For example, deaths are based primarily on the Complete state of structural damage, since partial or complete collapse of the building is assumed to dominate this type of loss. In contrast, direct economic loss (e.g., repair/replacement cost) is accumulated from all states of damage to both structural and nonstructural systems, since all are significant contributors to economic loss.

1.2.2 Building Classification

Buildings are classified both in terms of their use, or occupancy class, and in terms of their structural system, or model building type. Damage is predicted based on model building type, since the structural system is considered the key factor in assessing overall building performance, loss of function and casualties. Occupancy class is important in determining economic loss, since building value is primarily a function of building use (e.g., hospitals are more valuable than most commercial buildings, primarily because of their expensive nonstructural systems and contents, not because of their structural systems).

Thirty three occupancy classes are defined to distinguish among residential, commercial, industrial or other buildings; and 36 model building types are used to classify buildings within the overall categories of wood, steel, concrete, masonry or mobile homes. Building inventory data relate model building type and occupancy class on the basis of floor area, as illustrated in Figure 3, so that for a given geographical area the distribution of the total floor area of model building types is known for each occupancy class. For presentation purposes, Figure 3 shows only the four overall categories of occupancy and the five overall categories of construction, whereas FEMA/NIBS methodology calculations are based on all 28 occupancy classes and 36 model building types. Model building types are derived from the same classification system that is used in the NEHRP Handbook for the Seismic Evaluation of Buildings – A Prestandard [FEMA, 1998], but expanded to include mobile homes and to consider building height. Table 1 describes model building types and their heights. Typical building heights are used in the determination of generic-building capacity curve properties.

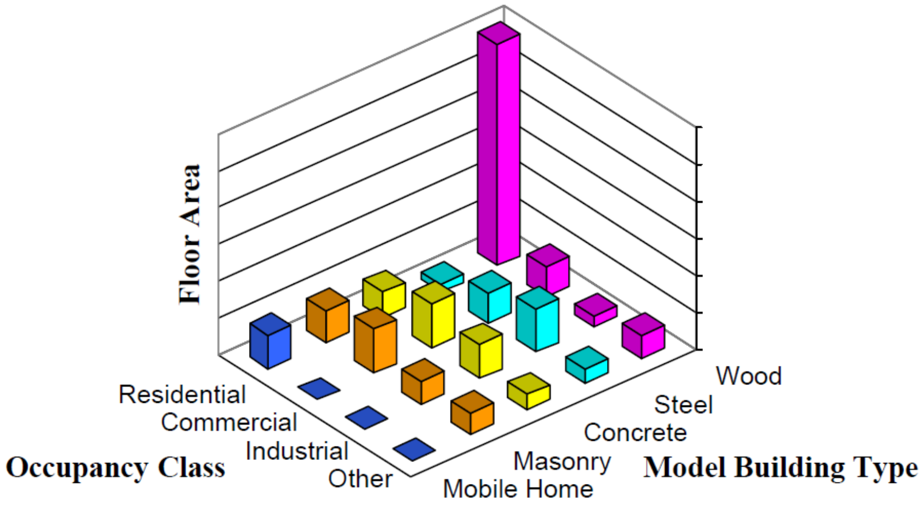

Figure 3: Example Inventory Relationship of Model Building Type and Occupancy Class (FEMA 2003)

Table 1: Model Building Types of Hazus (FEMA 2003)

No.	Label	Description	Height			
			Range		Typical	
			Name	Stories	Stories	Feet
1	W1	Wood, Light Frame (≤ 5,000 sq. ft.)		All	1	14
2	W2	Wood, Greater than 5,000 sq. ft.		All	2	24
3	S1L	Steel Moment Frame	Low-Rise	1-3	2	24
4	S1M		Mid-Rise	4-7	5	60
5	S1H		High-Rise	8+	13	156
6	S2L	Steel Braced Frame	Low-Rise	1-3	2	24
7	S2M		Mid-Rise	4-7	5	60
8	S2H		High-Rise	8+	13	156
9	S3	Steel Light Frame		All	1	15
10	S4L	Steel Frame with Cast-in-Place Concrete Shear Walls	Low-Rise	1-3	2	24
11	S4M		Mid-Rise	4-7	5	60
12	S4H		High-Rise	8+	13	156
13	S5L	Steel Frame with Unreinforced Masonry Infill Walls	Low-Rise	1-3	2	24
14	S5M		Mid-Rise	4-7	5	60
15	S5H		High-Rise	8+	13	156
16	C1L	Concrete Moment Frame	Low-Rise	1-3	2	20
17	C1M		Mid-Rise	4-7	5	50
18	C1H		High-Rise	8+	12	120
19	C2L	Concrete Shear Walls	Low-Rise	1-3	2	20
20	C2M		Mid-Rise	4-7	5	50
21	C2H		High-Rise	8+	12	120
22	C3L	Concrete Frame with Unreinforced Masonry Infill Walls	Low-Rise	1-3	2	20
23	C3M		Mid-Rise	4-7	5	50
24	C3H		High-Rise	8+	12	120
25	PC1	Precast Concrete Tilt-Up Walls		All	1	15
26	PC2L	Precast Concrete Frames with Concrete Shear Walls	Low-Rise	1-3	2	20
27	PC2M		Mid-Rise	4-7	5	50
28	PC2H		High-Rise	8+	12	120
29	RM1L	Reinforced Masonry Bearing Walls with Wood or Metal Deck Diaphragms	Low-Rise	1-3	2	20
30	RM1M		Mid-Rise	4+	5	50
31	RM2L	Reinforced Masonry Bearing Walls with Precast Concrete Diaphragms	Low-Rise	1-3	2	20
32	RM2M		Mid-Rise	4-7	5	50
33	RM2H		High-Rise	8+	12	120
34	URML	Unreinforced Masonry Bearing Walls	Low-Rise	1-2	1	15
35	URM M		Mid-Rise	3+	3	39
36	MH	Mobile Homes		All	1	12

1.2.3 Structural and Nonstructural Systems and Contents

Buildings are composed of both structural (load carrying) and nonstructural systems (e.g., architectural and mechanical components). While damage to the structural system is the most important measure of building damage affecting casualties and catastrophic loss of function (due to unsafe conditions), damage to nonstructural systems and contents tends to dominate economic loss. Typically, the structural system represents about 25% of the building's worth.

To better estimate different types of loss, building damage functions separately predict damage to: (1) the structural system, (2) drift-sensitive nonstructural components, such as partition walls that are primarily affected by building displacement, and (3) acceleration-sensitive nonstructural components, such as suspended ceilings, that are primarily affected by building shaking. Building contents are also considered to be acceleration sensitive. Distinguishing between driftand acceleration-sensitive nonstructural components, and contents, permits more realistic estimates of damage considering building response. Table 2 lists typical drift-sensitive and acceleration-sensitive components and building components.

Table 2: HAZUS Classification of Drift-Sensitive and Acceleration-Sensitive Nonstructural Components and Buidling Contents (FEMA 2003)

System Type	Component Description	Drift-Sensitive	Acceleration-Sensitive
Architectural	Nonbearing Walls/Partitions	•	
	Cantilever Elements and Parapets		•
	Exterior Wall Panels	•	
	Veneer and Finishes	•	
	Penthouses	•	
	Racks and Cabinets		•
	Access Floors		•
	Appendages and Ornaments		•
Mechanical and Electrical	General Mechanical (boilers, etc.)		•
	Manufacturing and Process Machinery		•
	Piping Systems		•
	Storage Tanks and Spheres		•
	HVAC Systems (chillers, ductwork, etc.)		•
	Elevators		•
	Trussed Towers		•
	General Electrical (switchgear, ducts, etc.)		•
	Lighting Fixtures		•
Contents	File Cabinets, Bookcases, etc.		•
	Office Equipment and Furnishings		•
	Computer/Communication Equipment		•
	Nonpermanent Manufacturing Equipment		•
	Manufacturing/Storage Inventory		•
	Art and Other Valuable Objects		•

1.2.4 Damage States

Damage states are defined separately for structural and nonstructural systems of a building. Damage is described by one of four discrete damage states: Slight, Moderate, Extensive or Complete, and Collapse as subset of Complete structural damage. Of course, actual building damage varies as a continuous function of earthquake demand. Ranges of damage are used to describe building damage, since it is not practical to have a continuous scale, and damage states provide the user with an understanding of the building's physical condition. Loss functions relate the physical condition of the building to various loss parameters (i.e., direct economic loss, casualties, and loss of function). For example, direct economic loss due to Moderate damage is assumed to correspond to 10% replacement value of structural and nonstructural components, on the average.

The four damage states of the FEMA/NIBS methodology are similar to the damage states defined in *Expected Seismic Performance of Buildings* [EERI, 1994], except that damage descriptions vary for each model building type based on the type of structural system and material. Table 3 provides structural damage states for W1 buildings (light frame wood) typical of the conventional construction used for single-family homes.

Table 3: Example Damage States – Light-Frame Wood Buildings (W1) (FEMA 2003)

Damage State		Description
	**Slight**	Small plaster cracks at corners of door and window openings and wall-ceiling intersections; small cracks in masonry chimneys and masonry veneers. Small cracks are assumed to be visible with a maximum width of less than 1/8 inch (cracks wider than 1/8 inch are referred to as "large" cracks).
	**Moderate**	Large plaster or gypsum-board cracks at corners of door and window openings; small diagonal cracks across shear wall panels exhibited by small cracks in stucco and gypsum wall panels; large cracks in brick chimneys; toppling of tall masonry chimneys.
	**Extensive**	Large diagonal cracks across shear wall panels or large cracks at plywood joints; permanent lateral movement of floors and roof; toppling of most brick chimneys; cracks in foundations; splitting of wood sill plates and/or slippage of structure over foundations.
	**Complete**	Structure may have large permanent lateral displacement or be in imminent danger of collapse due to cripple wall failure or failure of the lateral load resisting system; some structures may slip and fall off the foundation; large foundation cracks. Three percent of the total area of buildings with Complete damage is expected to be collapsed, on average.

1.2.5 Building Capacity Curves

A building capacity curve is a plot of a building's lateral load resistance as a function of a characteristic lateral displacement (i.e., a force-deflection plot). It is derived from a plot of static-equivalent base shear versus building displacement at the roof, known commonly as a pushover curve. In order to facilitate direct comparison with spectral demand, base shear is converted to spectral acceleration, and the roof displacement is converted to spectral displacement using modal properties that represent pushover response. Pushover curves and related-capacity curves, are derived from concepts similar to those of the *NEHRP Guidelines for the Seismic Rehabilitation of Buildings* [FEMA, 1997], and in *Seismic Evaluation and Retrofit of Concrete Buildings* [SSC, 1996], known as *ATC-40*.

Building capacity curves are constructed for each model building type and represent different levels of lateral force design and for a given loading condition, expected building performance. Each curve is defined by two control points:

(1) the "yield" capacity, and

(2) the "ultimate" capacity

The yield capacity represents the lateral strength of the building and accounts for design strength, redundancies in design, conservatism in code requirements and expected (rather than nominal) strength of materials. Design strengths of model building types are based on the requirements of current model seismic code provisions (e.g., 1994 *UBC* or *NEHRP Provisions*) or on an estimate of lateral strength for buildings not designed for earthquake loads. Certain buildings designed for wind, such as taller buildings located in zones of low or moderate seismicity, may have a lateral design strength considerably greater than those based on seismic code provisions.

The ultimate (plastic) capacity represents the maximum strength of the building when the global structural system has reached a full mechanism. Typically, a building is assumed capable of deforming beyond its ultimate point without loss of stability, but its structural system provides no additional resistance to lateral earthquake force. Up to yield, the building capacity curve is assumed to be linear with stiffness based on an estimate of the expected period of the building. From yield to the ultimate point, the capacity curve transitions in slope from an essentially elastic state to a fully plastic state. The capacity curve is assumed to remain plastic past the ultimate point. An example building capacity curve is shown in Figure 4.

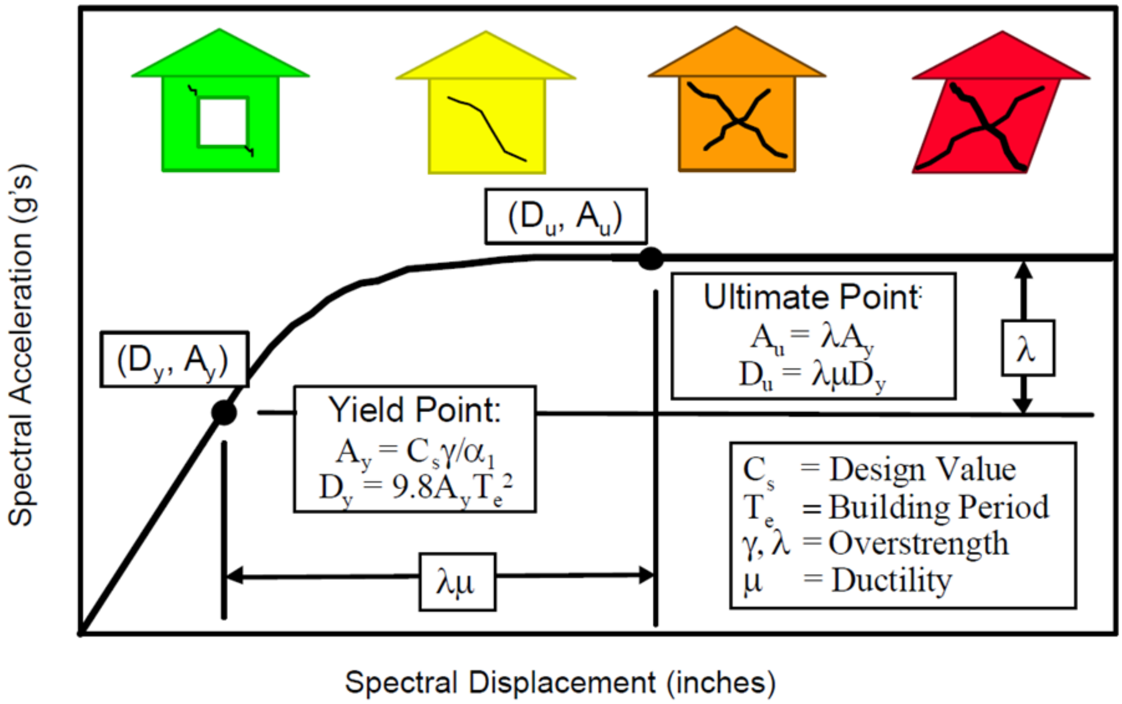

Figure 4: Example Building Capacity Curve and Control Points (FEMA 2003)

The following parameters define the yield point and the ultimate point of capacity curves as shown in Figure 4:

- **C_s** point of significant yielding of design strength coefficient (fraction of building's weight),
- **T_e** expected "elastic" fundamental- mode period of building (seconds),
- **α_1** fraction of building weight effective in the pushover mode,
- **α_2** fraction of building height at the elevation where pushover-mode displacement is equal to spectral displacement (not shown in Figure 4),
- **γ** "overstrength" factor relating "true" yield strength to design strength,
- **λ** "overstrength" factor relating ultimate strength to yield strength, and
- **μ** "ductility" ratio relating ultimate displacement to λ times the yield displacement (i.e., assumed point of significant yielding of the structure).

1.2.6 Building Response Calculation

Building response is determined by the intersection of the demand spectrum and the building capacity curve. Intersections are illustrated in Figure 5 for three example demand spectra representing what can be considered as weak, medium and strong ground shaking, and two building capacity curves representing weaker and stronger construction, respectively. As shown in Figure 5, stronger and stiffer construction displaces less than weaker and more flexible construction for the same level of spectral demand, and less damage is expected to the structural system and nonstructural components sensitive to drift. In contrast, stronger (and stiffer) construction will shake at higher acceleration levels, and more damage is expected to nonstructural components and contents sensitive to acceleration.

The demand spectrum is based on the 5%-damped response spectrum at the building's site (or center of a study area containing a group of buildings), reduced for effective damping when effective damping exceeds the 5% damping level of the input spectrum.

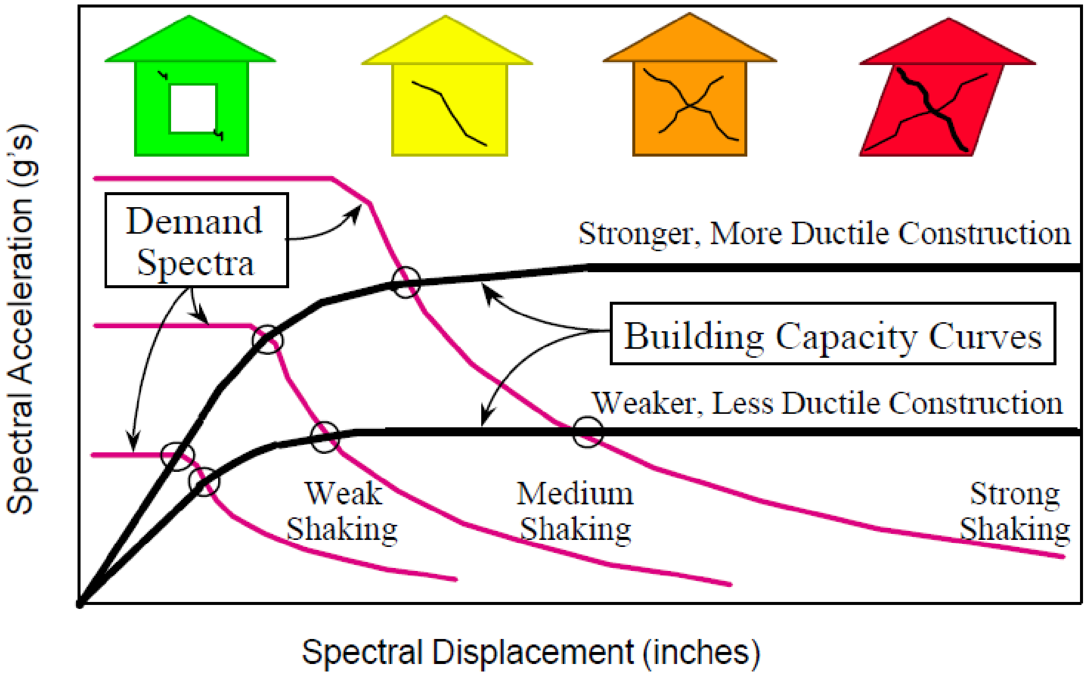

Figure 5: Example Intersection of Demand Spectra and Building Capacity Curves (FEMA 2003)

1.2.7 Building Fragility Curves

Building fragility curves are lognormal functions that describe the probability of reaching, or exceeding, structural and nonstructural damage states, given median estimates of spectral response, for example spectral displacement. These curves take into account the variability and uncertainty associated with capacity curve properties, damage states and ground shaking.

Figure 6 provides an example of fragility curves for the four damage states used in the FEMA/NIBS methodology and illustrates differences in damage-state probabilities for three levels of spectral response corresponding to weak, medium, and strong earthquake ground shaking, respectively. The terms "weak," "medium," and "strong" are used here for simplicity; in the actual methodology, only quantitative values of spectral response are used.

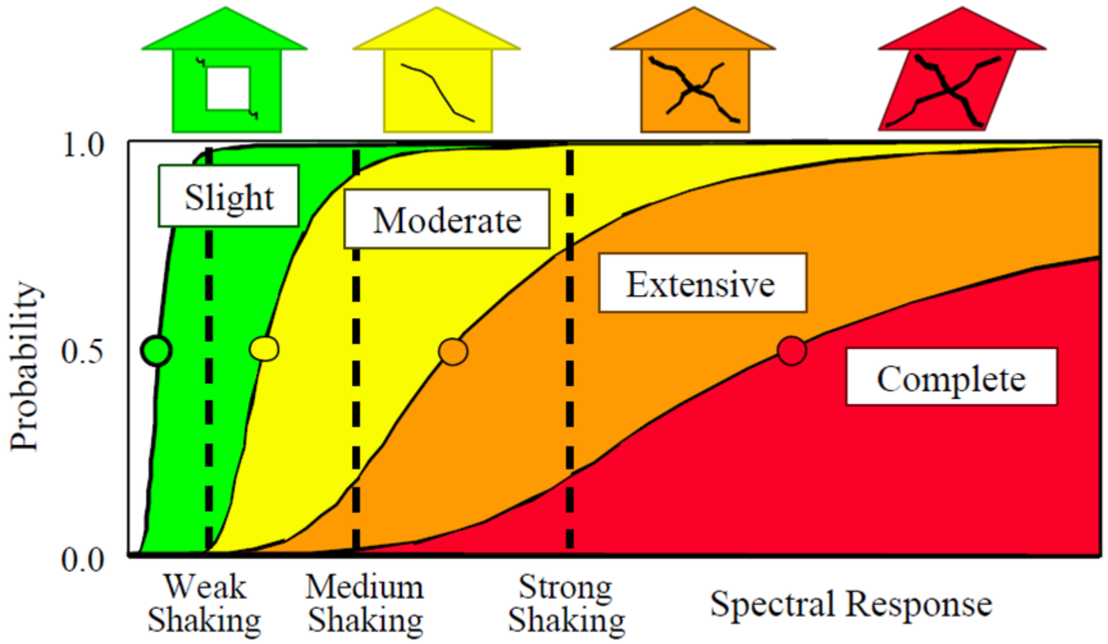

Figure 6: Example Fragility Curves for Slight, Moderate, Extensive and Complete Damage (FEMA 2003)

The fragility curves distribute damage among Slight, Moderate, Extensive and Complete damage states. For any given value of spectral response, discrete damage-state probabilities are calculated as the difference of the cumulative probabilities of reaching, or exceeding, successive damage states. Discrete damage-state probabilities are used as inputs to the calculation of various types of building-related loss.

Each fragility curve is defined by a median value of the demand parameter (e.g., spectral displacement) that corresponds to the threshold of that damage state and by the variability associated with that damage state.

The conditional probability of being in, or exceeding, a particular damage state, ds, given the spectral displacement, Sd, (or other seismic demand parameter) is defined by the following equation:

$$P\left[ds \middle| S_d\right] = \Phi\left[\frac{1}{\beta_{ds}} \ln\left(\frac{S_d}{\overline{S}_{d,ds}}\right)\right]$$

where:

ds a particular damage state

$S_{d,ds}$ is the median value of spectral displacement at which the building reaches the threshold of damage state, ds,

B_{ds} is the standard deviation of the natural logarithm of spectral displacement for damage state, ds, and

Φ is the standard normal cumulative distribution function.

1.3 Development of Capacity Curves and Response Parameters

1.3.1 Building Model and Pushover Criteria

This section guides users in the development capacity curves and related parameters that are used by Advanced Engineering Building Module (AEBM) to calculate building response as a function of ground shaking at the building site. It is assumed that the user has already performed nonlinear static (pushover) analysis of the building that conforms essentially to the methods of *NEHRP Guidelines* (or *ATC-40*) and to certain other criteria as set forth in this section.

The pushover analysis must appropriately represent the force-deflection and response characteristics of the building of interest. For use in developing fragility functions, the pushover analysis must also appropriately capture the damage patterns of elements and components of the building. In general, the latter requires more detailed and complex analysis than that required simply for evaluation of building response.

The *NEHRP Guidelines* (and *ATC-40*) provide users with a fairly complete description of the nonlinear static (pushover) method of analysis, including guidance on modeling and evaluation post-yield behavior of elements and components. Additional guidance is provided in this section for performing pushover analysis and using the results in loss estimation studies. Since the *NEHRP Guidelines* (and *ATC-40*) are design documents, the user should be aware that they intentionally (or unintentionally) include some conservatism that is not appropriate for loss estimation. For loss estimation, as compared to design procedures and building code rules, pushover analysis methods and models should fairly represent building (building group) without conservative bias. Building geometry, material strengths and response limits, etc. should all represent typical building conditions and likely response behavior, rather than being based on conservative or "worst-case" assumptions.

Users must determine how many different pushover models are required for loss estimation. For complex buildings, a model could be developed for each horizontal direction of response (if response is different in different directions) and for separate structural segments of the building. It is common for large buildings (in plan) to be composed of more than one structure, separated by construction joints. Each structure can have different capacity and response properties (and fragility and loss functions). For simple symmetrical buildings, a single pushover model would likely be sufficient to represent building behavior. If a single pushover model is used to evaluate a complex and/or irregular building, then the model would need to represent those modes of response and failure that are most likely to occur and cause damage and loss.

Consider, for example, a large tilt-up building, composed of three structural segments in a line (three by one rectangle in plan). Such buildings are commonly used for industrial manufacturing and warehousing facilities. The segments at each end are similar and have tilt-up panels of three sides. The segment in the middle is structurally different and has panels on only two opposing sides of the building. All three segments are strong in the plane of the tilt-up panels near the building's perimeter, but generally weak in the direction perpendicular to the panels away from building corners. All three segments have flexible diaphragms. Possible building response and failure modes include the following (there may be others):

- Local, out-of-plane failure of some tilt-up planes (due to failure of panel-to-roof connections) accentuated by diaphragm flexibility – most likely to occur at mid-span locations (away from building corners)
- Full collapse of center section in weak direction (perpendicular to tilt- up panels)
- Partial collapse of end sections in the weak direction (near joints with center section) accentuated by torsion response.

The user would likely develop multiple pushover models to evaluate the different modes of response and failure of the building, described above. Multiple pushover analyses could be converted into multiple building damage and loss models (one model per building segment) or folded into a single building damage and loss model. If multiple models of different building segments are developed, then damage and loss would be calculated separately for each and aggregated for the building as a whole.

Developing a single building damage and loss model (e.g., a single capacity curve) for a complex building requires users to judge the mode of failure, direction of response, etc., that best represents the most likely source of earthquake damage and loss. At the following paragraphs we assume that the user has resolved building complexity and describe methods for converting a single pushover curve into capacity and response parameters that are compatible with the AEBM.

Users must determine how many and to what degree elements and components are required to be explicitly modeled in pushover analyses used for loss estimation. For determining capacity curve properties, it is necessary that the pushover mode shape include all elements and components whose individual stiffness (flexibility) significantly affects global building response. From a dynamics standpoint, this requirement may also be thought of as including all "degrees of freedom" that significantly influence dynamic response of the 1st-mode of the building in the direction of interest.

Flexibility of the foundation, floor diaphragms, etc., should be explicitly modeled in the pushover analysis if the addition of the flexibility of these element/components to the pushover model would significantly change pushover mode shape and response. Similarly, no structural elements or components should be excluded from the pushover model simply because they are considered to be of secondary, rather than primary, importance to the structural system. Likewise, architectural elements and components that add significant stiffness to the building (e.g., hollow-clay tile used as in- fill partitions) should be modeled in the pushover analysis (and effectively removed from the model as they fail during pushover analysis).

1.3.2 Development of Capacity Curve Control Points

1.3.2.1 Conversion of Pushover Curve to Capacity Curve

The first step in developing capacity curve control points is to convert pushover coordinates of base shear force and control point (e.g., roof) displacement to spectral acceleration and displacement, respectively. The coordinate conversion is described somewhat vaguely as Method 2 in the commentary of the *NEHRP Guidelines* and more completely in *ATC-40*, the latter being consistent with *HAZUS* format and terminology.

The conversion of pushover to capacity is illustrated in Figure 7. An example pushover curve (normalized by the building's weight, W) is converted to capacity using pushover mode factors, α_1 and α_2. Each point on the normalized pushover curve (Dp, Ap) is factored by the pushover mode factors to create a corresponding point on the capacity curve (Dc, Ac). Provided the pushover curve was developed using a push force pattern based on the 1st-mode shape of the building, then the initial (pre-yield) slope of the capacity curve is directly related to the building's elastic (pre- yield) period (Te) as described by Equation 5. Axes are labeled in terms of Spectral Acceleration and Spectral Displacement in Figure 7, recognizing that while pushover and capacity curves can have the same units, they are in different coordinate systems.

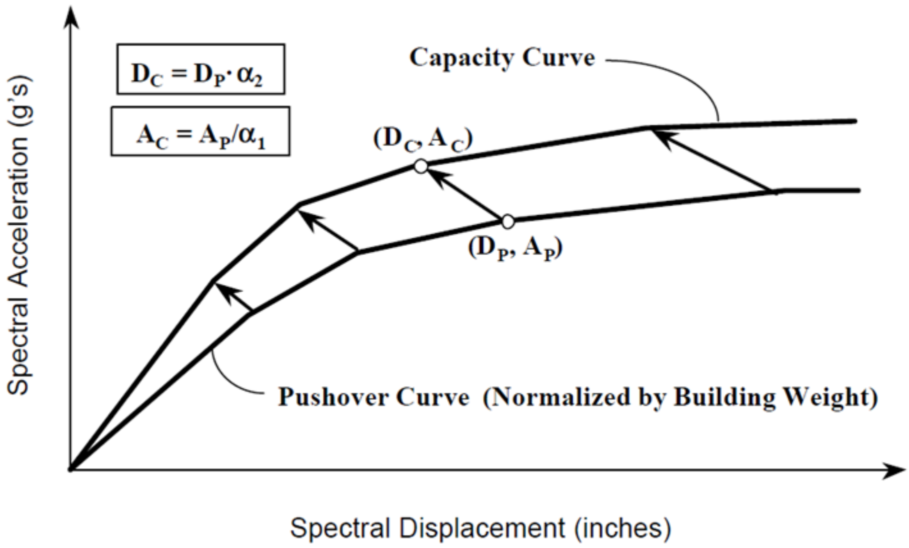

Figure 7: Example Conversion of Pushover Curve to Capacity Curve Using Pushover Mode Factors

HAZUS defines the two pushover mode factors:

- **α_1** fraction of building weight effective in pushover mode
- **α_2** fraction of building height at the elevation where pushover- mode displacement is equal to spectral displacement.

Consistent with *ATC-40* methods (and terms), a1 is defined by the distribution of building mass and pushover mode shape:

$$a_1 = \frac{\left[\sum_{i=1}^{N} (w_i \phi_{ip})/g\right]^2}{\left[\sum_{i=1}^{N} (w_i)/g\right]\left[\sum_{i=1}^{N} (w_i \phi^2_{ip})/g\right]} \qquad (1)$$

Where:

W_i / g = mass assigned to the ith degree of freedom

Φ_{ip} = amplitude of pushover mode at ith degree of freedom

Typically, the shape of the pushover mode is based on the 1st-mode of the building in the direction of interest. In general, the pushover mode shape is amplitude dependent, after elements and components begin to yield. While the most appropriate pushover shape would be the amplitude-dependent shape at the amplitude of interest, the pre-yield (1st-mode) shape may be used to calculate α_1 without significant loss of accuracy. This statement does not apply to element/component demands that are directly related to the post-yield changes to pushover mode shape. The term “degree of freedom” is used herein, rather than the term “level” of *ATC-40*, to indicate that there may be more than one node (degree of freedom) per floor (e.g., buildings with flexible diaphragms would need several nodes to represent diaphragm response).

Consistent with *ATC-40* (and discussion of the C0 factor in the commentary of the *NEHRP Guidelines*), the modal factor, α_2, is defined by amplitude of the normalized pushover mode shape at the control point and the pushover mode participation factor:

$$a_2 = \frac{1}{PF_p f_{cp,p}} = \frac{\sum_{i=1}^{N} (w_i \phi^2_{ip})/g}{\left[\sum_{i=1}^{N} (w_i \phi_{ip})/g\right] f_{cp,p}} \qquad (2)$$

Where:

$\mathbf{W_i / g}$ = mass assigned to the ith degree of freedom

$\mathbf{\Phi_{ip}}$ = amplitude of pushover mode at ith degree of freedom

$\mathbf{\Phi_{cp,p}}$ = amplitude of pushover mode at control point.

Typically, the roof is used as the location of the control point. The shape of the pushover mode is typically based on the 1st-mode of the building in the direction of interest and is, in general, amplitude dependent after elements and components begin to yield. As for the α_1 term, the most appropriate pushover shape would be the amplitude-dependent shape at the amplitude of interest, but the pre-yield (1st-mode) shape may be used to calculate α_2 in most cases without significant loss of accuracy.

The pushover mode factors are used directly to calculate the capacity curve from the pushover curve where each point on the capacity curve is defined by a spectral displacement, SD, and a spectral acceleration, SA:

$$\mathbf{SD = a_2 * \Delta_{CP}} \qquad (3)$$

$$\mathbf{SA = (V/W) / a_1} \qquad (4)$$

Where:

$\mathbf{\Delta_{CP}}$ = Pushover control point (e.g., roof) displacement

V = Pushover base shear force (kips)

W = Building weight (kips).

Certain structural analysis software programs (e.g., SAP2000 Nonlinear) automatically convert pushover curves to capacity curves using these formulas.

1.3.2.2 Yield and Ultimate Capacity Control Points

Capacity curve control points are determined from the capacity curve using both judgment and the following rules:

- Yield capacity control point (**Dy, Ay**) is selected as the point where significant yielding is just beginning to occur (slope of capacity curve is essentially constant up to the yield point).
- The expected period, **Te**, of the building, at or just below yield, should be the true "elastic" fundamental- mode period of the building:

$$T_e \cong 0.32\sqrt{\frac{D_y}{A_y}} \qquad (5)$$

- Ultimate capacity control-point acceleration, **Au**, is selected as the point of maximum spectral acceleration (maximum building strength), not to exceed the value of spectral acceleration at which the structure has just reached its full plastic capacity (i.e., ignore additional straining at the point at which the structure becomes a mechanism).
- Ultimate capacity control-point displacement, **Du**, is selected as the greater of either the spectral displacement at the point of maximum spectral acceleration or the spectral displacement corresponding to Equation 6:

$$D_u = 2 \cdot D_y \frac{A_u}{A_y} \qquad (6)$$

The *HAZUS* definition of the elastic period, **Te**, is the same as the initial period, Ti, of the *NEHRP Guidelines* and should not be confused with the definition of the effective period, Te, of the *NEHRP Guidelines*. The effective period, Te, of the *NEHRP Guidelines* is based on stiffness at 60% of the ultimate strength of the building and should not be used with *HAZUS* methods since it could significantly overestimate pre-yield displacement of the building.

Three sets of pushover and capacity curves and the **Control Points** selected for each using the rules described above are shown in Figures 8, 9 and 10, respectively. As shown in these figures, capacity curves typically extend beyond "ultimate" control-point displacement, **Du**, which defines the displacement at which the system is assumed to be fully plastic, but has not necessarily failed.

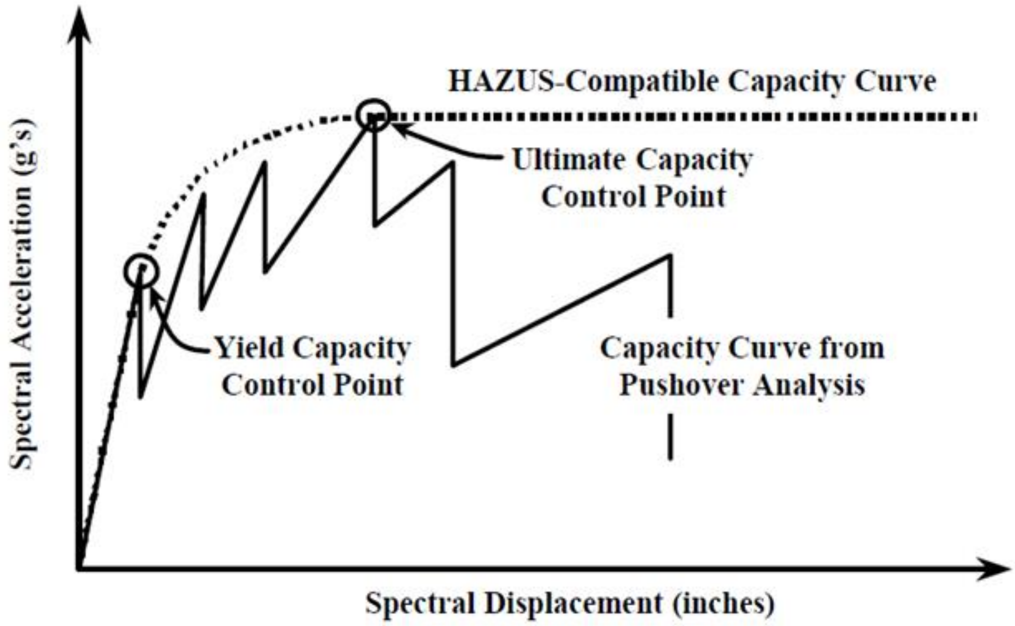

Figure 8: Example Development of the Capacity Curve for a Structure with "Saw-Tooth" Force-Deflection Behavior

In Figure 8, the first set of curves is for a structure that sustains shear failure and load reduction in a number of components at different levels of spectral displacement. The sequential shear failure of components creates a "saw-tooth" effect that is enveloped by the *HAZUS* capacity curve.

In Figure 9, the second set of curves represents "brittle" force-deflection behavior and catastrophic failure of the structure because it happened too quicly. The **Ultimate Capacity Control Point** is actually selected to be past the point of failure. This is not inappropriate, since the ultimate point does not define the fragility of the building, only the plateau of the capacity curve.

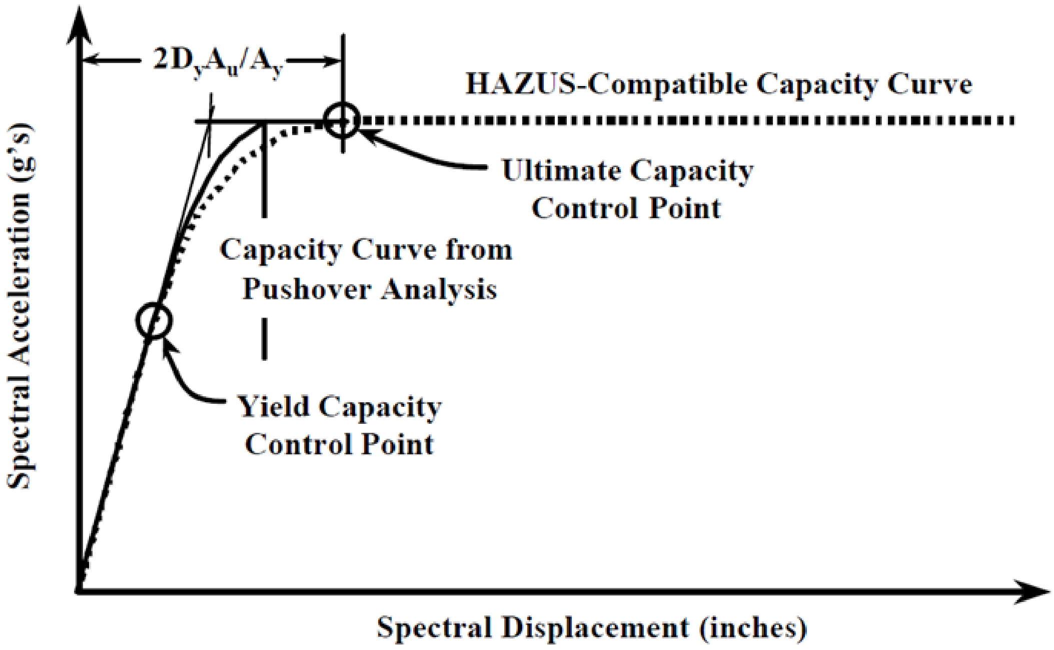

Figure 9: Example Development of the Capacity Curve for a Structure with "Brittle" Force-Deflection Behavior

The third set of curves shown in Figure 10 illustrates force-deflection behavior of a "ductile" building up to the formation of a complete mechanism (fully plastic state). The pushover curve indicates some additional strength beyond the fully plastic state due to strain hardening assumptions.

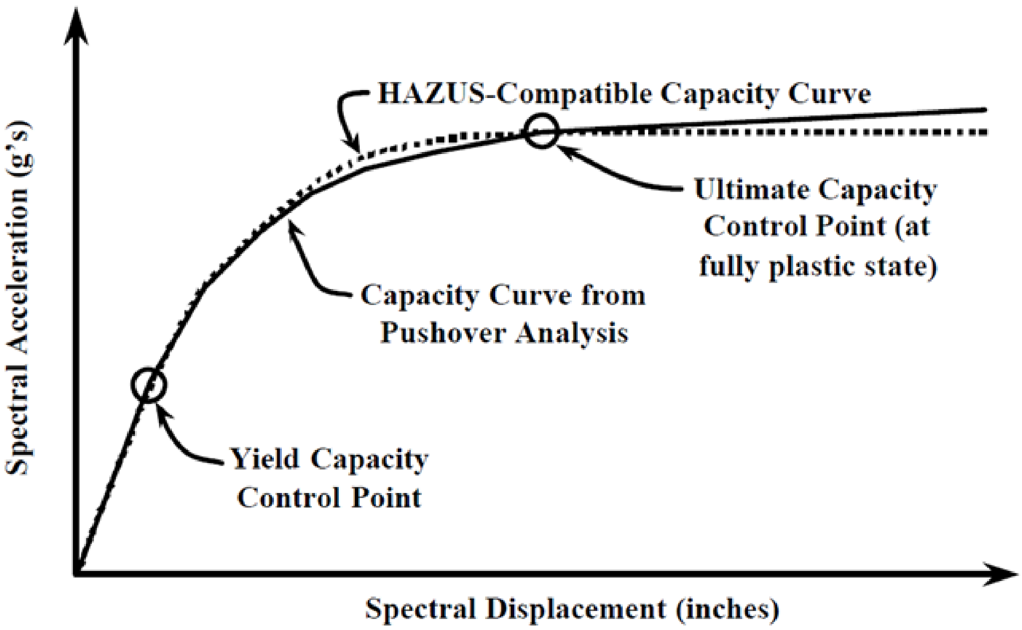

Figure 10: Example Development of the Capacity Curve for a Structure with "Ductile" Force-Deflection Behavior

Both the initial stiffness (i.e., elastic period, **Te**) and ultimate strength of the capacity curve will, in general, degrade with repeated cycles of post-yield earthquake demand. The effects of degradation of stiffness and strength on capacity and response of the building are accounted for by degradation factors. Development of degradation factors is described in the next subsection.

1.3.3 Development of Response Parameters

Response parameters include **Elastic Damping** and degradation (**Kappa**) factors that reduce hysteretic damping and affect the intersection capacity and demand, and the fraction of nonstructural components at lower- floors **(F_{ns})** which affects the calculation of demand on nonstructural-acceleration sensitive components. Background on the use of the elastic damping and degradation factors in the calculation of response is given in the following subsection.

1.3.3.1 Response Calculation

HAZUS characterizes ground shaking using a standard response spectrum shape, consistent with the format and parameters of the 1997 *NEHRP Provisions* and the *NEHRP Guidelines*. The standard shape consists of two primary parts: (1) a region of constant spectral acceleration at short periods and (2) a region of constant spectral velocity at long periods. Short-period spectral acceleration, S_s, is defined by 5%-damped spectral acceleration at a period of 0.3 seconds. The constant spectral velocity region has spectral acceleration proportional to 1/T and is anchored to the 1-second, 5%-damped spectral acceleration, S_1. A region of constant spectral displacement exists at very long periods, although this region does not usually affect calculation of building damage. Amplification of ground shaking to account for local site conditions is based on the short-period (Fa) and velocity-domain (Fv) soil factors of the 1997 *NEHRP Provisions.*

HAZUS modifies elastic system properties to simulate inelastic response by use of "effective" stiffness and damping properties of the building. Effective stiffness properties are based on secant stiffness, and effective damping is based on combined viscous and hysteretic measures of dissipated energy. Effective damping greater than 5% of critical is used to reduce spectral demand in a manner similar to the capacity-spectrum method of *ATC-40*.

Figure 11 illustrates the process of developing an inelastic response (demand) spectrum from the 5%-damped elastic response (input) spectrum. The demand spectrum is based on elastic response divided by amplitude-dependent damping reduction factors (i.e., Ra at periods of constant acceleration and Rv at periods of constant velocity). The demand spectrum intersects the building's capacity curve at the point of peak response displacement, D, and acceleration, A. The amount of spectrum reduction typically increases for buildings that have reached yield and dissipate hysteretic energy during cyclic response.

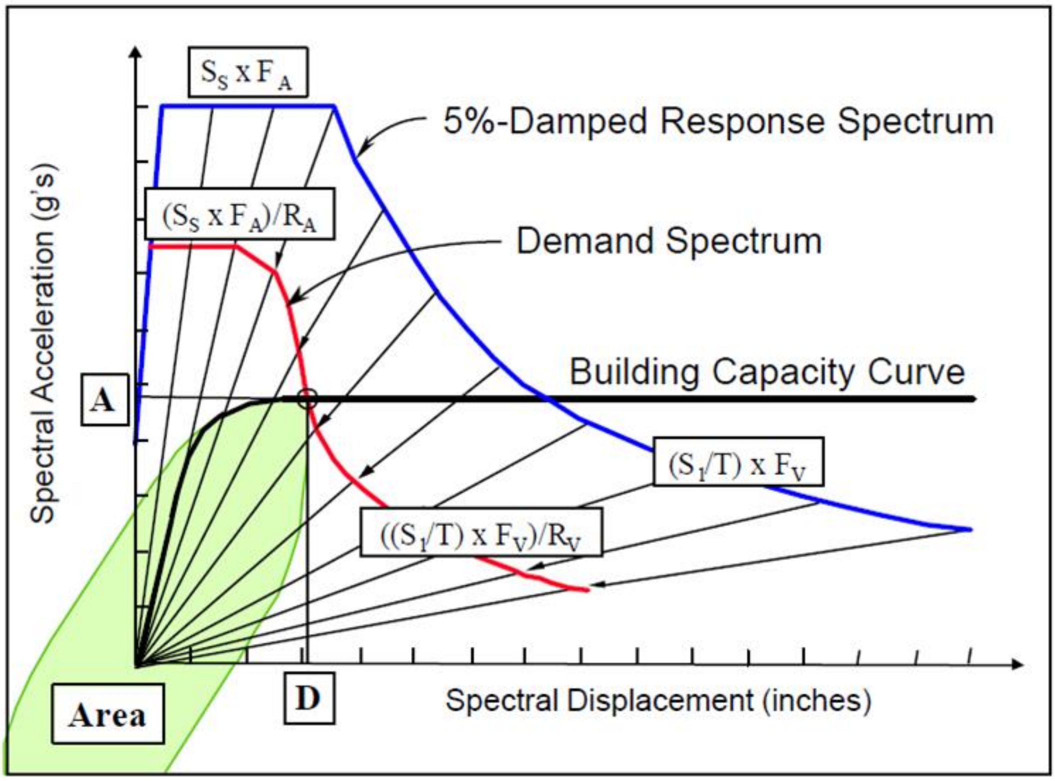

Figure 11: Example Demand Spectrum Construction and Calculation of Peak Response Point (D,A)

Spectrum reduction factors are a function of the effective damping of the building, beff, as defined by the following equations (yield reduction values of RA = 1.0 and RV = 1.0, respectively, for a value of beff = 5% of critical):

$$\mathbf{R_A = 2.12/(3.21 - 0.68\ ln(\beta_{eff}))} \qquad (7)$$

$$\mathbf{R_V = 1.65/(2.31 - 0.41\ ln(\beta_{eff}))} \qquad (8)$$

Effective damping, beff, is defined as the total energy dissipated by the building during peak earthquake response and is the sum of an elastic damping term, β_E, and a hysteretic damping term, β_H , associated with post-yield, inelastic response:

$$\boldsymbol{\beta_{eff} = \beta_E + \beta_H} \qquad (9)$$

The elastic damping term, β_E , is assumed to be a constant (i.e., amplitude independent) and follows the recommendations of Table 3 of *Earthquake Spectra and Design* for materials at or just below their yield points. The hysteretic damping term, β_H , is dependent on the amplitude of post-yield response and is based on the area enclosed by the hysteresis loop at peak response displacement, D, and acceleration, A, as shown in Figure 11. Hysteretic damping, bH, is defined in Equation 10:

$$\beta_H = \kappa \left(\frac{\text{Area}}{2\pi \, D \, A} \right) \qquad (10)$$

Where:

Area is the area enclosed by the hysteresis loop, as defined by a symmetrical push-pull of the building capacity curve up to peak positive and negative displacements, ±D, assuming no degradation of components

D is the peak displacement response of the capacity curve

A is the peak acceleration response at peak displacement, D

κ is a degradation factor that defines the fraction of the Area used to determine hysteretic damping

The κ (Kappa) factor in Equation 10 reduces the amount of hysteretic damping as a function of model building type, seismic design level and shaking duration to simulate degradation (e.g., pinching) of the hysteresis loop during cyclic response. Shaking duration is described qualitatively as either short, moderate or long, and is assumed to be primarily a function of earthquake magnitude, although proximity to fault rupture can also influence the duration of the level of shaking that is most crucial to building damage.

Figure 12 shows a typical capacity curve and three example demand spectra for damping levels corresponding to short (κ_s = 0.8), moderate (κ_M = 0.5) and long (κ_L= 0.3) duration ground shaking, respectively. In this example, building displacement due to long-duration ground shaking is more than twice that due to short-duration ground shaking (although building acceleration does not increase). Damage to the structural system and nonstructural, driftsensitive components and related losses increase significantly with increase in the duration of ground shaking for buildings that have reached yield

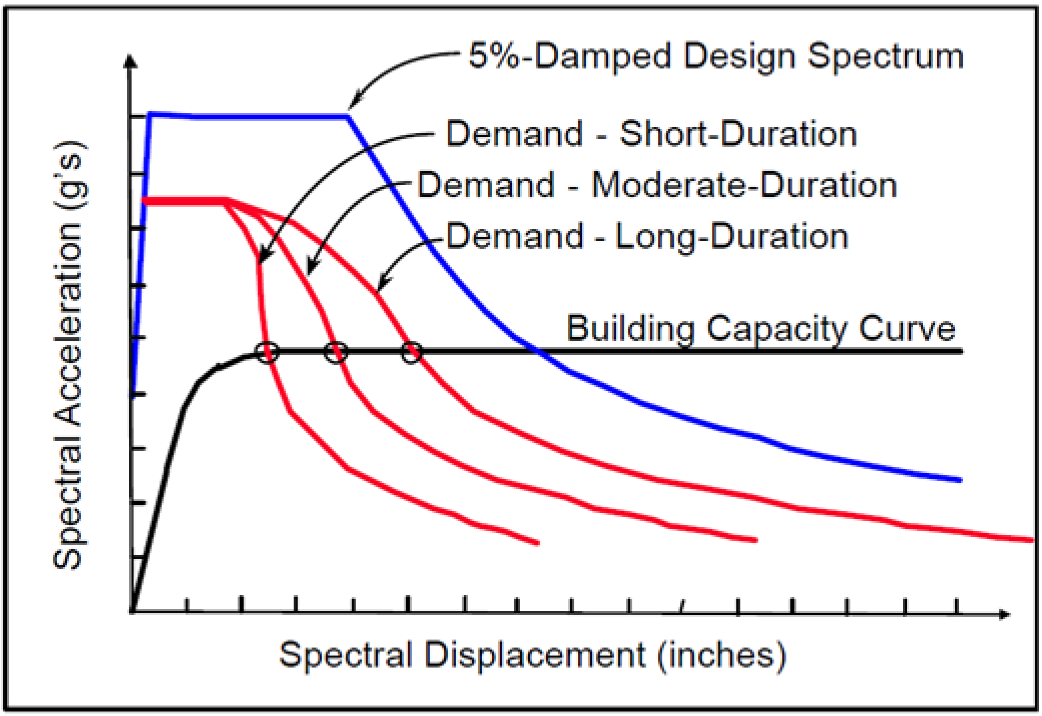

Figure 12: Example Demand Spectra – Post-Yield Response due to Strong Ground Shaking of Either Short, Moderate or Long-Duration

1.3.3.2 Elastic Damping Factors

As described in the preceding subsection, **Elastic Damping** factors estimate the damping of the building at or just below yield of the structural system. These values should be selected on the basis of the building type, reflecting the inherent differences in the damping behavior of different materials. In general, the **Elastic Damping** factors included in *HAZUS* for general building stock should be used without modification for building-specific applications. Table 4 summarizes the **Elastic Damping** values of *HAZUS* for different building types.

Table 4: Suggested Elastic Damping Values (FEMA 2003)

Building Type by Material	Damping (% of Critical)
Mobile Home	5%
Steel Buildings	5% - 7%
Reinforced-Concrete and Pre-cast Concrete Buildings	7%
Reinforced-Masonry Buildings	7% - 10%
Unreinforced-Masonry Bearing-Wall and In-Fill Buildings	10%
Wood Buildings	10% - 15%

1.3.3.3 Degradation Factors

Degradation (**Kappa**) factors are a function of the expected amplitude and duration (number of cycles) of post-yield building response. These parameters depend on the level of ground shaking, which is different for each building site and scenario earthquake. The default values of the Kappa factor developed for generic-building analysis assume that the building would have ground shaking strong enough to effect significant post-yield response of the structure, and degradation is based on the magnitude of the scenario event. The larger the magnitude of the event, the longer the assumed duration of ground shaking. In this sense, earthquake magnitude became a surrogate indicator of the duration of post- yield response, assuming shaking was strong enough to push the structure beyond the yield point. It should be recognized that if the ground shaking were not strong enough to yield the building, there would be little or no degradation, regardless of the magnitude of the scenario earthquake (or the type of structural system).

Kappa factors should be selected considering the extent to which brittle failure of the elements and components reduces the strength of the structural system. The capacity curve developed by pushover analysis provides some guidance on the selection of appropriate Kappa factors. If the capacity curve indicates a loss of strength at the ultimate capacity control point, then the Kappa factor should indicate a somewhat proportional reduction in hysteretic loop area. For example, in Figure 8 the capacity curve indicates about a 50% reduction in full strength, and a commensurate amount of degradation would be appropriate (e.g., κ_M = 0.50 for a moderate duration of post- yield response). In Figure 9, the capacity curve indicates nearly complete (brittle) failure (at the ultimate capacity control point) and a very low value of the degradation factor would be appropriate (e.g., κ_M = 0.10 for a moderate duration of post-yield response). In Figure 10, the capacity curve indicates nearly fully ductile behavior, and a relatively high value of the degradation factor would be appropriate (e.g., κ_M = 0.90 for a moderate duration of ground shaking).

Table 5 provides some general guidance on the selection of the degradation (Kappa) factor. The Kappa factors are shown as a function of the level of response (i.e., one- half yield, yield and post-yield levels of peak response) and for post-yield response as a function of post-yield shaking duration (i.e., short, moderate and long). The table also relates suggested values of Kappa factors to the seismic design level and quality of construction used to characterize generic building types of *HAZUS*.

Table 5: Suggested Values of the Degradation (Kappa) Factor (FEMA 2003)

Design Level and Construction Quality						Degradation (Kappa) Factor				
	Seismic Design Level[1]					At ½ Yield	At Yield	Post-Yield Shaking Duration		
	SHC	HC	MC	LC	PC			Short	Moderate	Long
QC[2]	S	S				1.0	1.0	1.0	0.9	0.7
		O	S			1.0	1.0	0.9	0.7	0.5
		I	O	S		1.0	0.9	0.7	0.5	0.3
			I	O	S	1.0	0.7	0.5	0.3	0.1
				I	O	1.0	0.5	0.3	0.1	0.0

1. Seismic Design Level Designation – Special High-Code (SHC), High-Code (HC), Moderate-Code (MC), Low-Code (LC) and Pre-Code (PC)
2. Construction Quality (QC) Designation – Superior (S), Ordinary (O) and Inferior (I)

The suggested values of the Kappa factor given in Table 5 do not apply to seismically rehabilitated buildings. If the user is developing damage functions for a building that been strengthened, or otherwise seismically improved, then the selection of Kappa's should be based on a seismic design level and quality of construction that reflects these improvements.

1.4 Development of Fragility Curves

1.4.1 Building Response and Performance Criteria

This section guides users in the development of fragility curves parameters that are used by Advanced Engineering Building Module (AEBM) to calculate damage as a function of building response. It is assumed (and essential) that the user has already performed a detailed nonlinear static (pushover) analysis of the building.

The pushover analysis must appropriately capture the damage patterns of elements and components of the building and evaluate modes of building failure (i.e., partial or full collapse of the structure). Users must carefully consider modes of building failure and develop appropriate and representative models of structural response and element/component behavior. More than one pushover model could be used to evaluate different modes of response and failure (e.g., of different building segments). In this thesis it is stated that the problem of the complexity of building has been solved and describes the methods for the development of the parameters of vulnerability from a non-linear static analysis (pushover).

Calculation of damage-state probability is a step in the sequential process of estimating earthquake losses. Some leeway is available to users in determining building-specific fragility curves, since the building-specific loss functions will also be developed based on the fragility assumptions. What is essential is that the amount and type of damage associated with each damage state be consistent with the amount and type of damage assumed in the development of loss functions. For example, the user may have a choice of 4 inches, 5 inches or 6 inches of spectral displacement to represent Moderate structural damage to the building. In this example, these spectral displacements represent a range of plausible estimates resulting in "moderate" damage to elements and components, but with distinct differences in the cost of repair. That is, 6 inches of spectral displacement would cause more damage and cost more to repair than 4 inches of spectral displacement. The user may choose either 4 inches, 5 inches or 6 inches of spectral displacement to represent Moderate structural damage, provided the loss functions for Moderate damage are developed for the same amount of spectral displacement.

Fragility curves define boundaries between damage states. That is, the median value of the Damage State of interest defines the threshold of damage, and this state of damage is assumed to exist up to next state of damage. This description is illustrated in Figures 13, which includes example fragility curves for Slight, Moderate, Extensive and Complete structural damage. In this illustration, a shaded region illustrates the probability-response space associated with Moderate damage. The boundary on the left of the shaded region is defined by the fragility curve for Moderate (or greater) structural damage, and the boundary on the right of the shaded region is defined by the fragility curve for Extensive (or greater) damage. The probability of Moderate damage at a given level of spectral demand is calculated as the difference of the probability of Moderate (or greater) damage less the probability of Extensive (or greater) damage – a probability of 0.40 at 6 inches of spectral displacement in the example shown in Figure 13.

Figure 13: Example Fragility Curves – Calculation of Damage-State Probability

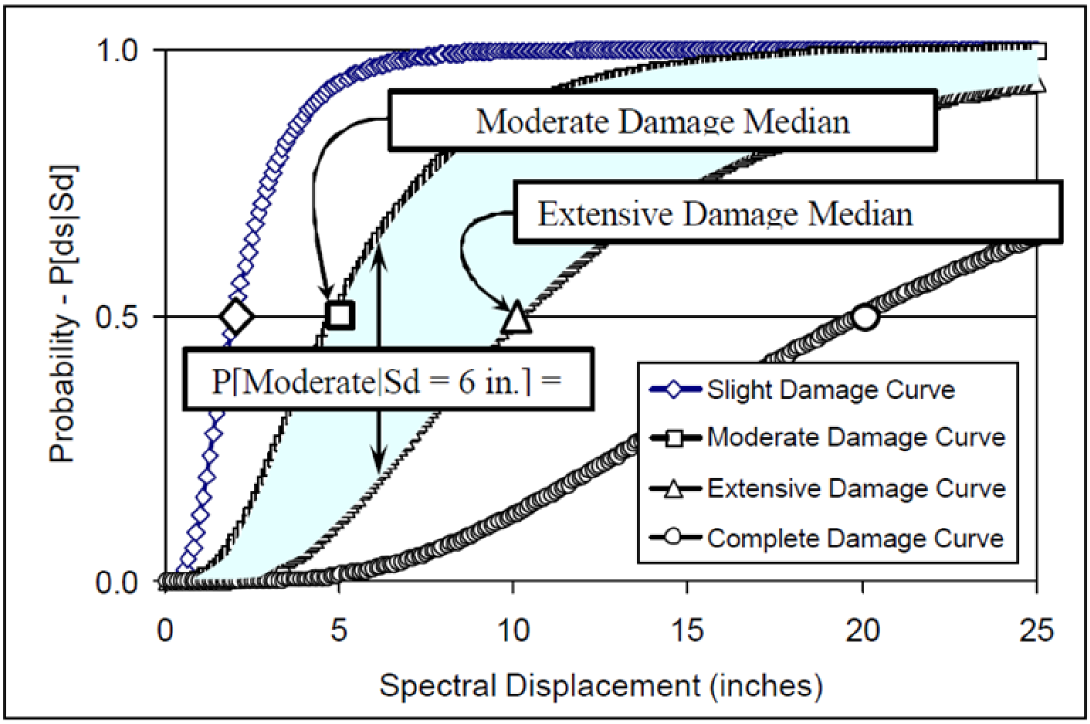

The slope of the fragility curve is controlled by the lognormal standard deviation value (Beta). The smaller the value of Beta, the less variable the damage state, and the steeper the fragility curve. The larger the value of Beta, the more variable the damage state, and the flatter the fragility curve.

Figure 14 illustrates this trend for fragility curves that share a common median (i.e., spectral displacement of 5 inches), but have Beta values ranging from 0.4 to 1.2. This range of Beta values approximately covers the range of Beta values that could be used for building-specific fragility curves.

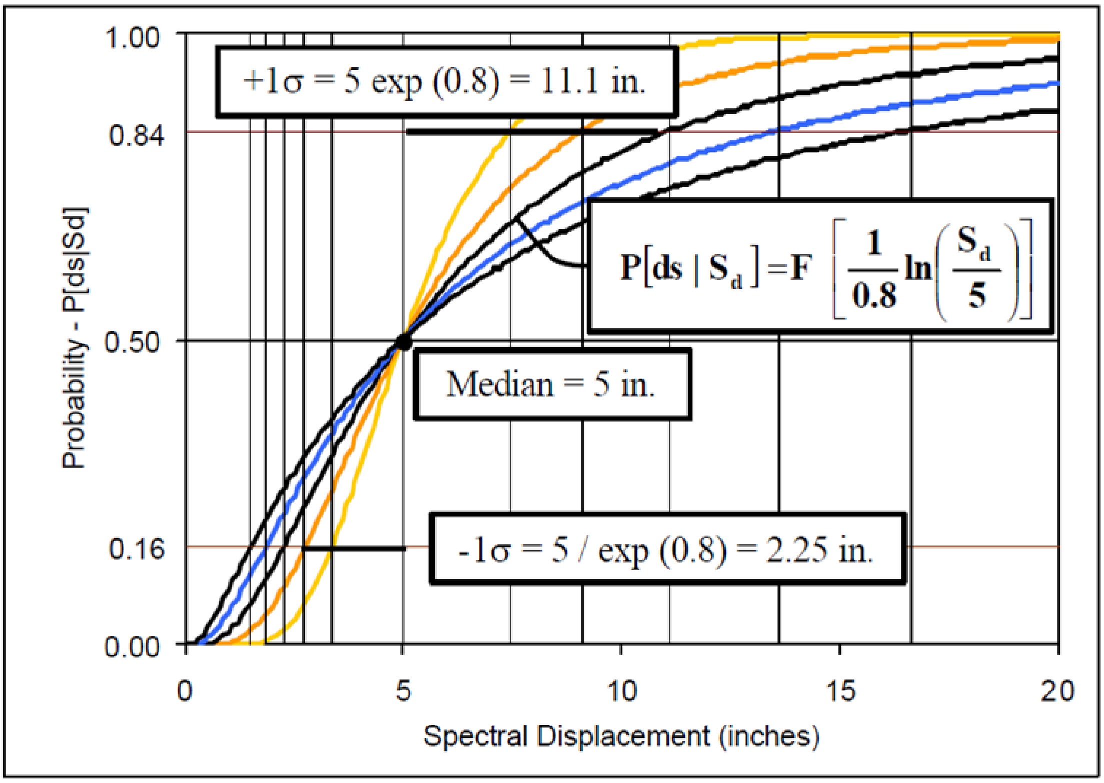

Figure 14: Example Lognormal Fragility Curves(Beta = 0.4, 0.6, 0.8, 1.0 and 1.2) and Calculation of ±1σ Spectral Displacement

1.4.2 Development of Damage-State Medians

Development of Damage-State Medians involves three basic steps:

- Develop a detailed understanding of damage to elements and components as a continuous function of building response (e.g., average inter-story drift or floor acceleration).
- Select specific values of building response that best represent the threshold of each discrete damage state.
- Convert damage-state threshold values (e.g., average inter-story drift) to spectral response coordinates (i.e., same coordinates as those of the capacity curve).

In general, the implementation of the three steps will be significantly different for structural and nonstructural systems. It is expected that detailed pushover analysis of the building will be the primary source of information regarding structural damage and selection of appropriate damagestate threshold values. In most cases, generic-building fragility values of *HAZUS* would not be used for the structural system (but could provide a “sanity check” of building-specific results). In contrast, pushover analysis typically provides only minimal information of nonstructural system performance, and users will rely primarily on the generic-building fragility values of *HAZUS* to determine threshold values of nonstructural damage states.

1.4.2.1 Structural System

Selection of **Damage-State Medians** should be consistent with the broad descriptions of structural damage given in Section 5.3.1 of the *HAZUS-MH Technical Manual* for different model building types. Descriptions of damage in *HAZUS* are sufficiently vague to permit user selection of values that best fit the damage patterns of dominant elements and components of the structural system. In addition, general guidance is provided below in Table 6 regarding the selection of appropriate **Damage-State Medians** for the structural system.

Table 6: General Guidance for Selection of Structural Damage-State Medians (FEMA 2003)

Damage State	Likely Amount of Damage, Direct Economic Loss, or Building Condition			
	Range of Possible Loss Ratios	Probability of Long-Term Building Closure	Probability of Partial or Full Collapse	Immediate Post-Earthquake Inspection
Slight	0% - 5%	P = 0	P = 0	Green Tag
Moderate	5% - 25%	P = 0	P = 0	Green Tag
Extensive	25% - 100%	P ≅ 0.5	P ≅ 0[1]	Yellow Tag
Complete	100%	P ≅ 1.0	P > 0	Red Tag

1. Extensive damage may include local collapse (e.g., out-of-plane failure of URM infill walls).

Pushover analysis results typically express performance in terms of component ductility demand, rather than in terms of physical damage. The structural criteria of Table 2-4 (Vertical Elements) and Table 2-5 (Horizontal Elements) of the *NEHRP Guidelines* provide some description of damage expected at various performance levels (e.g., component ductility) and may be used to relate element and component performance to physical description of damage. It is expected that the results of the pushover analysis, whether expressed in terms of physical damage (e.g., crack size) or in terms of component ductility demand, will be sufficient for users to tabulate the type and sequence of damage (and failure) of elements and components.

Damage to elements and components of the structural system should be tabulated as a function of the lateral displacement of the building, quantified by the average inter-story drift ratio (i.e., roof displacement divided by building height). Of course, individual stories of multi-story building would not all be expected to have the same drift, nor would inter-story drift be the same at all locations on a given floor if there was diaphragm flexibility or a rotational component to the pushover mode shape. However, average inter-story drift provides a convenient measure of building response that may be compared against default values of average inter-story drift that define damage states for generic building types of *HAZUS*.

The *NEHRP Guidelines* provide acceptance criteria that define deformation limits for large number of structural components and elements of different material types. These acceptance criteria imply various degrees of component or element damage and thus may be used to determine appropriate values of the average inter-story drift ration for each damage state of the structural system. However, in using the acceptance criteria of the *NEHRP Guidelines* users must be aware and account for each of the following four issues:

- Conservative Deformation Limits – The deformation limits of the NEHRP Guidelines are, in general, conservative estimates of true component or element capacity. In concept, the deformation limits are based on “backbone” curves that represent average multi-linear behavior of the subassembly of interest (e.g., as determined by cyclic-load testing).However, control points of idealized backbone curves necessarily incorporate some conservatism (that could be removed if the component or element were tested). Further, the Collapse Prevention deformation limits of primary components or elements are defined as 75% of that permitted for secondary elements, reflecting added conservatism for design of primary components or elements. The NEHRP Guidelines (like other seismic “codes”) include inherent conservatism in limit states. While appropriate for design, conservatism should be removed from deformation limits used to estimate actual damage and loss.
- Deformation Limits vs. Damage States – The NEHRP Guidelines provide limits on component or element deformation rather than explicitly defining damage in terms of degree of concrete cracking, nail pull-out, etc., or whether component of element

damage is likely to repairable (or not). For estimating direct economic loss it is important to understand the type of damage, not just the degree of yielding, to establish if repair would be required and what the nature (and cost) of such repairs would be.

- Global vs. Local Damage – Local damage (as inferred from the deformation limits of the NEHRP Guidelines) of individual components and elements must be accumulated over the entire structure to represent a global damage state. In general, any number of different combinations of local damage to components and elements could result in the same amount of global damage. Moderate damage could result due to a modest amount of damage to many components of elements, but would most likely be caused by significant damage to a limited number of components or elements that would cost 5% to 25% of the value of the structural system to repair (or replace).
- Collapse Failure – In general, collapse failures of the structural system require consideration of the interaction of components and elements and evaluation of possible global instability. The NEHRP Guidelines define "Collapse Prevention" deformation limits for components that are intended (with some degree of conservatism) to avoid local structural failure of components and elements. Reaching the "Collapse Prevention" deformation limit of components or elements does not necessarily imply structural collapse. Typically, structural systems can deform significantly beyond "Collapse Prevention" deformation limits before actually sustaining a local or global instability. It should be noted that while only a few buildings have actually collapsed during a major earthquake, case studies of the NEHRP Guidelines found that "Collapse Prevention" deformation limits were typically exceeded for strong ground shaking [FEMA, 1999].

Table 7 provides general guidance to users wishing to relate deformation (or deformation ratio) limits of the *NEHRP Guidelines* to average inter-story drift ratios of structural damage states. Table 7 provides two sets of criteria for each structural damage state. The first set of criteria establish damage states in terms of the fraction (by replacement value) of structural components reaching the control point "C" (or control point "E") on the idealized load versus deformation (backbone) curve. The second set of criteria establish an upper-bound on the average inter-story drift ratio of damage states by factors applied to the displacement at which 50% of structural components have reached their individual yield points (i.e., control point

“B”). Figure 15 (taken from Figure 2-5 of the *NEHRP Guidelines*, illustrates points B, C and E on the idealized load versus deformation (backbone) curve.

Table 7: General Guidance for Relating Component (or Element) Deformation to the Average Inter-Story Drift Ratios of Structural Damage-State Medians (FEMA 2003)

Damage State	Component (Criteria Set No. 1)[1]			Component (Criteria Set No. 2)[1]		
	Fraction[2]	Limit[3]	Factor[4]	Fraction[2]	Limit[3]	Factor[4]
Slight	> 0%	C	1.0	50%	B	1.0
Moderate	≥ 5%	C	1.0	50%	B	1.5
Extensive	≥ 25%	C	1.0	50%	B	4.5
Complete	≥ 50%	E	1.0 - 1.5[5]	50%	B	12

1. The average inter-story drift ratio of structural damage state is lessor of the two drift ratios defined by Criteria Sets No. 1 and No.2, respectively.

2. Fraction defined as the repair or replacement cost of components at limit divided by the total replacement value of the structural system.

3. Limit defined by the control points of Figure 14 and the acceptance criteria of *NEHRP Guidelines*.

4. Factor applied to average inter-story drift of structure at deformation (or deformation ratio) limit to calculate average inter-story drift ratio of structural damage-state median.

5. Complete factor is largest value in range for which the structural system is stable.

As an example of the use of the 1st set of criteria of Table 7, consider the development of damage-state medians for the “pushover” curve shown in Figure 15. This pushover curve corresponds to the “saw-tooth” capacity curve shown previously, except that curve is now shown in terms of base shear versus average inter-story drift ratio (i.e., roof displacement normalized by building height. This pushover curve is assumed to have been developed by nonlinear static analysis of the structure using the modeling and acceptance theory of the *NEHRP Guidelines*.

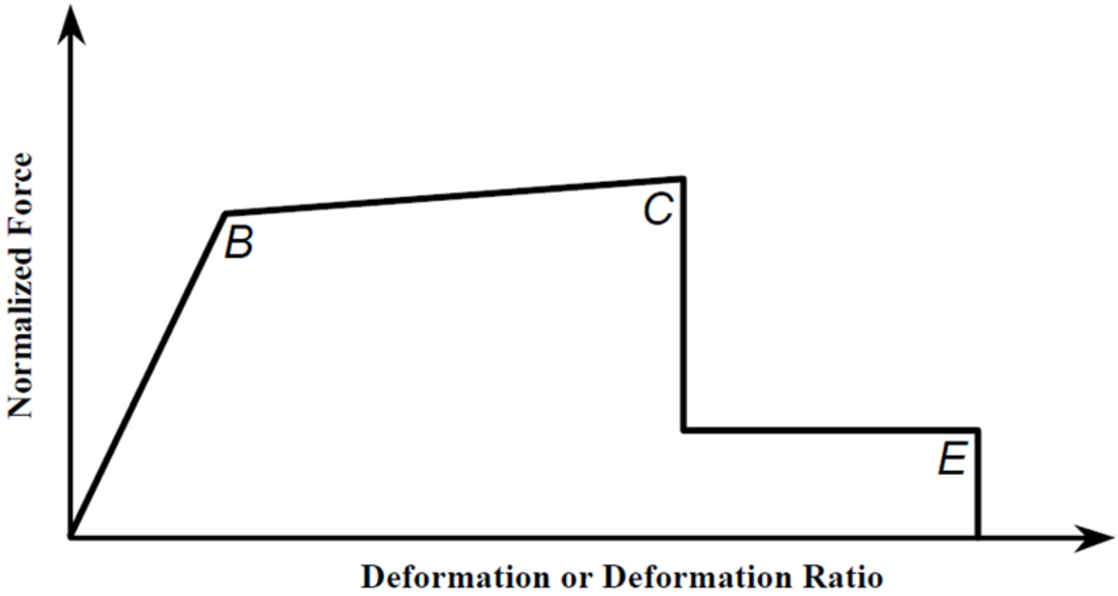

Figure 15: Idealized Component Load versus Deformation Curve (from Figure 2-5 of the NEHRP Guidelines)

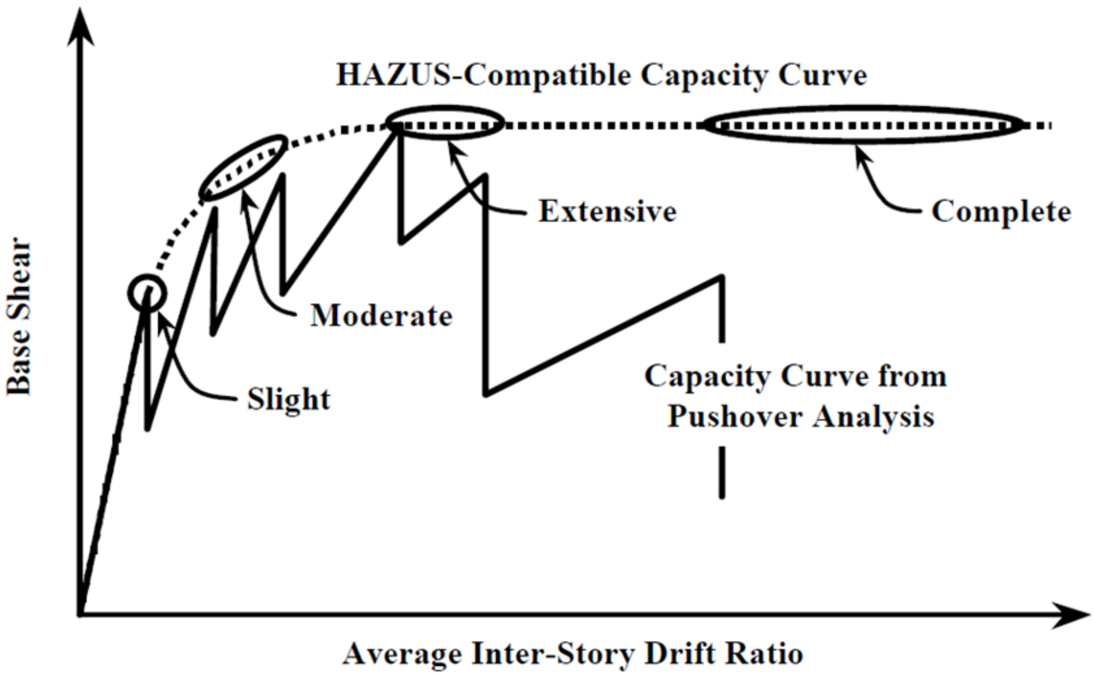

Figure 16: Example Damage-State Medians of "Saw-Tooth" Pushover Curve

Following the guidance of Table 7, the median of Slight damage is defined by the first structural component to reach control point C on its load deformation curve (i.e., point where component capacity of component drops, as illustrated in Figure 15). On a global basis, this point may be recognized as the first "tooth" of the capacity curve (i.e., point where structure capacity drops abruptly, as illustrated in Figure 16).

Moderate damage is defined by a median value for which a sufficient number of components have each reached control point C (on their respective load deformation curves) such that it will cost at least 5% of the replacement value of the structural system to repair (or replace) these components. Moderate damage is likely to be localized, since only a limited number of components can be repaired (or replaced) for 5% of the replacement value of the structural system. In Figure 16, an oval indicates that this extent damage might occur at the second or third "tooth" of the capacity curve, depending on type of repair, accessibility of damaged components and other factors that influence repair cost.

Extensive damage is defined by a median value similar to Moderate damage, except that damage repair now costs at least 25% of the value of the structural system. Extensive damage is likely to affect a number of components distributed throughout the building or affect all components at the most vulnerable story. Again, an oval indicates the sensitivity of the median to repair cost factors. The Extensive damage oval extends up to the point on the pushover curve for which there is a large drop in load capacity without significant recovery indicating (in this example) that a large number of elements would require repair or replacement at this level of response.

Complete damage is defined by a median value for which at least 50% (in terms of repair/replacement cost) of structural components have each lost full lateral capacity, as defined by control point E on their respective load deformation curves. Table 7 acknowledges the inherent conservatism in the values of control point E (as defined by the *NEHRP Guidelines*) and suggests that the median of the Complete damage state should be as much as 1.5 times greater than control point E, provided that the structure is not likely to collapse.

In Figure 16, a large oval indicates the range of possible median values for the Complete damage state. This range extends from 1.0 to 1.5 times the point of the last large drop in the load-carrying capacity of the pushover curve, indicating that most elements have reached their limit. The Complete damage state and related collapse failure modes are the most difficult to rationalize using engineering methods, even when evaluated using the sophisticated nonlinear methods of the *NEHRP Guidelines*. Correlation of predicted and observed damage and losses indicate that very liberal interpretations of engineering acceptance criteria are required to accurately predict Complete damage and the number of collapses that have actually occurred.

The average inter-story drift ratios of structural damage states of generic building types may be found in Table 6.4a and Tables 5.9a through 5.9d of the *HAZUS-MH Technical Manual*. These tables provide drift ratios of each model building type for Special High-Code, High-Code, Moderate-Code, Low-Code and Pre-Code seismic design levels, respectively. These drift ratios are also summarized below in Table 6.3. The *HAZUS* drift ratios for generic buildings may be used as a “sanity check” of building-specific values, recognizing that generic-building damagestate median values represent a typical building of the group and could be a factor of 2 or more greater (or less than) the medians of a specific building.

It should also be noted that Table 8 incorporates the effects of diaphragm flexibility (and other contributors to the overall flexibility of the structural system) in the values of average inter-story drift ratio that define the damage-state medians of generic buildings. In contrast, the control points and acceptance criteria of the *NEHRP Provisions* apply strictly to the component of interest. For structural systems with very stiff components (e.g., URM buildings), average interstory drift ratios developed from pushover analysis using the modeling and acceptance criteria of the *NEHRP Guidelines* should also incorporate diaphragm (and other sources of) flexibility before comparison with the default values summarized in Table 8 for generic building types.

Table 8: HAZUS Average Inter-Story Drift Ratio (Δds) of Structural Damage States

Model Building Type		Structural Damage States			
		Slight	Moderate	Extensive	Complete
Low-Rise Buildings – High-Code Design Level					
W1, W2		0.004	0.012	0.040	0.100
S1		0.006	0.012	0.030	0.080
C1, S2		0.005	0.010	0.030	0.080
C2		0.004	0.010	0.030	0.080
S3, S4, PC1, PC2, RM1, RM2		0.004	0.008	0.024	0.070
Low-Rise Buildings – Moderate-Code Design Level					
W1, W2		0.004	0.010	0.031	0.075
S1		0.006	0.010	0.024	0.060
C1, S2		0.005	0.009	0.023	0.060
C2		0.004	0.008	0.023	0.060
S3, S4, PC1, PC2, RM1, RM2		0.004	0.007	0.019	0.053
Low-Rise (LR) Buildings – Low-Code Design Level					
W1, W2		0.004	0.010	0.031	0.075
S1		0.006	0.010	0.020	0.050
C1, S2		0.005	0.008	0.020	0.050
C2		0.004	0.008	0.020	0.050
S3, S4, PC1, PC2, RM1, RM2		0.004	0.006	0.016	0.044
S5, C3, URM		0.003	0.006	0.015	0.035
Low-Rise (LR) Buildings – Pre-Code Design Level					
W1, W2		0.003	0.008	0.025	0.060
S1		0.005	0.008	0.016	0.040
C1, S2		0.004	0.006	0.016	0.040
C2		0.003	0.006	0.016	0.040
S3, S4, PC1, PC2, RM1, RM2		0.003	0.005	0.013	0.035
S5, C3, URM		0.002	0.005	0.012	0.028
Mid-Rise Buildings[1]					
All	Mid-Rise Building Types	2/3 * LR	2/3 * LR	2/3 * LR	2/3 * LR
High-Rise Buildings[1]					
All	High-Rise Building Types	1/2 * LR	1/2 * LR	1/2 * LR	1/2 * LR

1. Mid-rise and high-rise buildings have damage-state drift values based on low-rise (LR) drift criteria reduced by factors of 2/3 and 1/2, respectively, to account for higher-mode effects and differences between average inter-story drift and individual inter-story drift.

As the final step in the development of **Damage-State Medians** for the structural system, average inter-story drift values for each damage state are converted to the corresponding amount of spectral displacement using the modal factor, a_2, and other terms:

$$S_{d,ds} = \Delta_{ds} * H_R * a_2 \qquad (11)$$

Where:

$S_{d,ds}$ = Median spectral displacement value of damage state, ds (inches)

Δds = Average inter-story drift ratio at the threshold of damage state, ds, determined by user (consistent with generic values of Table 7)

HR = Height of building at the roof level (inches)

a2 = Pushover modal factor from Equation (2).

1.4.2.2 Nonstructural Components

In most applications, **Damage-State Medians** for nonstructural components may be based directly on the default values of *HAZUS*. Exceptions include buildings with nonstructural components or contents that are either significantly more rugged or significantly more vulnerable than the normal make-up of components of nonstructural systems in a typical commercial building. Examples of buildings with particularly vulnerable systems include certain manufacturing facilities (e.g., buildings with clean rooms), laboratories, computer facilities, historical buildings (architectural components), art museums and other buildings with special contents. Examples of buildings with particularly rugged systems include certain military, industrial or emergency facilities whose nonstructural systems and contents have been specially anchored or braced to resist earthquake shaking.

HAZUS default values for the drift ratio of the threshold of each damage state are summarized in Table 9 for drift-sensitive nonstructural components. These damage-state drift ratios are assumed to be the same for all building types and seismic design levels. The same values of drift ratio are also assumed to be appropriate for special buildings, such as emergency facilities, since drift-sensitive components (partitions) typically do not receive special design or detailing to accommodate building displacement.

HAZUS default values of peak floor acceleration defining the threshold of each damage state are summarized in Table 9 for acceleration-sensitive nonstructural components (and contents). These damage-state accelerations are assumed to be the same for all building types, but to vary by seismic design level. Similarly, emergency or other facilities that have special anchorage and bracing requirements for nonstructural components and equipment (Special High-Code design level) have damage-state accelerations increased by a factor of 1.5.

Table 9: HAZUS Damage-State Criteria for Nonstructural Systems and Contents

Design Level	Nonstructural Damage States – All Building Types			
	Slight	Moderate	Extensive	Complete
Inter-Story Drift Ratio (Δ_{ds}) - Drift-Sensitive Components				
All	0.004	0.008	0.025	0.050
Peak Floor Acceleration ($A_{max,ds}$) - Acceleration-Sensitive Components/Contents (g's)				
Special High-Code	0.45	0.9	1.8	3.6
High-Code	0.30	0.6	1.2	2.4
Moderate-Code	0.25	0.5	1.0	2.0
Low-Code	0.20	0.4	0.8	1.6
Pre-Code	0.20	0.4	0.8	1.6

Considering the importance to the estimates of certain types of loss, in particular estimates of direct economic loss, it would seem desirable to develop building-specific damage-state parameters for nonstructural components and contents, rather than rely on generic building data. However, rigorous development of nonstructural parameters would require detailed evaluation of component capacity, similar to that used to evaluate the structural system, only much more difficult to perform due to the complexity and variety of different nonstructural systems and components. Nonstructural systems and contents would need to be thoroughly inspected (detailed field survey). Capacity of anchorage and bracing would need to be evaluated (possibly requiring dynamic analysis of complex systems such as piping runs). Fragility values would then need to be developed based on the results of the analysis, available test data (e.g., of similar equipment), and/or experience data. This process is not practical for most applications and would likely be limited to a "walk-down" of nonstructural systems and building contents.

If the user has access to the building and is concerned that nonstructural components and/or contents are not "typical," then it is recommended that a building "walk-down" be performed using checklists and other guidance provided by *FEMA 74* [FEMA, 1994] or *FEMA 310* [FEMA, 1998]. These documents do not estimate damage or loss but are useful in spotting potential deficiencies in typical nonstructural systems. The user need not perform calculations, but may rely on judgement to estimate the approximate drift ratio (for drift-sensitive components) or peak floor acceleration (for acceleration-sensitive components) at which different nonstructural components would begin to fail and require repair or replacement.

Damage-State Medians for drift-sensitive nonstructural components must be converted from drift ratio to spectral displacement in a manner similar to that used for the structural system. Inter-story drift ratios for each damage state are converted to the corresponding amount of spectral displacement using the modal factor, a_2, and other terms:

$$\mathbf{S_{d,\,ds} = F_{fP,ds} * \Delta_{ds} * H_R * a_2} \qquad (12)$$

Where:

$\mathbf{S_{d,\,ds}}$ Median spectral displacement value of damage state, ds (inches)

$\mathbf{F_{fP,\,ds}}$ Factor relating average inter-story drift to the drift ratio of the component at damage state, ds, as defined by Equation (13)

$\mathbf{\Delta_{ds}}$ Component drift ratio corresponding to threshold of damage state, ds, determined by user (consistent with the generic values of Table 8)

$\mathbf{H_R}$ Height of building at the roof level (inches)

$\mathbf{a_2}$ Pushover modal factor from Equation (2).

The factor, $\mathbf{F_{fP,ds}}$, is used to relate average inter-story drift to maximum inter-story drift to account for the effects of an uneven distribution of drift over the height of the building. Uneven distribution of drift causes damage to occur at certain stories sooner than at other stories. The factor, $\mathbf{F_{fP,ds}}$, is based on both the shape of the pushover mode and damage-state loss ratio:

$$\mathbf{F_{fp,ds} = [\Phi_{R,P} * (1 - NSP) / (H_R * \Delta_{max})] - NSD_{ds}} \quad (13)$$

Where:

$\mathbf{\varphi_{R,P}}$ Roof displacement of the pushover mode for damage state, ds (inches)

$\mathbf{NSD_{ds}}$ Nonstructural drift-sensitive component loss ratio of damage state, ds

(expressed as a fraction)

$\mathbf{H_R}$ Height of building at the roof level (inches)

$\Delta_{max,P}$ Maximum inter-story drift ratio (considering torsion) over the height of the building corresponding to the roof displacement, $\varphi_{R,P}$.

The factor, $F_{fP,ds}$, makes use of the results of the pushover analysis to better predict localized damage and loss for buildings that have a structural irregularity (e.g., soft story). When drift is uniformly distributed over building height, the value of the factor is equal 1.0. When drift is not uniformly distributed over building height, the factor reduces median values to reflect the lower thresholds of damage associated with accentuated drift of critical stories. The factor varies with the loss ratio of the damage state, effectively reducing the influence of localized damage on the more extensive states of damage (i.e., factor is 1.0 for Complete Damage).

Damage-State Medians for nonstructural acceleration-sensitive components (and contents) are developed in terms of peak floor acceleration. In general, medians expressed in terms of spectral acceleration are taken as equal to peak floor acceleration values since spectral acceleration (obtained by the intersection of pushover curve and spectral demand) is assumed to represent peak floor acceleration of a typical upper floor of the building. Demand on components (and contents) at ground level is based directly on peak ground acceleration and is also assumed to represent peak (ground) floor acceleration.

The trivial equation summarizing conversion peak floor acceleration of each damage state to the corresponding amount of spectral acceleration is:

$$\mathbf{S_{a,\,ds}} = \mathbf{A_{max,ds}} \qquad (14)$$

Where:

$S_{a,ds}$ Median spectral acceleration value of damage state, ds (units of g)

$A_{max,ds}$ Peak floor acceleration of the threshold of damage state, ds (units of g) determined by user or based on generic values of Table 8.

The assumption that peak floor acceleration is the same as spectral acceleration demand ignores higher-mode shaking effects (not included in the pushover analysis) and the uneven distribution of floor acceleration over building height. Higher-mode effects can significantly increase upperfloor accelerations, although they may not cause failure of systems that have some ductility. Users concerned about higher-mode response could reduce median values by a factor inversely proportional to the increase in (damaging) floor acceleration associated with higher-mode response.

Peak floor acceleration will vary over the height of the building, typically with the largest accelerations at the roof. The intersection of the pushover and demand spectrum corresponds to building response at a floor elevation of about α_2 x H_R. Users concerned that this location is not representative of a typical upper floor of nonstructural acceleration-sensitive components (e.g., all the equipment is on the roof) could modify median values based on the location of the components and the shape of the pushover mode. Such modification would have little effect on the prediction of damage for most buildings with well distributed nonstructural systems.

1.4.3 Development of Damage-State Variability

Lognormal standard deviation (**Beta**) values describe the total variability of fragility-curve damage states. Three primary sources contribute to the total variability of any given state, namely, the variability associated with the capacity curve, β_C, the variability associated with the demand spectrum, β_D, and the variability associated with the discrete threshold of each damage state, $\beta_{T,\,ds}$, as described in Equation (15):

$$\beta_{ds} = \sqrt{(\mathrm{CONV}[\beta_C, \beta_D])^2 + (\beta_{T,ds})^2} \qquad (15)$$

Where:

βds is the lognormal standard deviation parameter that describes the total variability of damage state, ds,

βC is the lognormal standard deviation parameter that describes the variability of the capacity curve,

βD is the lognormal standard deviation parameter that describes the variability of the demand spectrum (values of **βD** = 0.45 at short periods and **βD** = 0.50 at long periods were used to develop Tables 10 – 12),

βT,ds is the lognormal standard deviation parameter that describes the variability of the threshold of damage state, ds.

Since the demand spectrum is dependent on building capacity, a convolution process is required to combine their respective contributions to total variability. This is referred to as "CONV" in Equation (15). The third contributor to total variability, βT,ds, is assumed mutually independent of the first two variables and is combined with the results of the CONV process using the squareroot- sum-of-the squares (SRSS) method. Additional background on the calculation of **Damage- State Beta's** is provided in the *HAZUS-MH Technical Manual* and the *Earthquake Spectra* paper "Development of Building Damage Functions for Earthquake loss Estimation" [Kircher et al., 1997a].

The variability of the demand spectrum (i.e., variability of ground shaking) is a key parameter in the calculation of damage-state variability. The values of demand variability, β_D = 0.45 at short periods and β_D = 0.50 at long periods, are the same as those used to calculate the default fragility curves of the *HAZUS-MH Technical Manual*. These values are consistent with the variability (e.g., dispersion factor) of ground shaking attenuation functions used by *HAZUS* to predict response spectra for large-magnitude events in the Western United States (WUS). It may be noted that if there were no variability of demand (response spectrum is known exactly), then Equation (15) would become:

$$\beta_{ds} = \sqrt{(\beta_C)^2 + (\beta_{T,ds})^2} \qquad (16)$$

This equation provides a lower-bound on the damage-state variability appropriate for use in probabilistic calculations of damage and loss that are based on the integration of the fragility with hazard functions that have already incorporated ground shaking variability in the hazard calculations. Similarly, Equation (16) also provides a lower-bound on damage-state variability for calculation of damage and loss using a response spectrum that is reasonably well known (i.e., response spectrum of recorded ground shaking). Arguably, there would always be some amount variability (uncertainty) in ground shaking demand, β_D, but such can be ignored in the calculation of total damage-state variability, β_{ds}, when substantially less than both capacity curve variability, β_C, and damage-state threshold variability, $\beta_{T,ds}$.

The convolution process involves a complex numerical calculation that would be very difficult for most users to perform. To avoid this difficulty, sets of pre-calculated values of **Damage- State Beta's** have been compiled in Tables 10 through 12 from which users may select appropriate values of variability for the structural system, nonstructural drift-sensitive components and nonstructural acceleration-sensitive components. The Beta values of these tables are a function of the following building characteristics and criteria:

- Building Height Group - Low-Rise Buildings (Table 10), Mid-Rise Buildings (Table 11) and High-Rise Buildings (Table 12)
- Post-Yield Degradation of the Structural System – Minor, Major and Extreme Degradation
- Damage-State Threshold Variability – Small, Moderate or Large Variability
- Capacity Curve Variability – Very Small, Small, Moderate or Large Variability.

The Beta values of the tables are applicable to all model building types. For example, a low-rise concrete-frame building (C1L) would have the same set of Beta’s as a low-rise braced steel frame building (S2L), provided the two buildings have the same amount of capacity curve and damage-state threshold variability, and the same amount of post-yield degradation of the structural system.

Post-yield degradation of the structural system is defined by a Kappa factor, which is a direct measure of the effects of seismic design level and construction quality on the variability of response. Buildings that are seismically designed and/or have superior construction are less likely to degrade during post-yield earthquake shaking, and therefore have more predictable response, than buildings that are not seismically designed and/or have inferior construction.

To select a set of building-specific **Damage-State Beta’s** (i.e., a structural Beta, a nonstructural drift-sensitive Beta and a nonstructural acceleration-sensitive Beta), users must first determine the building height group that best represents the specific building of interest. The height groups are defined by the same criteria as those used by *HAZUS* to define generic building types. For example, a 5-story, reinforced concrete building would be classified as a mid-rise building as per the height criteria of Table 1.

Tables 10 through 12 (referred to as the Beta tables) provide recommended sets of **Damage-State Beta’s** for each of the three building height groups, respectively. In each of these tables, the Beta’s are based on 36 possible combinations of capacity curve variability, damage threshold variability and the amount of post-yield degradation expected for the structural system.

Estimation of structural system degradation (minimum or maximum) is made on the basis of **Kappa** factors suggested by Table 5 and the degree of post-yield response expected for the damage state of interest. **Kappa** factors decrease with increase in response level (and damage). Slight damage corresponds to response between ½ yield and full yield; Moderate damage to response at or just beyond yield; and Extensive and Complete damage correspond to post-yield response for the duration of scenario earthquake shaking. Beta values are given in Tables 10 through 12 for $k > 0.9$ (minor degradation), $k = 0.5$ (major degradation) and $k < 0.1$ (extreme degradation) of the structural system; and linear interpolation may used to establish Beta's for other values of the **Kappa** factor.

Estimation of the variability of the capacity curve (β_C) and the variability of the threshold of the damage state ($\beta_{T,ds}$) must be made by users on a judgmental basis (with some guidance provided herein). To assist the user, the Beta tables express capacity curve and damage threshold variability qualitatively (e.g., Small Variability) and in term of the numerical value used to develop the Beta's in the CONV process. Numerical values of variability (β_C and $\beta_{T,ds}$) are lognormal standard deviation parameters and may be used, as illustrated in Figure 14, to construct the distribution of capacity or damage threshold that they represent.

The variability of capacity curves and the damage-state thresholds are influenced by:

- Uncertainty in capacity curve properties and the thresholds of damage states, and
- Building population (i.e., individual building or group of buildings).

Relatively low variability of damage states would be expected for an individual building with well known properties (e.g., complete set of as-built drawings, material test data, etc.) and whose performance and failure modes are known with confidence. The taller the building the greater the variability in damage state due to uncertainty in the prediction of response and damage using pushover analysis. Relatively high variability of damage states would be expected for a group of buildings whose properties are not well known and for which the user has low confidence in the results (of pushover analysis) that represent performance and failure modes of all buildings of the group. The latter case essentially describes the original development of damage-state fragility curves for generic model building that were based on capacity variability, $\beta_C = 0.3$, and damagestate threshold variability, $\beta_{T,ds} = 0.3$ (Structure), $\beta_{T,ds} = 0.5$ (NSD) and $\beta_{T,ds} = 0.6$ (NSA). The generic model building types represent large populations of buildings for which properties are not well known.

Table 10: Low-Rise Building Fragility Beta's

Building System[2]	Post-Yield Degradation of Structural System[3]								
	Minor Degradation (κ >= 0.9)			Major Degradation (κ = 0.5)			Extreme Degradation (κ <= 0.1)		
	Damage Variability[4] ($\beta_{T,ds}$)			Damage Variability[4] ($\beta_{T,ds}$)			Damage Variability[4] ($\beta_{T,ds}$)		
	Small (0.2)	Mod. (0.4)	Large (0.6)	Small (0.2)	Mod. (0.4)	Large (0.6)	Small (0.2)	Mod. (0.4)	Large (0.6)
Structural Systems with Very Small Capacity Curve Variability[5] (β_C = 0.1)									
Structure	0.70	0.80	0.90	0.85	0.90	1.00	0.95	1.00	1.10
NSD	0.65	0.75	0.90	0.85	0.90	1.00	0.95	1.00	1.10
NSA	0.35	0.50	0.65	0.35	0.50	0.65	0.35	0.50	0.65
Structural Systems with Small Capacity Curve Variability[5] (β_C = 0.2)									
Structure	0.70	0.80	0.90	0.85	0.90	1.00	0.95	1.05	1.15
NSD	0.70	0.75	0.90	0.85	0.90	1.00	0.95	1.00	1.10
NSA	0.35	0.50	0.65	0.35	0.50	0.65	0.35	0.50	0.65
Structural Systems with Moderate Capacity Curve Variability[5] (β_C = 0.3)									
Structure	0.75	0.80	0.95	0.85	0.95	1.05	1.00	1.05	1.15
NSD	0.70	0.80	0.90	0.85	0.95	1.05	1.00	1.05	1.15
NSA	0.35	0.50	0.65	0.35	0.50	0.65	0.35	0.50	0.65
Structural Systems with Large Capacity Curve Variability[5] (β_C = 0.4)									
Structure	0.80	0.85	0.95	0.90	1.00	1.10	1.05	1.10	1.20
NSD	0.75	0.85	0.95	0.90	1.00	1.05	1.00	1.05	1.15
NSA	0.35	0.50	0.65	0.35	0.50	0.65	0.35	0.50	0.65

1. Building Systems include the Structure, Nonstructural Drift-Sensitive Components (NSD) and Nonstructural Acceleration-Sensitive (NSA) components.

Table 11: Mid-Rise Building Fragility Beta's

Building System[2]	Post-Yield Degradation of Structural System[3]								
	Minor Degradation ($\kappa >= 0.9$)			Major Degradation ($\kappa = 0.5$)			Extreme Degradation ($\kappa <= 0.1$)		
	Damage Variability[4] ($\beta_{T,ds}$)			Damage Variability[4] ($\beta_{T,ds}$)			Damage Variability[4] ($\beta_{T,ds}$)		
	Small (0.2)	Mod. (0.4)	Large (0.6)	Small (0.2)	Mod. (0.4)	Large (0.6)	Small (0.2)	Mod. (0.4)	Large (0.6)
Structural Systems with Very Small Capacity Curve Variability[5] ($\beta_C = 0.1$)									
Structure	0.60	0.70	0.80	0.70	0.80	0.90	0.85	0.95	1.05
NSD	0.60	0.70	0.80	0.80	0.85	0.95	0.90	1.00	1.10
NSA	0.35	0.50	0.65	0.35	0.50	0.65	0.35	0.50	0.65
Structural Systems with Small Capacity Curve Variability[5] ($\beta_C = 0.2$)									
Structure	0.65	0.75	0.85	0.75	0.85	0.95	0.95	1.00	1.10
NSD	0.65	0.70	0.85	0.80	0.85	1.00	0.95	1.00	1.10
NSA	0.35	0.50	0.65	0.35	0.50	0.65	0.35	0.50	0.65
Structural Systems with Moderate Capacity Curve Variability[5] ($\beta_C = 0.3$)									
Structure	0.65	0.75	0.85	0.80	0.85	0.95	0.95	1.00	1.10
NSD	0.65	0.75	0.85	0.80	0.90	1.00	0.95	1.05	1.15
NSA	0.35	0.50	0.65	0.35	0.50	0.65	0.35	0.50	0.65
Structural Systems with Large Capacity Curve Variability[5] ($\beta_C = 0.4$)									
Structure	0.70	0.75	0.90	0.80	0.90	1.00	1.00	1.05	1.15
NSD	0.70	0.75	0.90	0.85	0.90	1.00	1.00	1.05	1.15
NSA	0.35	0.50	0.65	0.35	0.50	0.65	0.35	0.50	0.65

1. Building Systems include the Structure, Nonstructural Drift-Sensitive Components (NSD) and Nonstructural Acceleration-Sensitive (NSA) components.

Table 12: High-Rise Building Fragility Beta's

Building System[2]	Post-Yield Degradation of Structural System[3]								
	Minor Degradation (κ >= 0.9)			Major Degradation (κ = 0.5)			Extreme Degradation (κ <= 0.1)		
	Damage Variability[4] ($\beta_{T,ds}$)			Damage Variability[4] ($\beta_{T,ds}$)			Damage Variability[4] ($\beta_{T,ds}$)		
	Small (0.2)	Mod. (0.4)	Large (0.6)	Small (0.2)	Mod. (0.4)	Large (0.6)	Small (0.2)	Mod. (0.4)	Large (0.6)
Structural Systems with Very Small Capacity Curve Variability[5] (β_C = 0.1)									
Structure	0.55	0.65	0.80	0.65	0.75	0.85	0.80	0.90	1.00
NSD	0.55	0.65	0.80	0.75	0.80	0.95	0.90	0.95	1.05
NSA	0.35	0.50	0.65	0.35	0.50	0.65	0.35	0.50	0.65
Structural Systems with Small Capacity Curve Variability[5] (β_C = 0.2)									
Structure	0.60	0.65	0.80	0.70	0.80	0.90	0.90	0.95	1.05
NSD	0.60	0.70	0.80	0.75	0.85	0.95	0.95	1.00	1.10
NSA	0.35	0.50	0.65	0.35	0.50	0.65	0.35	0.50	0.65
Structural Systems with Moderate Capacity Curve Variability[5] (β_C = 0.3)									
Structure	0.60	0.70	0.80	0.70	0.80	0.90	0.95	1.00	1.10
NSD	0.60	0.70	0.85	0.80	0.85	0.95	0.95	1.05	1.15
NSA	0.35	0.50	0.65	0.35	0.50	0.65	0.35	0.50	0.65
Structural Systems with Large Capacity Curve Variability[5] (β_C = 0.4)									
Structure	0.60	0.70	0.85	0.75	0.80	0.95	0.95	1.00	1.10
NSD	0.60	0.70	0.85	0.80	0.90	1.00	1.00	1.05	1.15
NSA	0.35	0.50	0.65	0.35	0.50	0.65	0.35	0.50	0.65

1. Building Systems include the Structure, Nonstructural Drift-Sensitive Components (NSD) and Nonstructural Acceleration-Sensitive (NSA) components.

2 Features of Territorial Movement in Near Field Seismic Stimulation

2.1 Introduction

The ground motions near a fault can be significantly different from those who are away from the seismic source. Theoretically, the near-field zone faults defined approximately 20 - 60km of a fault. Within this zone, the ground motions are significantly affected by the rupture mechanism, the propagation direction of rupture in relation to the area and possible permanent ground displacements as a result of the fault slip. These factors lead to results which are called as rupture directivity and fling step.

2.1.1 The effect of directionality

The forward directivity is the phenomenon in which the propagation of rupture and direction of the fault slip are in the same area. This is because the velocity of rupture in the fault is nearly identical to the shear wave velocity of the rock near the source. As illustrated in Figure 17 for horizontally sliding mechanism wherein the front burst propagates away from the hypocenter and to a region, the energy accumulated near the front burst of each successive zone of sliding along the fault. The front of the wave reaches as a large pulse of motion characterized by a large range between long periods and short duration.

In the case of the propagation of rupture is opposite to the studied area, the arrival of each pulse at individual seismic rupture occurs at the end of the previous. This phenomenon is called backward directivity and is characterized by movements with relatively long duration and small range. The neutral directivity occurs when the rupture is neither toward and neither away from the area.

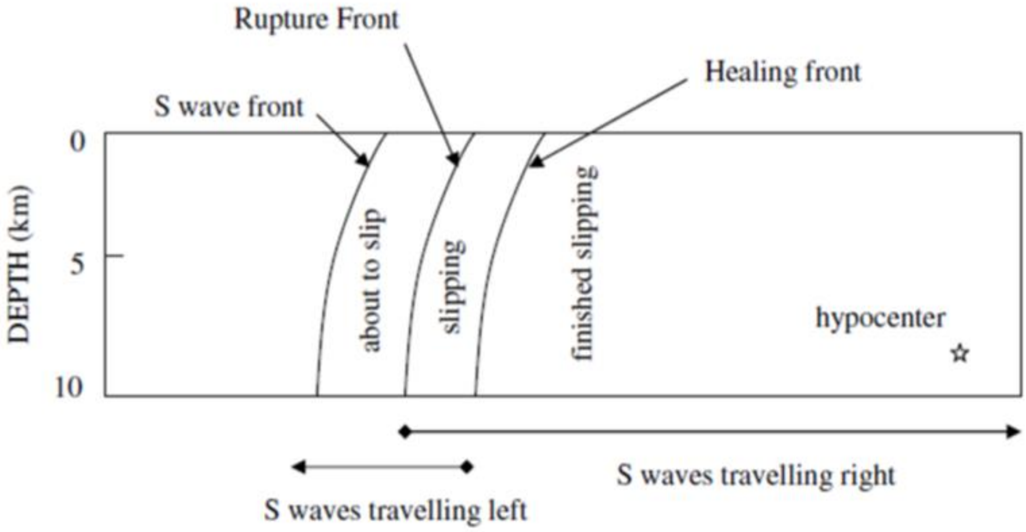

Figure 17: Schematic effects of rupture directivity on horizontal slip fault. Rupture begins from the hypocenter and propagates with a speed approximately equal to 80% of the speed of shear waves. Figure shows a snapshot of the front rupture at a given time (Somerville et al 1997a)

An example of soil displacements that are affected from directivity are the displacements that recorded during the Loma Prieta earthquake in 1989 and presented in Figure 18. At the epicenter of the earthquake the horizontal soil movements are moderate in both perpendicular and parallel to the fault component which is attributed to the backward directivity. At the ends of the fault the forward directivity causes the horizontal ground motions in the vertical direction of the fault to be pulsed and much larger than the movements of the parallel components of the fault, which are similar to those near the epicenter. Large pulsations movements appear only perpendicular to the fault component (fault normal) and only away from the epicenter.

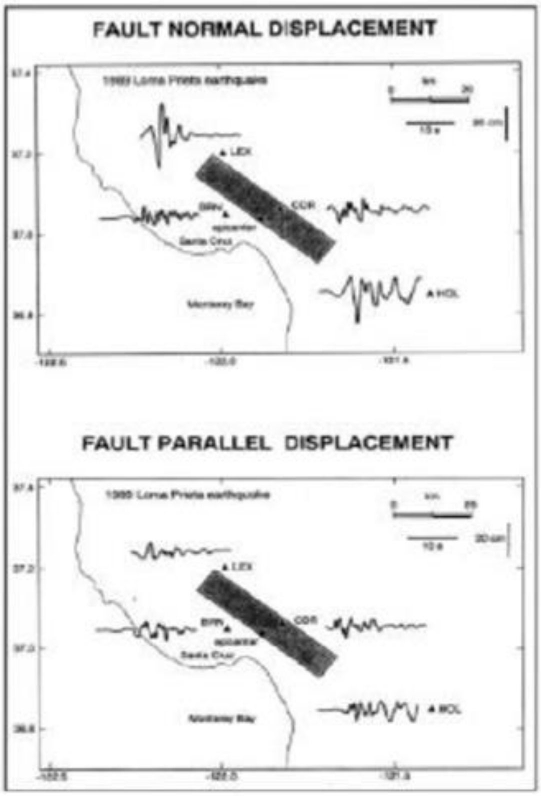

Figure 18: Results of rupture directivity of the recorded time-histories movements of earthquake Loma Prieta 1989 for the verticals (up) and the parallels (down) on the fault components. (EERI, 1995)

In modern digital recordings of near -field ground motions observed permanent ground movements. These static displacements are called fling step and is the result of the total slip of the fault. These movements appear parallel to sliding direction and not directly related to the aforementioned dynamic movements called pulse directivity of rupture. At horizontal slip faults the directivity pulse appears on the vertical component and the remaining movement in parallel. At vertical immersion fault the remaining movement and the pulse directivity appear in the vertical component. The orientations of the remaining movement and pulse directivity for faults horizontal slip and vertical immersion presented in Figure 19, and the time-histories in which they appear together and individually are presented in Figure 20.

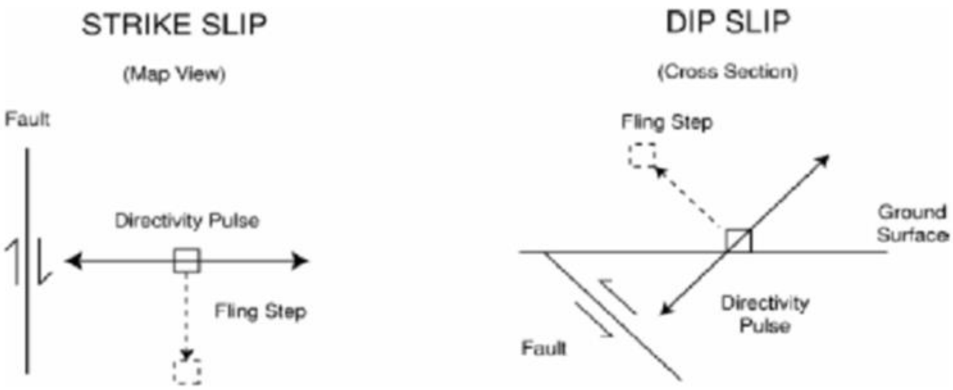

Figure 19: Schematic orientation of the rupture directivity pulse and fault displacement ("fling step") for strike-slip (left) and dip-slip (right) faulting

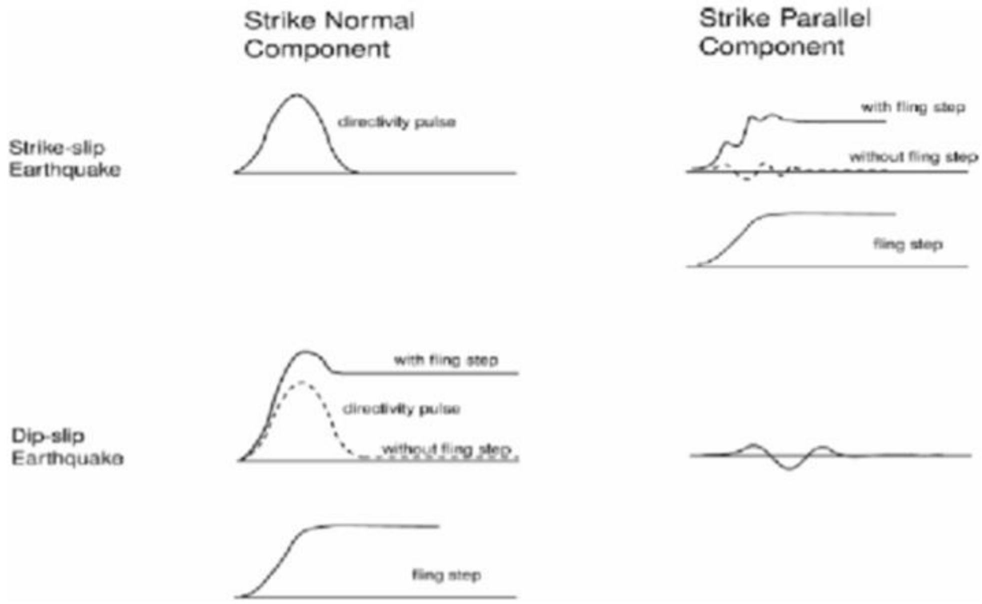

Figure 20: Schematic diagram of the time-histories for the horizontal slip fault and the vertical immersion fault which the fling step and directivity pulse show together and separate.

2.1.2 Customization of near-field ground motions

The Somerville et al (1997a) studied the conditions leading to the forward and backward directivity. The recordings are affected by the phenomenon of forward directivity show enhancement of spectral values to the area in the medium and long periods, with this increase to be more pronounced the larger the portion of the crack internal elapsed between the outbreak and the recording site. As shown in Figure 1.5, the difference in the effect of directivity depends on two factors, the angle between the direction of propagation of the rupture and the direction of the waves traveling from the fault in the area (θ for the horizontal slip fault and φ for vertical immersion fault), and from the part of the surface rupture of the fault lying between the hypocenter and the test region (X for horizontal slip fault and Y for vertical immersion fault).

To take into account the results of the directivity Somerville et al (1997a) correlated the converted to an average range of values of response spectra (5% damping) with the geometrical parameters defined in Figure 21. The results are shown in Figure 22. The ground motion parameters that modified are the average horizontal response spectra and the ratio of response spectra for the perpendicular and parallel to the fault component.

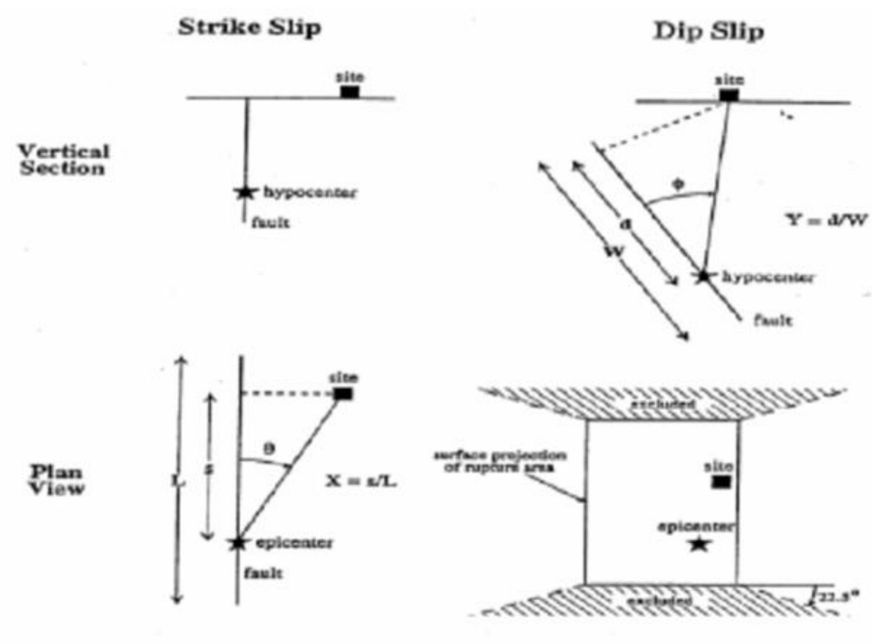

Figure 21: The parameters used to interpret rupture directivity conditions (Somerville et al 1997a)

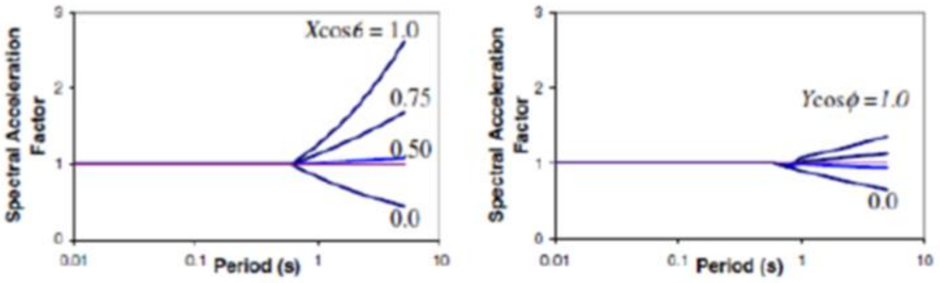

Average rate of spectral response with dependence on parameters of the period and direction

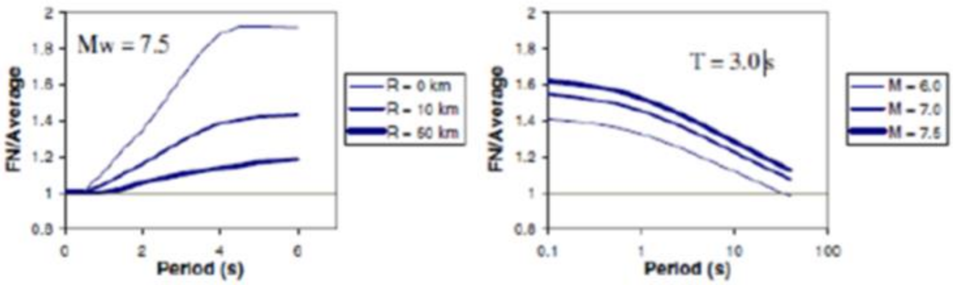

Ratio of horizontal spectral response vertical to the rupture to the mean horizontal for conditions of forward directivity (Xcosθ=1).

Figure 22: Predictions from the relation of Somerville et al (1997a) between different conditions directivity

Research on the response of structures to earthquakes near-field showed that a representative time history of movements is preferred by a representation of a response spectrum (eg Somerville (1998), Alavi and Kranwinkler (2000), Sasani and Bertero (2000), Rodriguez-Marek (2000)). This is because the ground motions affected by the phenomena of directivity and remaining movement, the energy is concentrated in one or more pulses by a simple form in the time history velocity.

Studies of Kranwinkler and Alavi (1998) and Sasani and Bertero (2000) have shown that simplified visa pulse speed can "capture" the salient features of response of structures subjected to near-field ground motions. Some simplified pulses are shown in Figure 23.

Table 13 provides definitions of parameters near-field ground motions, which are illustrated in Figure 24. A simple characterization is possible using the maximum horizontal speed

(PHV), the approximate period of the dominant pulse (Tv) and the number of significant semi-pulses of motion in the vertical direction at greater fault.

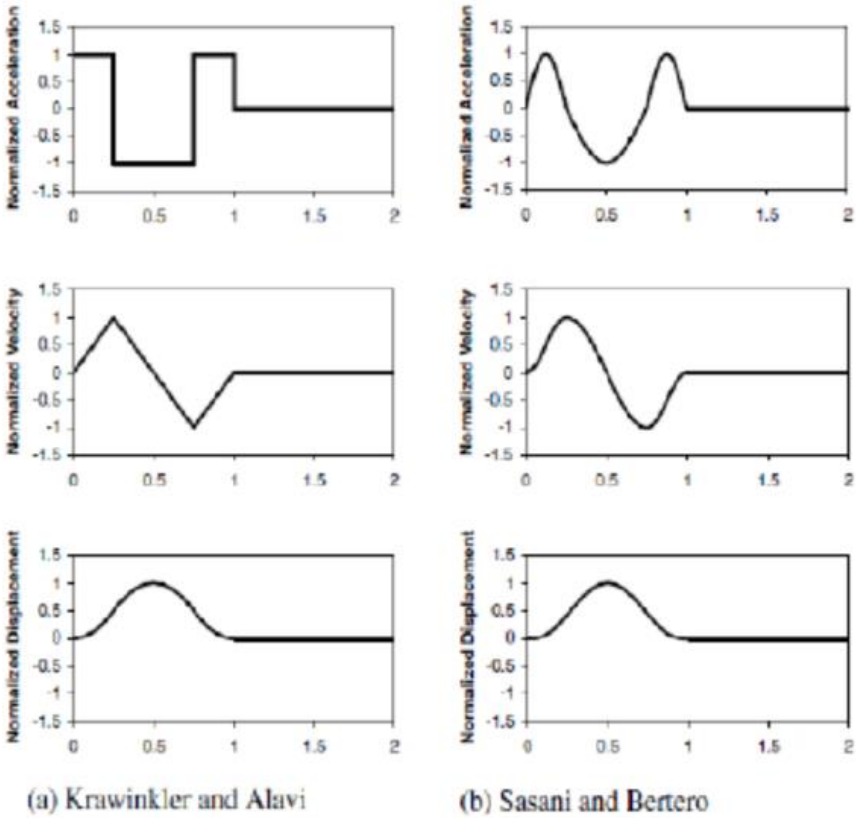

Figure 23: Simplified pulses have been used by researchers

The determination of the pulse period using either the time needed to pass the values of the zero axis (zero crossing time) or the time at which the velocity equals 10 % of the maximum speed for this pulse. Certainly there is a degree of uncertainty in estimates of Tv, but the uncertainty associated with predicting of Tv from seismological variables is much larger than the errors in the calculation of the nulls. Kranwinkler and Alavi (1998) define the pulse speed of a clear and comprehensive top peak in the spectrum response speed of ground motion. Therefore, this estimate of the equivalent pulse period (Tv-p) is relatively clear. For single-pulse movements these different definitions of pulse period provide roughly equivalent results. Overall, the ratio between the Tv and Tv-p is 0.84 with a standard deviation of 0.28 (Rodriguez-Marek 2000). The coincidence of a Tv for earthquake ground motion shows that the speed pulse contains energy in a particular zone periods.

Table 13: Factors used to determine the simplified ground motion of sine pulse (Rodriguez-Marek 2000)

Parameter	Abbreviation	Methodology to obtain parameter
Number of significant pulses.	N	Number of half-cycle pulses in the velocity-time history with amplitudes at least 50% of the peak ground velocity of the record.
Pulse period.	$T_{v,i}$	For each half sine pulse, $T_{v,i} = 2\ (t_2 - t_1)$, where t_1 and t_2 are either the zero-crossing time, or the time at which velocity is equal to 10% of the peak velocity for the pulse if this time is significantly different than the zero crossing time. T_v corresponding to the pulse with maximum amplitude is the overall representative velocity pulse period.
Predominant period from pseudo-velocity response spectra.	$T_{p\text{-}v}$	Period corresponding to a clear and global peak in the pseudo-velocity response spectra at 5% damping.
Pulse amplitude.	A_i	For each half sine pulse, the peak ground velocity in the time interval $[t_1, t_2]$.
Peak ground velocity	PHV	Maximum velocity, defined by the maximum value of A_i. Note, however, that in very few exceptions, the maximum value of A_i in the fault parallel direction does not occur concurrently with the fault normal pulse.
Ratio of fault parallel to fault normal amplitude	$PHV_{P/N}$	Defined by the ratio of maximum A_P divided by maximum A_N, where the subscripts P and N denote fault-parallel and fault-normal motions respectively.
Time delay between fault normal and fault parallel pulse	t_{off}	Time of initiation of fault parallel pulse minus the time of initiation of fault normal pulse.

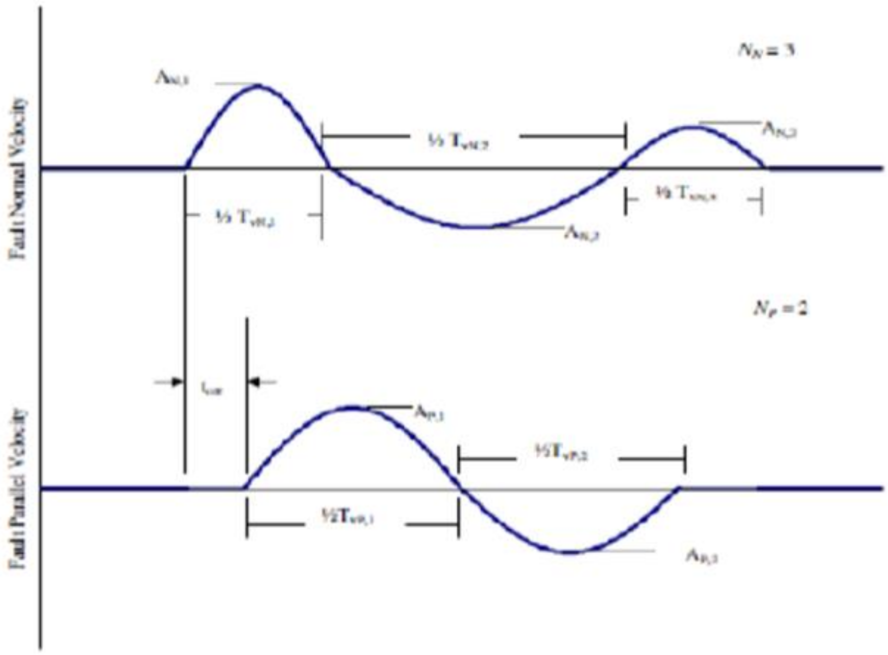

Figure 24: Factors that needed to establish the parallel and perpendicular to the fault component for simplified velocity pulses. N, P correspond to the vertical and parallel motions relative to the direction of the fault respectively (Rodriguez-Marek 2000).

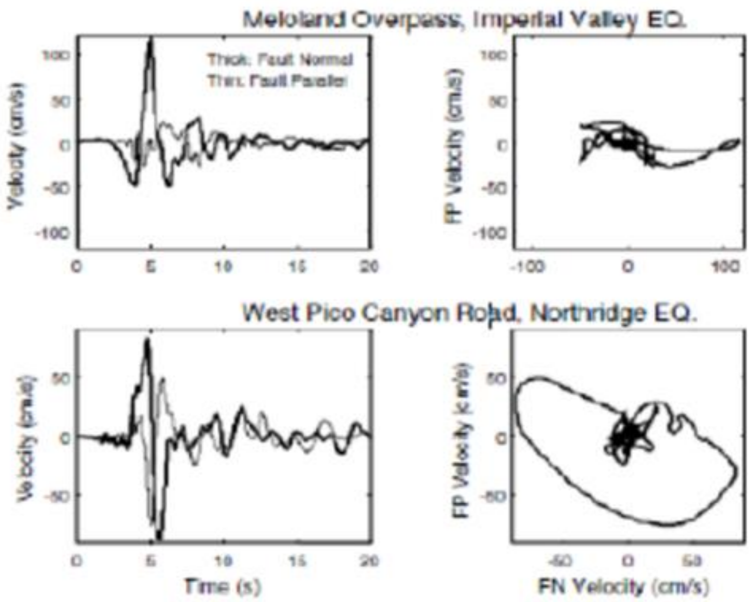

Figure 25: Velocity time-histories and horizontal orbital plans for vertical (FN) and parallel (FP) to the fault component for two near fault records. Both records show significant "vertical" velocities but Meloland has smaller "parallel" velocities.

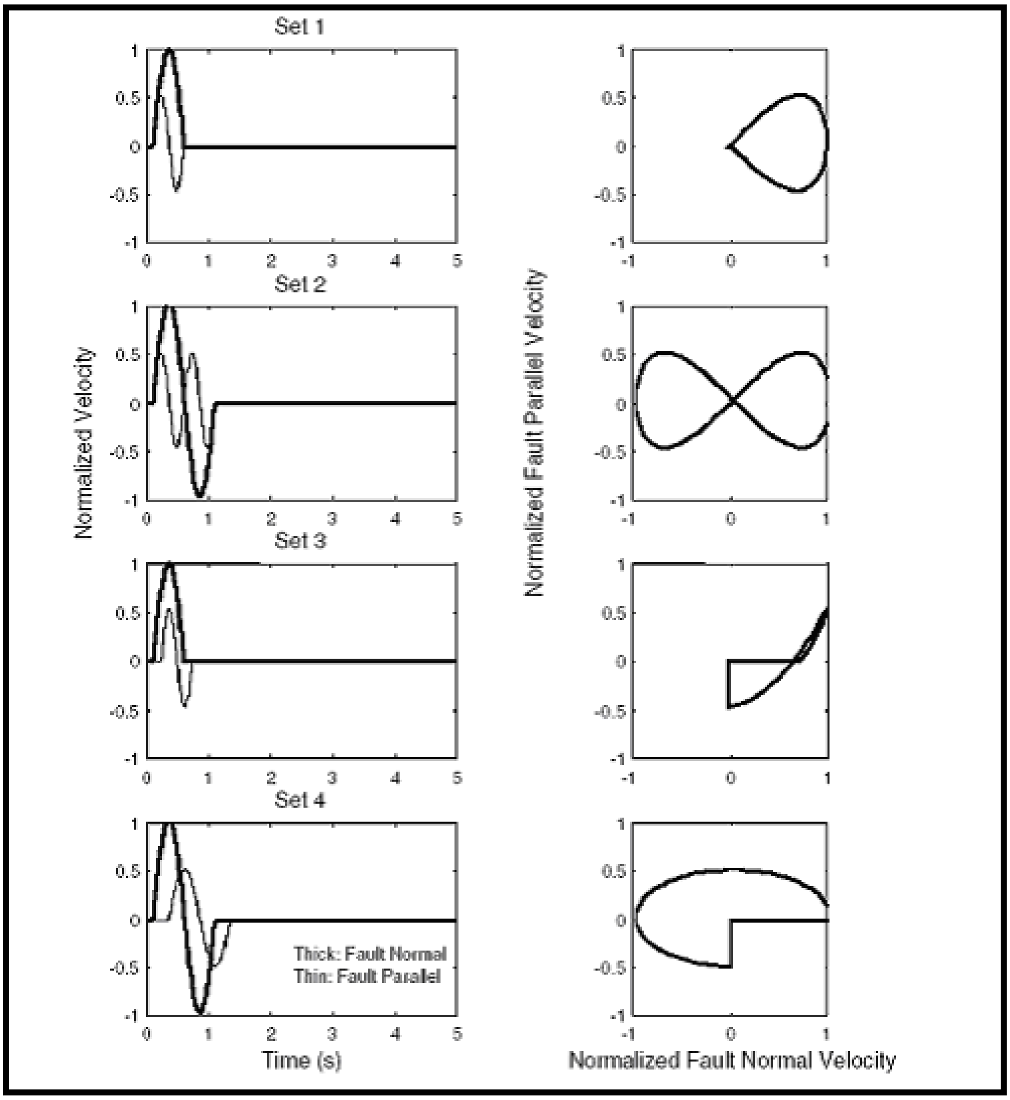

Figure 26: Simplified representation sine pulse for near field ground motions. PHV (Peak Horizontal Velocity) for parallel to the fault component corresponds to 50% of PHV vertical to the fault component (Rodriguez-Marek 2000).

The studies of the responce of structures in near-field movements have focused on the results of the largest vertical component of the fault (eg Alavi and Kranwinkler 2000). However , there are applications for which the parallel component of the fault may also be important. Nonlinear analyzes of soil response by Rodriguez - Marek (2000) show that local soil conditions can affect the values of PHV and Tv in both directions. Two near-field movements with significantly different movements of the parallel component of the fault shown in Figure 25. Additional research allows to distinguish the effects of vibration in two directions of response of soil and structures in near- fault zone where the two components of horizontal ground motion can vary significantly. By examining recorded near-field movements showing the forward directivity Rodriguez - Marek (2000), found that simplified movements presented in Figure 26 could be used to investigate the importance of vibration at two directions in future studies. If they are important to the behavior of the structures then the vertical movements of the near-field area can also be calculated.

2.2 Simulation models for near-field earthquakes

Spectral acceleration

The Somerville et al (1997a) and Abrahamson (2000) presented models for the modification of response spectra with damping $\zeta = 5$ % through damping relationship of Abrahamson and Silva (1997). The models were developed with regression variables of this damping relationship at geometrical parameters of the near-field of the fault (Figure 21). The models presented for the modification of the geometric mean of the two horizontal components and the ratio of vertical to horizontal average spectral component. The details of the models shown in the first two rows of Table 14.

Duration and equal number of similar cycles

The Somerville et al (1997a) presented a model for amending 5-75 % of considerable duration from the damping relationship Abrahamson and Silva (1996). The model was developed with regression variables of this damping relationship at geometrical parameters of the near-field of the fault (Figure 21). The model is valid for the duration of the geometric mean of both horizontal components. A similar model was developed by Liu (2001) for the equivalent number of similar cycles (N). The details of models duration and number (N) shown in the last two rows of Table 14.

Table 14: Ground motion parameter changes on the assessment of the effects of directivity. Parameters X,Y,θ,φ declared at Figure 21. Changes present at Figure 22.

Ground Motion Parameter (Reference)	Description	Equation	Range of Applicability
Spectral Acceleration: Ratio of data/model (Somerville et al., 1997a; Abrahamson, 2000)	y=Bias in average horizontal response spectral acceleration (ln units) with respect to Abrahamson and Silva (1997)	Strike-Slip faults: $y = c_1 + 1.88c_2 X\cos\theta$ $(X\cos\theta \leq 0.4)$ $y = c_1 + 0.75c_2$ $(X\cos\theta > 0.4)$ Dip-Slip faults: $y = c_1 + c_2 Y\cos\phi$	$m > 6.5$ For $m < 6.5$, replace y with $T_m \times y$ Where $T_m = 0$ for $m \leq 6$ and $T_m = 1 + (m-6.5)/0.5$ for $6.5 > m > 6$ $r < 30$ km For $r > 30$, replace y with $T_d \times y$ Where $T_d = 0$ for $r > 60$ and $T_d = 1-(r-30)/30$ for $60 > r > 30$ km
Spectral Acceleration: Ratio of Strike Normal/Average Amplitude (Somerville et al., 1997a)	Natural logarithm of the ratio of strike normal to average horizontal spectral acceleration	$y = \cos 2\xi\,[C_1 + C_2 \ln(r+1) + C_3(m-6)]$	$6.0 \leq m \leq 7.5$ $0 \leq r \leq 50$ km $\xi = \theta$ for strike-slip, ϕ for dip-slip. $0 < \xi < 90°$ C_1, C_2, C_3 function of period. Given separately for cases in which dependence on ξ is included, and cases in which dependence on ξ is ignored.
5-75% sig. duration: Ratio of data/model (Somerville et al., 1997a)	Bias in duration of acceleration with respect to Abrahamson and Silva (1996)	Strike-Slip faults: $y = C_1 + C_2 X\cos\theta$ Dip-Slip faults: $y = C_1 + C_2 Y\cos\phi$	$6.5 \leq m \leq 7.5$ $0 \leq r \leq 20$ km
Number of Cycles (N): Ratio of data/model (Liu et al., 2001)	Bias in N with respect to Liu et al. (2001)	Strike-Slip faults: $y = C_1 + C_2 X\cos\theta$ Dip-Slip faults: $y = C_1 + C_2 Y\cos\phi$	$6.5 \leq m \leq 7.5$ $0 \leq r \leq 20$ km

Maximum horizontal velocity (PHV)

The PHV is significantly influenced by the magnitude of the earthquake , the distance from the fault and the soil conditions of the examination area . The Somerville (1998) proposed the use of a bilinear relationship between the logarithm PHV, the magnitude and the logarithm of the distance. The Somerville (1998) performed a regression analysis using data from 15 recorded time-histories which have increased from 12 artificial time-histories. The records correspond to magnitudes m = 6.2-7 and distance r = 0-10km. To avoid unrealistic predictions of PHV at short distances, Somerville (1998) used a minimum distance of 3km. The relationship of Somerville (1998) for the PHV near the fault is:

$$\mathbf{ln(PHV)=-2.31+1.15m-0.5ln(r)} \tag{17}$$

where r is the minimum distance from the fault but is limited in at least 3km.

A similar study correlates the PHV, the magnitude and distance presented by Alavi and Kranwinkler (2000) based on the same set of data that used by Somerville (1998). The relationship of the PHV by Alavi and Kranwinkler (2000) are:

$$\mathbf{ln(PHV)=-5.11+1.59m-0.58ln(r)} \tag{18}$$

The Rodriguez-Marek (2000) were performed regression analyzes using 48- velocity time-histories of 11 events. The data were for areas with distances r <20km and m = 6.1-7.4. Separate analyzes were performed for the motions recorded on rock and soil. Based on the analysis of this records suggested the following relationship for PHV:

$$\mathbf{ln(PHV)= \alpha+b\ m +c\ ln(r2+d2)+\eta i+\varepsilon ij} \tag{19}$$

where the PHV is in units of cm / s, the a, b, c, d are parameters, r is the minimum distance from the fault, m is the magnitude and ηi and εij are the error terms.

The values of model parameters Rodriguez - Marek (2000) are presented in Table 15.

Data Set	a	b	c	d	σ	τ	σ_{total}
All Motions	2.44	0.50	-0.41	3.93	0.47	0.41	0.62
Rock	1.46	0.61	-0.38	3.93	0.53	0.25	0.59
Soil	3.86	0.30	-0.42	3.93	0.43	0.41	0.59

Table 15: Parameters of Rodriguez-Marek(2000)'s model for PHV

Figure 27 compares the relationship proposed by Rodriguez - Marek (2000) with the relations developed by Somerville (1998) and Alavi and Kranwinkler (2000). Relations particularly differ in effect of magnitude m . The differences are likely due to a larger amount of data contained in a recent study.

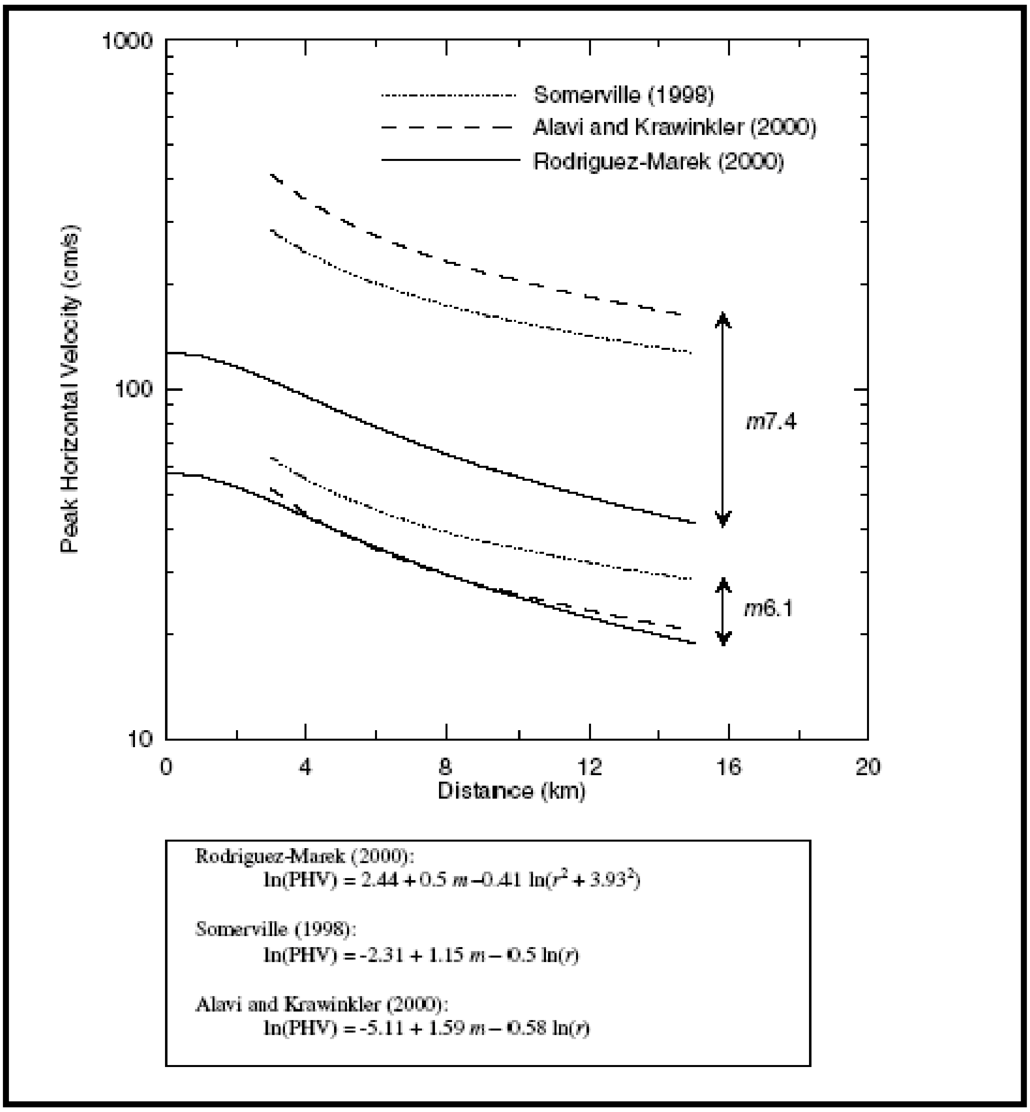

Figure 27: Compare of the results of analysis for assessing the PHV with relationships suggested by various researchers with data from databases earthquakes near-field and with the phenomenon of forward directivity (Rodriguez-Marek 2000)

Pulse Period

The relationship of Somerville (1998) for the pulse period is:

$$\mathbf{Log10Tv=-2.5+0.425m} \qquad (20)$$

where Tv is the period of greatest circle of speed and m is the size. In a larger study of slip distributions using slip models for 15 earthquakes by Somerville et al (1999) provide the following equation:

$$\mathbf{log10Tv=-3.0+0.5m} \qquad (21)$$

The period of the pulse speed associated with the time duration of the fault slip tR, which measures the duration of slip at a specific point in the fault. The relationship between the pulse period and the time duration tR is (Somerville 1998):

$$\mathbf{Tv=2.2\ tR} \qquad (22)$$

The relationship between the pulse period and time duration tR can also be derived from the natural phenomenon of rupture. If a fault is formed as a point (point source) and directivity effects are ignored, the duration of the motion will be equal to the time duration tR (Somerville 1998). The finite dimensions of the fault and the directivity effects contribute to the widening of the pulse. The time duration of the fault slip tR is then a lower limit of the pulse.

The Alavi and Kranwinkler (2000) determined the pulse period as dominant period in response spectrum velocity (Tv-p). The relationship that uses this definition for the pulse period is:

$$\mathbf{Log10Tv\text{-}p=-1.76+0.31m} \qquad (23)$$

Rodriguez-Marek (2000) developed the following relationship for the pulse period:

$$\mathbf{ln(Tv)ij=a+b\ m+\eta i+\varepsilon ij} \qquad (24)$$

where(Tv)ij is the period of the pulse of record j by the fact i, a and b are the parameters of the model, ηi and εij are error conditions.

Estimates are provided for the period of the pulse, Tv, and the dominant period of velocity spectrum Tv-p. The values of model parameters are presented in Table 16. The relation is valid for m = 6.1-7.4 and r <20km.

Figure 28 compares the relation recently proposed by Rodriguez - Marek (2000) with the relations developed by Somerville (1998) and Alavi and Kranwinkler (2000). Relationships Rodriguez - Marek (2000) for the Tv and Tv-p give smaller pulse periods than the relationships developed by Somerville (1998) for the Tv and by Alavi and Kranwinkler (2000) for the Tv-p. The differences are not so great for large earthquake magnitude m> 7, where there are uncertainties in the estimation of the pulse period.

Table 16: Parameters of Rodriguez-Marek(2000)'s model for pulse period

a) Tv

Data Set	a	b	σ	τ	σ_{total}
All Motions	-8.33	1.33	0.36	0.40	0.54
Rock	-11.10	1.70	0.31	0.41	0.51
Soil	-5.81	0.97	0.32	0.40	0.51

b) Tv-p

Data Set	a	b	σ	τ	σ_{total}
All Motions	-6.92	1.08	0.48	0.45	0.66
Rock	-9.53	1.42	0.37	0.61	0.71
Soil	-5.66	0.91	0.41	0.45	0.61

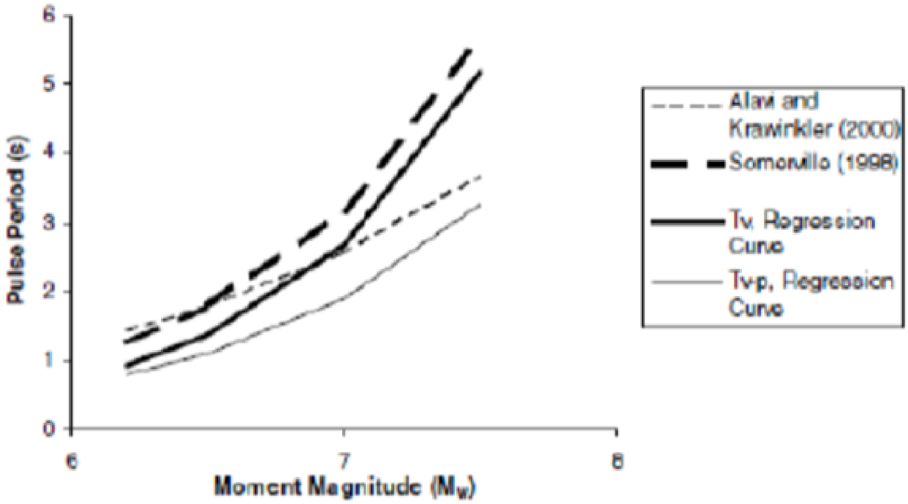

Figure 28: Compare of the Rodriguez-Marek(2000)'s model with relations that have been developed by Somerville(1998) for Tv and from Alavi and Kranwinkler(2000) for Tv-p (Rodriguez-Marek 2000)

The effect of soil conditions can be investigated through the use of relationships Rodriguez - Marek (2000) for the pulse period for rock and soil (Figure 29). The difference between the values of the pulse period for rock and soil is small for large magnitude events (m> 7), but the period of the pulse is greater over land than for rock sites for events with lower magnitude. The examination of paired stations rock and soil and the effects of non-linear response analyzes confirm this observation (Rodriguez-Marek 2000).

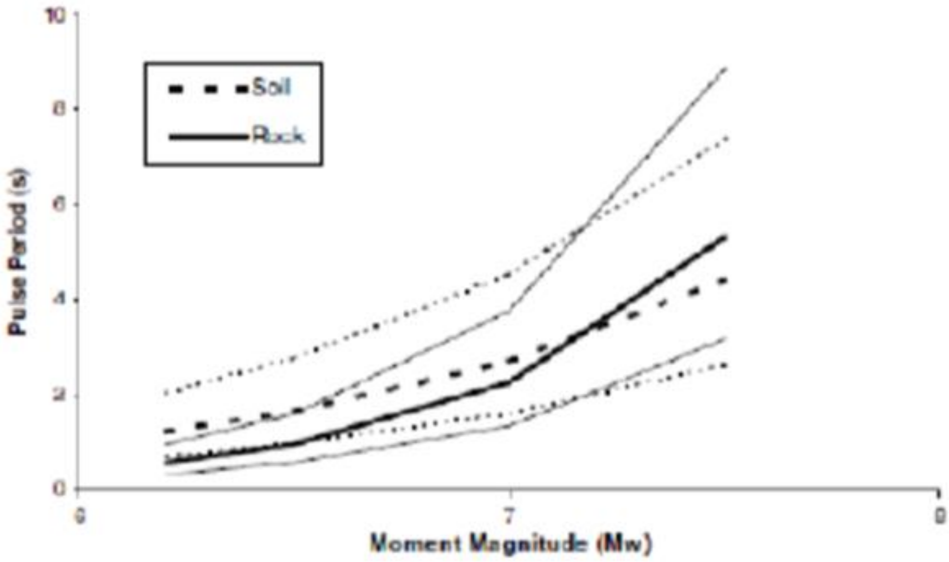

Figure 29: Rodriguez-Marek(2000)'s model for the assessment of pulse period for rocks and ground. Bold curves represent the mean and lightened curves the standard deviations (Rodriguez-Marek 2000)

Number of significant pulses

The number of pulses of motion (called as number of significant pulses Nv) is defined as the number of half cycles velocity having amplitudes at least 50 % of the maximum velocity of ground motion (Table 14) . To calculate the number of significant velocity pulses only the vertical component of the fault motion is examined . The number of significant pulses to the vertical component 48 recordings presented in Table 17. Most records contain two major pulses (ie a full circle of ground motion). The Somerville (1998) suggests the number of sine pulses in the time history of velocity linked to the number of heterogeneous ruptures (asperities) on a fault, which is then connected to distribution fault slip. There is no model available for predicting the number of significant pulses in the time-history of velocity. For most cases, the Nv will vary between 1 and 3 with Nv = 2 as a good value used for earthquakes.

Table 17: Number of pulses (Nv) for 48 near field movements. Rodriguez-Marek(2000)'s model for pulse period. The values in the bracket are the numbers of semicycles of velocity pulse which have ranges at least 33% of PHV (Rodriguez-Marek 2000)

Earthquake	Year	Number of Records	Number of Records with given number of half-cycle pulses (N_v)			
			1 pulse	2 pulses	3 pulses	> 3 pulses
Parkfield	66	2	0 (0)	1 (1)	0 (0)	1 (1)
San Fernando	71	1	1 (0)	0 (0)	0 (1)	0 (0)
Imperial Valley	79	13	1 (0)	10 (1)	1 (7)	1 (5)
Morgan Hill	84	2	0 (0)	0 (0)	1 (0)	1 (2)
Superstition Hills(B)	87	2	1 (0)	1 (1)	0 (0)	0 (1)
Loma Prieta	89	8	0 (0)	4 (0)	1 (1)	3 (7)
Erzincan, Turkey	92	1	0 (0)	0 (0)	1 (1)	0 (0)
Landers	92	1	1 (0)	0 (1)	0 (0)	0 (0)
Northridge	94	10	3 (0)	4 (4)	3 (2)	0 (4)
Kobe	95	4	0 (0)	1 (0)	0 (1)	3 (3)
Kocaeli,Turkey	99	4	0 (0)	3 (2)	0 (0)	1 (2)
Totals		48	7 (0)	24 (10)	7 (13)	10 (25)

2.3 Effects of Fling Step

The effects of fling step of territorial motion in response to the construction were considered less important than the influence of the directivity. The recent earthquakes in Turkey (Izmit 1999) and Taiwan (Chi-Chi 1999), stressed the importance of residual deformation associated with the rupture surface in the response of buildings. The distinct territorial shifts, differential settlements and ground deformation are some aspects of this phenomenon.

The fling step as a result of static displacement soil is characterized by a unidirectional pulse velocity and a monotonic step in the time history of displacements. The step in the time history of displacements occurs along the direction of fault slip (ie along the rupture).

For all types of faults, the maximum displacement (MD) of fault in m may be associated with the earthquake magnitude (m) of that fact by the equation:

$$\mathbf{log10(MD)=-5.46+0.82m} \qquad (25)$$

valid for earthquake magnitude range m = 5.2-8.1 and range from MD 0.01m to 14.6m.

The mean displacement (AD) fault for all types of faults is:

$$\mathbf{log10(AD)=-4.80+0.69m} \qquad (26)$$

valid for earthquake magnitude range m = 5.6-8.1.

The fling step of surface as a result of rupture faults can vary significantly with distance from the trace of fault. The tectonic shift away from the fault can be detected in trace quadratic faults and other discontinuities.

3 Presentation and Description of the Building

3.1 General Description of the Building

The building has been studied in this thesis is of reinforced concrete, has eight (8) floors with pilotis. The height of the pilotis is 2,55 m and height of all other floors is 2,75 m. The specific weight of the concrete has taken 25,0 kN / m³.

Some assumptions which have been used to study the building are shown below:

Loads:

General coatings	2.0 kN/m²
Live Loads for Plates	2.0 kN/m²
Live Loads for Balconies	5.0 kN/m²
Live Loads for Scales	3.5 kN/m²
Live Loads for Ground Floor	5.0 kN/m²

Materials:

Concrete quality: C 20/25

Quality steel: S 500

Quality steel fasteners: S 500

The characteristic strength of concrete is fc = 20 MPa and the characteristic value of the yield for the steel is fy = 500 MPa (these are the strengths of the materials that also defined in the program). The elastic modulus of materials defined by Greek Regulation for Reinforced Concrete 2000 (Ε.Κ.Ω.Σ 2000) is as follows: Ec = 29 GPa for concrete and Es = 200 GPa for steel.

Concerning the seismic activity, the building has been constructed in an area of seismic hazard I (a = 0,16 g), the importance class has defined as II, category of foundation soil is B (T1 = 0,15 sec, T2 = 0.6sec) the seismic behavior factor is q = 3,5 and the percentage of critical damping is $\zeta = 0.05$.

Figure 30 shows the plan view of the building with the dimensions and Figure 31 the 3D view of the building.

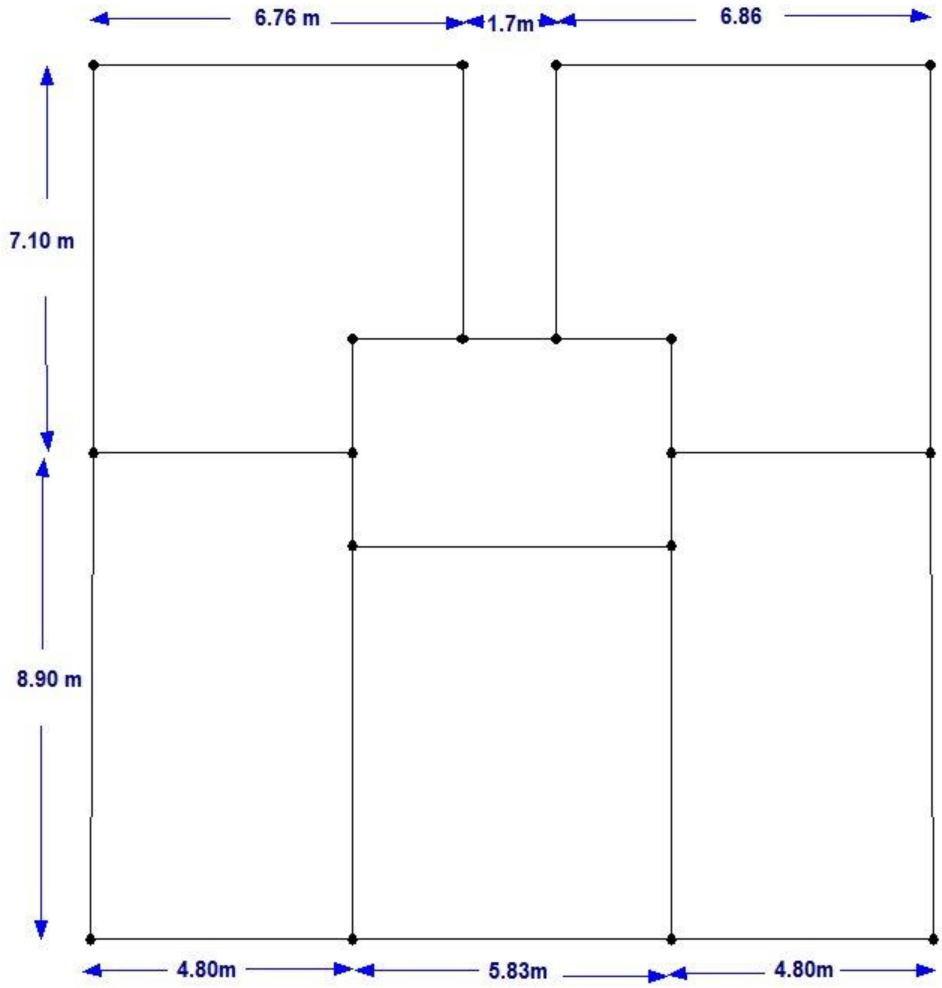

Figure 30: Plan View of the building with dimensions

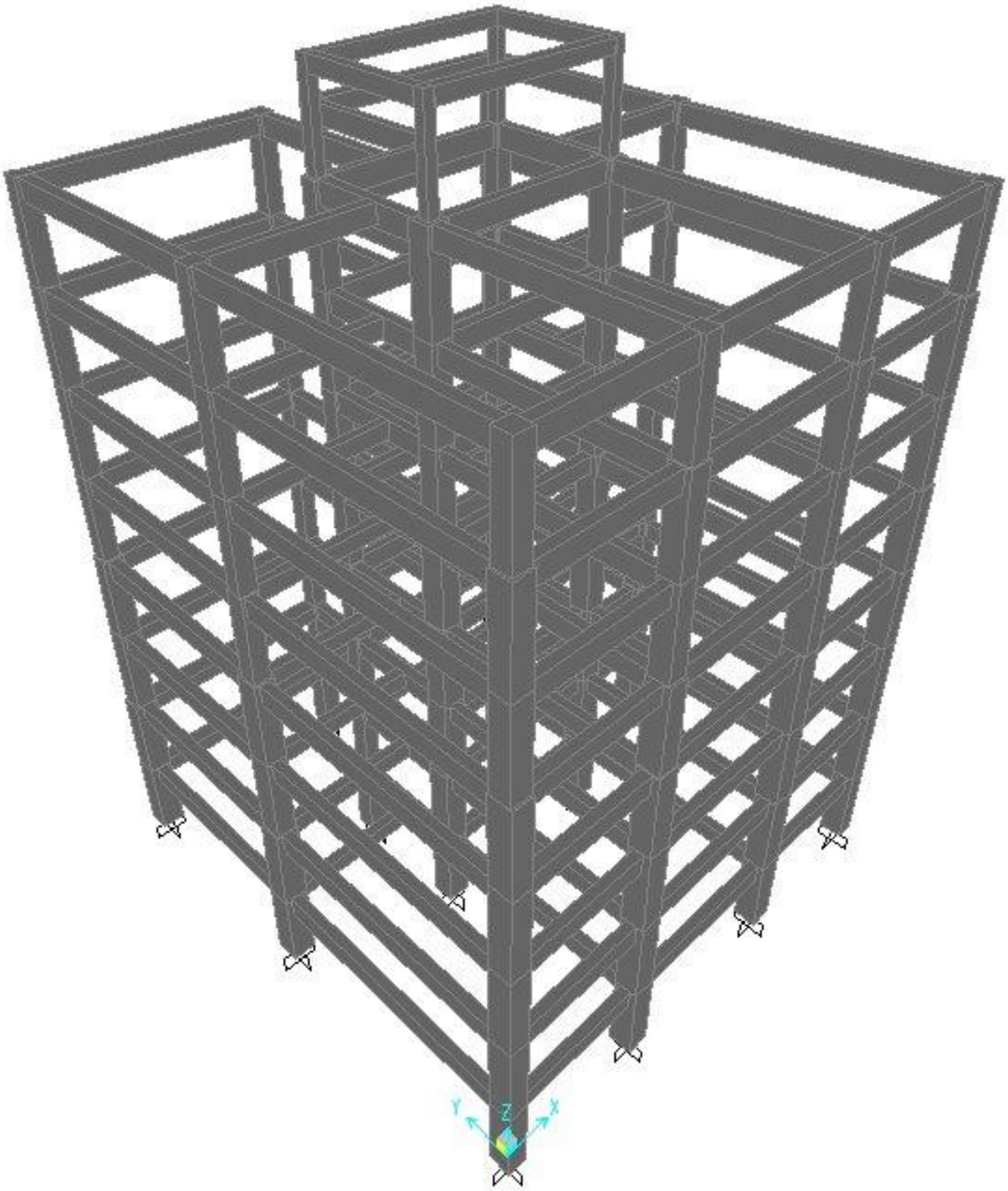

Figure 31: 3D view of the building

Other assumptions which had used to simulate the building are as follows:

- At the base of all the columns defined anchors.
- The mass of the structure is set by the mass corresponding to the load combination $1{,}0 \cdot G + 0{,}3 \cdot Q$,in which the dead loads are multiplied by factor of 1.0 while the live loads by reduction factor of 0.3.
- The construction is considered symmetrical in X-axis and for this reason during seismic loading is not developed torsion, ie there are no bends in the Z-axis.

4 Eigen periods, Push-Over Curve, Capacity Curve and Fragility Curves

4.1 Fundamental eigenperiods of the building

The eigenperiods of the building under investigation are computed through Modal Analysis, which has been performed using SAP2000 software. The first two eigenmodes are:

- T1 = 1.165sec
- T2 = 1.113ec

4.2 Push-Over Curve

The structure is subjected to non-linear static analysis (push-over analysis) using the SAP2000 software. In particular, plastic hinges were used in the model to simulate the non-linear behaviour of both columns and beams of the reinforced concrete building under incremental horizontal seismic loading in the X-direction. In both cases (column and beam plastic hinges) a fully elastoplastic behavior was assumed with no hardening (Figure 32).

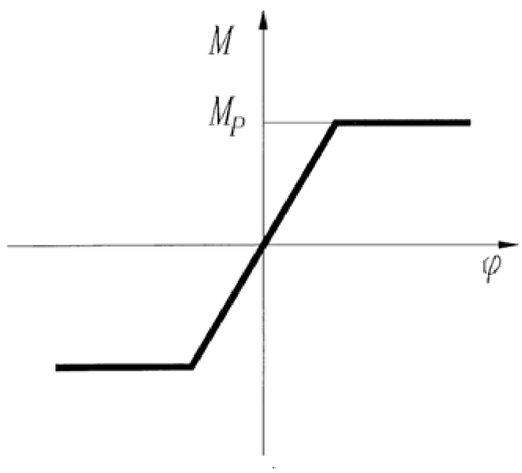

Figure 32: Non-linear elastoplastic behaviour considered for structural elements

More specifically, in the case of beams, plastic hinges were applied at both edges of the horizontal frame elements, by defining a simple moment-rotation relationship (M3), as described above and providing the "Acceptance criteria", which correspond to the damage limit states of each plastic hinge, according to FEMA 356. In the case of columns a different type of plastic hinge was used that takes into account the interaction of both bending moments of the column with the axial load (P-M2-M3). Different acceptance criteria were provided for columns. The values of element rotation for each damage stage are provided in Table 18.

Table 18: Acceptance Criteria (Plastic rotation values) for frame hinge properties used in SAP2000

Damage level	**Beam**	**Column**
Immediate Occupancy (IO)	0.01	0.003
Life Safety (LS)	0.02	0.012
Collapse Prevention (CP)	0.025	0.018

The push-over curve, i.e. the total base shear of the building in terms of the horizontal displacement of joint 340 of top (8^{th}) floor of the building, is provided in Figure 33.

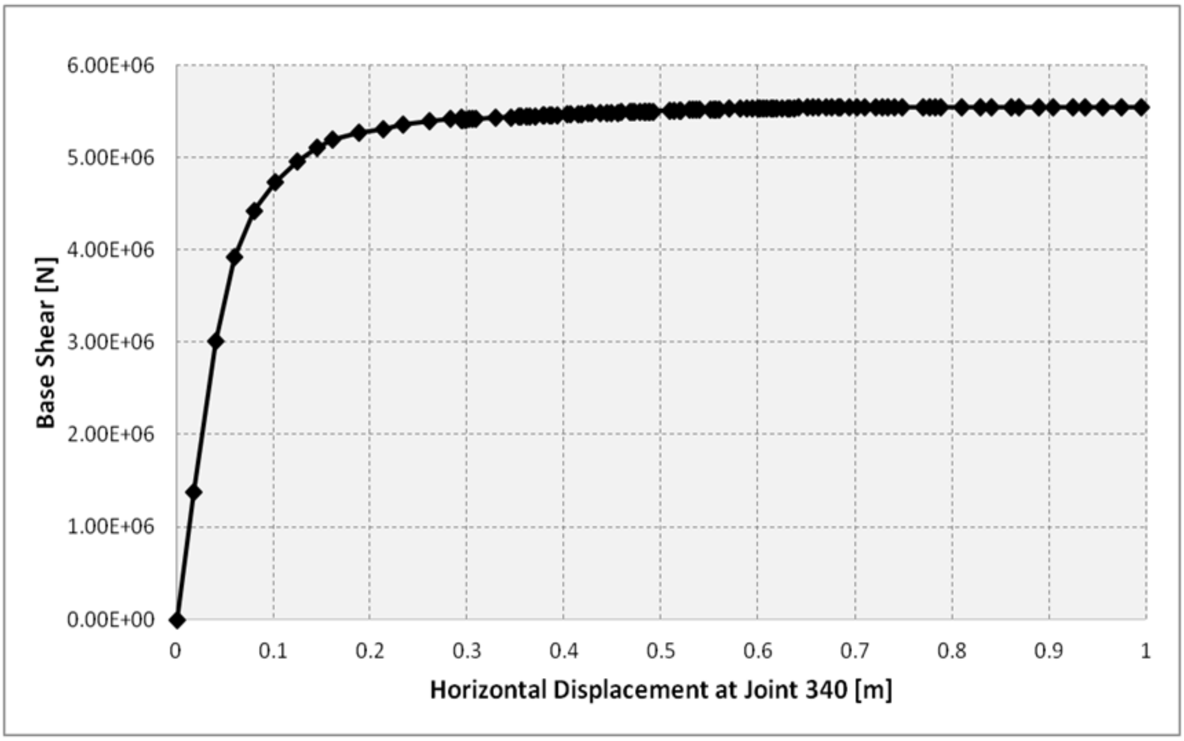

Figure 33: Push over curve, obtained from the non-linear static analysis of the 8-storey building in the X-direction (1^{st} mode)

4.3 Capacity Curve

In order to convert pushover coordinates of base shear force and control point (Joint 340 at the 8th floor) displacement to spectral acceleration and spectral displacement, respectively. The conversion of pushover to capacity is described in section 1.3 in this thesis and HAZUS (Section 5.2.1) and the procedure is based on the calculation of two mode factors α_1 and α_2:

$$\alpha_1 = \frac{\left[\sum_{i=1}^{N} (w_i \phi_{ip})/g\right]^2}{\left[\sum_{i=1}^{N} (w_i)/g\right]\left[\sum_{i=1}^{N} (w_i \phi^2_{ip})/g\right]}$$

$$\alpha_2 = \frac{1}{PF_p \varphi_{cp,p}} = \frac{\sum_{i=1}^{N} (w_i \phi^2_{ip})/g}{\left[\sum_{i=1}^{N} (w_i \phi_{ip})/g\right] \varphi_{cp,p}}$$

Where: w_i/g = mass assigned to the i^{th} degree of freedom

Φ_{ip} = amplitude of pushover mode at i^{th} degree of freedom

$\Phi_{cp,p}$ = amplitude of pushover mode at control point (Joint 340)

The spectral acceleration can be computed from the normalised base shear, V, by the total weight of the building, W, as follows:

$$S_a = A_p/\alpha_1 = \frac{V}{W}/\alpha_1$$

The spectral displacement can be computed in terms of the top-floor displacement (control point), U_x, as follows:

$$S_d = \alpha_2 * U_x$$

The assigned masses for each floor are taken from SAP2000 using the ability to export the Assembled Joint Masses in the form of table and summarise the masses of the corresponding joints at each floor. The amplitudes of the first eigenmode, which corresponds to the push-over load pattern, at each floor are also taken from SAP2000 output and the following table (Table 19) is formed:

Table 19: Data for the calculation of the modal factor α_2

Floor	*Level [m]*	*m_i (Kg)*	*Φip*	*m*Φip^2*	*m*Φip*
1	2.55	269729	5.36E-05	0.00077	14.45
2	5.30	240130	1.70E-04	0.00694	40.82
3	8.05	239649	3.06E-04	0.02237	73.21
4	10.80	239208	4.34E-04	0.04499	103.74
5	13.55	238111	5.60E-04	0.07464	133.32
6	16.30	237962	6.66E-04	0.10542	158.39
7	19.05	237819	7.42E-04	0.13090	176.44
8	21.80	247831	7.88E-04	0.15397	195.34
	Sum:	**1950440**	**---**	**0.540**	**895.71**

So the modal factor α_1 is:

$$\alpha_1 = \frac{895.71^2}{1950440 * 0.54} = 0.7617$$

and the modal factor α_2 is:

$$\alpha_2 = \frac{0.54}{7.88 * 10^{-4} * 895.71} = 0.765$$

Using the above values of the two modal factors the push-over curve is converted to the capacity curve, shown in Figure 34.

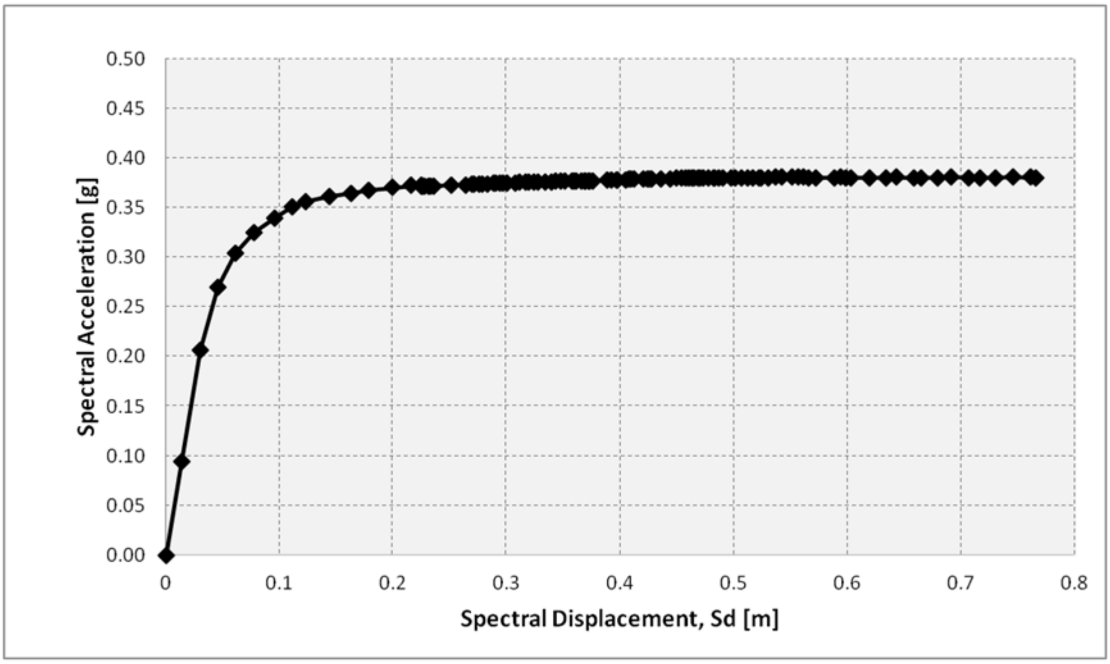

Figure 34: Capacity curve of the 8-sory building in the X-direction

4.4 Development of Fragility Curves

4.4.1 Structural damage states

For the development of the fragility curves of the building, it is necessary to define the structural damage states on the push over curves, in terms of top horizontal displacement. HAZUS provides the average inter-storey drift ratios ($\mathbf{\Delta_{ds}}$) of structural damage states of generic building types. The building under consideration is a concrete moment frame high-rise building, so according to Table 1 (Table 2.1 in HAZUS) it is labelled as C1H. Using Table 8 (Table 6.3 in HAZUS) and assuming Moderate-Code design level the average inter-storey drift ratios for the case of Low-rise buildings are obtained for each damage state. The corresponding drift ratios for the case of High-rise buildings are computed by multiplying those values with 0.5. The average inter-storey drift ratios are then multiplied with the total height of the building, i.e. 21.80m to give the corresponding damage state limit in terms of horizontal displacement of the top floor (see Table 20). Figure 35 shows the corresponding damage states on the push over curve of the building, while Figure 36 shows the damage states on the capacity curve.

Table 20: Structural damage states of the considered building in terms of average inter-storey drift ratios and top-floor displacement.

Damage state	Δ_{ds}	$Ux = H^*\Delta_{ds}$
Slight	0.0025	0.0545 m
Moderate	0.0045	0.0981 m
Extensive	0.0115	0.3270 m
Complete	0.03	0.6540 m

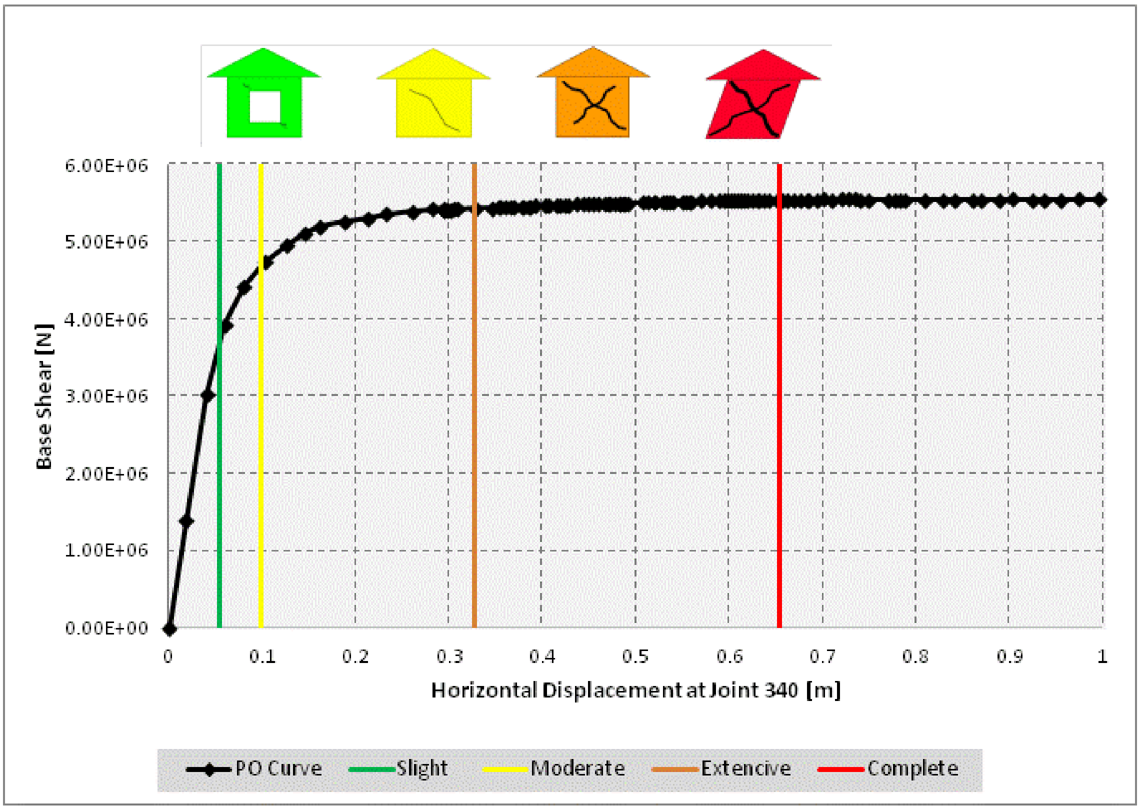

Figure 35: Damage limit-states on the push over curve of the 8-storey building

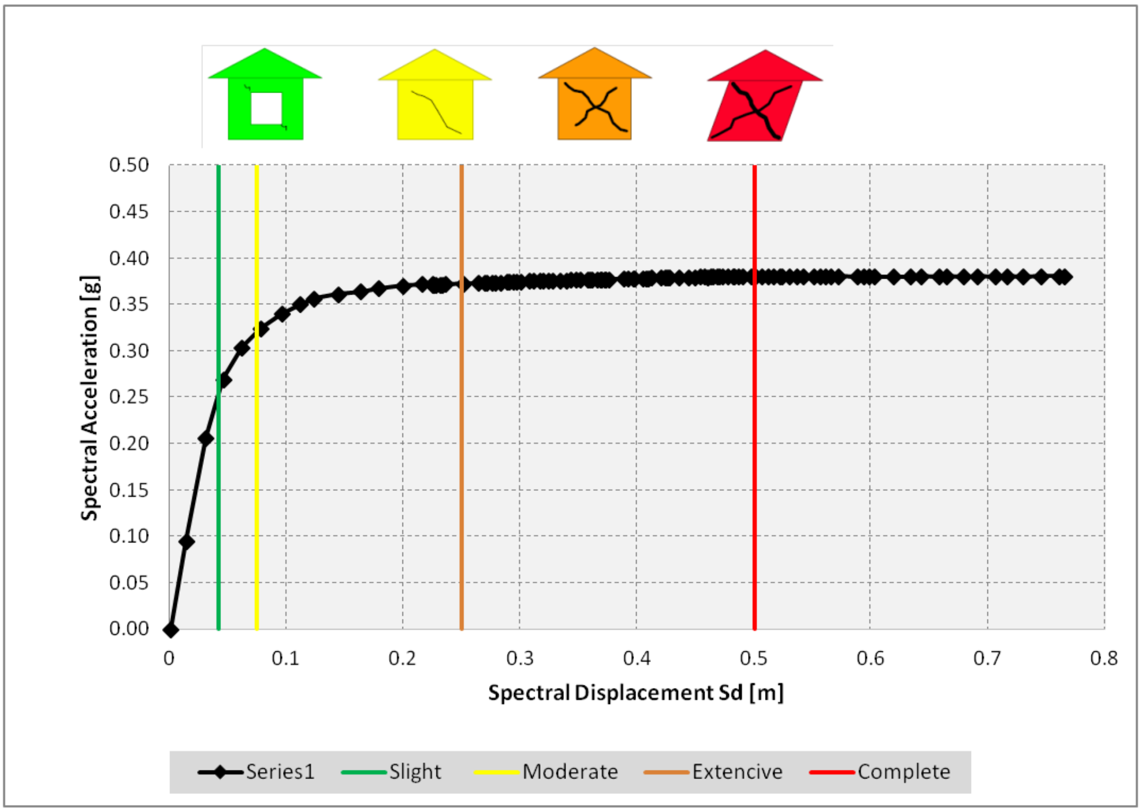

Figure 36: Damage limit-states on the capacity curve of the 8-storey building

Moreover, Figures 37-40 show the deformation of the building and the states of the hinges in different colours, for each damage-limit-state, as have been obtained from the push over analysis, using SAP2000. It is observed that for the 'Slight damage' limit state only some yielding occurs for the beams of the lower floors (Figure 37). In the case of 'Moderate Damage' the number of beam hinges that have been yielded is increased and spread to upper storeys, while some yielding occurs to columns of the internal frame at Y=11m (Figure 38). Figure 39 shows that in the case of 'Extensive Damage' some beam hinges at the lower floors fail (θ > 0.025), as well as some column hinges of the internal frame at Y=11m. Moreover, yielding occurs to beam hinges of the upper floors, to the base of the columns at the ground floor, as well as to the columns of the 5th floor. In the case of 'Complete Damage' state, nearly all the beams of the first four floors have failed, as well as the column hinges at the base and the 5th floor of the building. Failure is also observed at the columns of the internal frame at Y=11m (Figure 40), while the whole structure seems to become a mechanism.

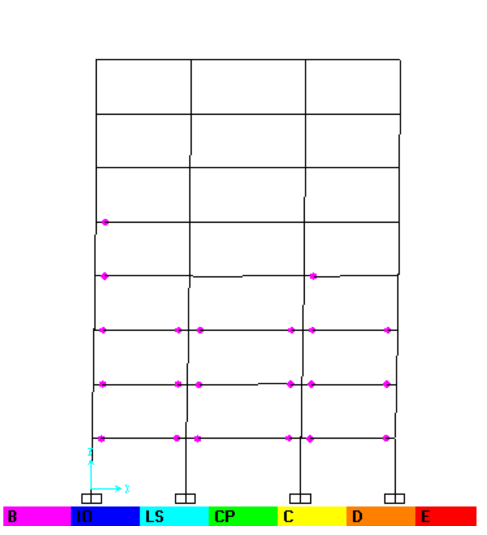

@Y=0.00m

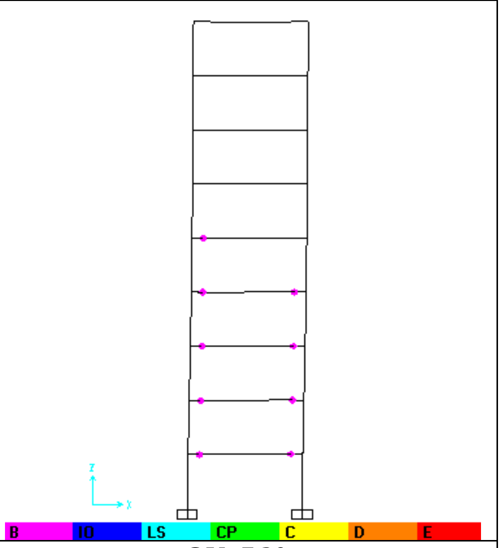

@Y=7.20m

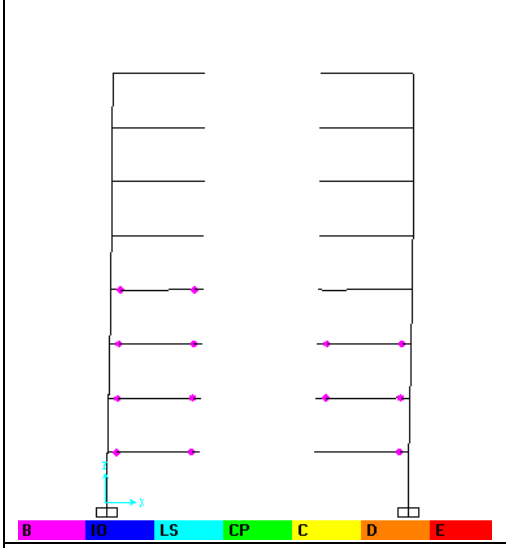

@Y=8.90m

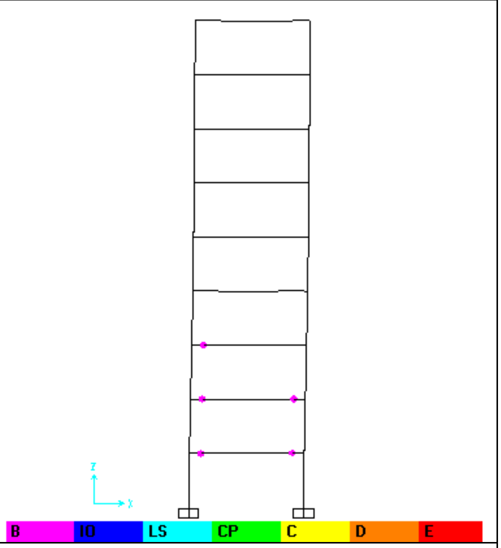

@Y=11.00m

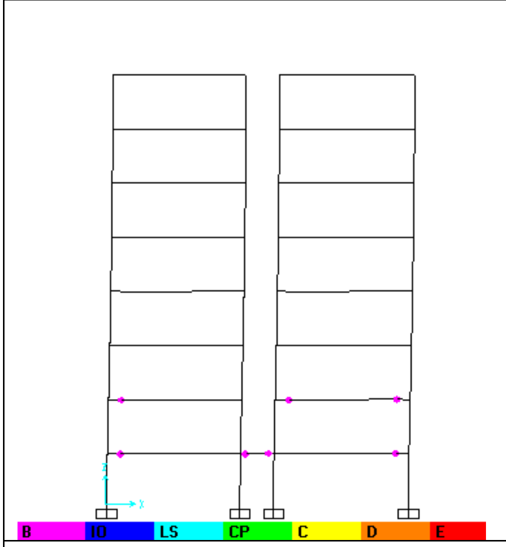

@Y=16.00m

Legend

B	Yielding
IO	Immediate Occupancy
LS	Life safety
CP	Collapse prevention
C **D** **E**	Failure

Figure 37: Hinge states at 'Slight Damage' limit-state

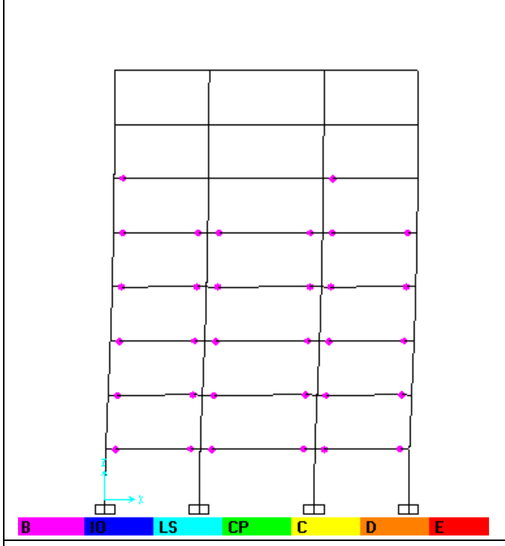

@Y=0.00m

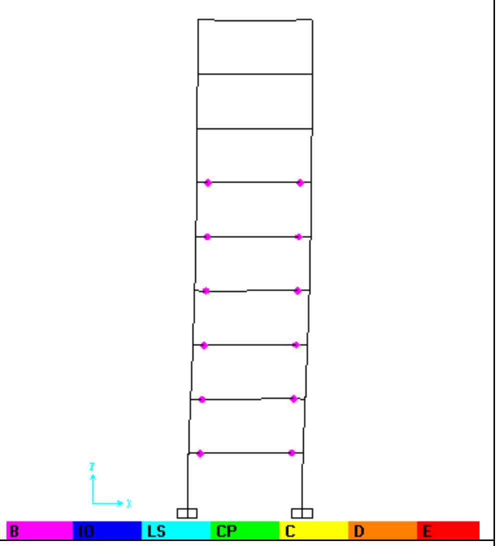

@Y=7.20m

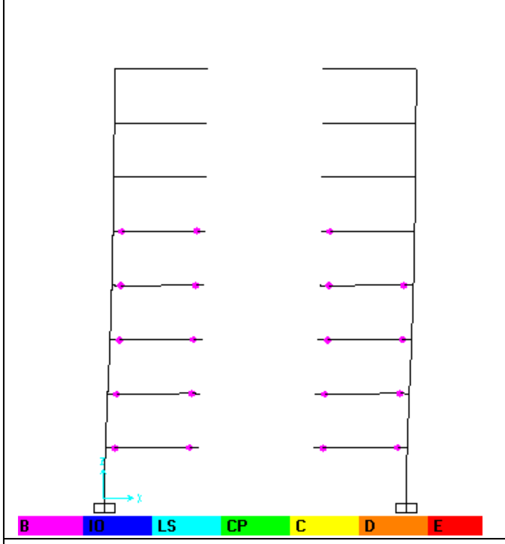

@Y=8.90m

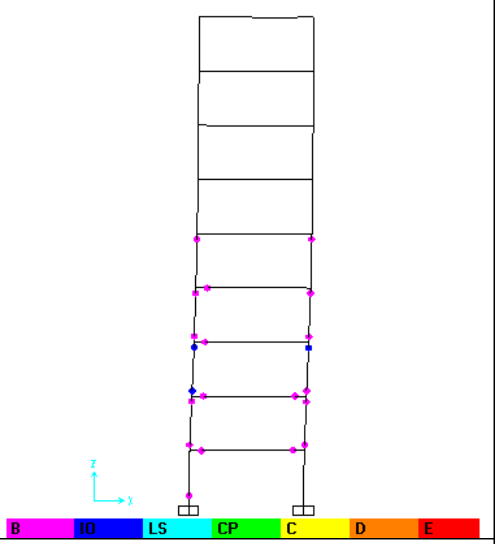

@Y=11.00m

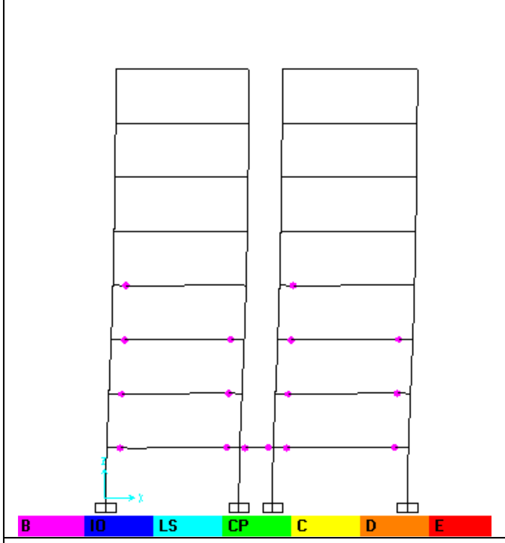

@Y=16.00m

Legend

B	Yielding
IO	Immediate Occupancy
LS	Life safety
CP	Collapse prevention
C **D** **E**	Failure

Figure 38: Hinge states at 'Moderate Damage' limit-state

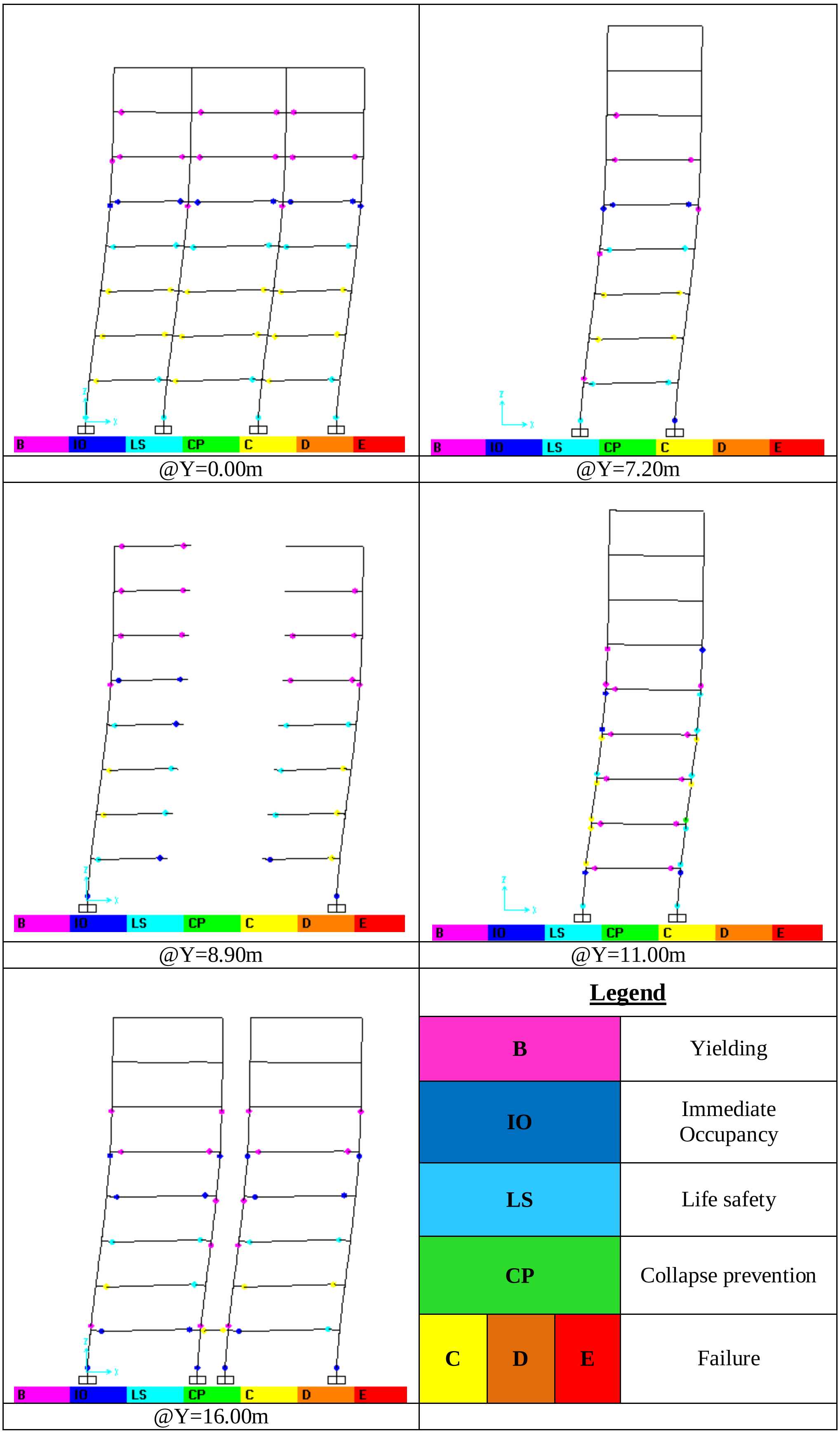

Figure 39: Hinge states at ‘Extensive Damage’ limit-state

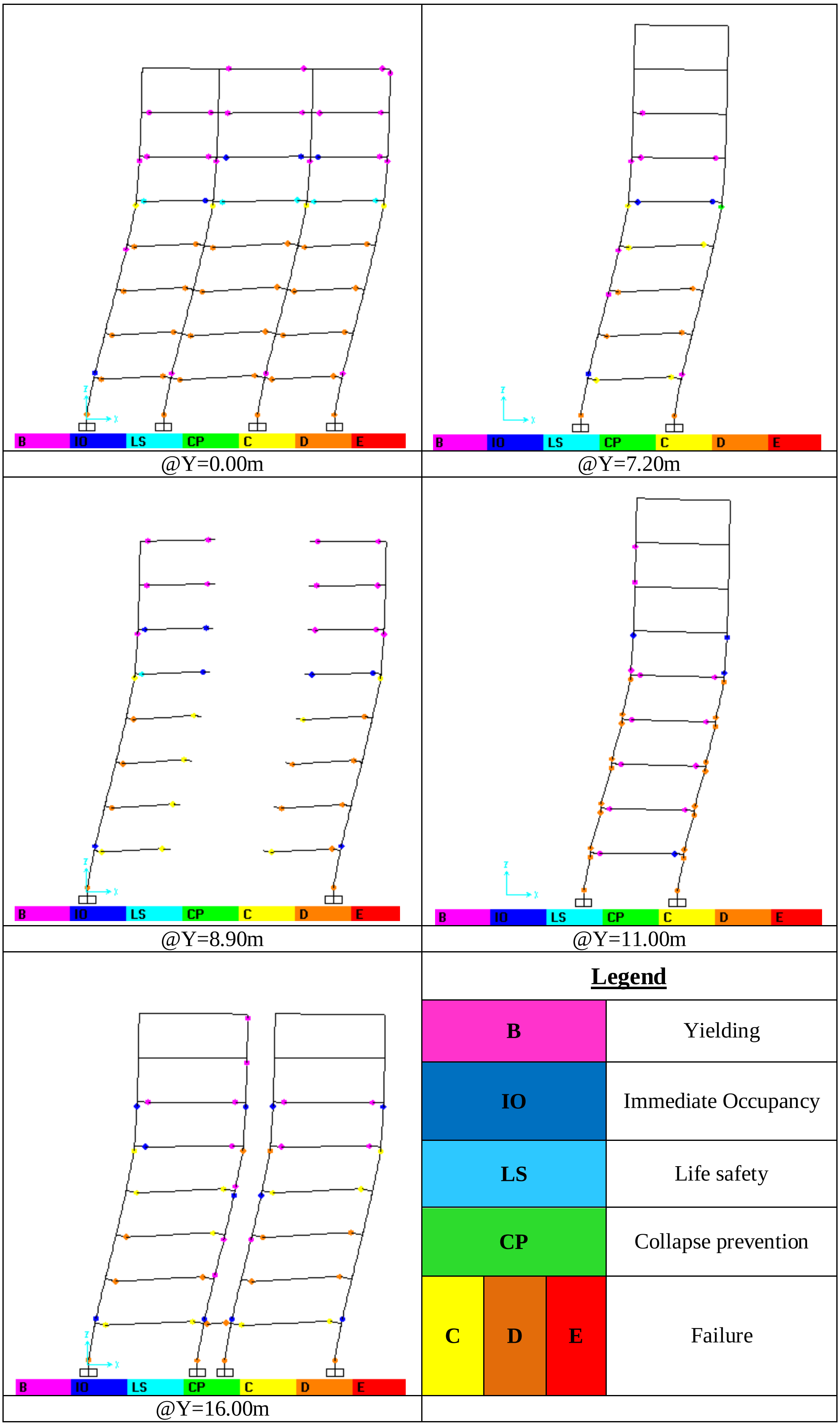

Figure 40: Hinge states at 'Complete Damage' limit-state

4.4.2 Damage-State Variability (Beta)

Lognormal standard deviation (Beta) values describe the total variability of fragility-curve damage states, which depends on the variability associated with the capacity curve, β_C and the variability associated with the discrete threshold of each damage state, $\beta_{T,ds}$:

$$\beta_{ds} = \sqrt{(\beta_C)^2 + (\beta_{T,ds})^2}$$

Where:

- β_{ds} is the lognormal standard deviation parameter that describes the total variability of damage state, *ds*,
- β_C is the lognormal standard deviation parameter that describes the variability of the capacity curve,
- $\beta_{T,ds}$ is the lognormal standard deviation parameter that describes the variability of the threshold of damage state, *ds*.

The values of βds can be obtained from HAZUS and particularly from Table 12 (Table 6.7 in HAZUS) which represents the group of High-rise buildings and gives the Beta values in terms of the post-yield degradation of the structure (Kappa factor), the Damage-State Threshold Variability and the Capacity Curve Variability.

The Kappa (κ) factors are obtained from Table 5 (Table 5.2 in HAZUS), based on the Seismic Design Level Designation and the Construction Quality of the building. For the particular case, Moderate Code (MC) requirements are considered and Ordinary (O) construction quality. Therefore the values of the Kappa factors are: 0.9 at yield, 0.7 at short post-yield response, 0.5 at moderate post-yield response and 0.3 at long at post-yield response. Moderate values of both damage variability ($\beta_{T,ds}$ = 0.4) and capacity curve variability (β_C = 0.3) are assumed. So the values of the β_{ds} of the fragility curves for each one of the damage states are obtained from Table 21, as follows:

Slight damage curve:

Degradation at Yield: κ=0.9 → β_{ds} = 0.70

Moderate damage curve:

Degradation at Yield: κ=0.7 → β_{ds} = 0.75

Extensive damage curve:

Degradation at Yield: κ=0.5 → β_{ds} = 0.80

Complete damage curve:

Degradation at Yield: κ=0.3 → β_{ds} = 0.90

The beta values for Kappa factors κ=0.7 and κ= 0.3 are obtained after linear interpolation.

4.4.3 Fragility curves in terms of the top-floor displacement

Building fragility curves are lognormal functions that describe the probability of reaching, or exceeding, structural and non-structural damage states, given median estimates of structural response, in this case the top-floor displacement. The conditional probability of being in, or exceeding, a particular damage state, *ds*, given the building's top-floor displacement, U_x, is defined by:

$$P[ds|U_x] = \Phi[\frac{1}{\beta_{ds}} * \ln\left(\frac{U_x}{U_{x,ds}}\right)]$$

where:

$U_{x,ds}$ is the median value of top-floor displacement at which the building reaches the threshold of damage state, *ds*,

Φ is the standard normal cumulative distribution function.

So, the fragility curves are obtained by substituting the values of $U_{x,ds}$, given in Table 20, in the above equation, along with the standard deviation (Beta) values that are calculated above. Figure 41 shows the fragility curves in terms of top-floor displacement of the building.

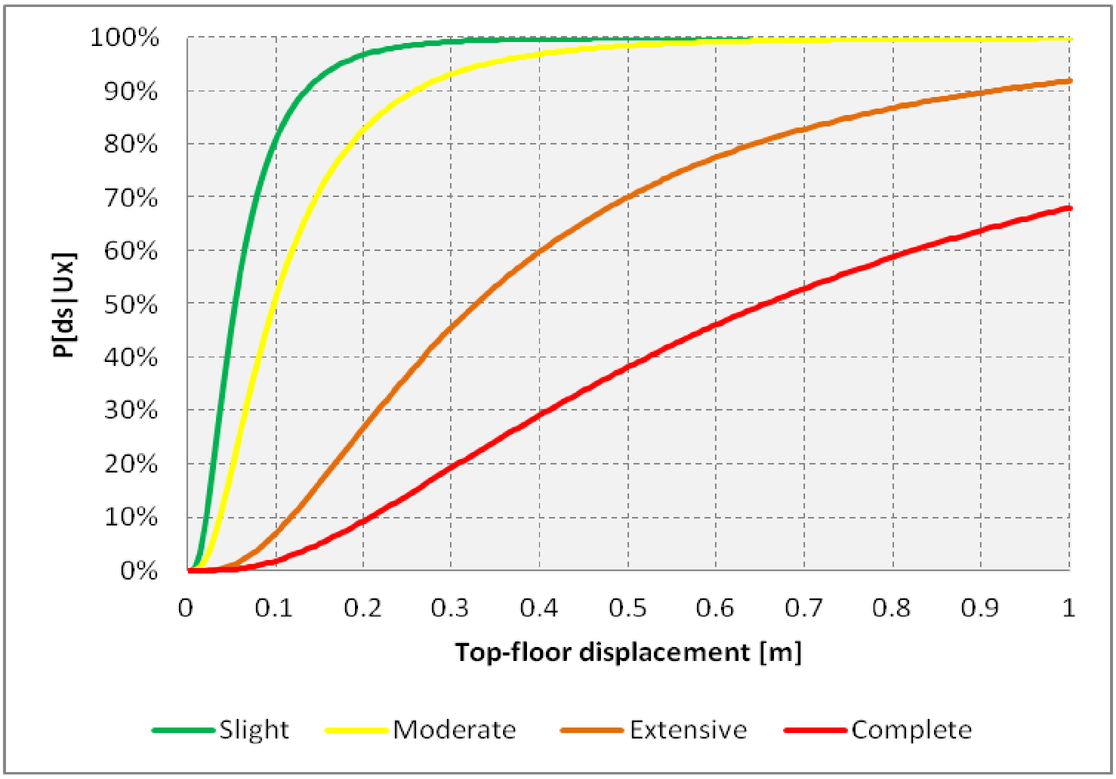

Figure 41: Fragility curves of the 8-storey building, in terms of the top-floor displacement

5 Selected near-fault ground motions

A set of seismic records have been selected for the assessment of the 8-storey building, based on their near-fault characteristic and their relatively large value of maximum spectral displacement (SDmax), as displayed in Table 21, which is provided by a large database of seismic records. The set includes, in total, 18 ground-acceleration time-histories, since each seismic recording consists of two orthogonal seismic components. Here is the description of the header of each column of Table 21:

F/M: Fault Mechanism:

SS: Strike slip,

RV: Reverse,

OB: Obverse.

S/C: Site Code:

HR: hard rock,

SR: sedimentary and conglomerate rock,

SL: soil and alluvium.

DIR/TY: Directivity:

F: forward,

N: neutral,

B: backward.

C/D: Closest distance:

Normal distance from fault trace for events: 1, 2, 4, 5, 7

Normal distance from fault plane for events: 3, 6

COMP.: Direction of seismic components (angle with north)

SDmax: Maximum spectral displacement (for both components)

Table 21: Characteristics of the selected near-fault ground motions

#	LOCATION	DATE	Mw	F/M	STATION	S/C	DIR/TY	C/D	COMP.	SDmax
1	Tabas, Iran	16/9/1978	7.1	RV	Tabas (TAB)	SL	N	1.2	74 - 344	243.73 - 131.32
2	Imperial Valley, CA,USA	15/10/1979	6.4	SS	El Centro Array 4, Anderson Rd (E04)	SL	F	6.0	230	123.84
					El Centro Array 5, James Rd (E05)	SL	F	2.7	140 – 230	112.33 - 127.06
					El Centro Array 6, Huston Rd (E06)	SL	F	0.3	230	155.55
					El Centro Array 7, Imperial Val. Cl (E07)	SL	F	1.8	230	117.6
					Meloland Route Overpass (EMO)	SL	F	1.2	270	111.05
3	Northridge, CA, USA	17/1/1994	6.7	RV	Jensen Filtration Plant (JFA)	SL	F	5.2	22 – 292	109.88 - 72.43
					Sylmar Converter Station (SCG)	SL	F	5.1	52 – 142	131.88 - 87.25
					Sylmar Converter Station East (SCH)	SL	F	5.0	11	97.63
4	Hanshin (Kobe), Japan	17/1/1995	6.8	SS	Takatori (TAK)	SL	F	1.1	0 – 90	114.89 - 95.42
					Kobe Port Island,Surface (KPI)	SL	F	3.2	0	77.52
5	Izmit, Turkey	17/8/1999	7.4	SS	Yarimca Petkim (YPT)	SL	F	2.6	0 - 270	107.42 - 145.02
					Arcelik Arge Lab (ARC)	SR	F	14.0	270	78.02

6	Chi-Chi, Taiwan	20/9/1999	7.6	RV	CHY101	SL	F	7.7	90 – 360	107.61 - 223.06
					TCU053	SL	F	4.6	360	166.76
					TCU065	SL	F	0.1	90 – 360	248.53 - 182.93
					TCU068	SL	F	0.2	90 – 360	597.22 – 768.98
					TCU102	SL	F	0.6	90	199.98
					TCU103	SL	F	4.4	90	180.67
7	Duzce, Turkey	12/11/1999	7.1	OB	Duzce (DZC)	SL	N	8.3	180 – 270	145.65 - 159.53
					Bolu (BOL)	SL	F	19.9	0	49.54

The following figures (Figure 42 – Figure 59) present some seismological information about the selected ground motions, including the map of epicentre, the rupture extent and the station location. Some parameters that are related to directivity effects are also provided in the figures (Shahi and Baker, 2012).

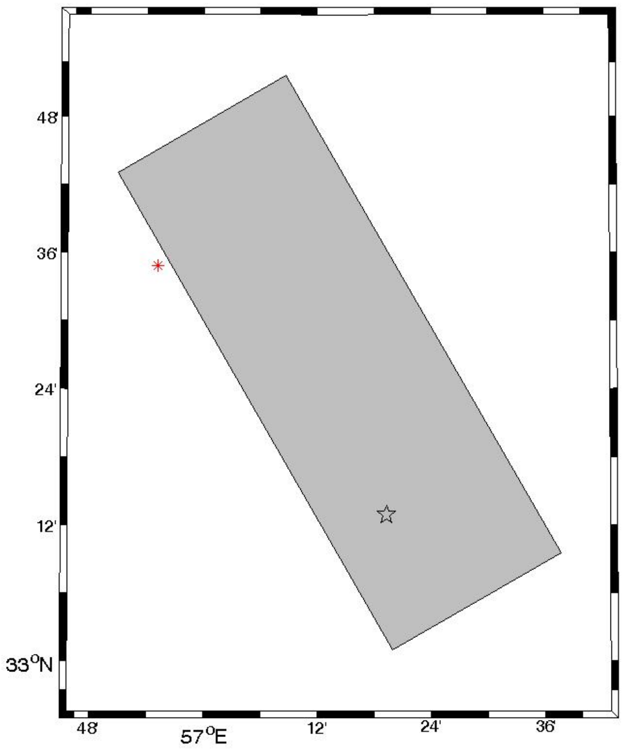

Directivity parameters:

X = 0.6
s = 53.92 km
θ = 12.6

Y = 0.32
d = 11.27 km
φ = 0.6

IDP = 0.8
Rowshandel parameter = 0.28

Epicenter
Surface projection of rupture
Recording station

Figure 42: Map of epicentre, rupture extent and station location for: 1978 Tabas, Iran, Tabas

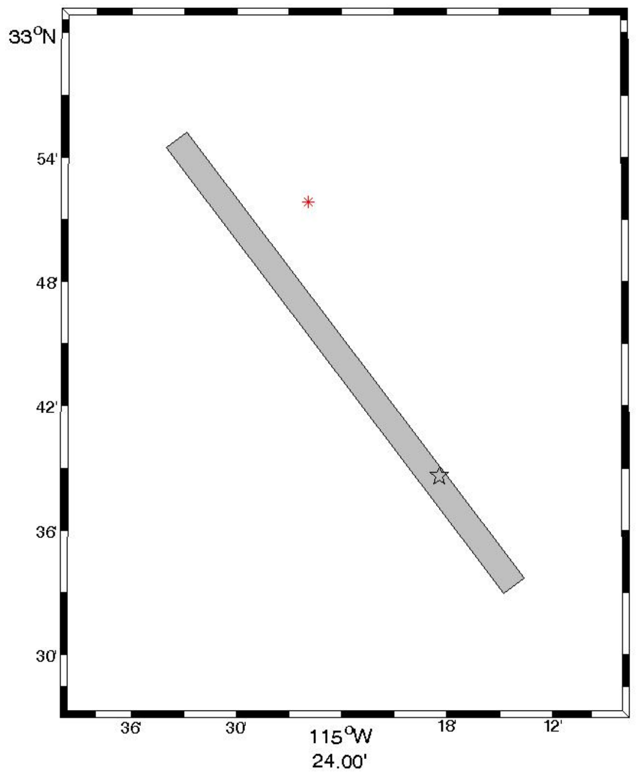

Directivity parameters:

X = 0.53
s = 26.59 km
θ = 11.5

Y = 0.68
d = 8.87 km
φ = 38.5

IDP = 2.21
Rowshandel parameter = 0.05

Epicenter
Surface projection of rupture
Recording station

Figure 43: Map of epicentre, rupture extent and station location for: 1979 Imperial Valley, El Centro A#4

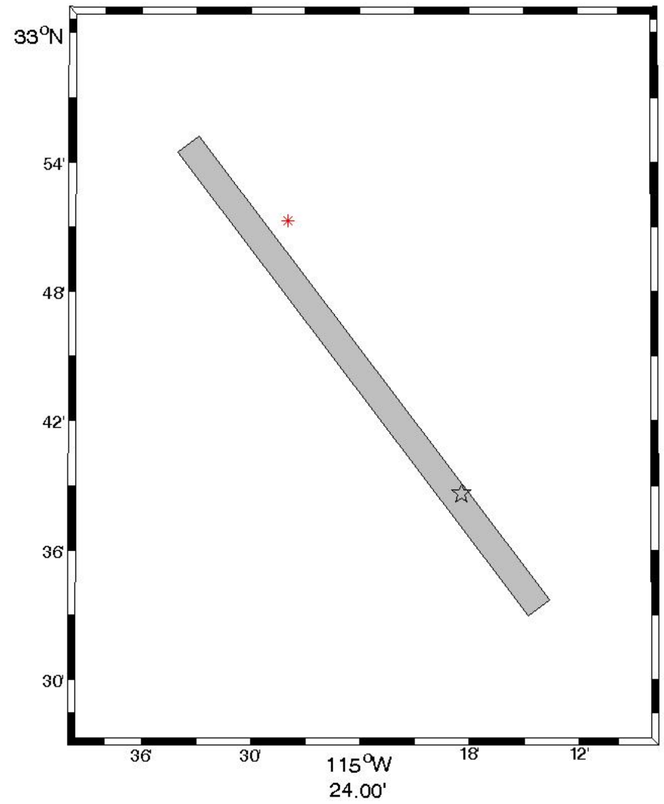

Directivity parameters:

X = 0.55
s = 27.71 km
θ = 4.7

Y = 0.72
d = 9.42 km
φ = 22.8

IDP = 3.04
Rowshandel parameter = 0.1

☆ Epicenter
Surface projection of rupture
* Recording station

Figure 44: Map of epicentre, rupture extent and station location for: 1979 Imperial Valley, El Centro A#5

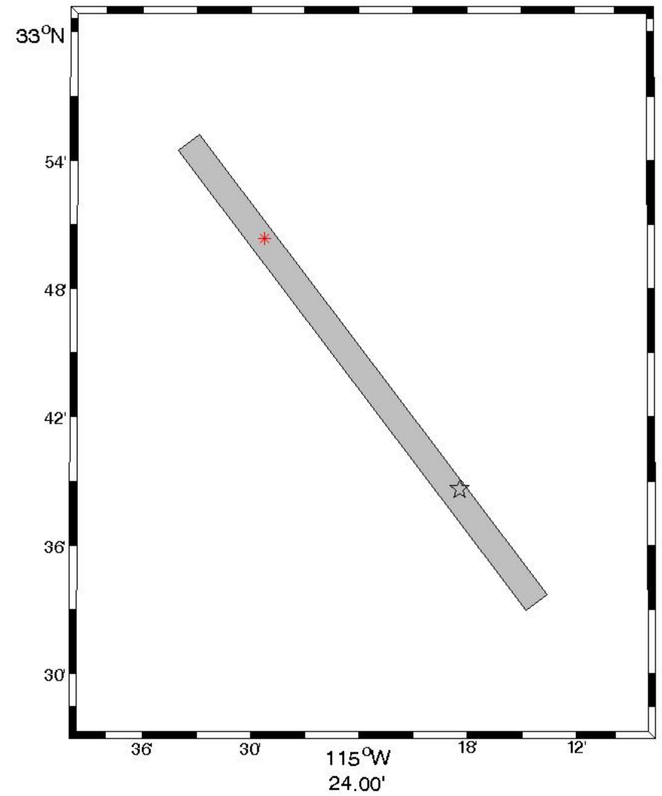

Directivity parameters:

X = 0.55
s = 27.47 km
θ = 0.8

Y = 0.76
d = 9.87 km
φ = 7.9

IDP = 3.1
Rowshandel parameter = 0.1

☆ Epicenter
Surface projection of rupture
* Recording station

Figure 45: Map of epicentre, rupture extent and station location for: 1979 Imperial Valley, El Centro A#6

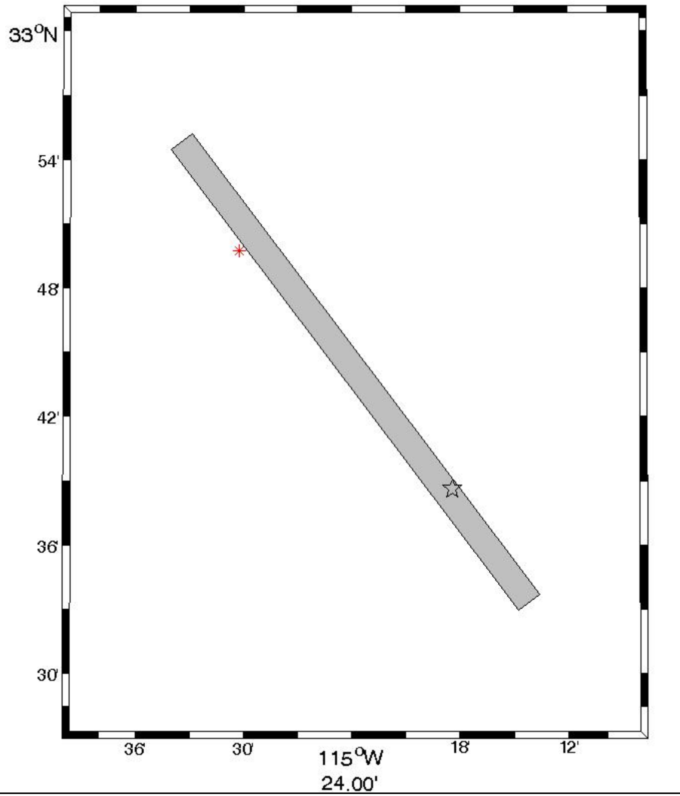

Directivity parameters:

X = 0.55
s = 27.54 km
θ = 4.8

Y = 0.78
d = 10.11 km
φ = 3.1

IDP = 3.11
Rowshandel parameter = 0.1

☆ Epicenter
Surface projection of rupture
* Recording station

Figure 46: Map of epicentre, rupture extent and station location for: 1979 Imperial Valley, El Centro A#7

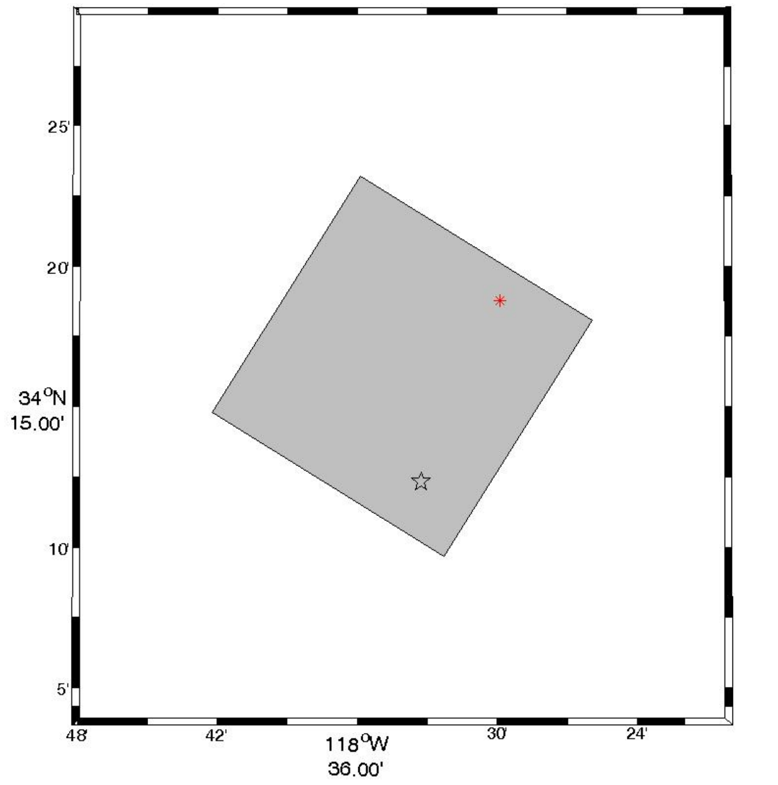

Directivity parameters:

X = 0.1
s = 1.76 km
θ = 82.2

Y = 0.81
d = 19.5 km
φ = 13.7

IDP = 2.55
Rowshandel parameter = 0.43

☆ Epicenter
Surface projection of rupture
* Recording station

Figure 47: Map of epicentre, rupture extent and station location for: Northridge 1994, Jensen Filter Plant Station

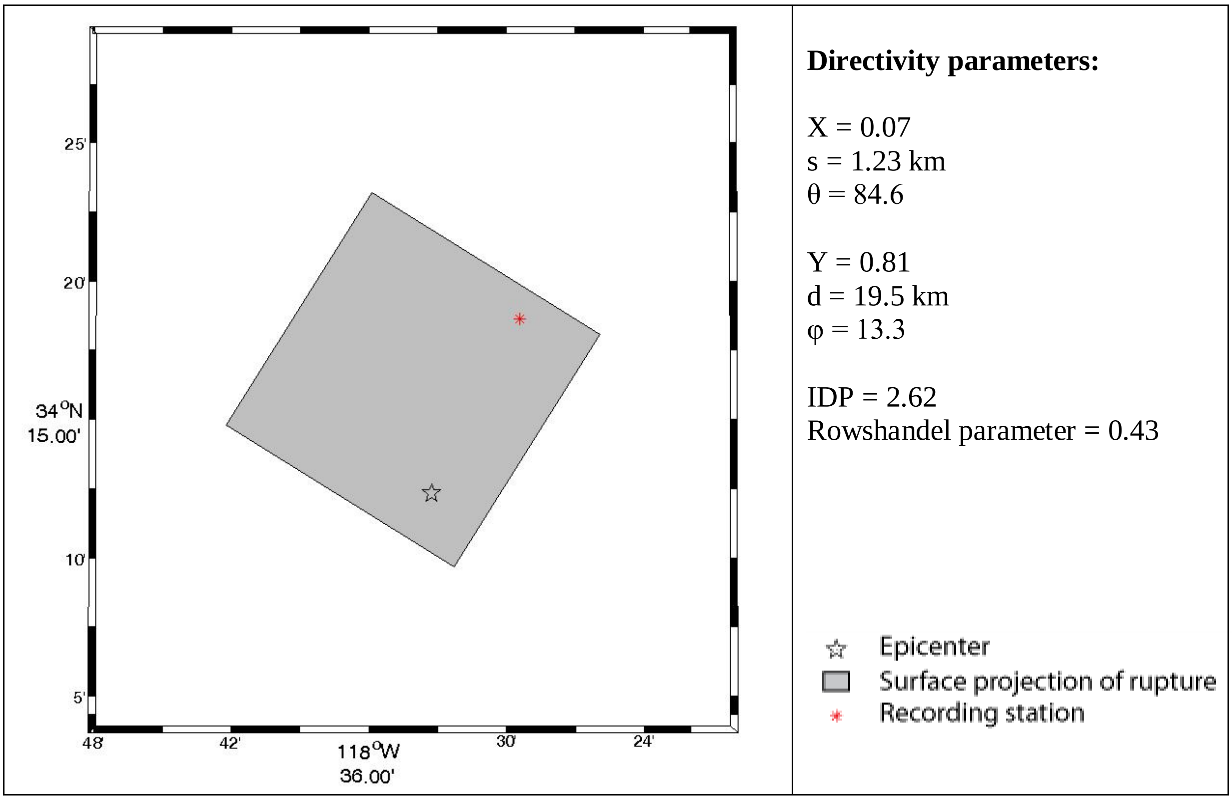

Directivity parameters:

X = 0.07
s = 1.23 km
θ = 84.6

Y = 0.81
d = 19.5 km
φ = 13.3

IDP = 2.62
Rowshandel parameter = 0.43

Figure 48: Map of epicentre, rupture extent and station location for: Northridge 1994, Sylmar-Converter Station

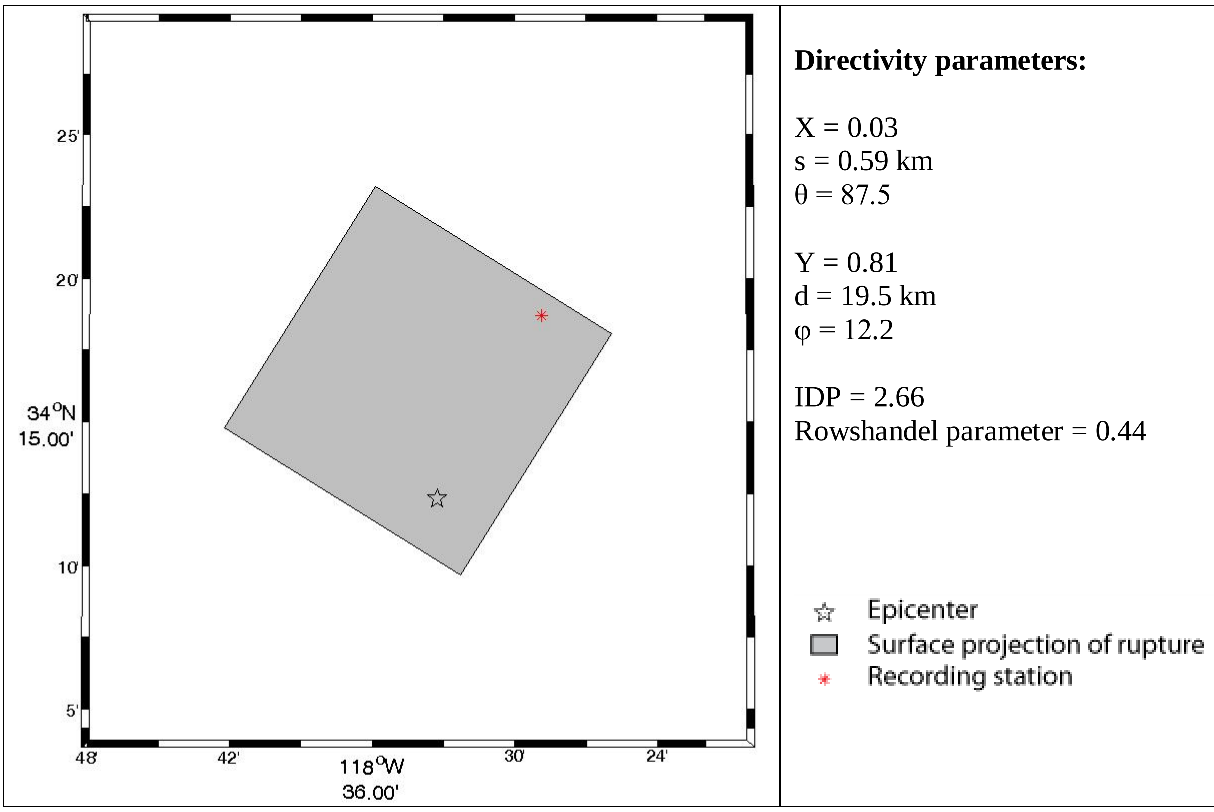

Directivity parameters:

X = 0.03
s = 0.59 km
θ = 87.5

Y = 0.81
d = 19.5 km
φ = 12.2

IDP = 2.66
Rowshandel parameter = 0.44

Figure 49: Map of epicentre, rupture extent and station location for: Northridge 1994, Jensen Filter Plant Station East

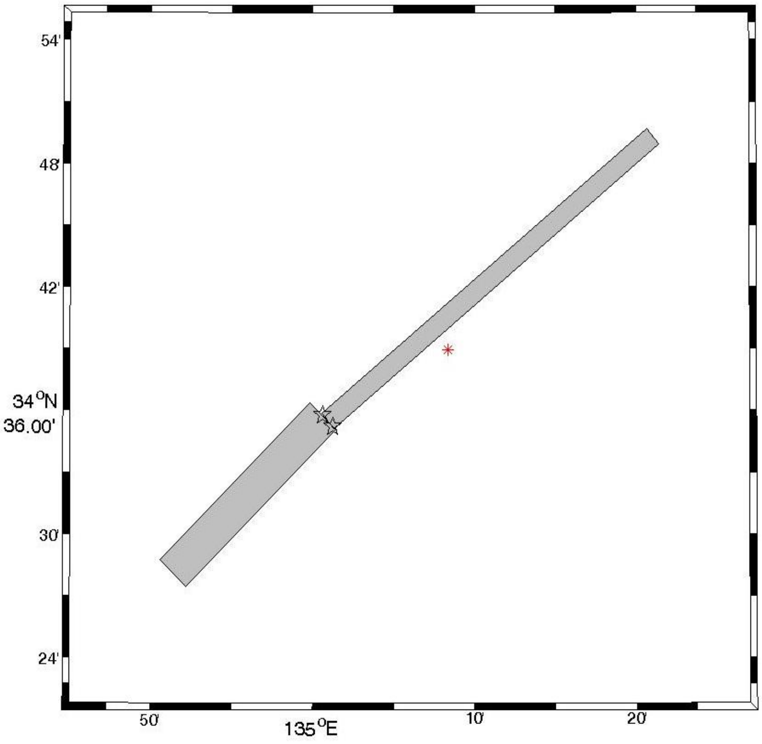

Directivity parameters:

X = 0.21
s = 12.81 km
θ = 13.3

Y = 0.87
d = 17.77 km
φ = 13.5

IDP = 1.65
Rowshandel parameter = -0.37

☆ Epicenter
Surface projection of rupture
* Recording station

Figure 50: Map of epicentre, rupture extent and station location for: 1995 Kobe, Japan, Takatori

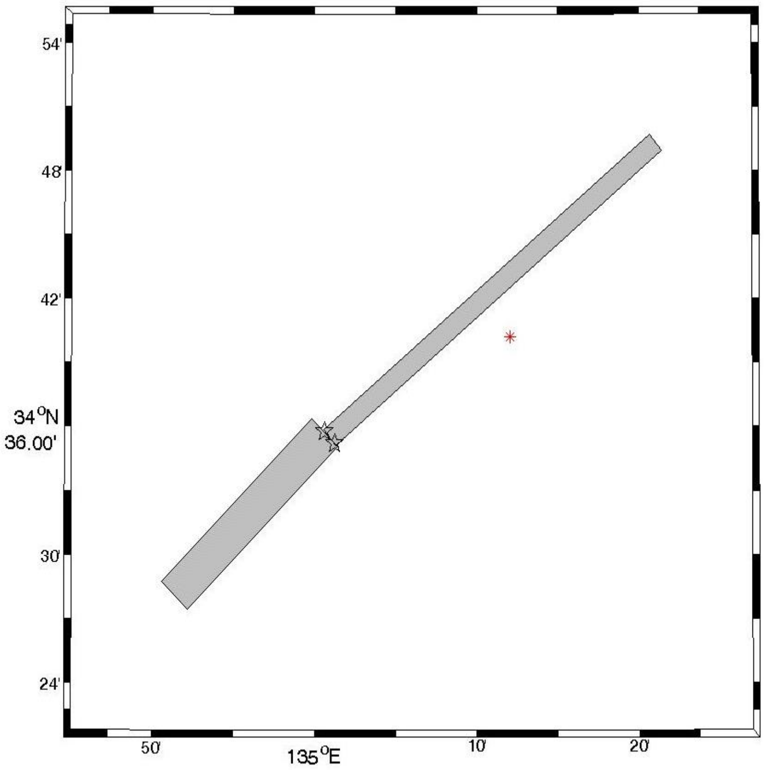

Directivity parameters:

X = 0.31
s = 18.66 km
θ = 14.6

Y = 0.86
d = 17.77 km
φ = 19.4

IDP = 2.04
Rowshandel parameter = -0.24

☆ Epicenter
Surface projection of rupture
* Recording station

Figure 51: Map of epicentre, rupture extent and station location for: 1995 Kobe, Japan, Port Island

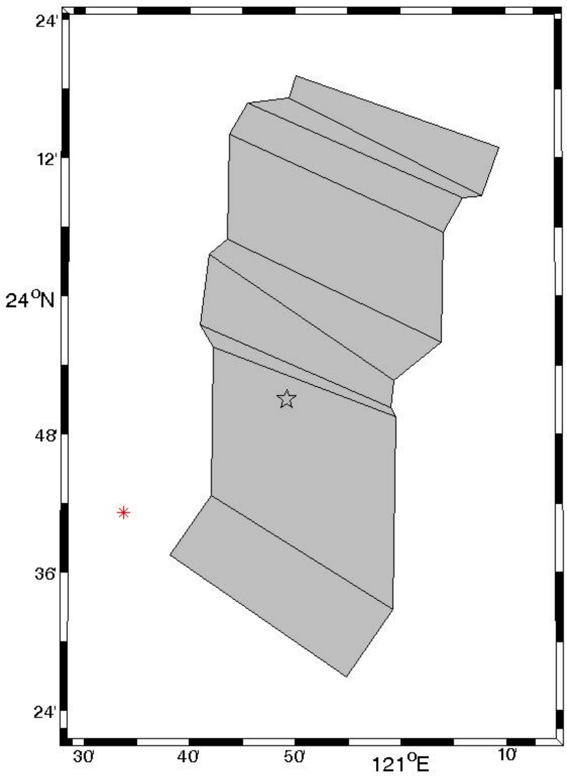

Directivity parameters:

X = 0.32
s = 29.51 km
θ = 58.7

Y = 0.3
d = 11.1 km
φ = 4.3

IDP = 0.46
Rowshandel parameter = -0.23

Figure 52: Map of epicentre, rupture extent and station location for: 1999 Chi-Chi, Taiwan, CHY101

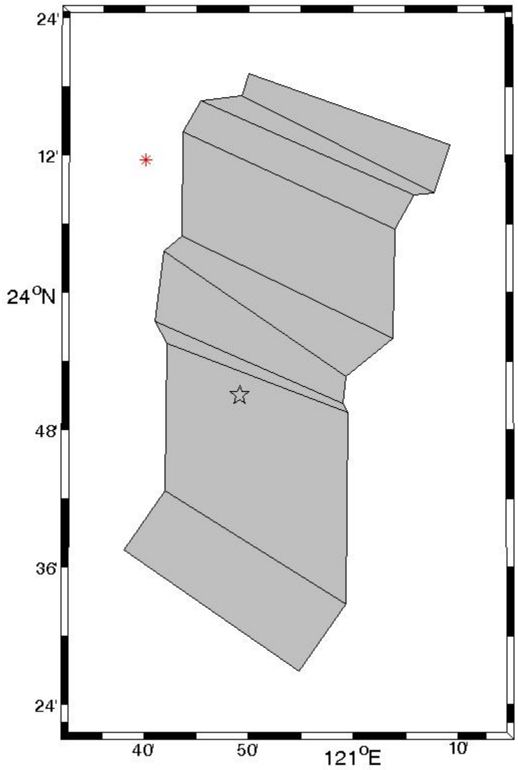

Directivity parameters:

X = 0.4
s = 36.16 km
θ = 43

Y = 0.4
d = 14.8 km
φ = 12.3

IDP = 3.17
Rowshandel parameter = 0.12

Figure 53: Map of epicentre, rupture extent and station location for: 1999 Chi-Chi, Taiwan, TCU053

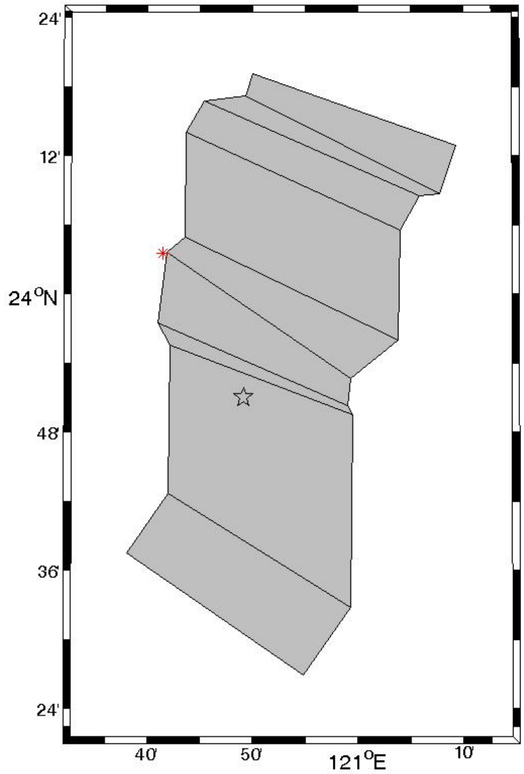

Directivity parameters:

X = 0.21
s = 19.53 km
θ = 44.9

Y = 0.38
d = 14.1 km
φ = 6

IDP = 2.55
Rowshandel parameter = -0.08

☆ Epicenter
Surface projection of rupture
* Recording station

Figure 54: Map of epicentre, rupture extent and station location for: 1999 Chi-Chi, Taiwan, TCU065

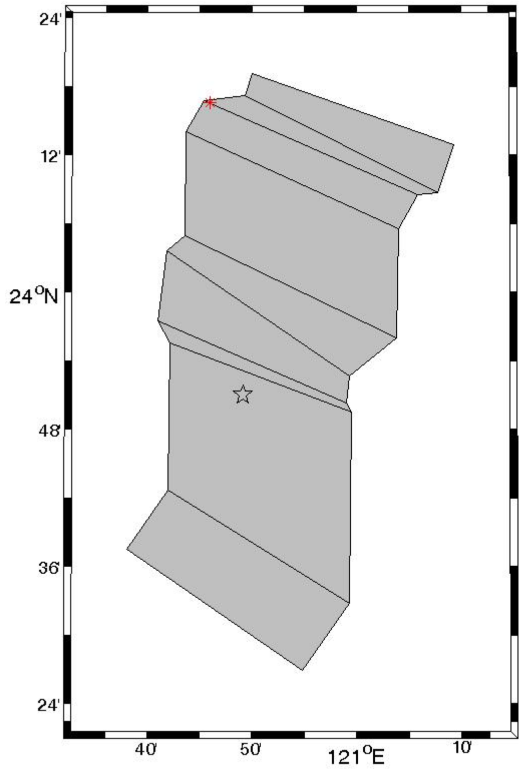

Directivity parameters:

X = 0.48
s = 43.78 km
θ = 34.5

Y = 0.39
d = 14.56 km
φ = 7

IDP = 2.94
Rowshandel parameter = 0.25

☆ Epicenter
Surface projection of rupture
* Recording station

Figure 55: Map of epicentre, rupture extent and station location for: 1999 Chi-Chi, Taiwan, TCU068

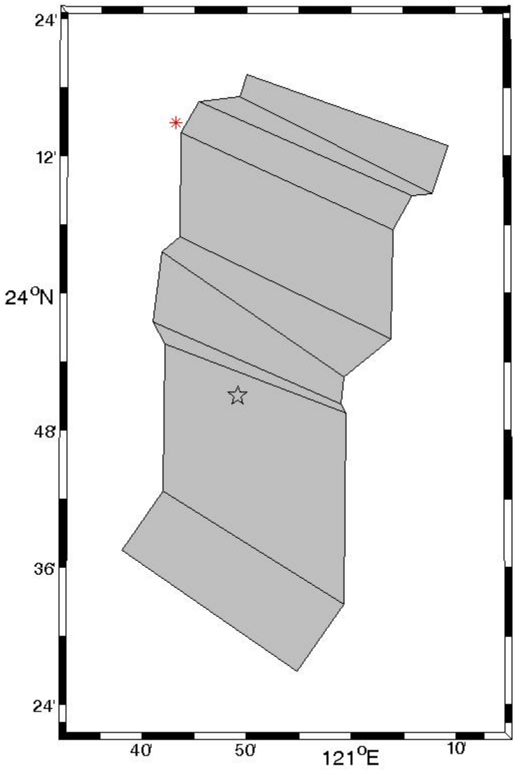

Directivity parameters:

X = 0.43
s = 39.24 km
θ = 34.9

Y = 0.4
d = 14.8 km
φ = 10.1

IDP = 2.96
Rowshandel parameter = 0.2

☆ Epicenter
Surface projection of rupture
* Recording station

Figure 56: Map of epicentre, rupture extent and station location for: 1999 Chi-Chi, Taiwan, TCU102

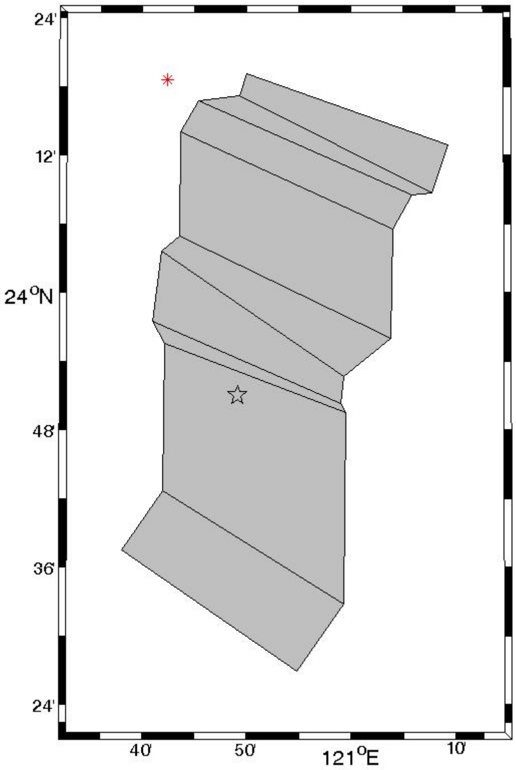

Directivity parameters:

X = 0.49
s = 44.16 km
θ = 40

Y = 0.4
d = 14.8 km
φ = 12.7

IDP = 3.11
Rowshandel parameter = 0.26

☆ Epicenter
Surface projection of rupture
* Recording station

Figure 57: Map of epicentre, rupture extent and station location for: 1999 Chi-Chi, Taiwan, TCU103

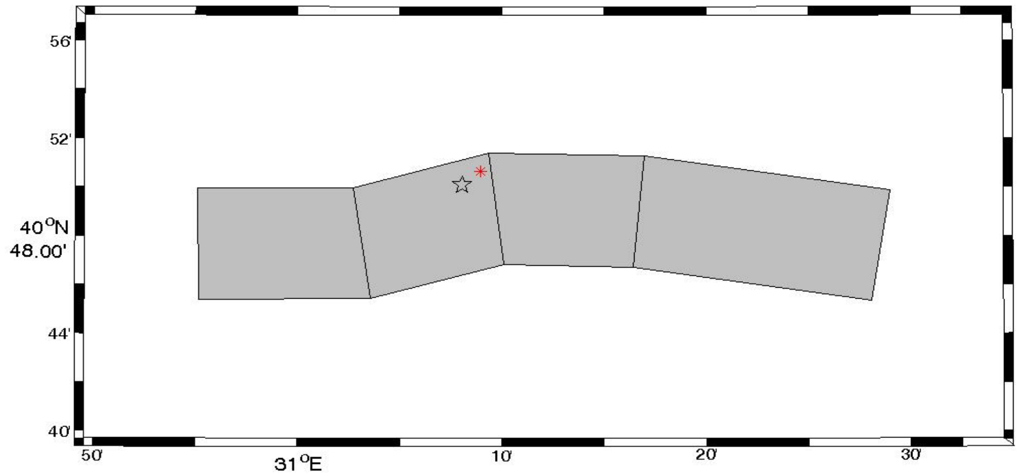

Directivity parameters:

X = 0.03
s = 1.45 km
θ = 25.3

Y = 0.62
d = 12.34 km
φ = 37.5

IDP = 0.58
Rowshandel parameter = -0.58

☆ Epicenter
Surface projection of rupture
* Recording station

Figure 58: Map of epicentre, rupture extent and station location for: 1999 Duzce, Turkey, Duzce

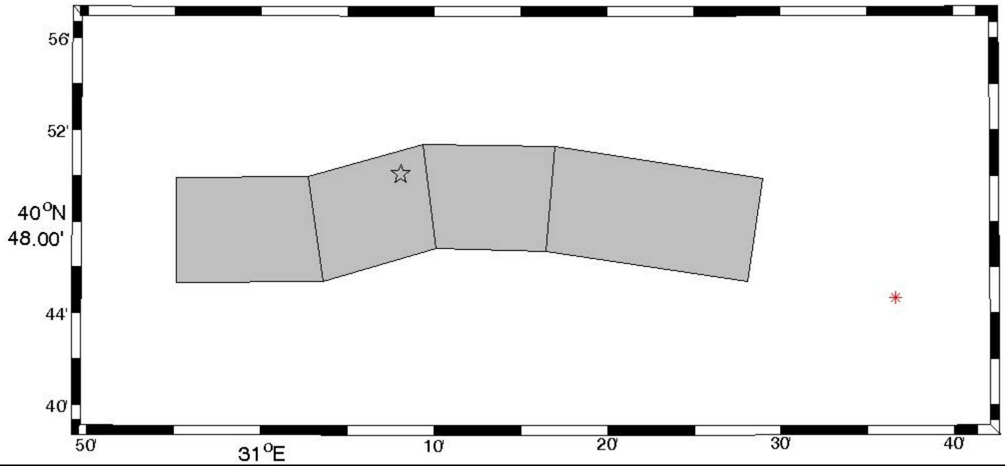

Directivity parameters:

X = 0.61
s = 29.34 km
θ = 14.4

Y = 0.77
d = 15.38 km
φ = 4.8

IDP = 3.1
Rowshandel parameter = 0.14

☆ Epicenter
Surface projection of rupture
* Recording station

Figure 59: Map of epicentre, rupture extent and station location for: 1999 Duzce, Turkey, Bolu

5.1 Displacement response spectra and spectral displacements

The displacement response spectrum is produced for each one of the ground motions, considering a damping ratio of 5% and period values up to 3 sec. Figures 60 to 66 present the displacement response spectra of the above seismic records, while Table 22 provides the corresponding spectral displacements (S_d) for the fundamental eigenperiod of the 8-storey building (T_1 = 1.165sec), as obtained from the corresponding response spectra. The peak ground accelerations (PGA) for the various seismic records are also provided in Table 22.

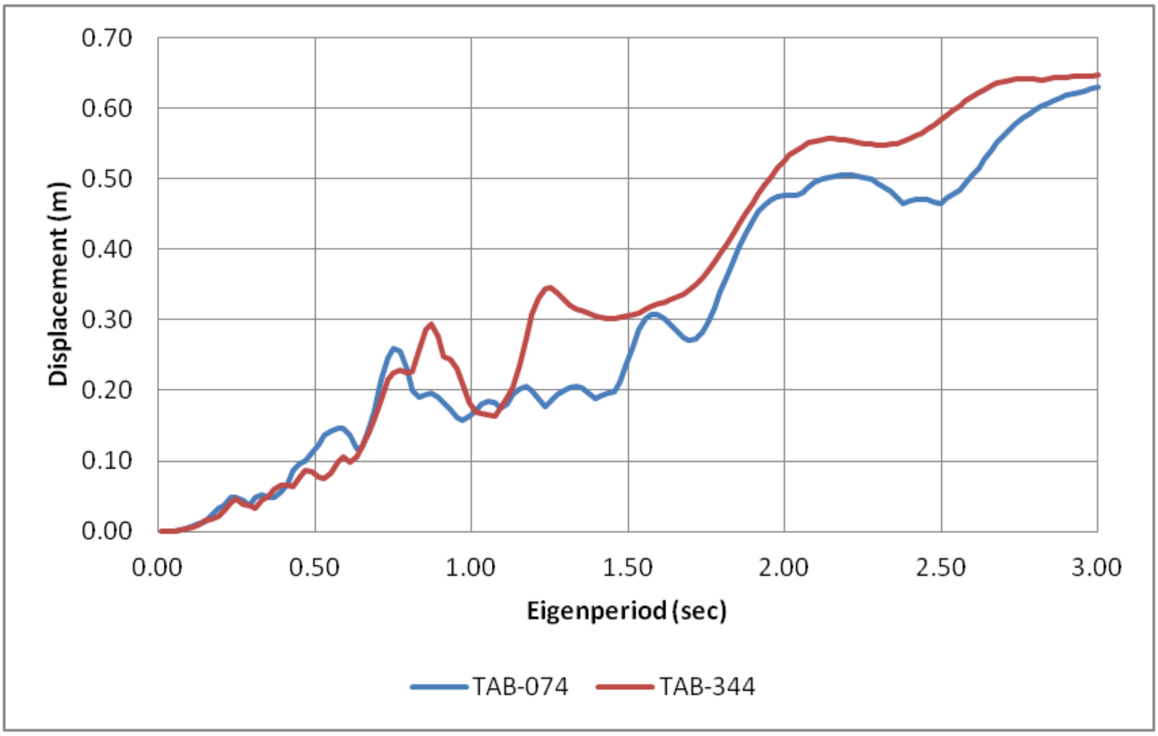

Figure 60: Displacement response spectrum of the seismic records of Tabas (Iran) Earthquake

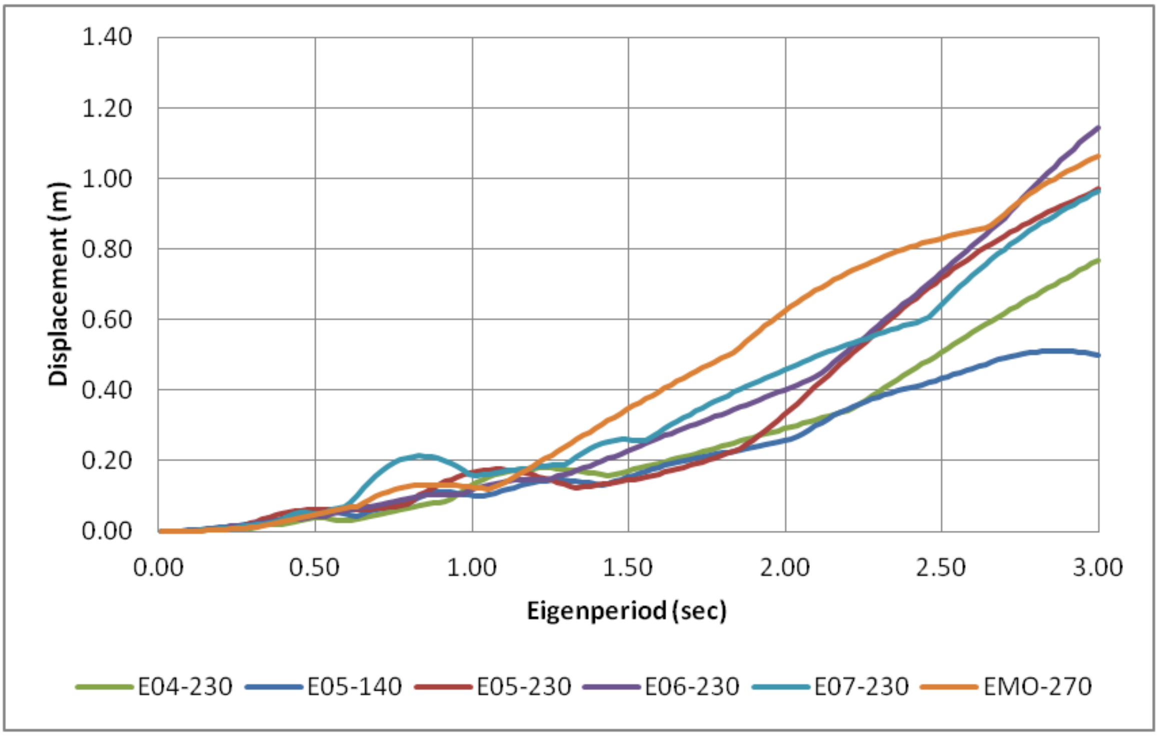

Figure 61: Displacement response spectrum of the seismic records of Imperial Valley Earthquake

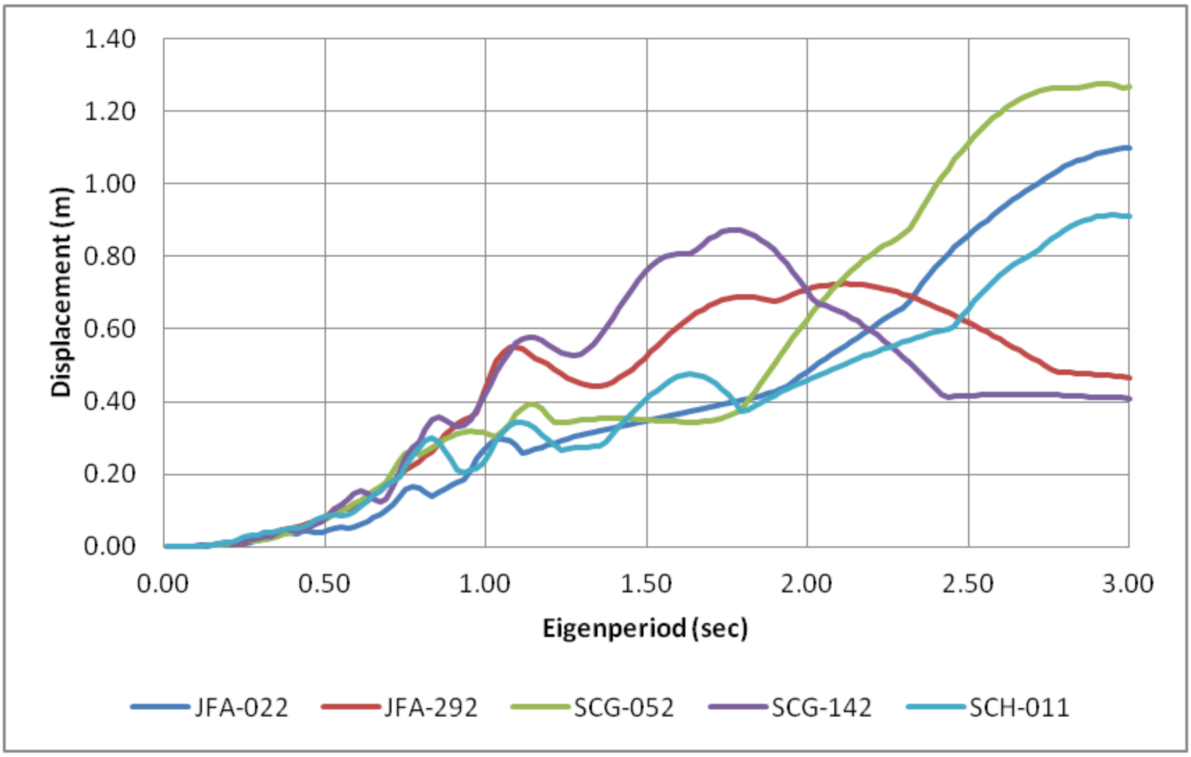

Figure 62: Displacement response spectrum of the seismic records of Northridge Earthquake

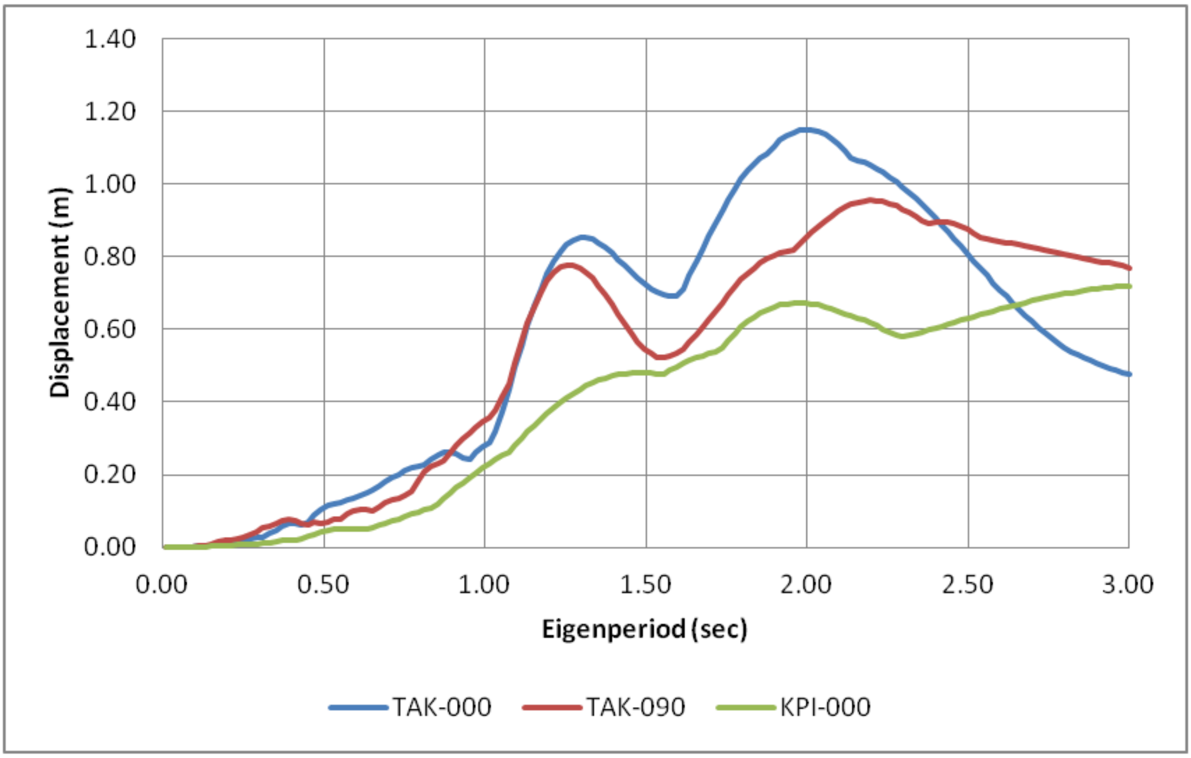

Figure 63: Displacement response spectrum of the seismic records of Kobe Earthquake

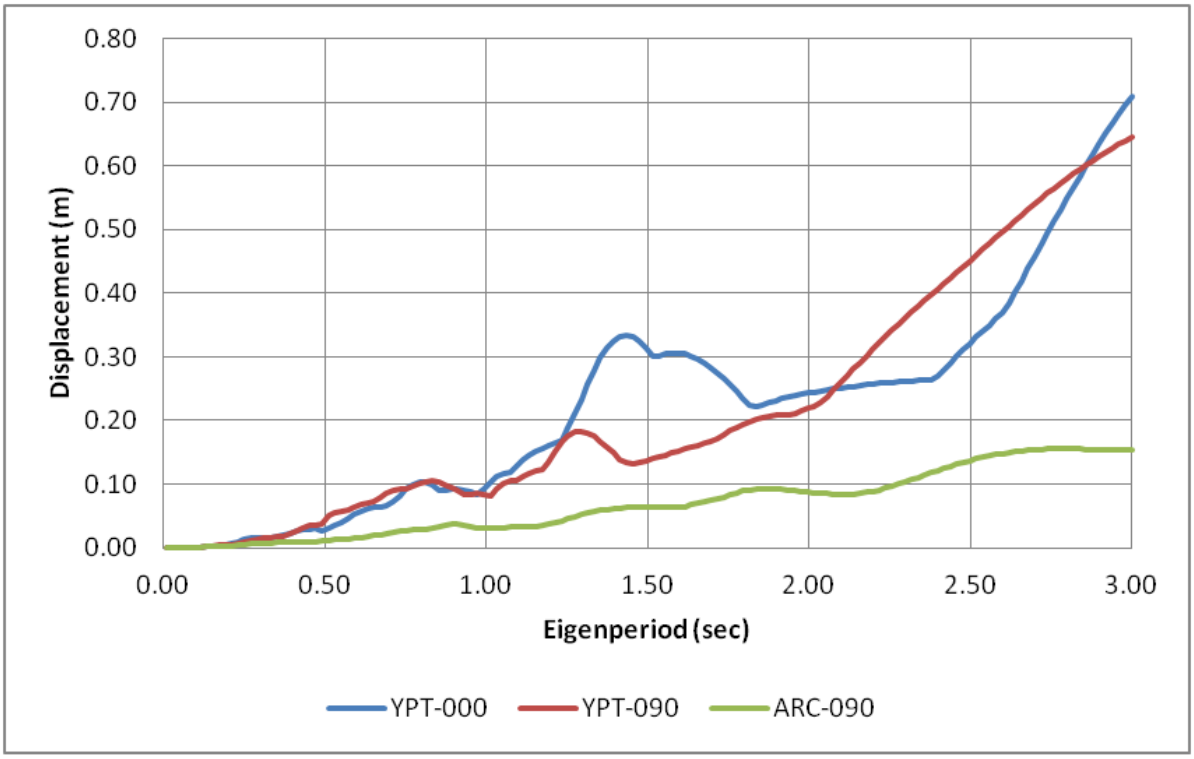

Figure 64: Displacement response spectrum of the seismic records of Izmit (Turkey) Earthquake

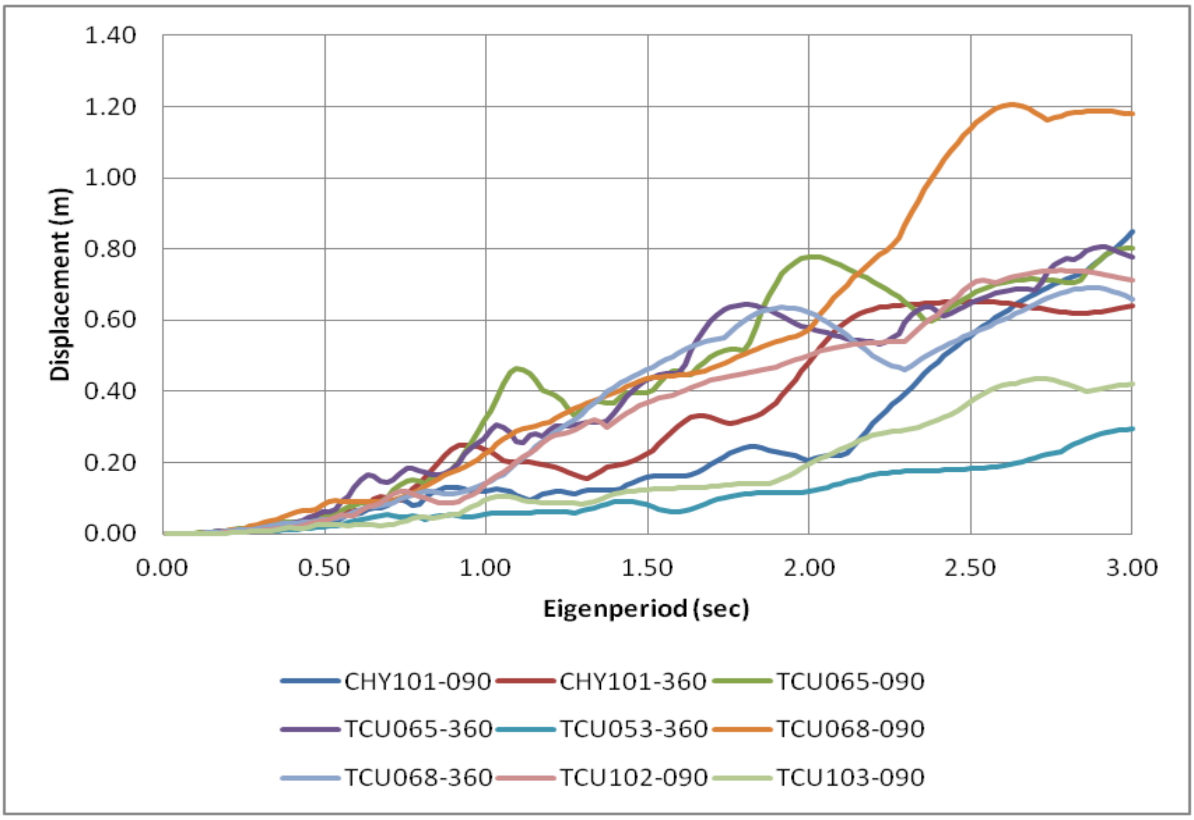

Figure 65: Displacement response spectrum of the seismic records of Chi-Chi (Taiwan) Earthquake

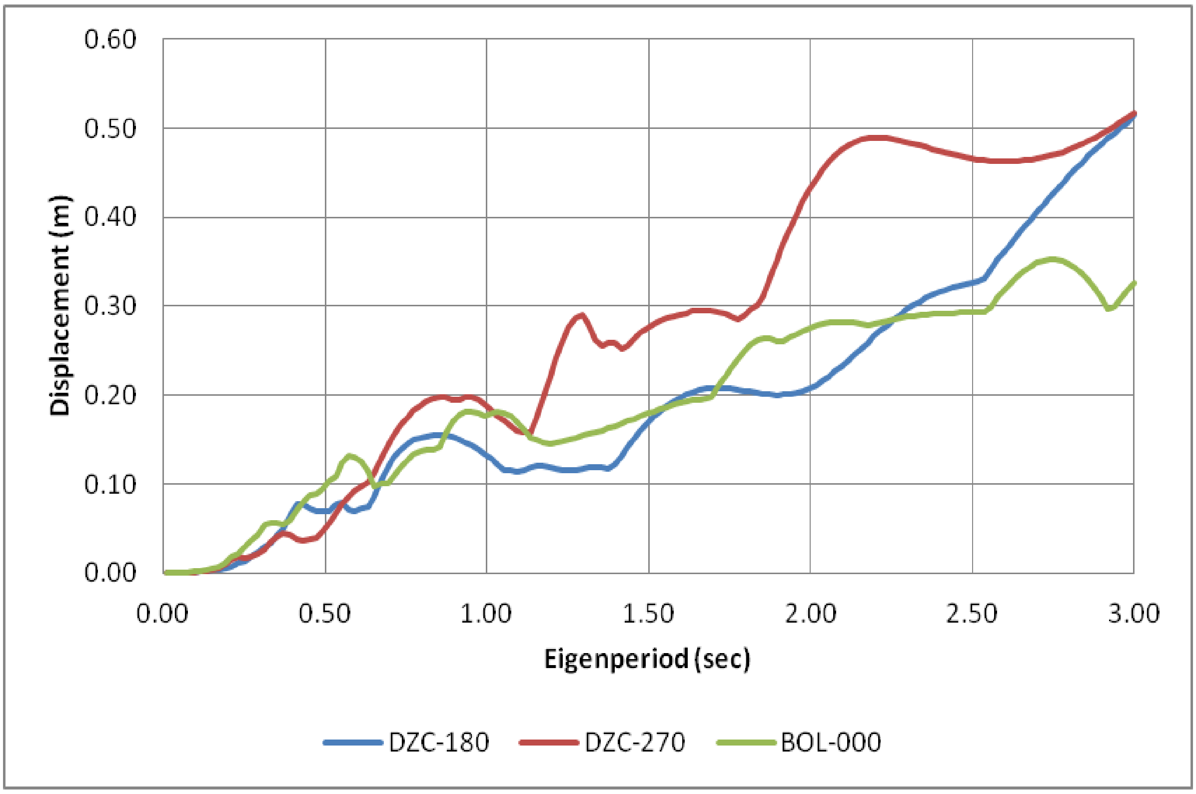

Figure 66: Displacement response spectrum of the seismic records of Duzce (Turkey) Earthquake

Table 22: Peak ground accelerations of the seismic records and spectral displacements that correspond to the fundamental period of the 8-storey building

#	LOCATION	STATION	COMP.	PGA [m/sec^2]	Sd (T=1.165sec) [m]
1	Tabas, Iran	Tabas (TAB)	74 – 344	8.36 – 8.20	0.2038 – 0.2519
2	Imperial Valley, CA,USA	El Centro Array 4, Anderson Rd (E04)	230	3.75	0.1759
		El Centro Array 5, James Rd (E05)	140 – 230	5.49 – 3.82	0.1307 – 0.1667
		El Centro Array 6, Huston Rd (E06)	230	4.52	0.1473
		El Centro Array 7, Imperial Val. Cl (E07)	230	4.68	0.1772
		Meloland Route Overpass (EMO)	270	3.68	0.1684
3	Northridge, CA, USA	Jensen Filtration Plant (JFA)	22 – 292	4.08 – 6.20	0.2711 – 0.5174
		Sylmar Converter Station (SCG)	52 – 142	5.93 – 7.39	0.3864 – 0.5729
		Sylmar Converter Station East (SCH)	11	8.15	0.3180
4	Hanshin (Kobe), Japan	Takatori (TAK)	0 – 90	5.99 – 6.04	0.6845 – 0.6796
		Kobe Port Island,Surface (KPI)	0	3.09	0.3434
5	Izmit, Turkey	Yarimca Petkim (YPT)	0 - 270	3.50 – 2.63	0.1533 – 0.1219
		Arcelik Arge Lab (ARC)	270	1.49	0.0349
6	Chi-Chi, Taiwan	CHY101	90 – 360	3.46 – 4.32	0.1051 – 0.1981

		TCU053	360	1.37	0.0602
		TCU065	90 – 360	7.99 – 5.92	0.4200 – 0.2775
		TCU068	90 – 360	5.55 – 4.53	0.3053 – 0.2522
		TCU102	90	2.92	0.2464
		TCU103	90	1.31	0.0889
7	Duzce, Turkey	Duzce (DZC)	180 – 270	3.41 – 5.25	0.1207 – 0.1855
		Bolu (BOL)	0	7.14	0.1483

5.2 Method for assessing the seismic damage (HAZUS)

According to HAZUS, the level of damage that a certain structure will have after a specific ground motion can be estimated using the fragility curves that correspond to the specific structure or type of structure. In the current case, have been produced the fragility curves in terms of the top-floor displacement, which correspond to the response of the particular 8-storey building (*HAZUS – Umax method*).

5.2.1 Damage assessment using the building's top-floor displacement (Method HAZUS – Umax)

According to this method, the level of structural damage under a specific ground motion is assessed using the fragility curves, in terms of top-floor displacement (see Figure 41), and the value of the maximum absolute top-floor displacement of the building. The later can be obtained from the dynamic analysis of the structure, subjected to the specific ground motion. Table 23 provides the various structural damage states as a function of the relationship between the top-floor displacement and the mean values (damage limit states) of the fragility curves of Figure 41 (Table 20).

Table 23: Characterisation of overall structural damage, based on top-floor displacement and its relation to the various damage limits, as defined in the corresponding fragility curves ("*HAZUS-Umax method"*).

Damage state	Condition
PRE-YIELDING	$\max\lvert U_{x,\,Top}\rvert < 0.0545$ m
SLIGHT	0.0545 m $< \max\lvert U_{x,\,Top}\rvert < 0.0981$ m
MODERATE	0.0981 m $< \max\lvert U_{x,\,Top}\rvert < 0.3270$ m
EXTENSIVE	0.3270 m $< \max\lvert U_{x,\,Top}\rvert < 0.6540$ m
COMPLETE	$\max\lvert U_{x,\,Top}\rvert > 0.6540$ m

5.3 Time-history analysis

The considered building was subjected to non-linear time-history analysis, using the above near-fault ground-motion records and the SAP2000 software. The same building model with the same properties of the frame hinges were considered as in the case of push-over analysis. P-Delta effects and large displacements were also taken into account in the analyses, while the Hilber-Hughes-Taylor direct integration method was employed. In total, 31 dynamic analyses were performed, using the 31 ground acceleration recordings and applying them in the X-direction of the structural axes of the building. From each analysis, the maximum absolute displacement at the top-floor of the building (at joint 340) and the damage statuses of the hinge properties are obtained.

5.3.1 Damage assessment based on hinges damage states ("Observation method")

When performing non-linear time-history analysis in SAP2000, the damage state of the building under a certain ground-motion can be defined based on the location and the damage states of the individual frame hinges, as formed after the end of the corresponding analysis. In particular, the hinges undergoing the various damage states are printed in different colours in SAP2000, as described in previous, enabling the user to make a visual estimation of the overall performance of the simulated structure under the specific earthquake record. The estimation of the damage state of the structure after an earthquake is performed based on guidelines provided in Table 24. The guidelines are based on the observed response of the building under the push-over analysis and specifically on the observed damage at each damage limit state, as shown in Figures 37-40.

Table 24: General guidelines for the characterisation of the structural damage, based on the observations of hinges statuses from time-history analysis

<table>
<tr><th>Condition</th><th>Damage state</th></tr>
<tr><td>No yielding occurs</td><td>PRE-YIELDING</td></tr>
<tr><td>Beams have yielded at lower floors</td><td>SLIGHT</td></tr>
<tr><td>Beams have yielded at lower and upper floors</td><td rowspan="2">MODERATE</td></tr>
<tr><td>Columns at Y=11m have yielded</td></tr>
<tr><td>Beams have failed at lower floors</td><td rowspan="4">EXTENSIVE</td></tr>
<tr><td>Ground-floor columns have passed the LS limit at their base</td></tr>
<tr><td>Some columns have yielded at middle floors</td></tr>
<tr><td>Some columns have failed at Y=11m</td></tr>
<tr><td>Significant number of beams at lower floors have failed</td><td rowspan="2">COMPLETE</td></tr>
<tr><td>All ground-floor columns have failed at their base</td></tr>
</table>

5.3.2 Results from time-history analyses

The elevations of the five frames of the building in the X-direction with the resulting damage on element hinges, displayed in various colours, are provided in Figures 67 to 97 for each one of the considered seismic records. The name of the record, the maximum absolute top-floor displacement, a short description of the observed damage and the corresponding damage state, according to Table 24 ("*Observation method*"), are also provided. In addition, for more easy comparison with the "*HAZUS – Umax method*", a graph with the fragility curves of the building, where its top-floor displacement under the corresponding ground motion is indicated, is also provided in each figure.

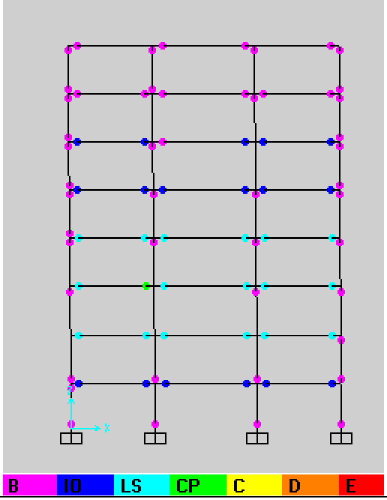

@Y=0.00m

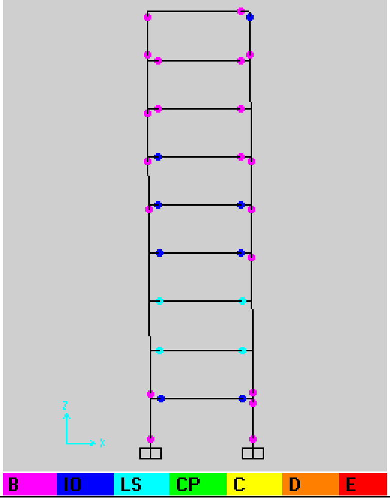

@Y=7.20m

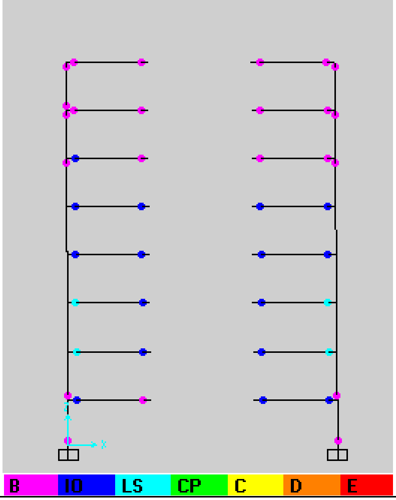

@Y=8.90m

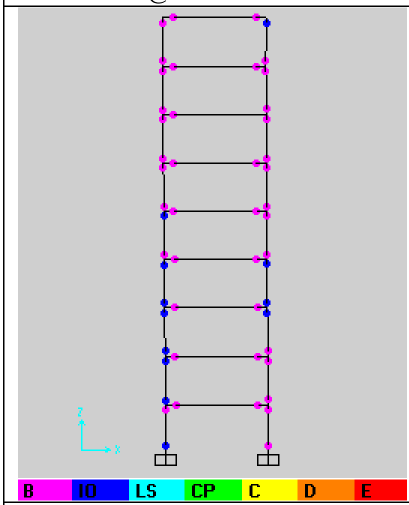

@Y=11.00m

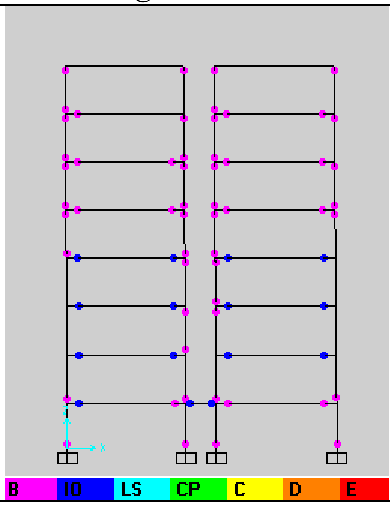

@Y=16.00m

Record: TAB-074

Max abs $Ux_{,Top} = 0.2618$ m

Estimated damage state:
MODERATE

Description:

- Yielding at lower & upper floors
- No failures

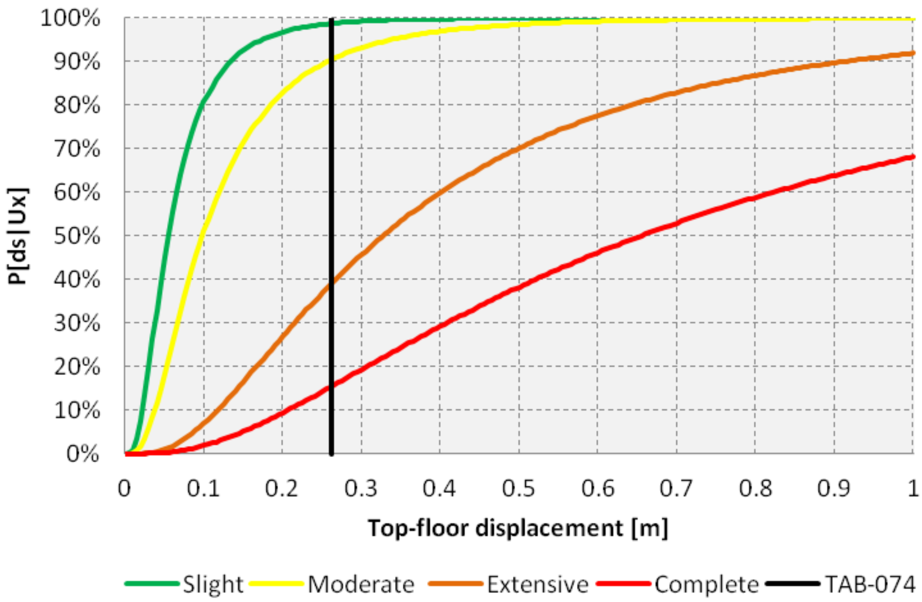

Figure 67: Damage due to the TAB-074 component of the Tabas, Iran (1978) earthquake

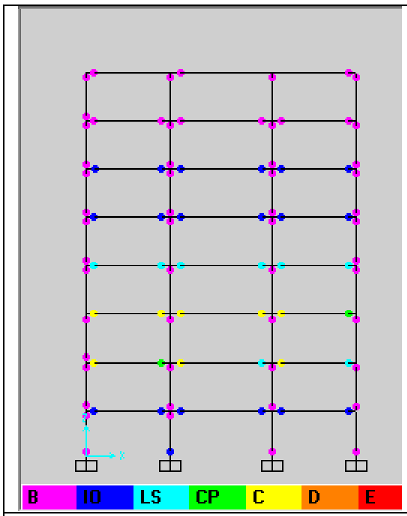

@Y=0.00m

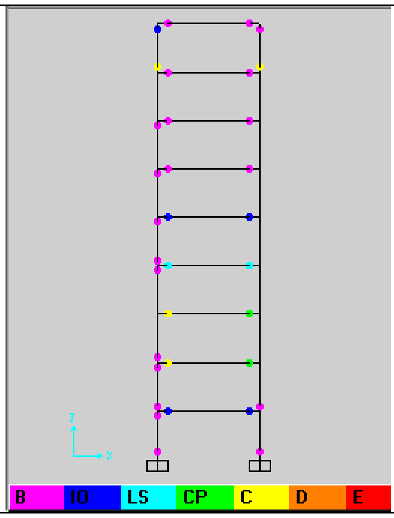

@Y=7.20m

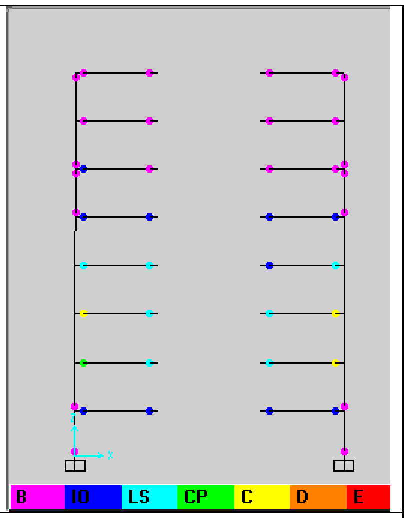

@Y=8.90m

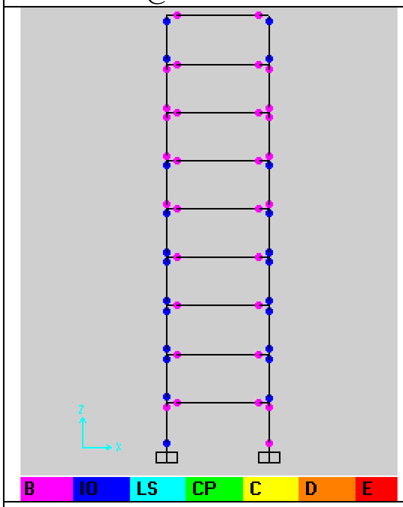

@Y=11.00m

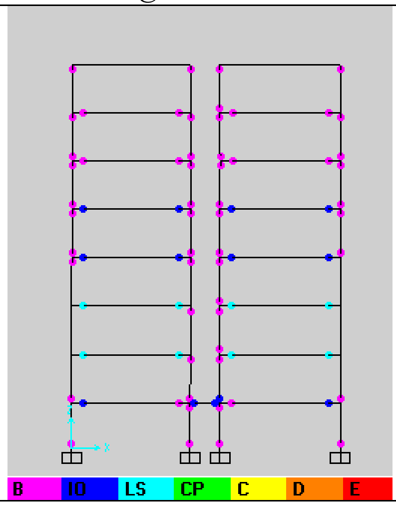

@Y=16.00m

Record: TAB-344

Max abs $Ux_{,Top}$ = 0.3012 m

Estimated damage state:
EXTENSIVE

Description:

- Columns yielded at middle floors
- Failure at some beams

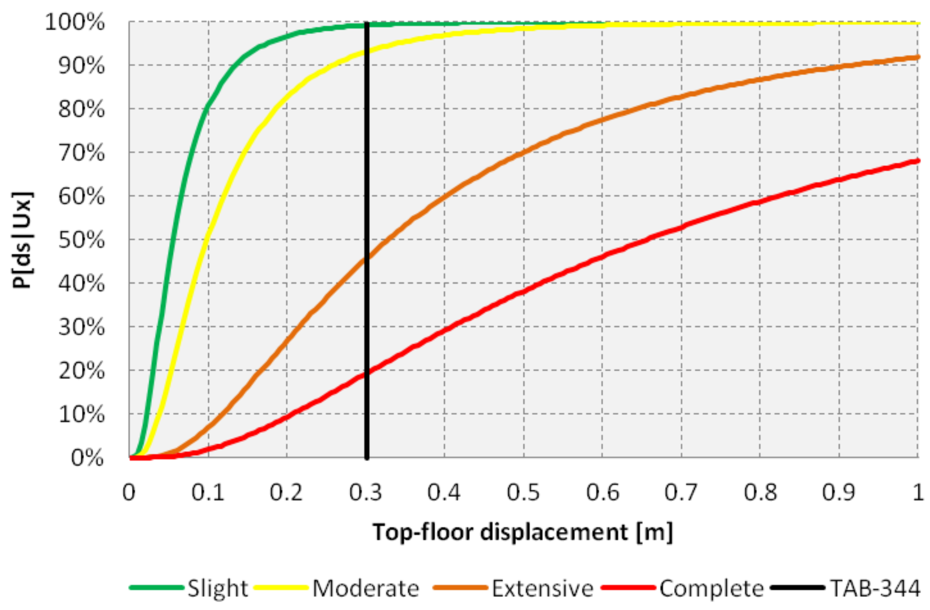

Figure 68: Damage due to the TAB-344 component of the Tabas, Iran (1978) earthquake

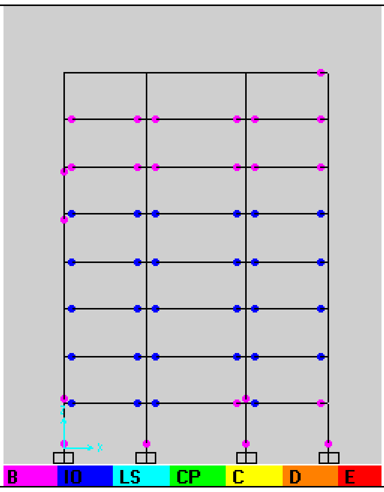

@Y=0.00m

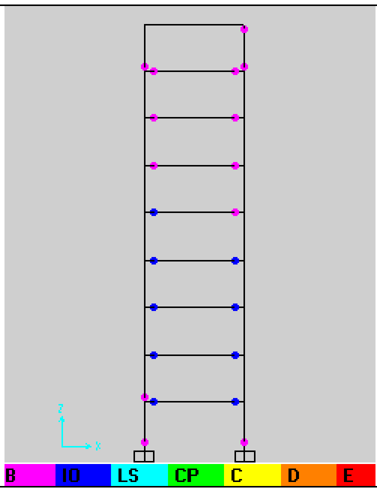

@Y=7.20m

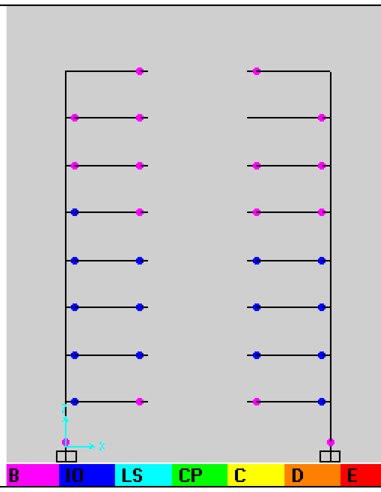

@Y=8.90m

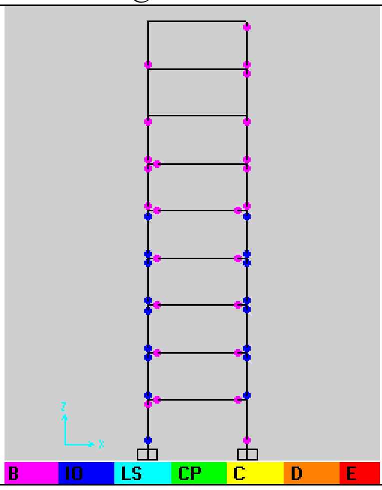

@Y=11.00m

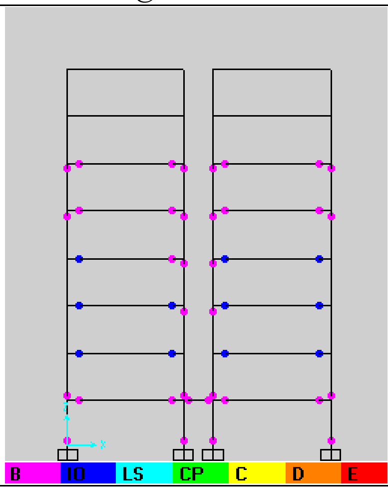

@Y=16.00m

Record: E04-230

Max abs $Ux_{,Top}$ = 0.2192 m

Estimated damage state:
MODERATE

Description:

- Yielding at lower & upper floors
- No failures

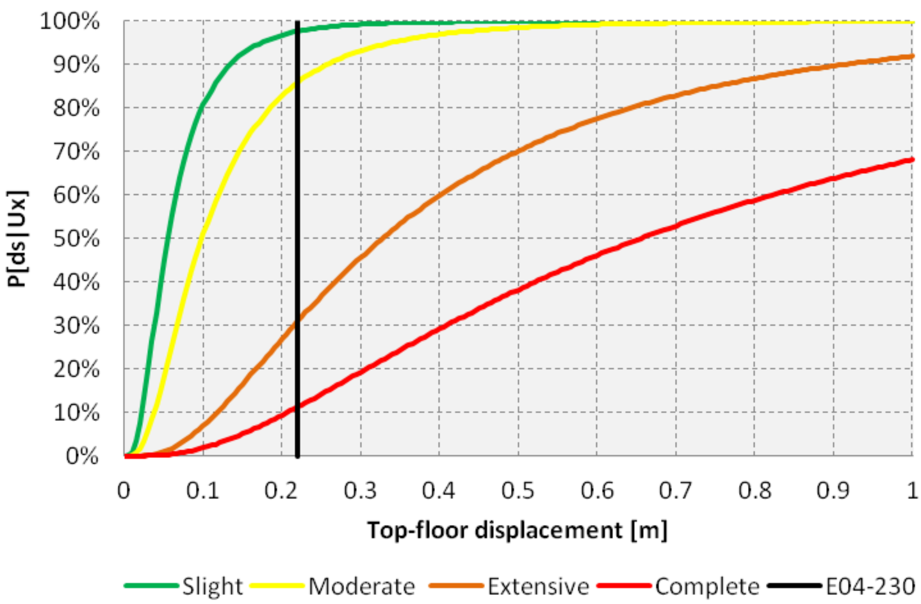

Figure 69: Damage due to the E04-230 component of the Imperial Valley, CA, USA (1979) earthquake

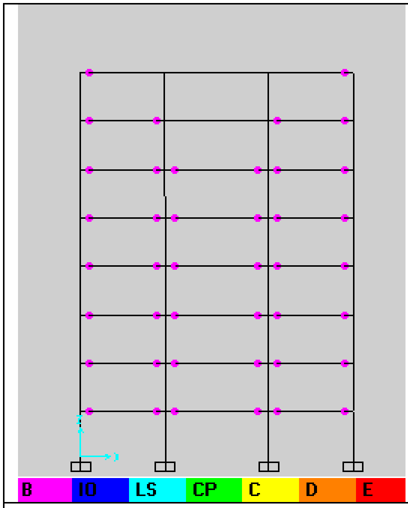

@Y=0.00m

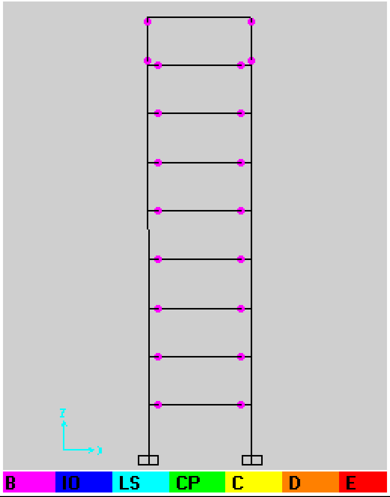

@Y=7.20m

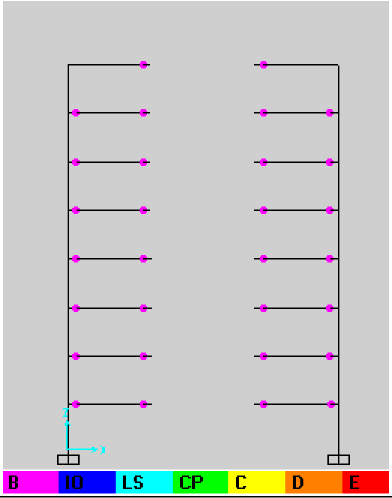

@Y=8.90m

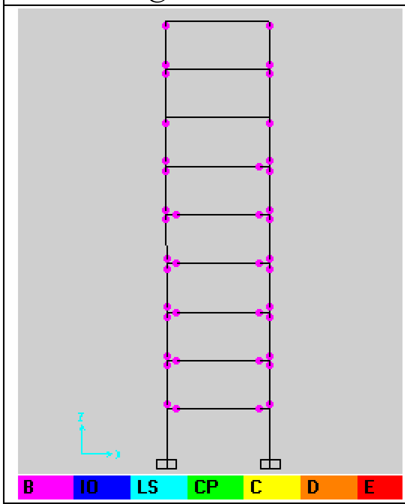

@Y=11.00m

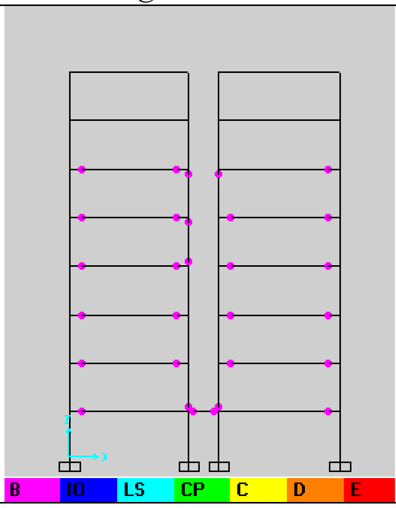

@Y=16.00m

Record: E05-140

Max abs $Ux,_{Top}$ = 0.1168 m

Estimated damage state:
MODERATE

Description:

- Yielding at lower & upper floors
- No failures

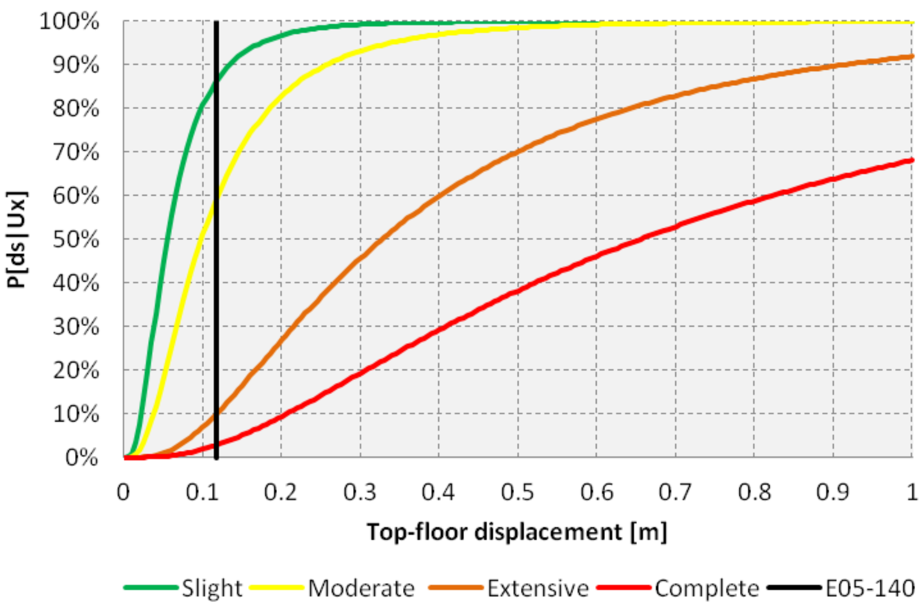

Figure 70: Damage due to the E05-140 component of the Imperial Valley, CA, USA (1979) earthquake

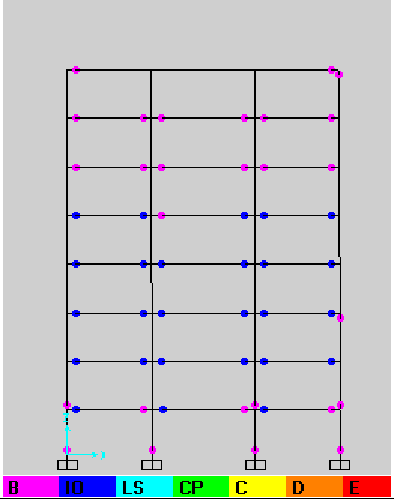

@Y=0.00m

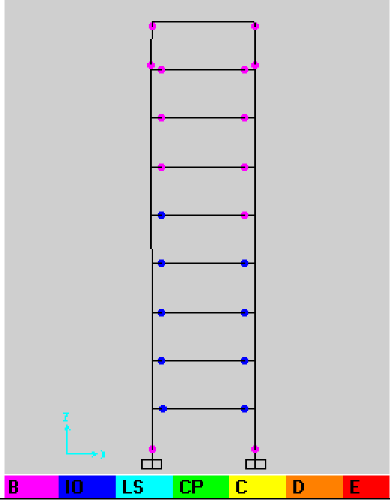

@Y=7.20m

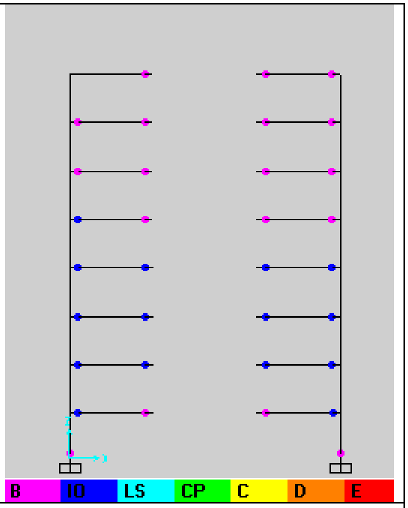

@Y=8.90m

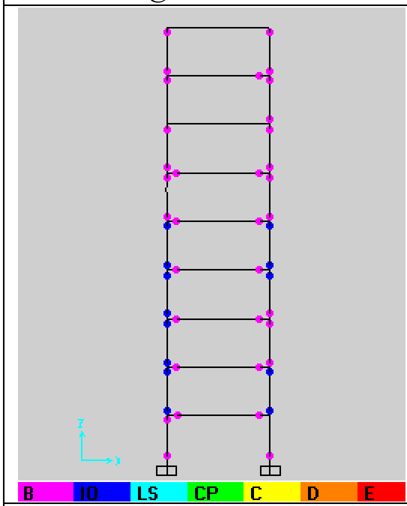

@Y=11.00m

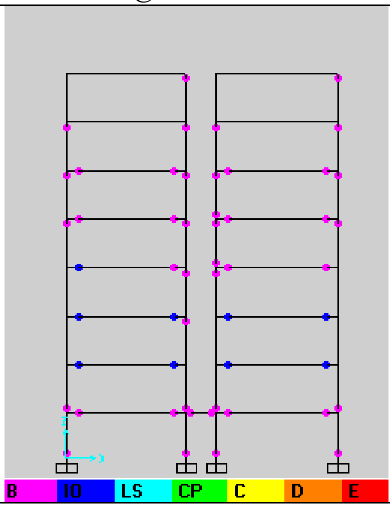

@Y=16.00m

Record: E05-230

Max abs $Ux_{,Top}$ = 0.2069 m

Estimated damage state:
MODERATE

Description:

- Yielding at lower & upper floors
- No failures

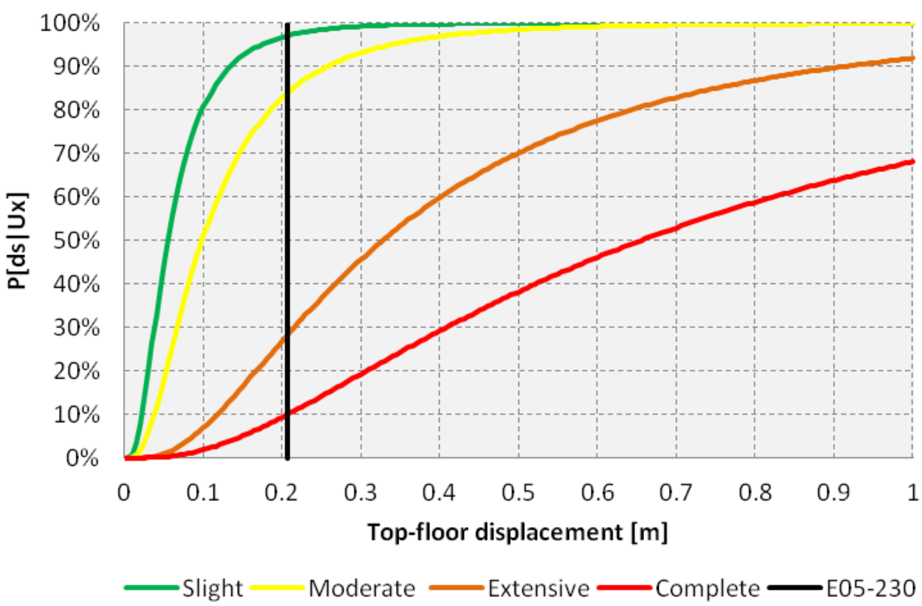

Figure 71: Damage due to the E05-230 component of the Imperial Valley, CA, USA (1979) earthquake

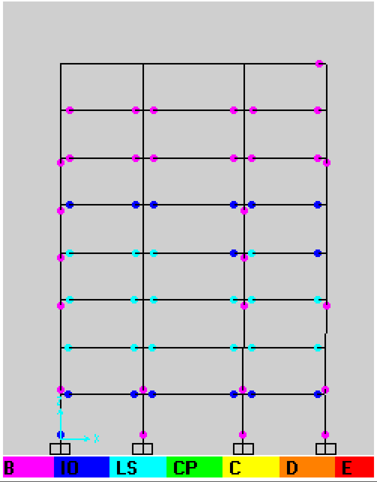

@Y=0.00m

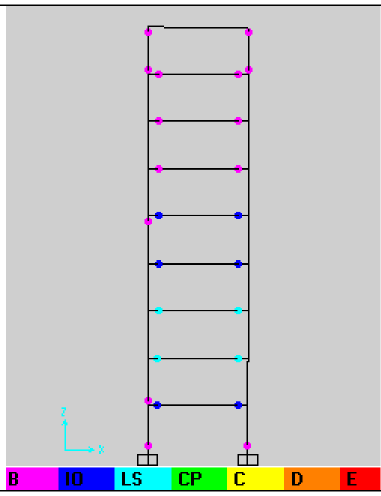

@Y=7.20m

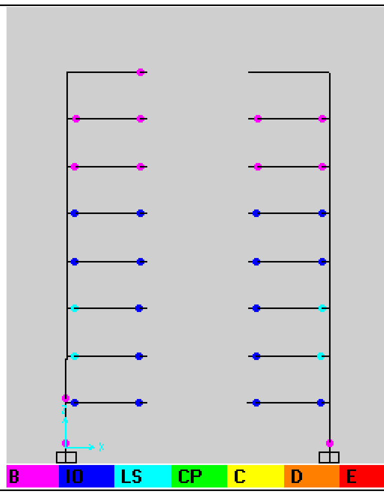

@Y=8.90m

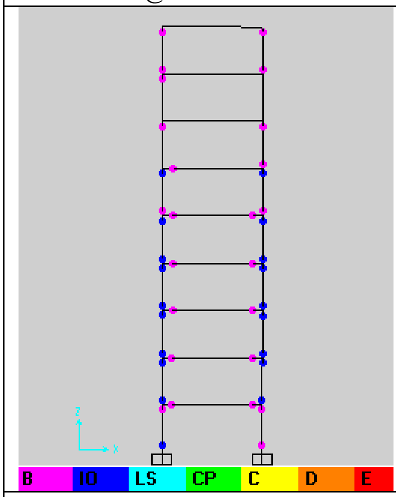

@Y=11.00m

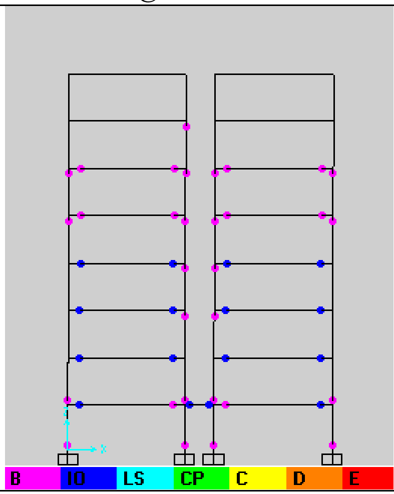

@Y=16.00m

Record: E06-230

Max abs $Ux_{,Top}$ = 0.2669 m

Estimated damage state:
MODERATE

Description:

- Yielding at lower & upper floors
- No failures

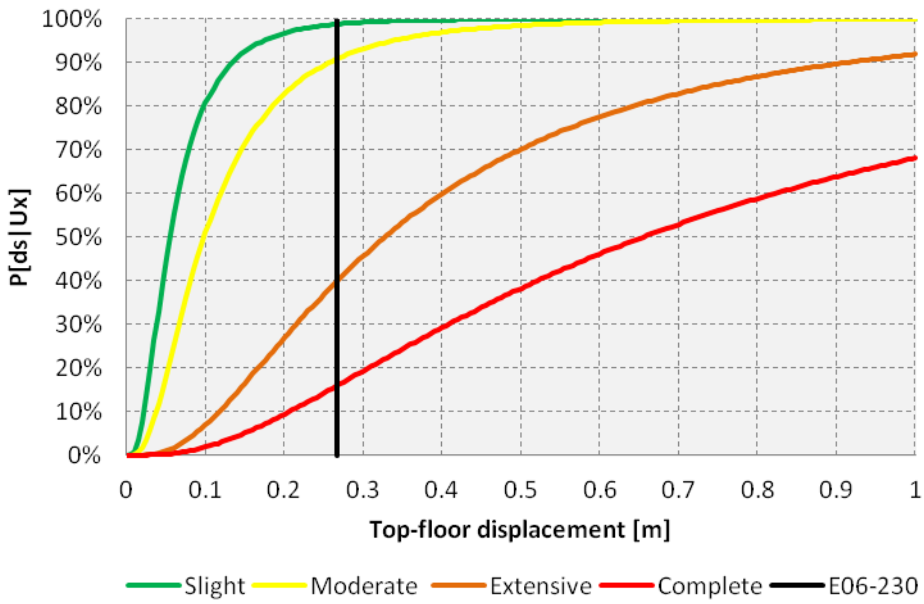

Figure 72: Damage due to the E06-230 component of the Imperial Valley, CA, USA (1979) earthquake

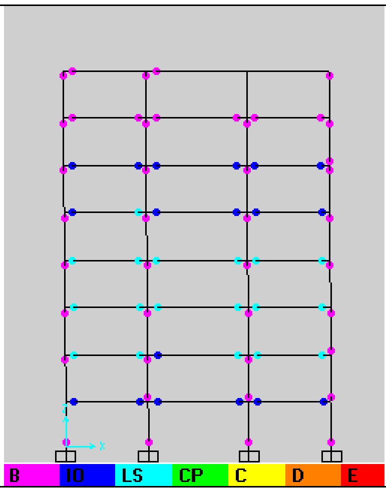

@Y=0.00m

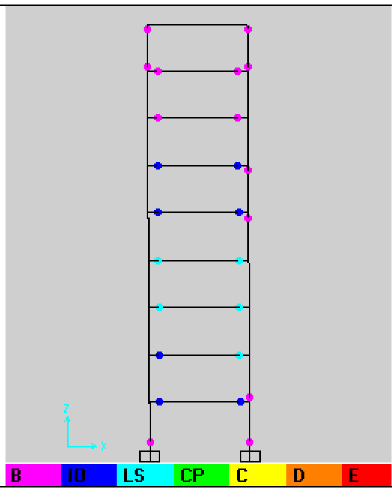

@Y=7.20m

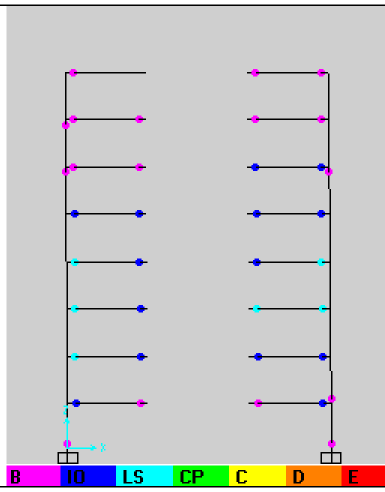

@Y=8.90m

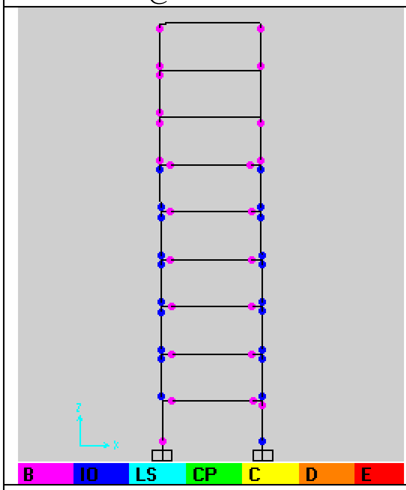

@Y=11.00m

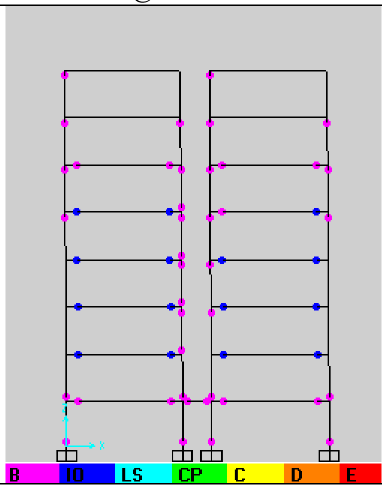

@Y=16.00m

Record: E07-230

Max abs $Ux_{,Top}$ = 0.29 m

Estimated damage state:
MODERATE

Description:

- Yielding at lower & upper floors
- No failures

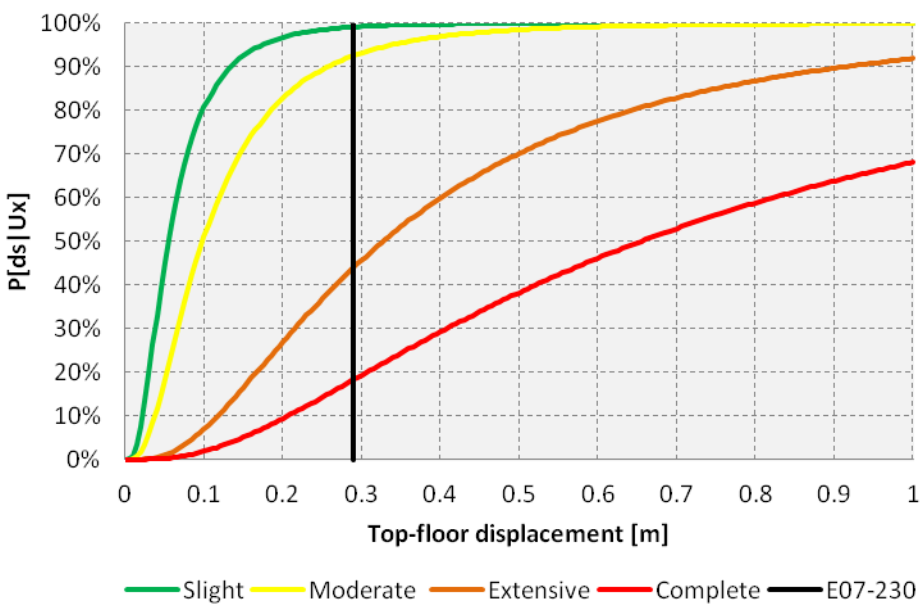

Figure 73: Damage due to the E07-230 component of the Imperial Valley, CA, USA (1979) earthquake

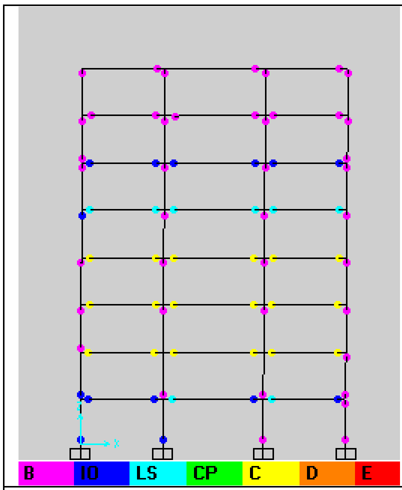

@Y=0.00m

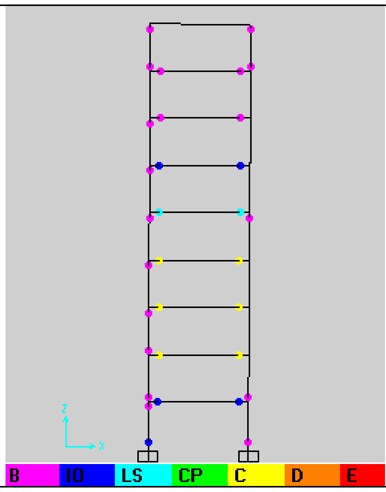

@Y=7.20m

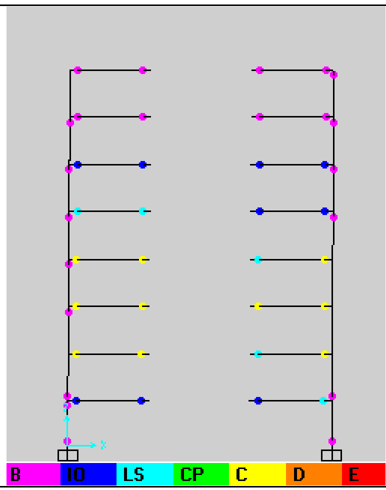

@Y=8.90m

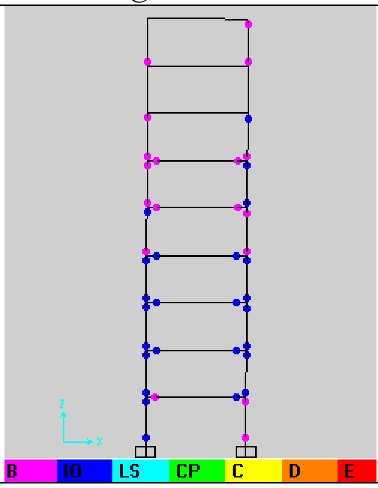

@Y=11.00m

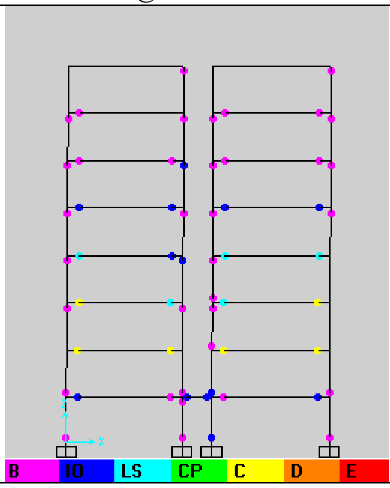

@Y=16.00m

Record: EMO-270

Max abs $Ux_{,Top}$ = 0.3714 m

Estimated damage state:
EXTENSIVE

Description:

- Failure at some beams
- Columns yielded at middle floors

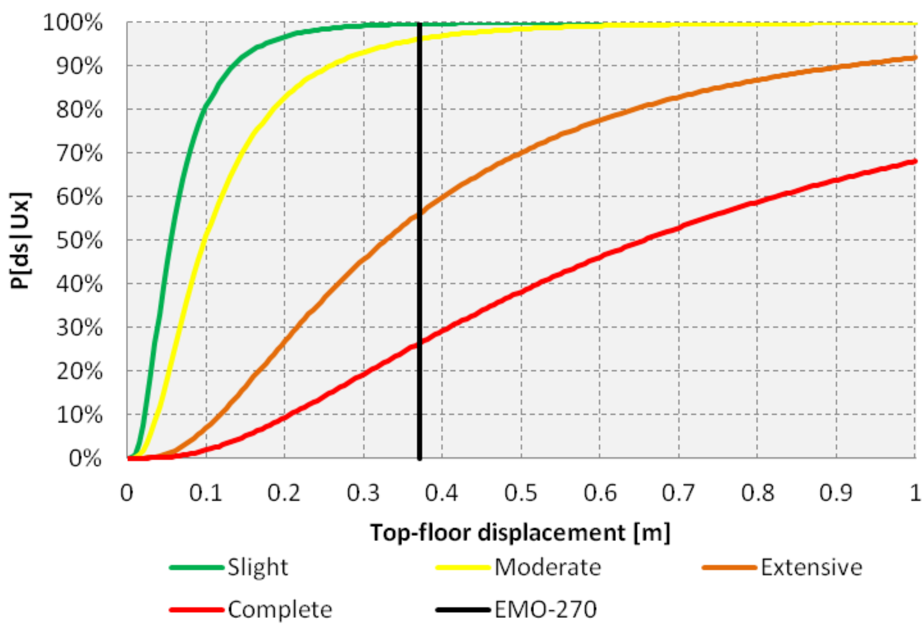

Figure 74: Damage due to the EMO-270 component of the Imperial Valley, CA, USA (1979) earthquake

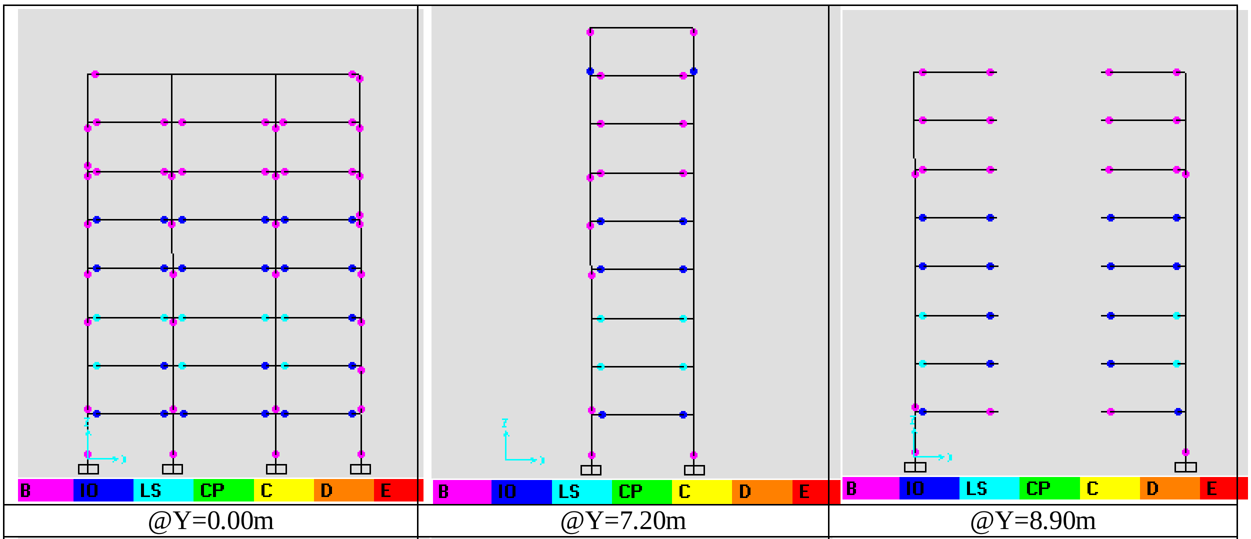

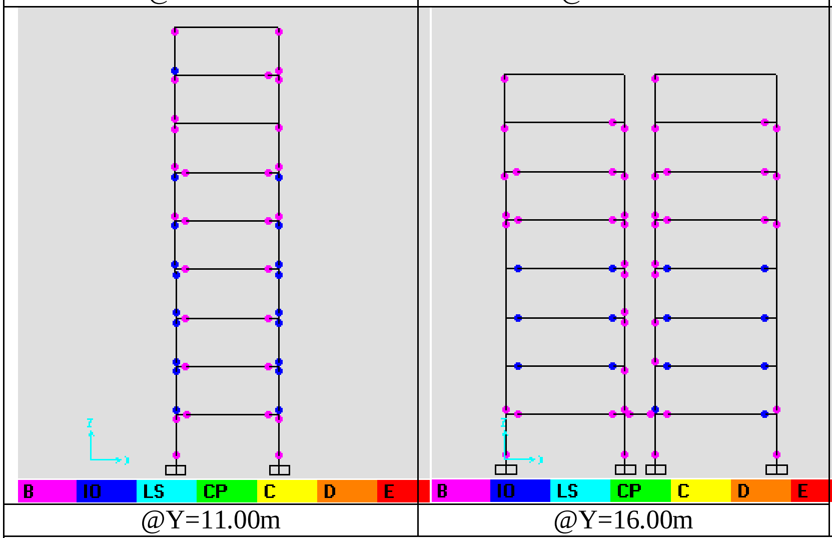

Record: JFA-022

Max abs $Ux_{,Top}$ = 0.2431 m

Estimated damage state:
MODERATE

Description:

- Yielding at lower & upper floors
- No failures

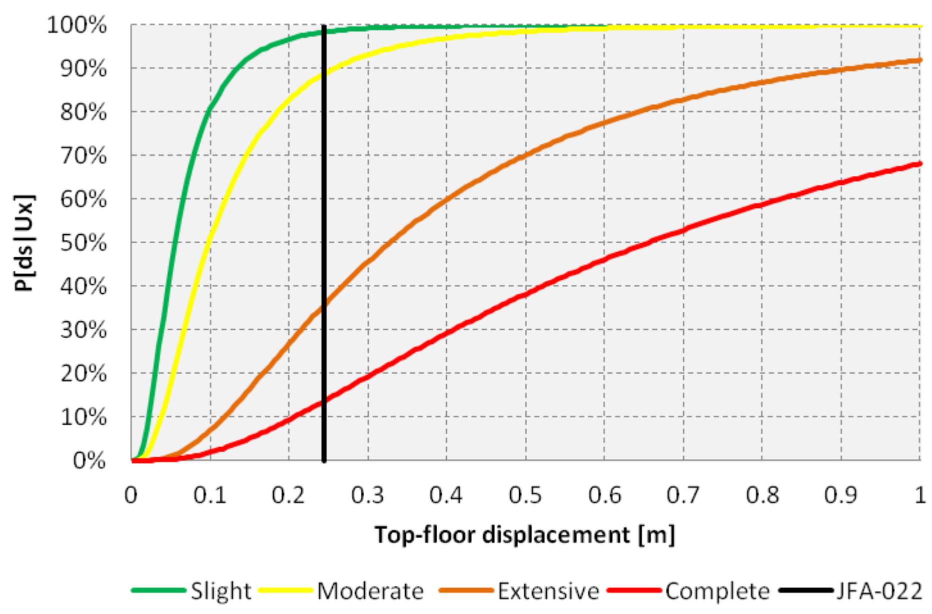

Figure 75: Damage due to the JFA-022 component of the Northridge, CA, USA (1994) earthquake

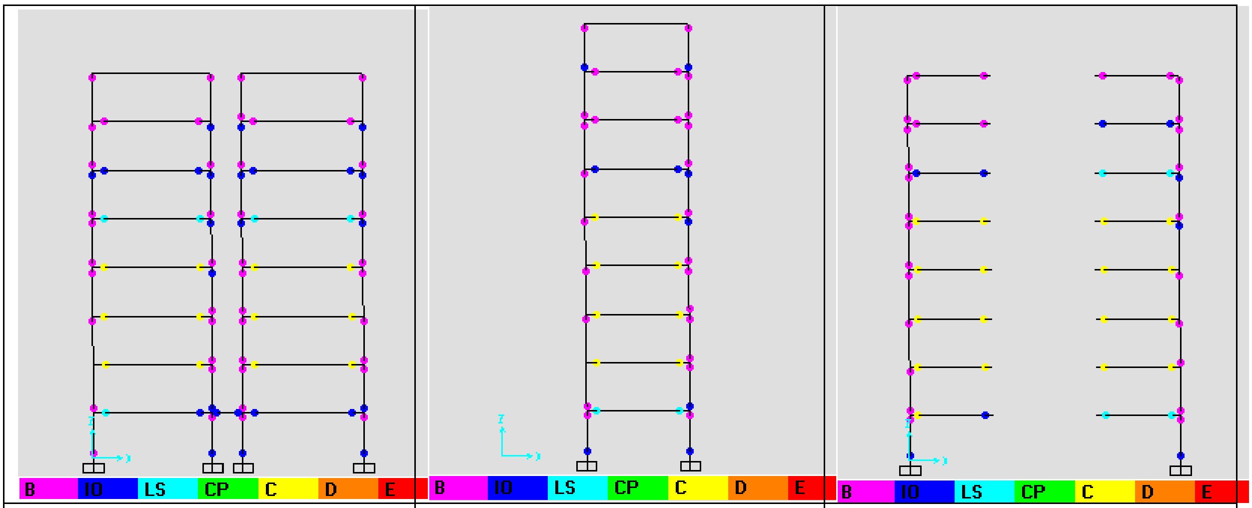

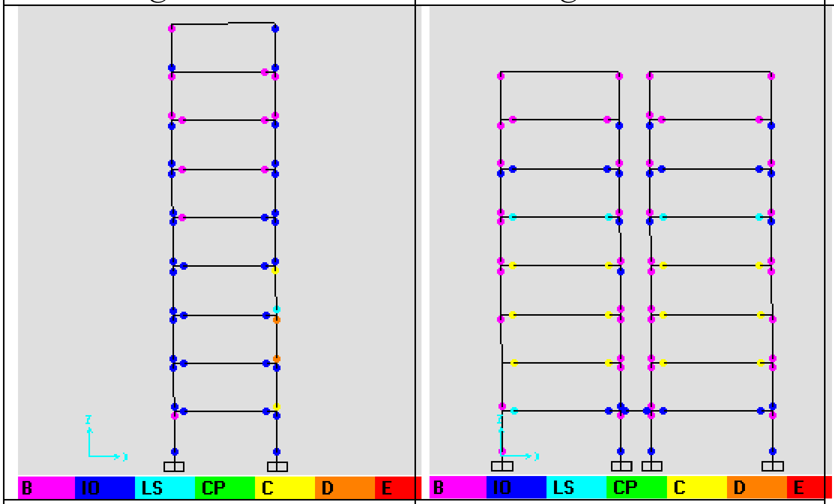

Record: JFA-292

Max abs $Ux_{,Top}$ = 0.4952 m

Estimated damage state:
EXTENSIVE

Description:

- Failure at some beams
- Columns passed the LS limit at base

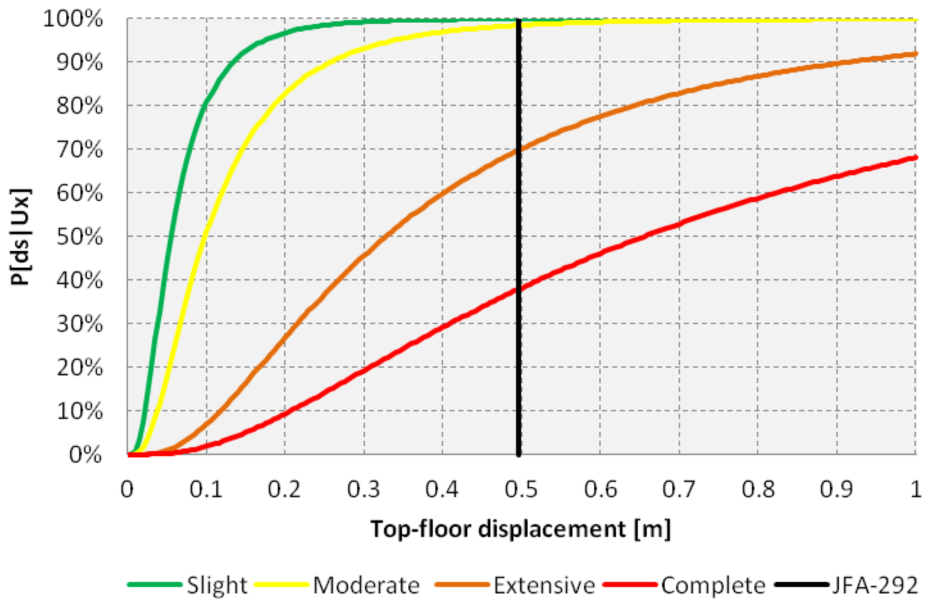

Figure 76: Damage due to the JFA-292 component of the Northridge, CA, USA (1994) earthquake

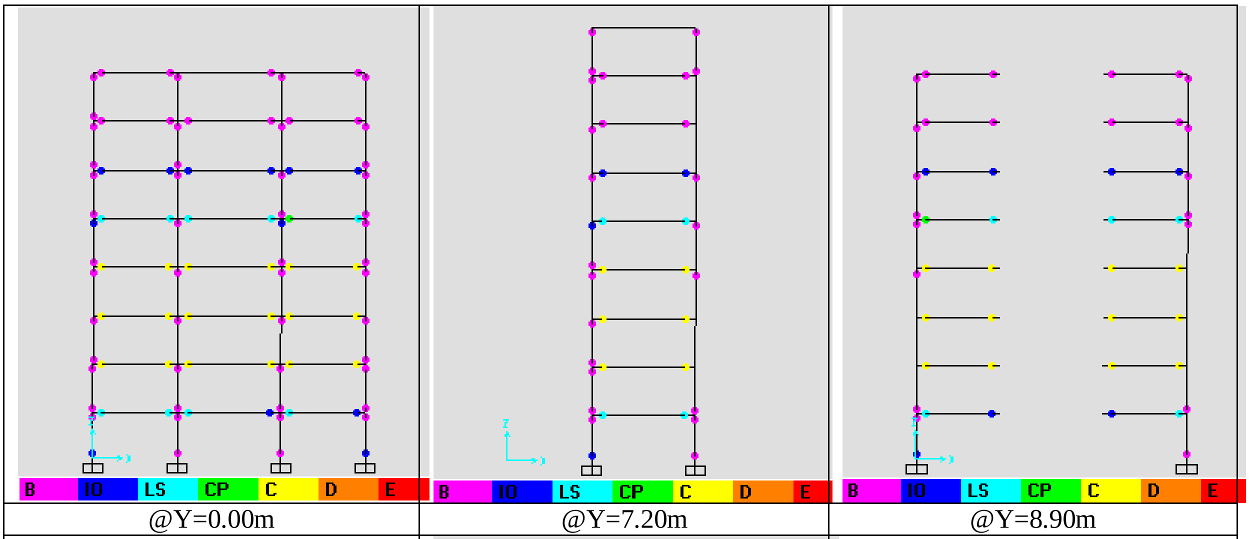

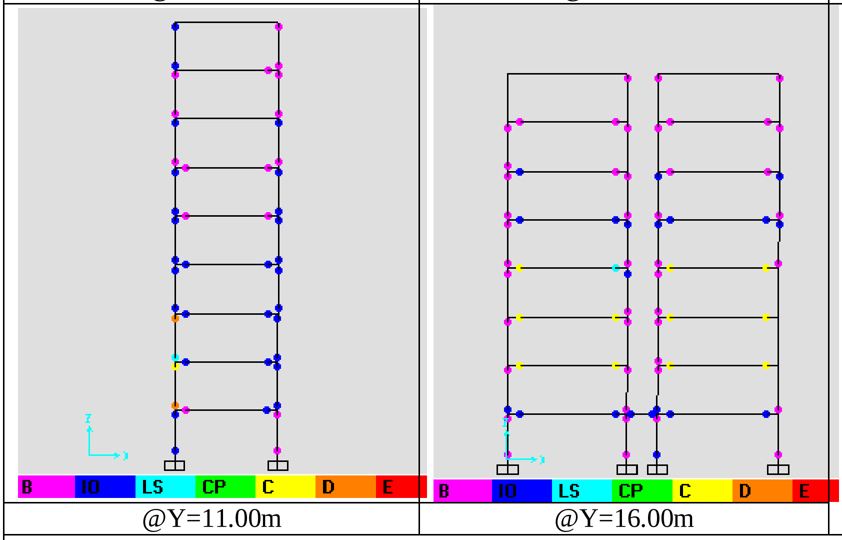

Record: SCG-052

Max abs $Ux_{,Top}$ = 0.4038 m

Estimated damage state:
EXTENSIVE

Description:

- Failure at some beams
- Columns yielded at middle floors
- Column failure at Y=11m

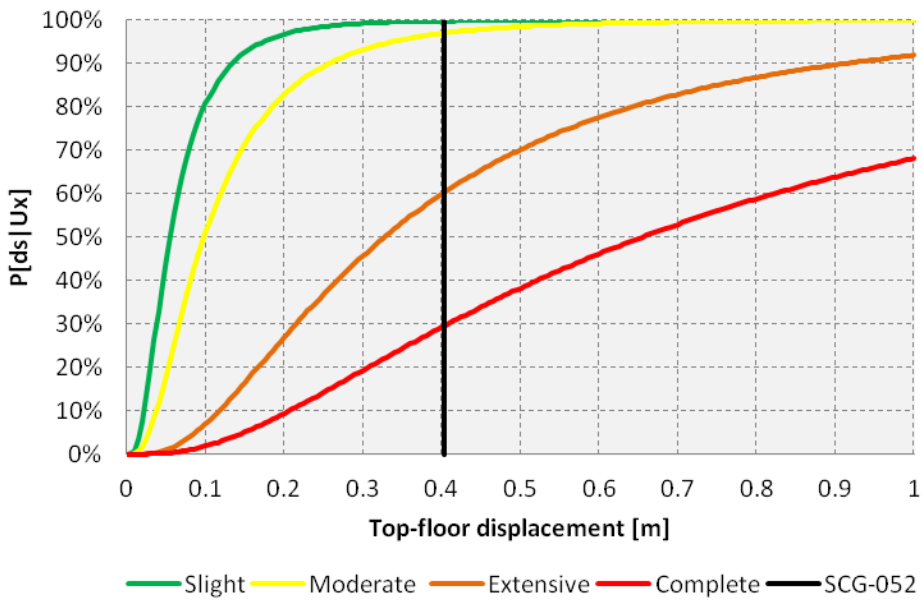

Figure 77: Damage due to the SCG-052 component of the Northridge, CA, USA (1994) earthquake

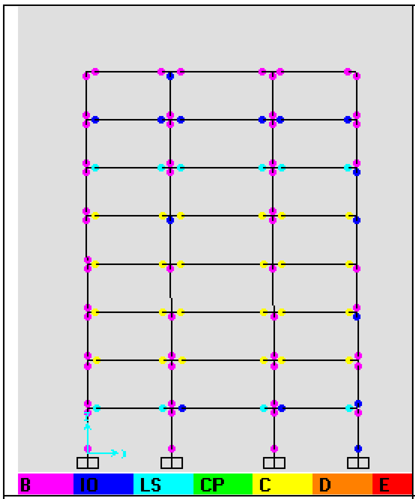

@Y=0.00m

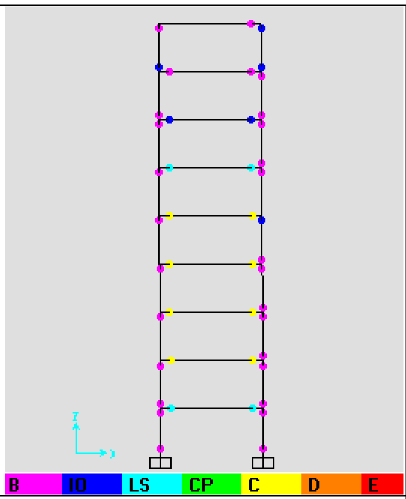

@Y=7.20m

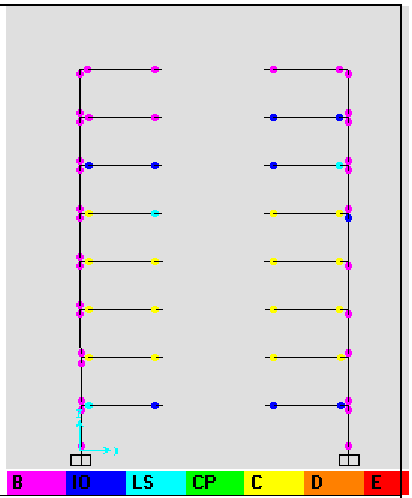

@Y=8.90m

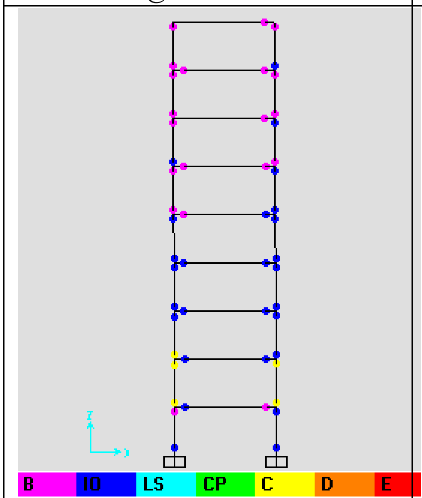

@Y=11.00m

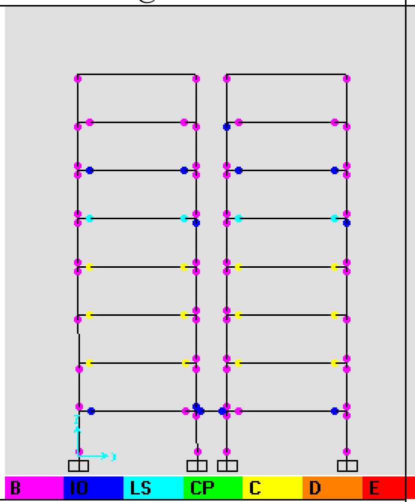

@Y=16.00m

Record: SCG-142

Max abs $Ux_{,Top}$ = 0.46 m

Estimated damage state:
EXTENSIVE

Description:

- Failure at some beams
- Columns yielded at middle floors

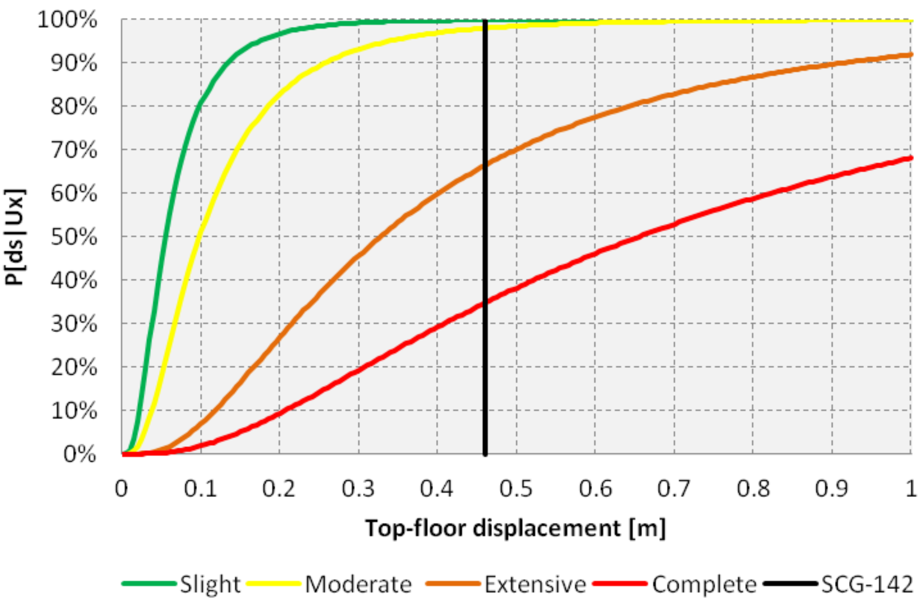

Figure 78: Damage due to the SCG-142 component of the Northridge, CA, USA (1994) earthquake

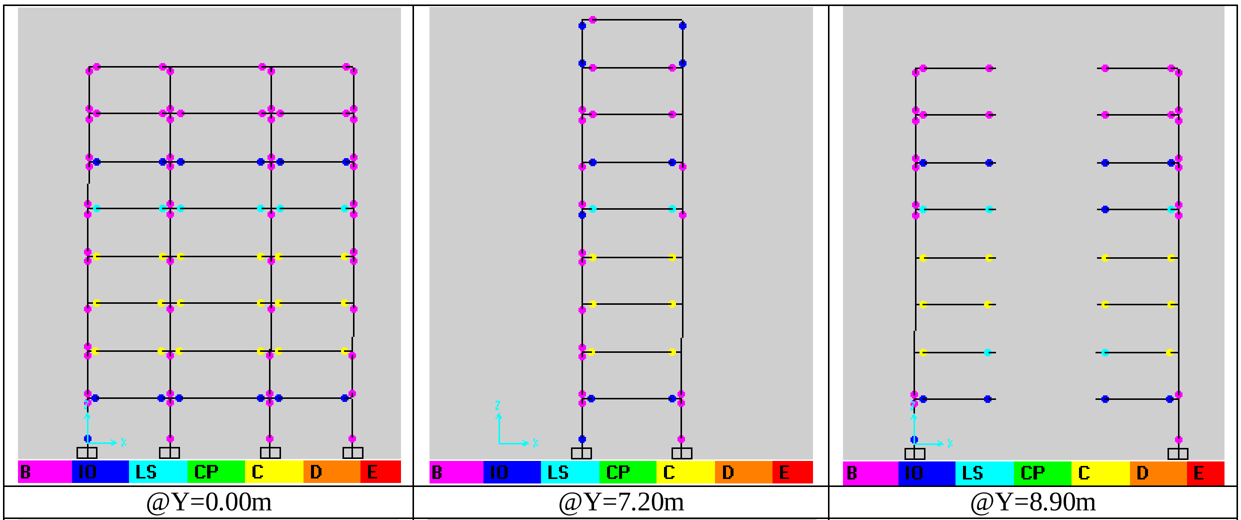

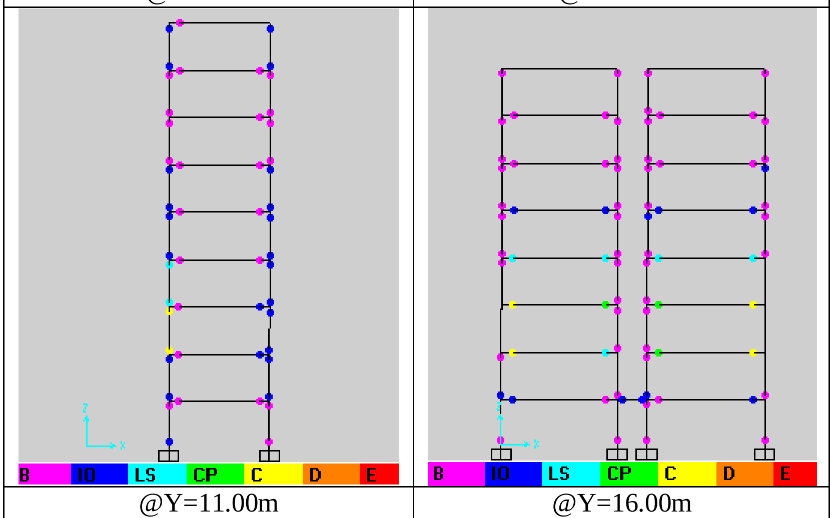

Record: SCH-011

Max abs $Ux_{,Top}$ = 0.3762 m

Estimated damage state:
EXTENSIVE

Description:

- Failure at some beams
- Extensive column yielding

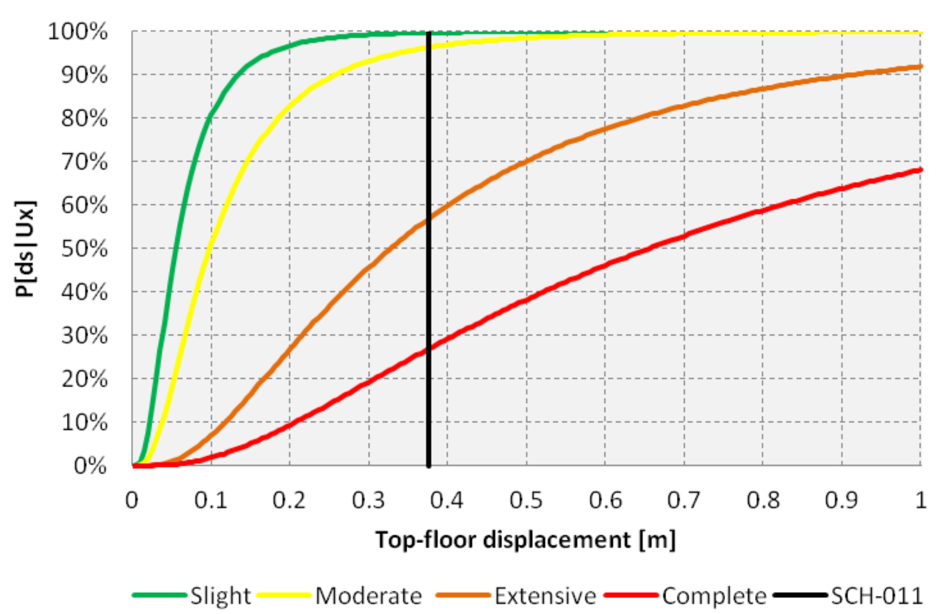

Figure 79: Damage due to the SCH-011 component of the Northridge, CA, USA (1994) earthquake

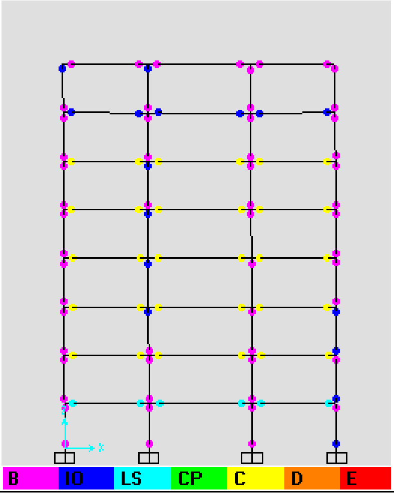

@Y=0.00m

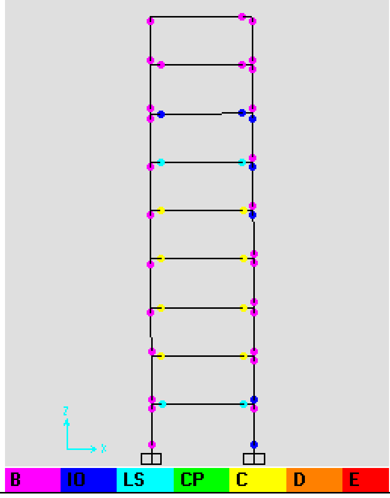

@Y=7.20m

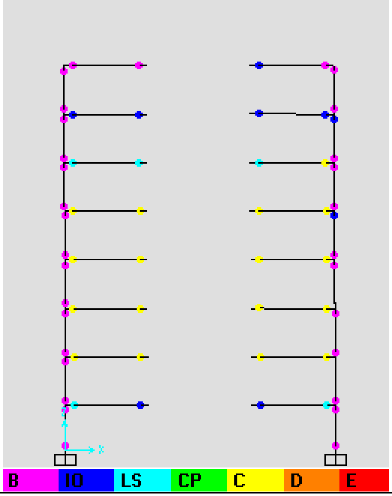

@Y=8.90m

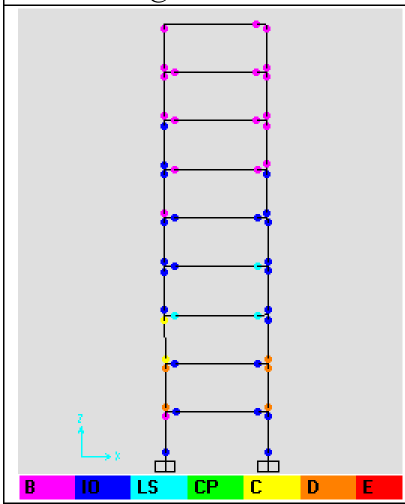

@Y=11.00m

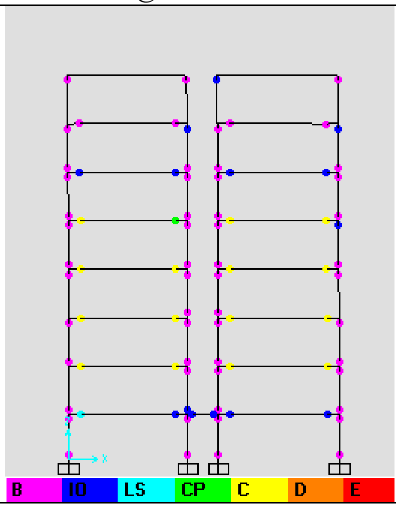

@Y=16.00m

Record: TAK-000

Max abs Ux,$_{Top}$ = 0.5148 m

Estimated damage state: **EXTENSIVE**

Description:

- Failure at some beams
- Extensive column yielding
- Column failure at Y=11m

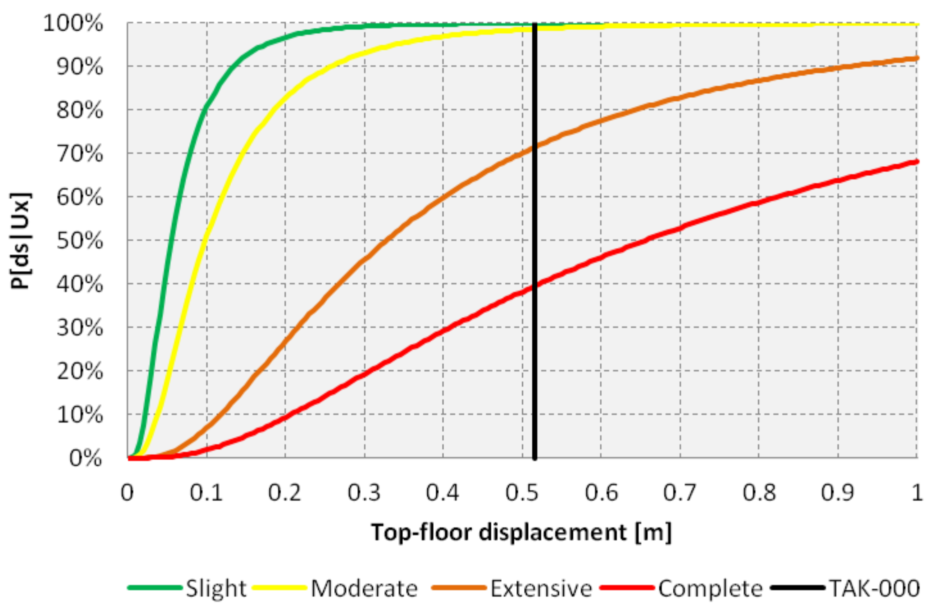

Figure 80: Damage due to the TAK-000 component of the Kobe, Japan (1995) earthquake

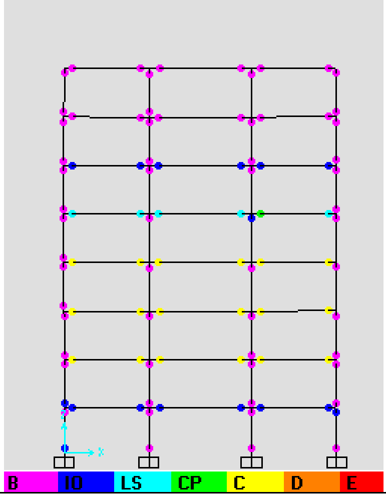

@Y=0.00m

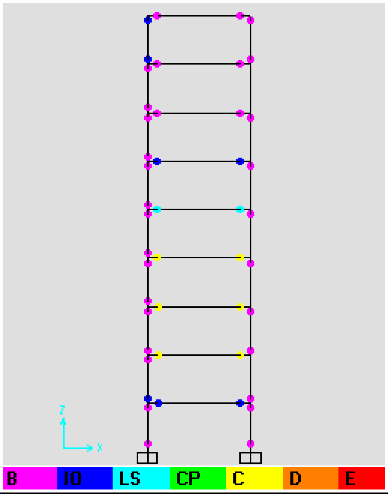

@Y=7.20m

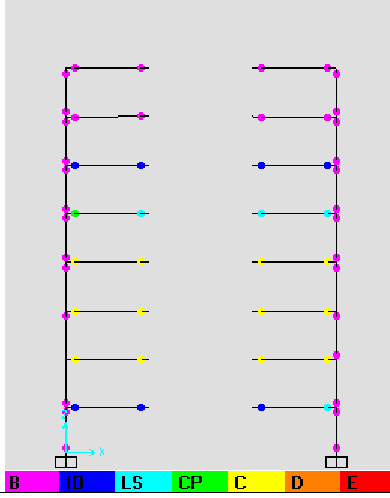

@Y=8.90m

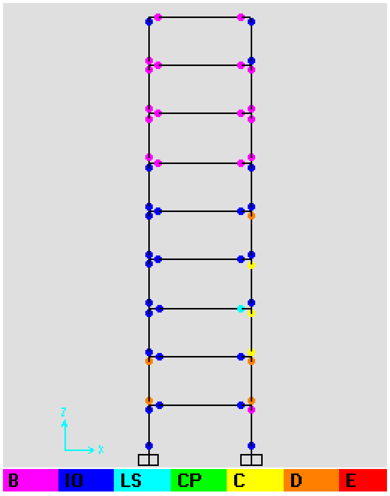

@Y=11.00m

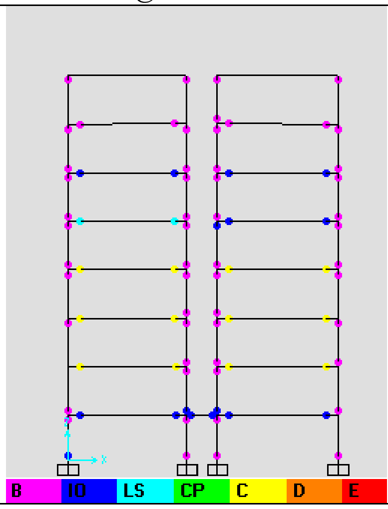

@Y=16.00m

Record: TAK-090

Max abs Ux,$_{Top}$ = 0.3963 m

Estimated damage state:
EXTENSIVE

Description:

- Failure at some beams
- Extensive column yielding
- Column failure at Y=11m

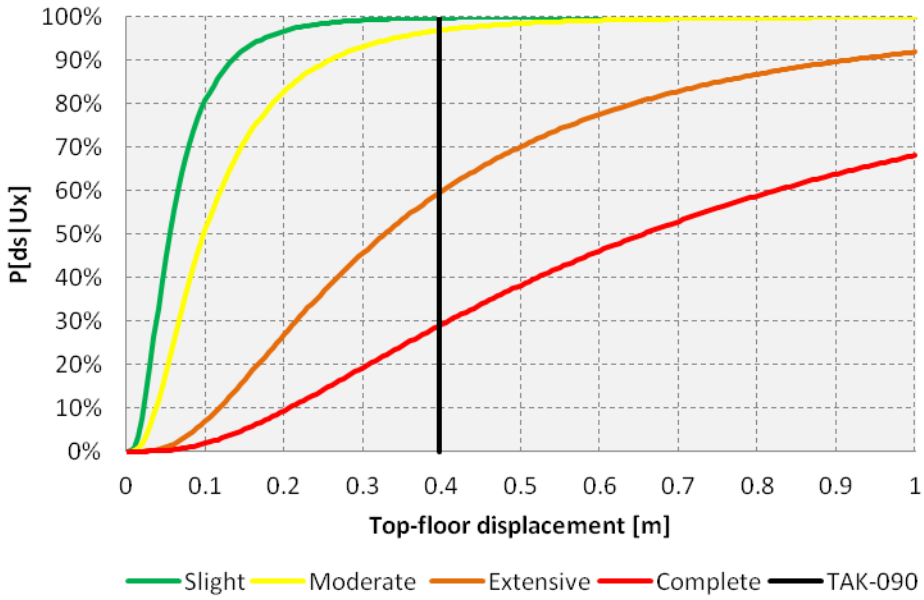

Figure 81: Damage due to the TAK-090 component of the Kobe, Japan (1995) earthquake

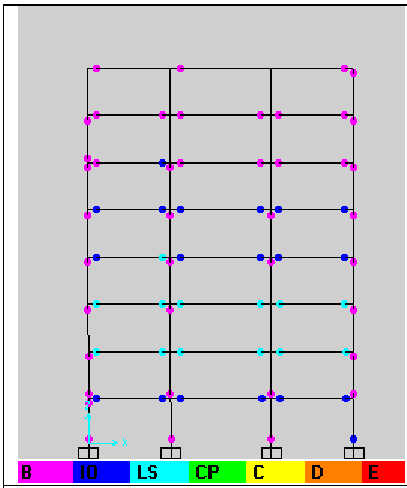

@Y=0.00m

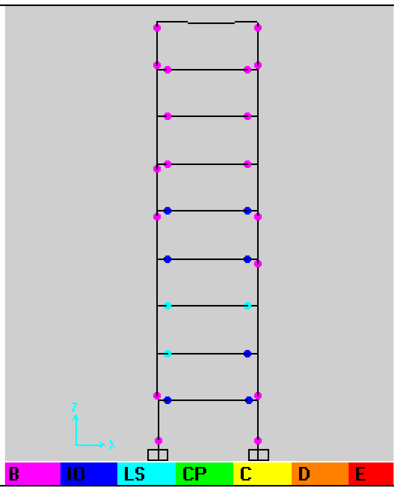

@Y=7.20m

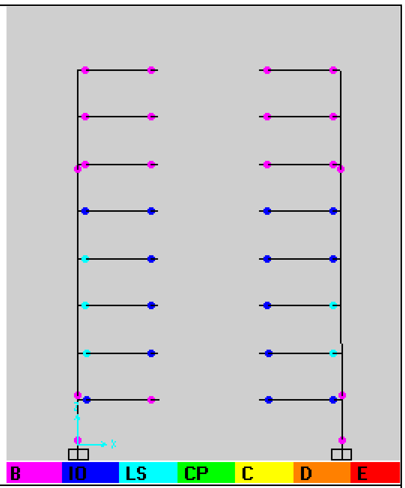

@Y=8.90m

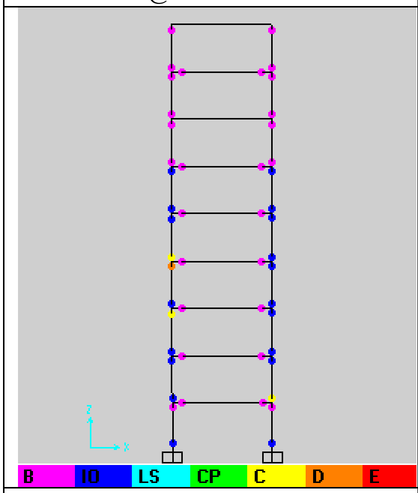

@Y=11.00m

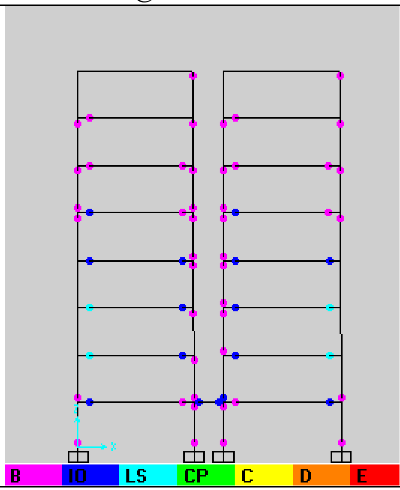

@Y=16.00m

Record: KPI-000

Max abs $Ux,_{Top}$ = 0.2666 m

Estimated damage state:
MODERATE

Description:

- Yielding at lower & upper floors
- No beam failures

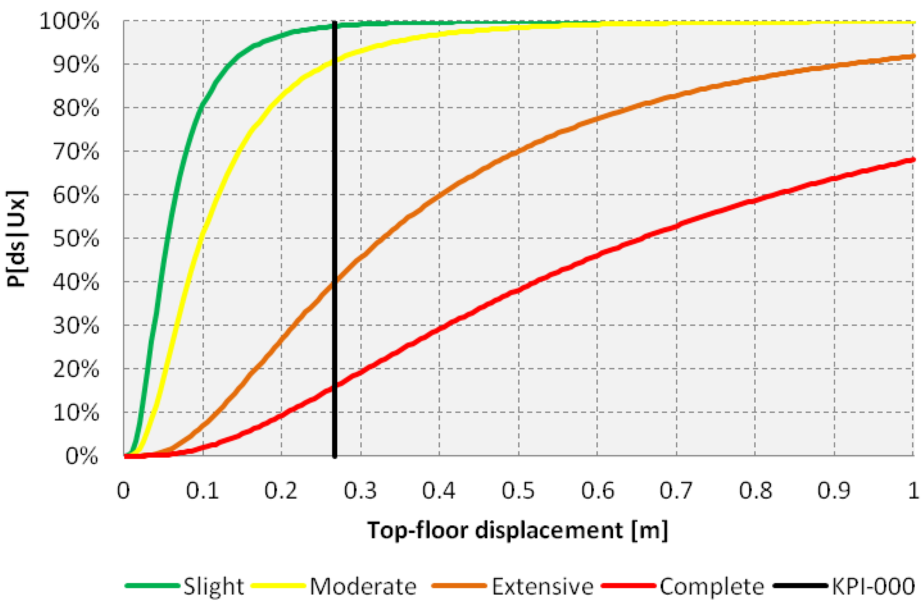

Figure 82: Damage due to the KPI-000 component of the Kobe, Japan (1995) earthquake

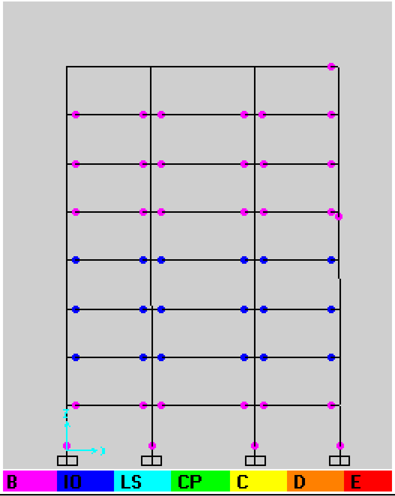

@Y=0.00m

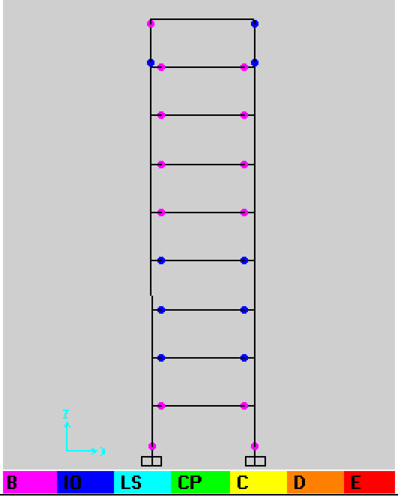

@Y=7.20m

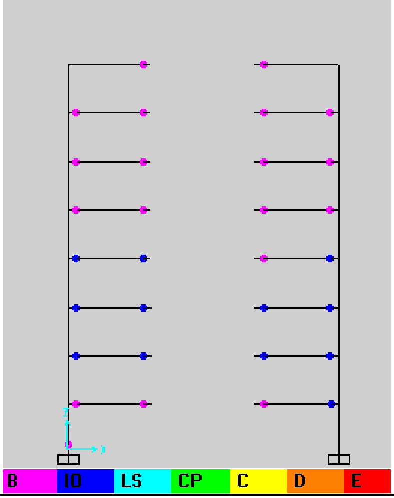

@Y=8.90m

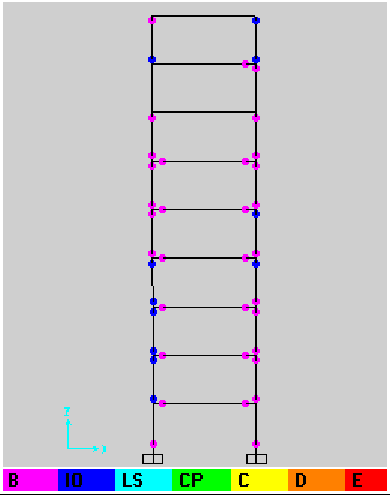

@Y=11.00m

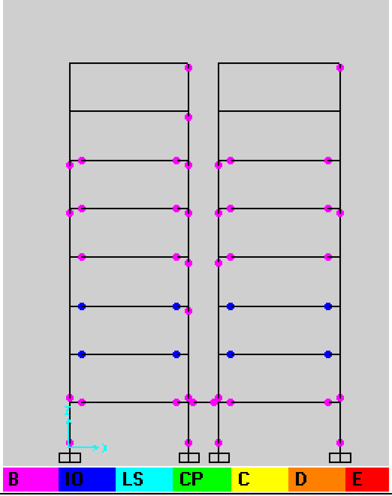

@Y=16.00m

Record: YPT-000

Max abs $Ux_{,Top}$ = 0.1838 m

Estimated damage state:
MODERATE

Description:

- Yielding at lower & upper floors
- No failures

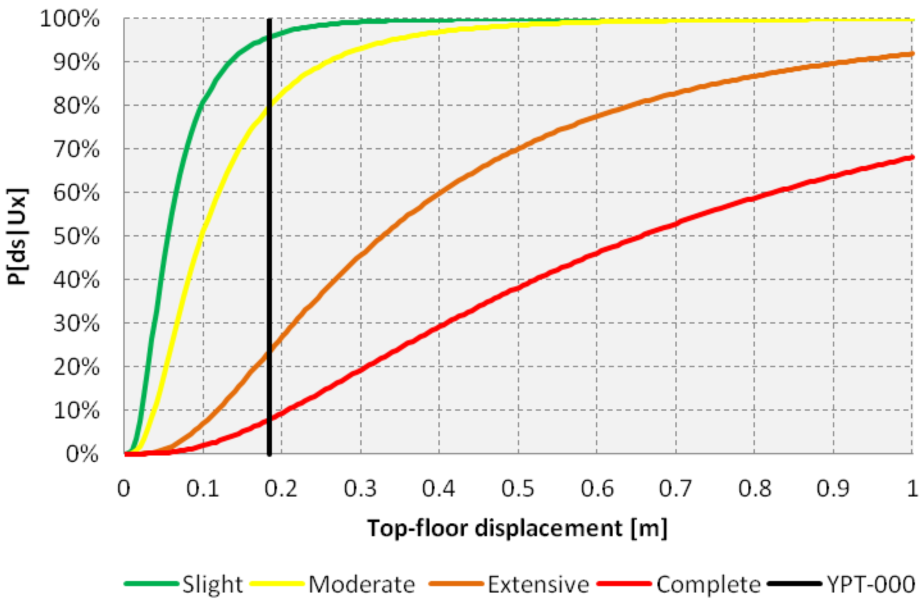

Figure 83: Damage due to the YPT-000 component of the Izmit, Turkey (1999) earthquake

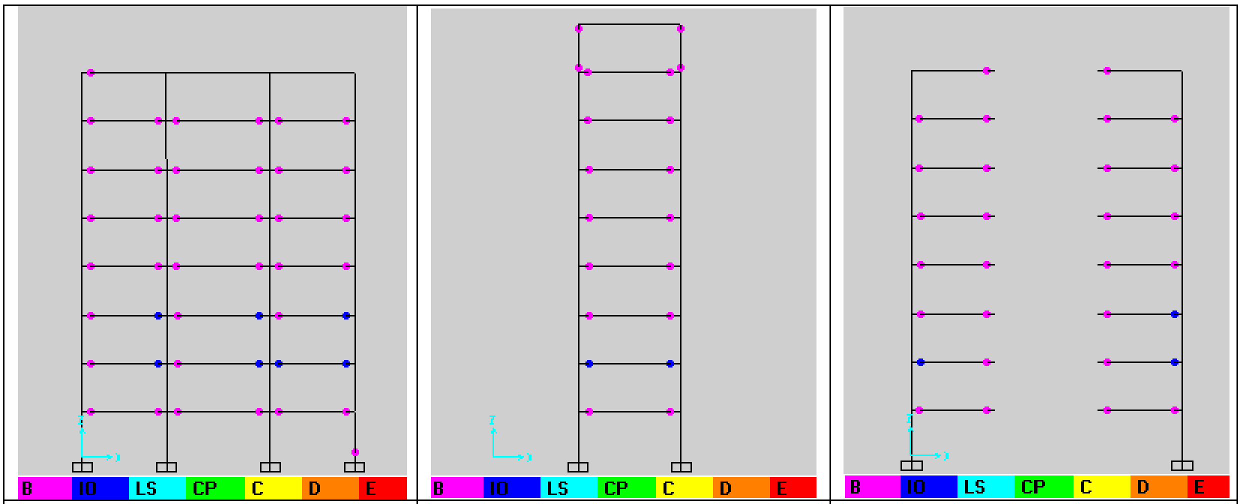

@Y=0.00m @Y=7.20m @Y=8.90m

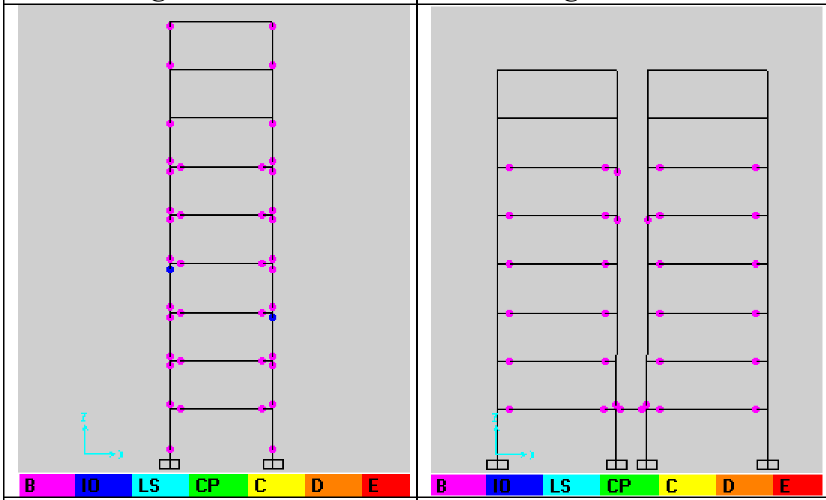

@Y=11.00m @Y=16.00m

Record: YPT-270

Max abs $Ux_{,Top}$ = 0.1354 m

Estimated damage state:
MODERATE

Description:

- Yielding at lower & upper floors
- No failures

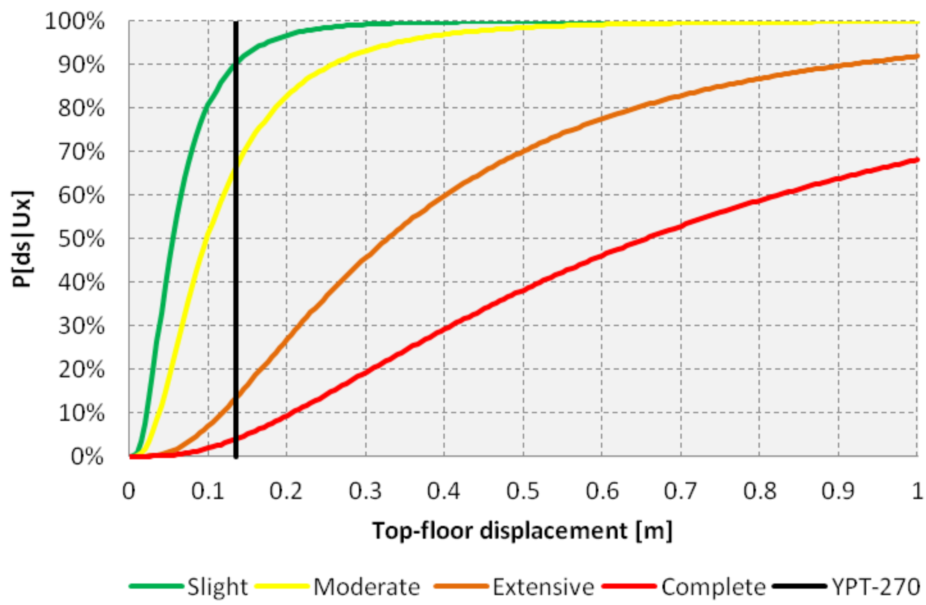

Figure 84: Damage due to the YPT-270 component of the Izmit, Turkey (1999) earthquake

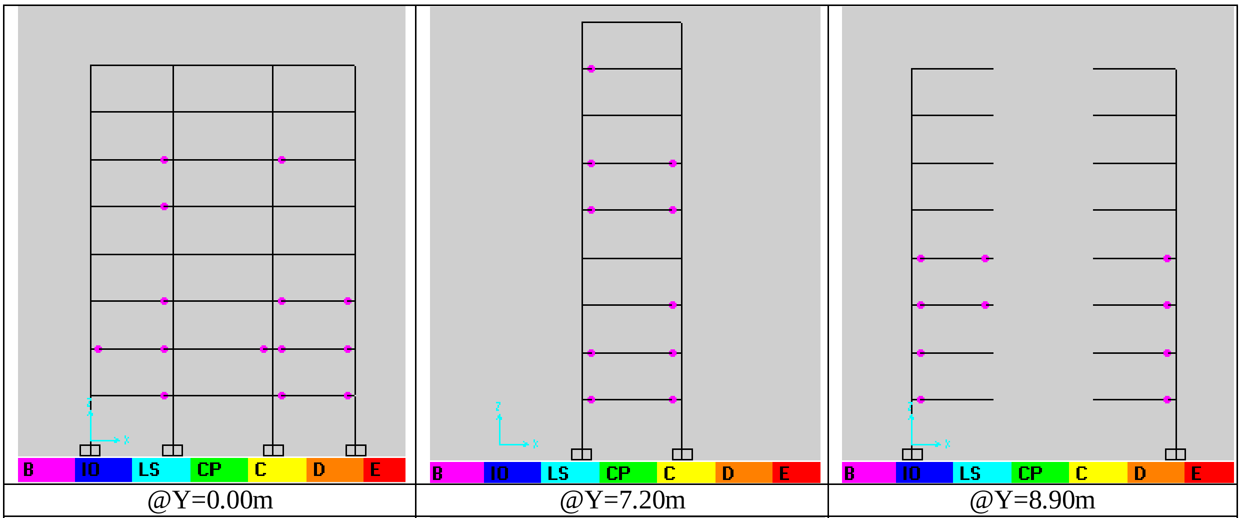

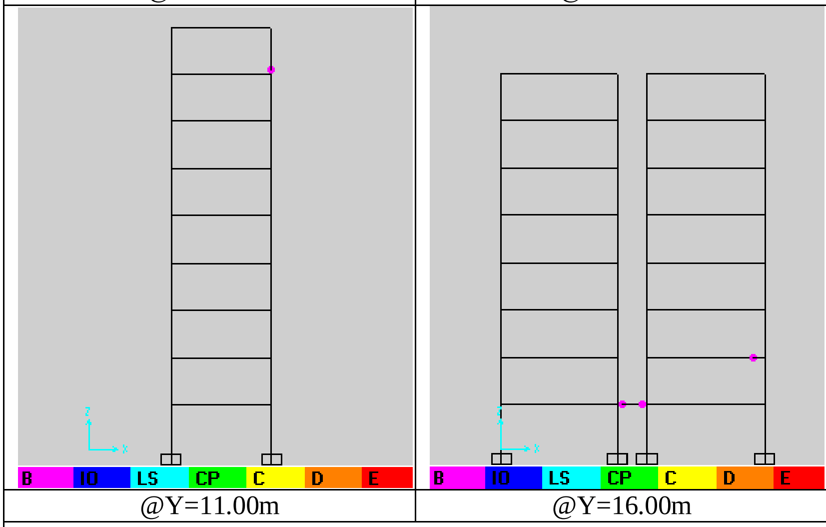

Record: ARC-270

Max abs Ux,$_{Top}$ = 0.04273 m

Estimated damage state: **SLIGHT**

Description:

- Some yielding at lower floors
- No failures

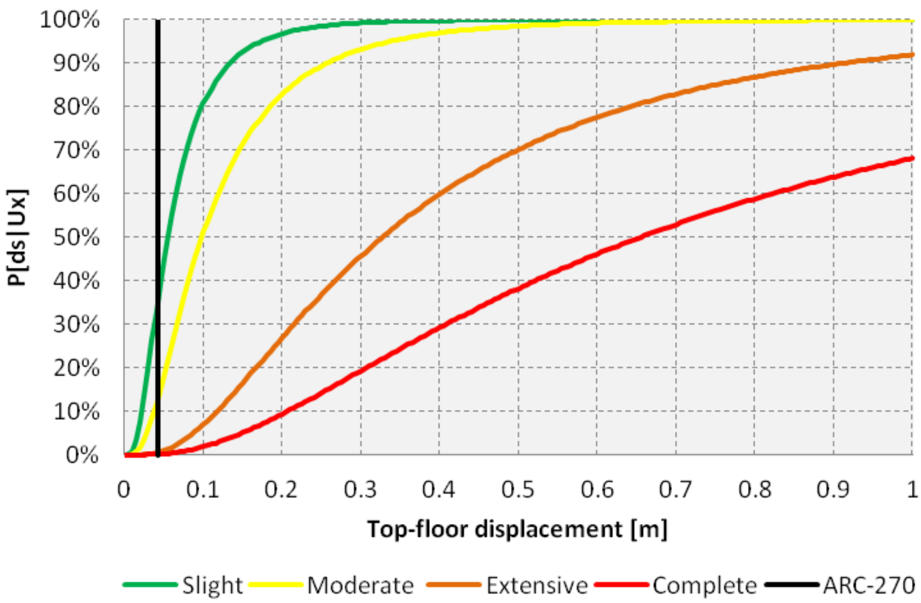

Figure 85: Damage due to the ARC-270 component of the Izmit, Turkey (1999) earthquake

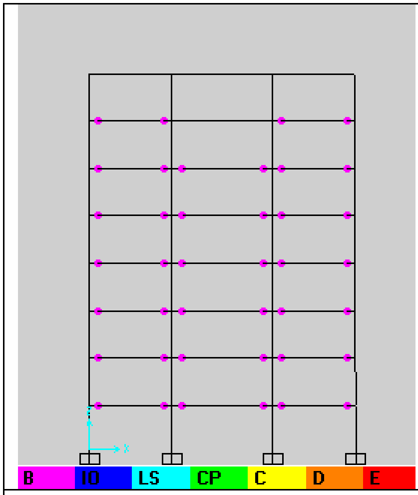

@Y=0.00m

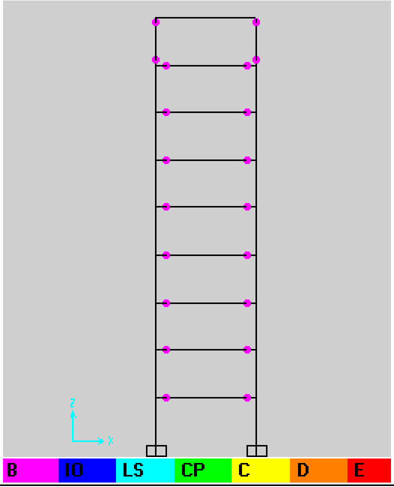

@Y=7.20m

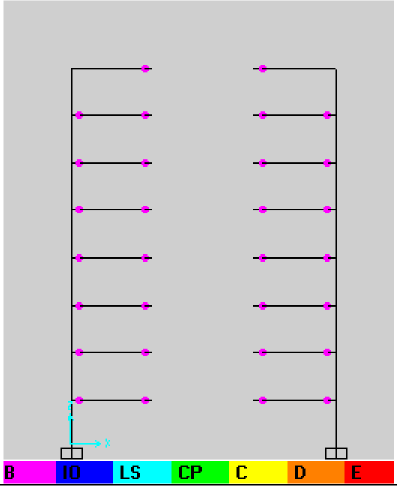

@Y=8.90m

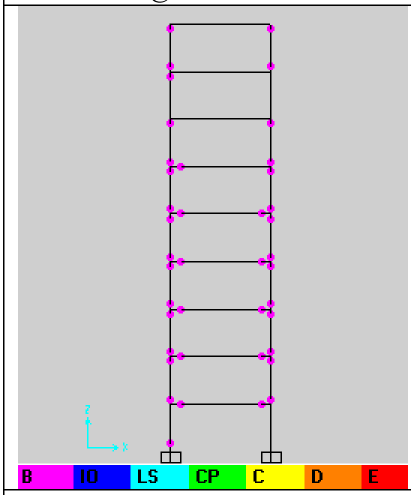

@Y=11.00m

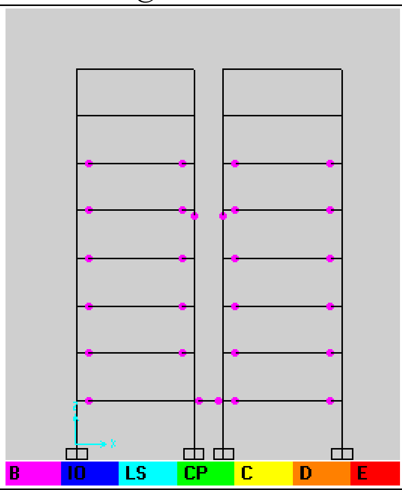

@Y=16.00m

Record: CHY101-090

Max abs $Ux_{,Top}$ = 0.1202m

Estimated damage state:
MODERATE

Description:

- Yielding at lower & upper floors
- No failures

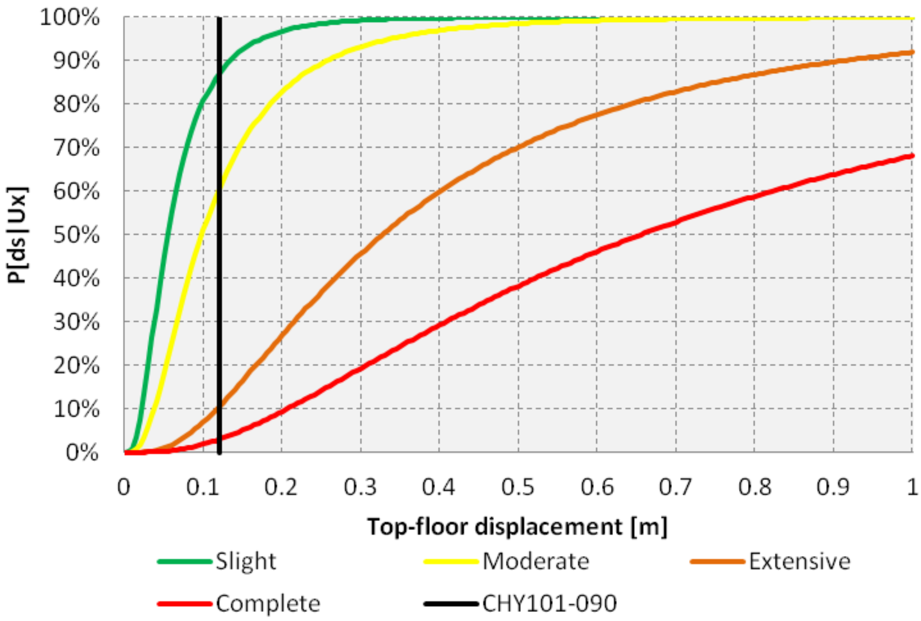

Figure 86: Damage due to the CHY101-090 component of the Chi-Chi, Taiwan (1999) earthquake

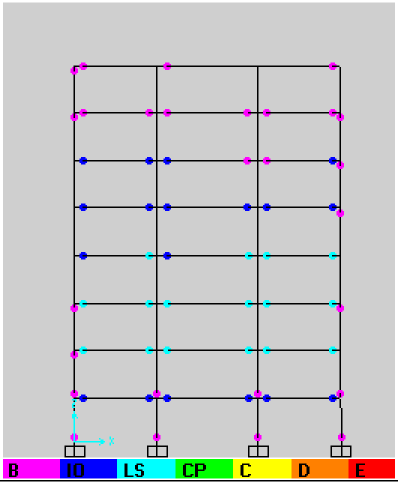

@Y=0.00m

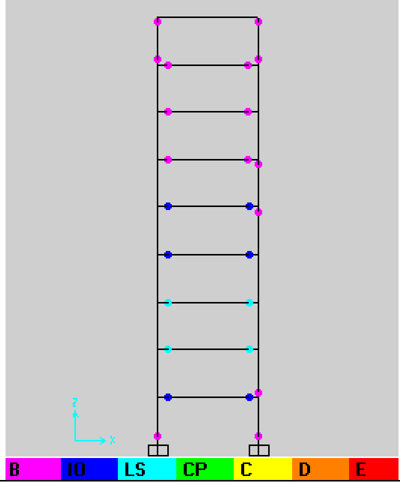

@Y=7.20m

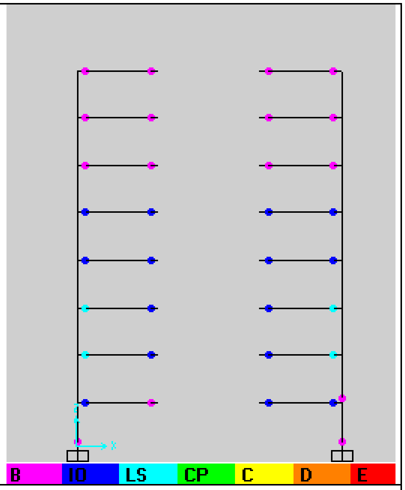

@Y=8.90m

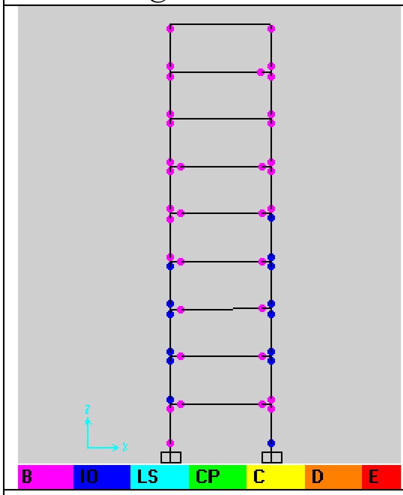

@Y=11.00m

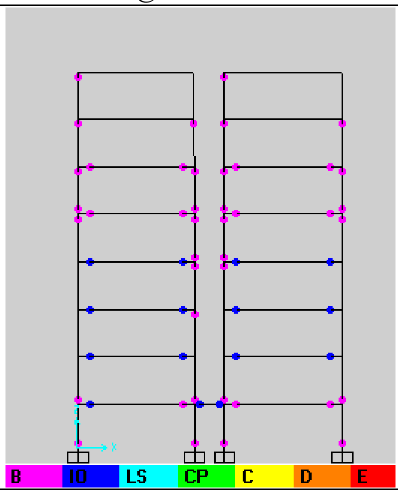

@Y=16.00m

Record: CHY101-360

Max abs $Ux,_{Top}$ = 0.268m

Estimated damage state:
MODERATE

Description:

- Yielding at lower & upper floors
- No failures

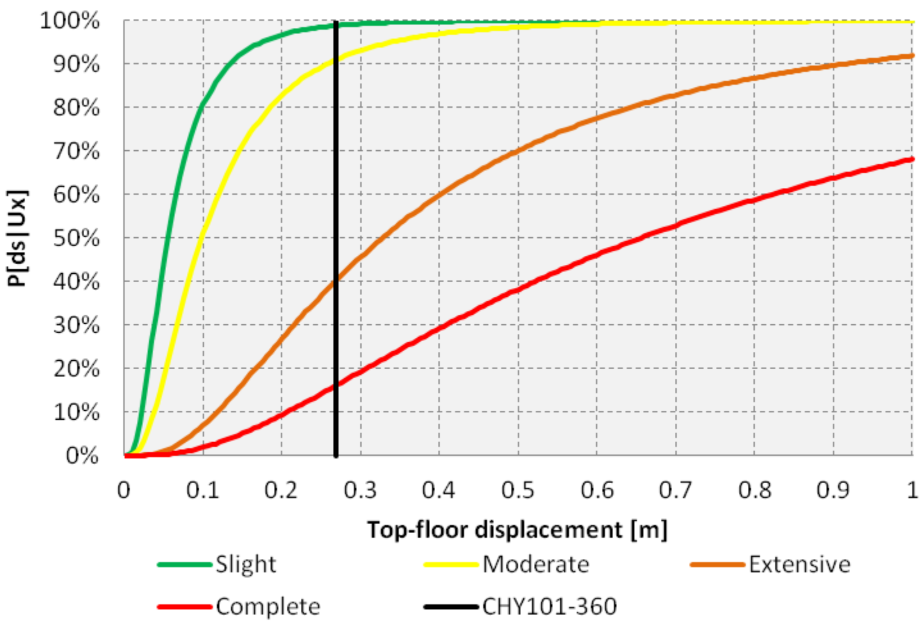

Figure 87: Damage due to the CHY101-360 component of the Chi-Chi, Taiwan (1999) earthquake

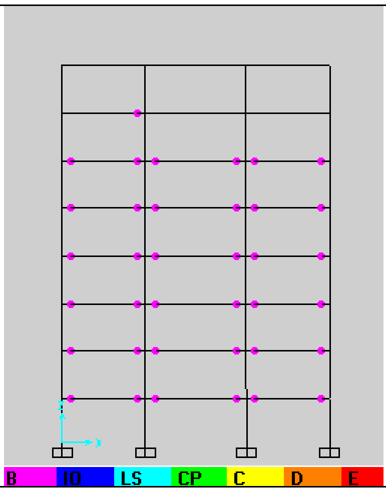

@Y=0.00m

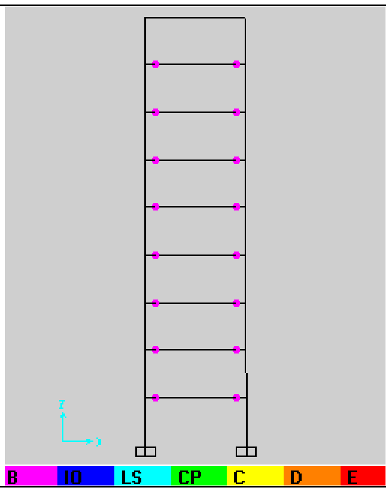

@Y=7.20m

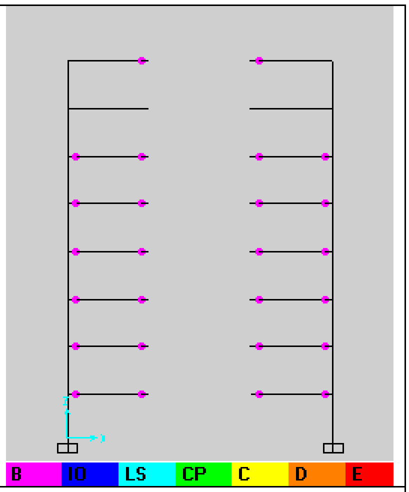

@Y=8.90m

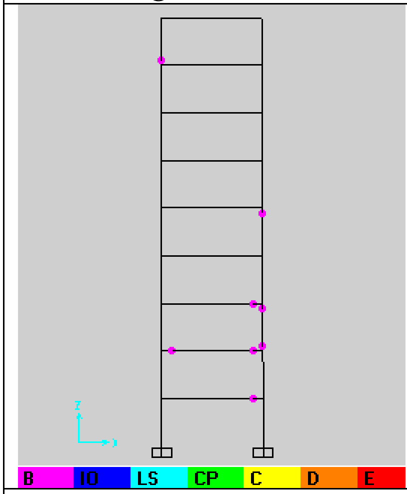

@Y=11.00m

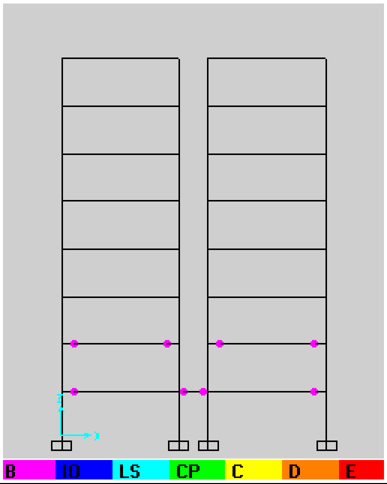

@Y=16.00m

Record: TCU053-360

Max abs $Ux,_{Top}$ = 0.06743 m

Estimated damage state:
MODERATE

Description:

- Yielding at lower & upper floors
- No failures

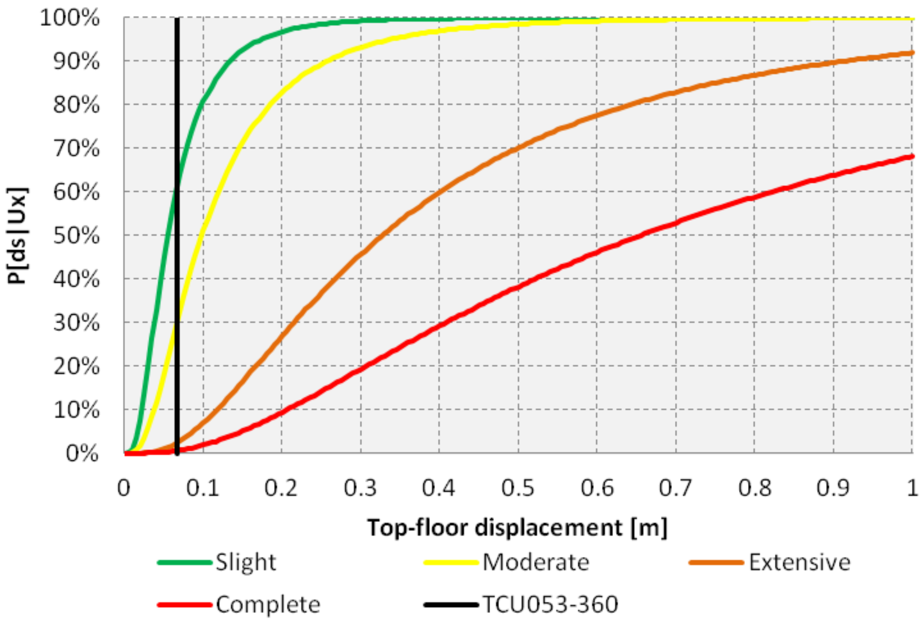

Figure 88: Damage due to the TCU053-360 component of the Chi-Chi, Taiwan (1999) earthquake

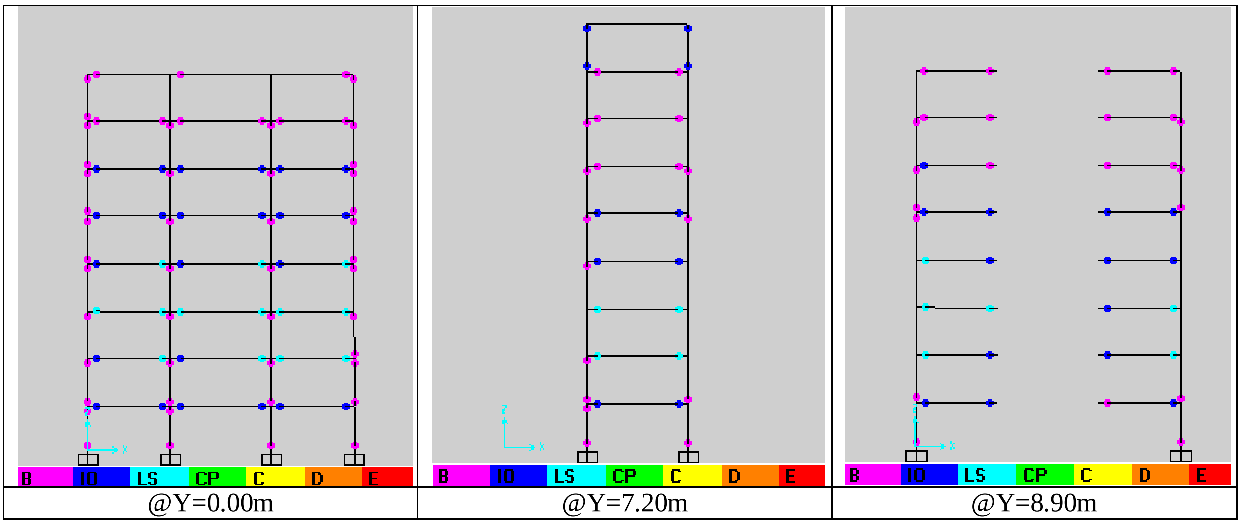

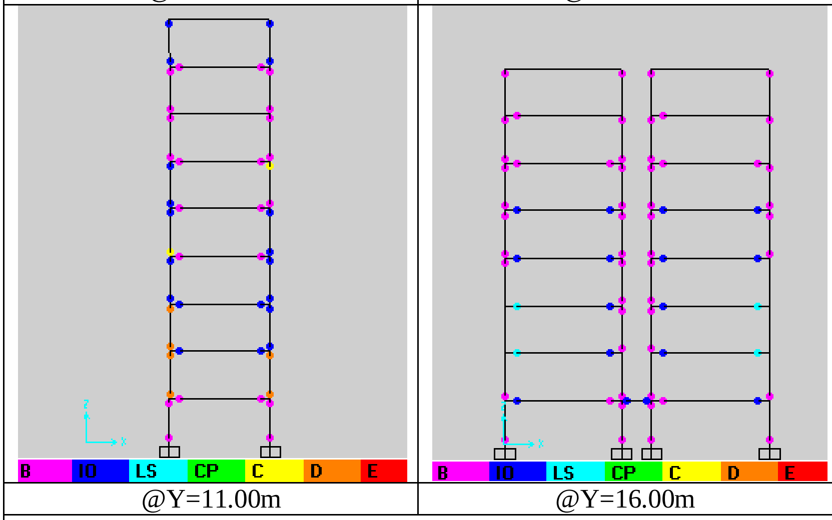

Record: TCU065-090

Max abs $Ux,_{Top}$ = 0.2826 m

Estimated damage state:
MODERATE

Description:
- Yielding at lower & upper floors
- No beam failures

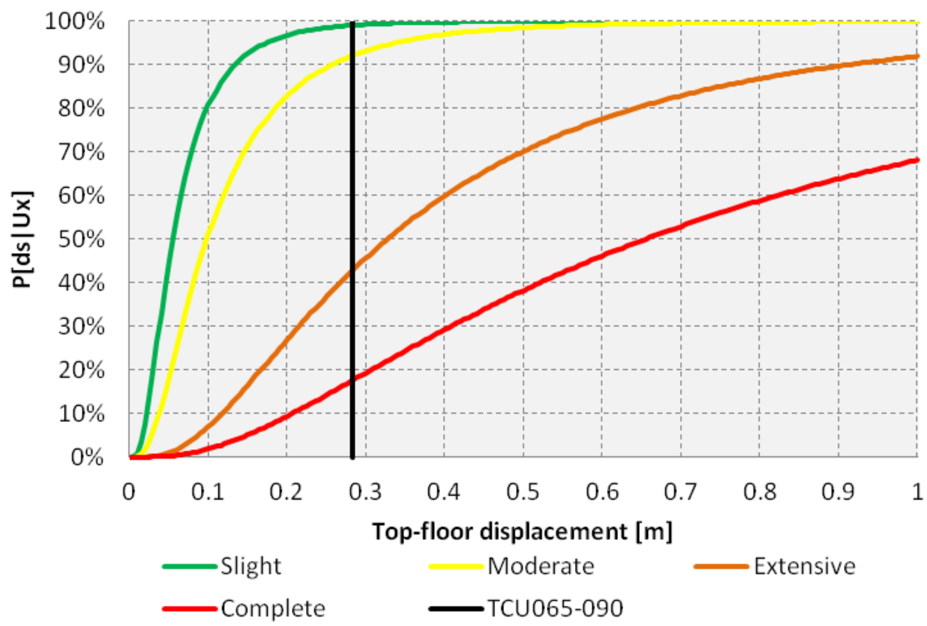

Figure 89: Damage due to the TCU065-090 component of the Chi-Chi, Taiwan (1999) earthquake

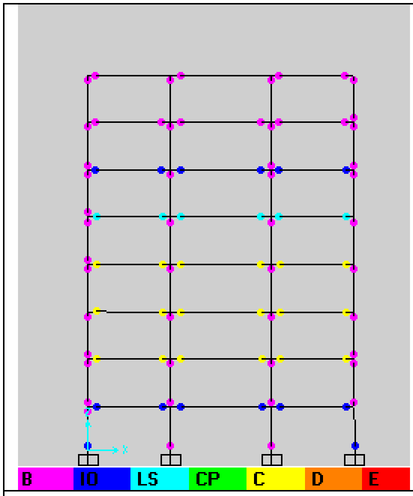

@Y=0.00m

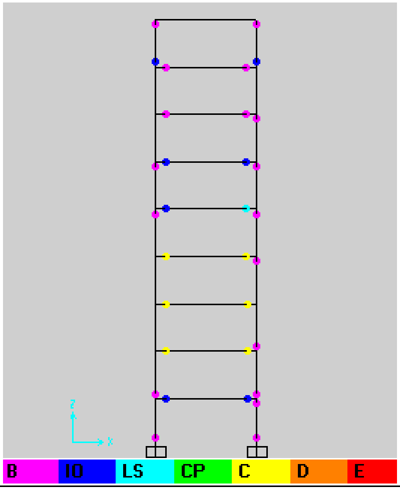

@Y=7.20m

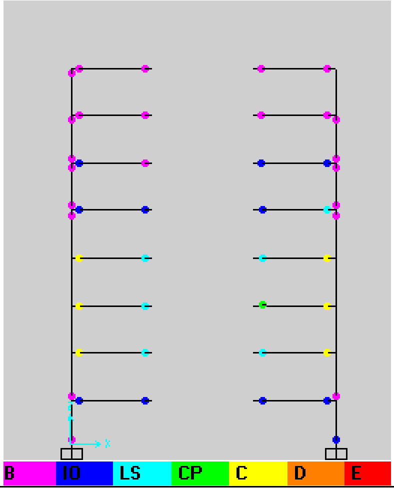

@Y=8.90m

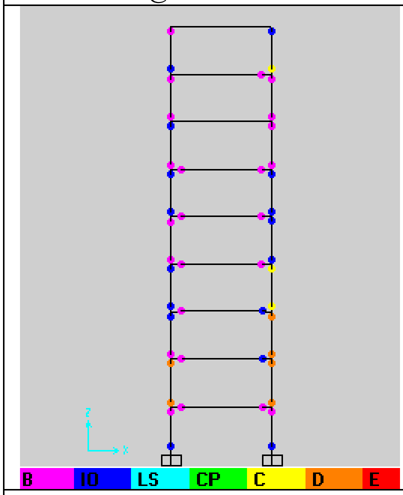

@Y=11.00m

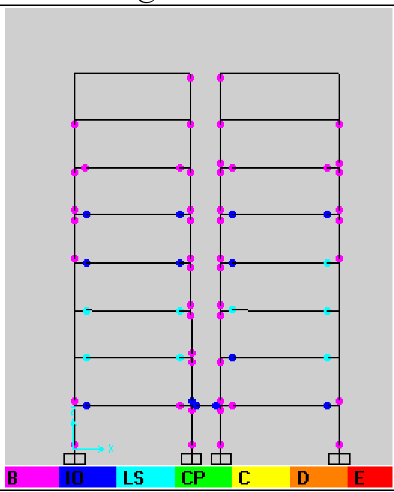

@Y=16.00m

Record: TCU065-360

Max abs $Ux_{,Top}$ = 0.3344 m

Estimated damage state:
EXTENSIVE

Description:

- Failure at some beams
- Extensive column yielding
- Column failure at Y=11m

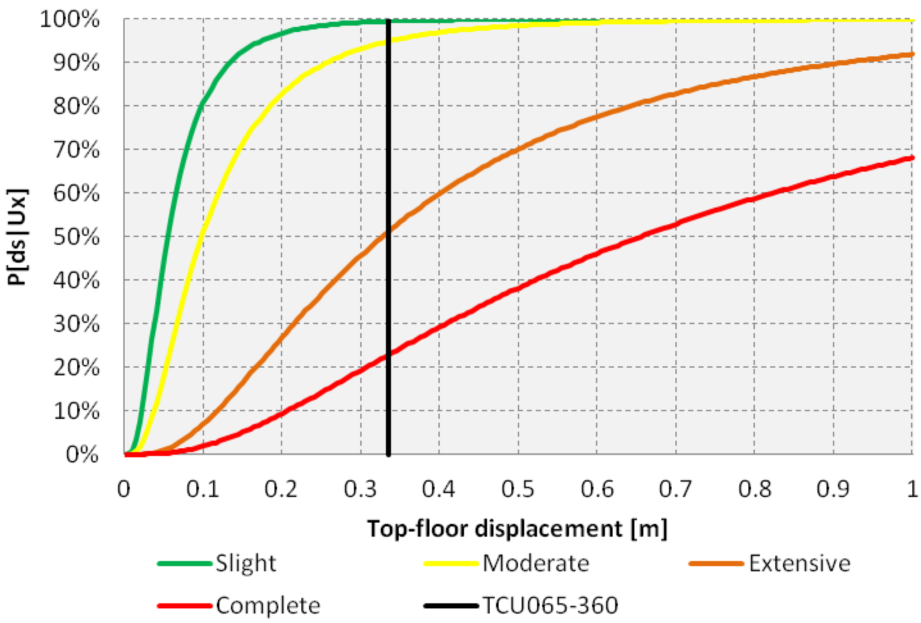

Figure 90: Damage due to the TCU065-360 component of the Chi-Chi, Taiwan (1999) earthquake

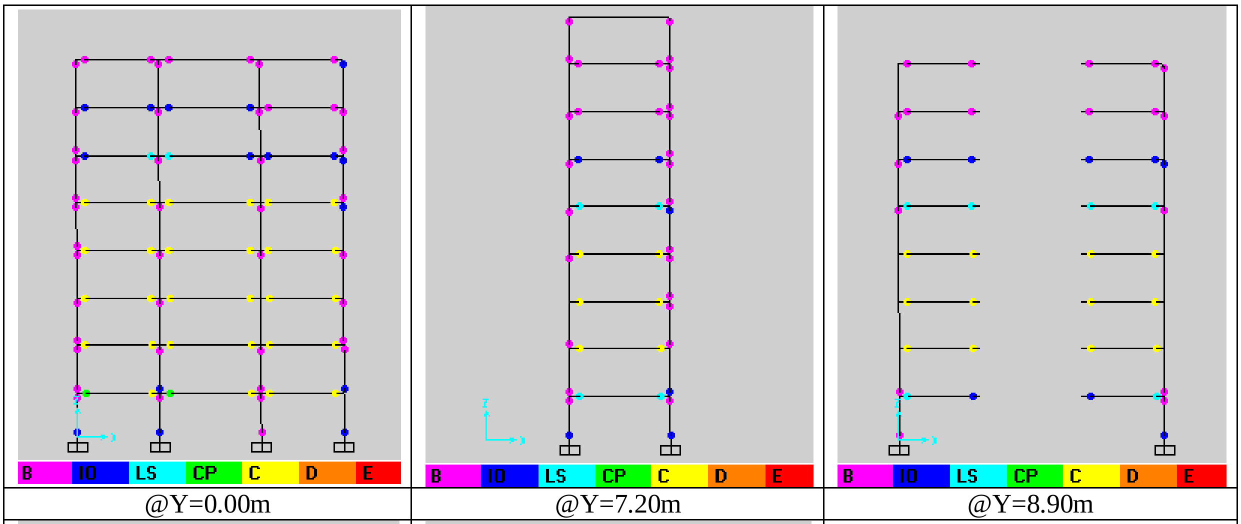

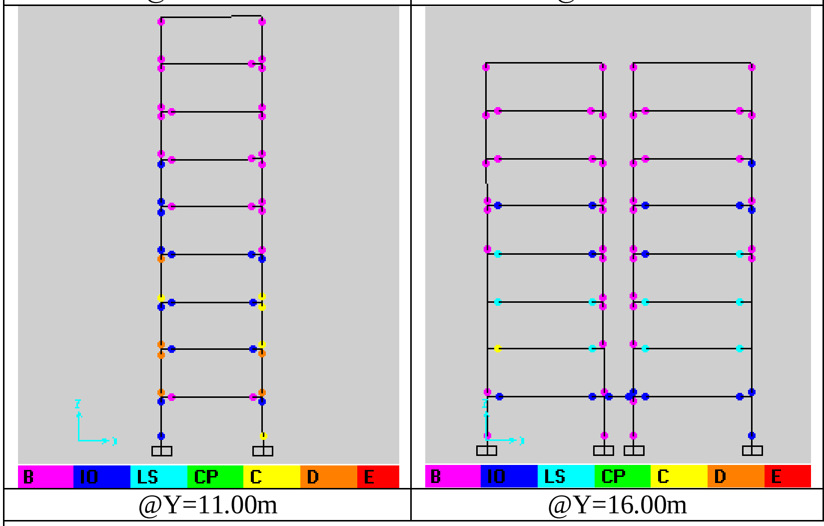

Record: TCU068-090

Max abs $Ux,_{Top}$ = 0.4157 m

Estimated damage state: **EXTENSIVE**

Description:

- Failure at some beams
- Extensive column yielding
- Column failure at Y=11m

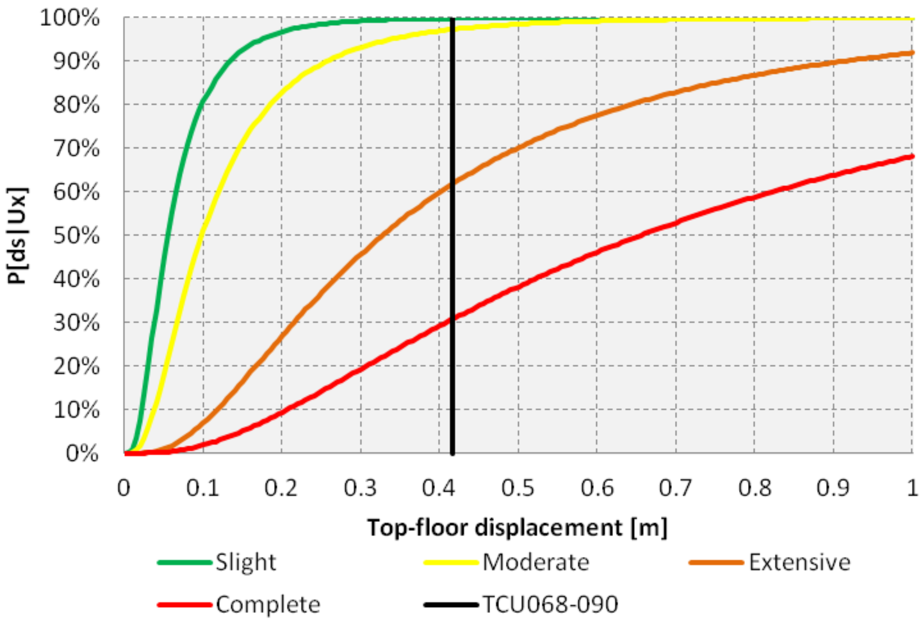

Figure 91: Damage due to the TCU068-090 component of the Chi-Chi, Taiwan (1999) earthquake

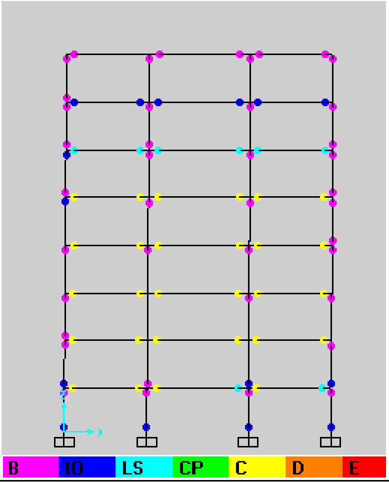

@Y=0.00m

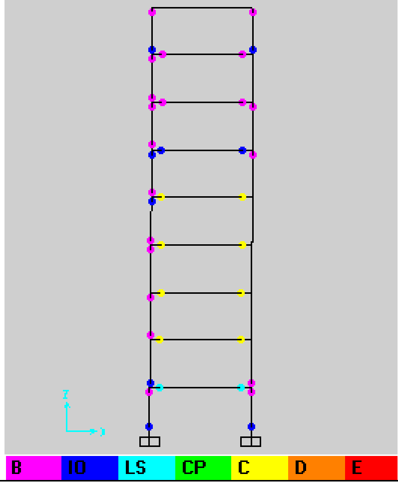

@Y=7.20m

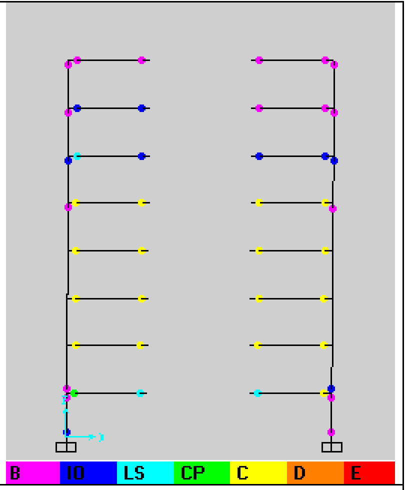

@Y=8.90m

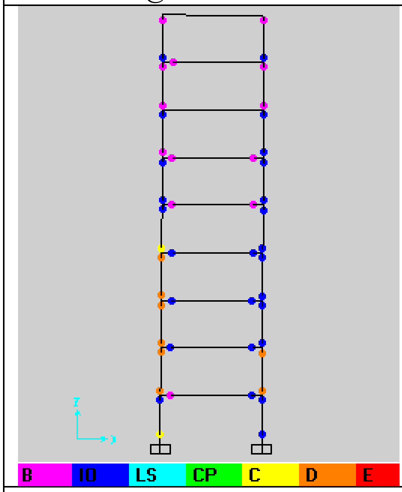

@Y=11.00m

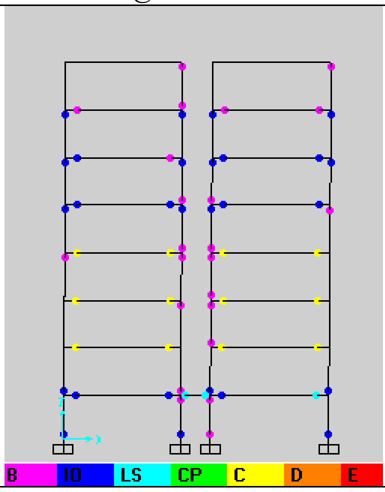

@Y=16.00m

Record: TCU068-360

Max abs $Ux,_{Top}$ = 0.4982 m

Estimated damage state:
EXTENSIVE

Description:

- Failure at some beams
- Extensive column yielding
- Column failure at Y=11m

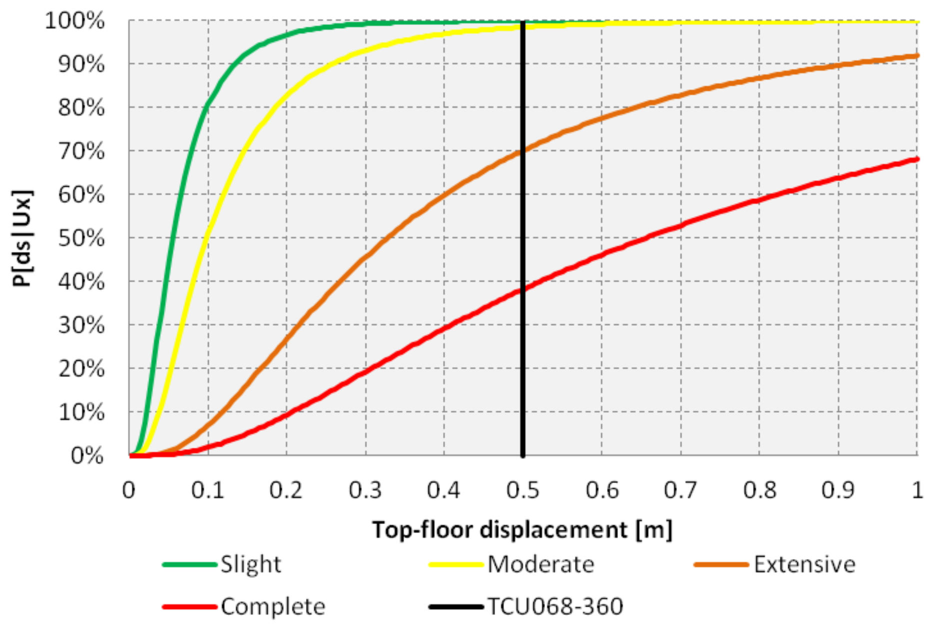

Figure 92: Damage due to the TCU068-360 component of the Chi-Chi, Taiwan (1999) earthquake

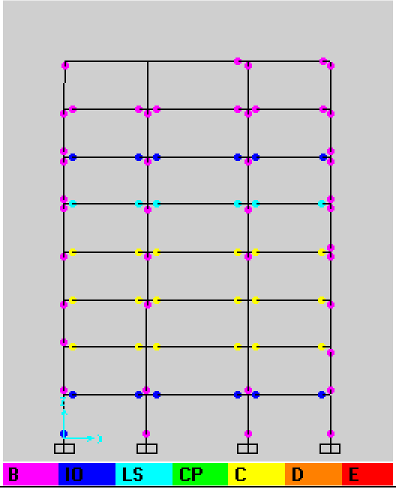

@Y=0.00m

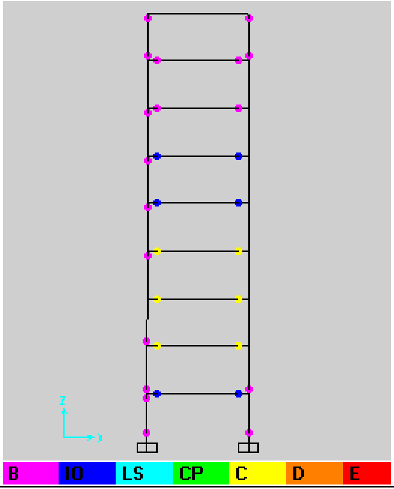

@Y=7.20m

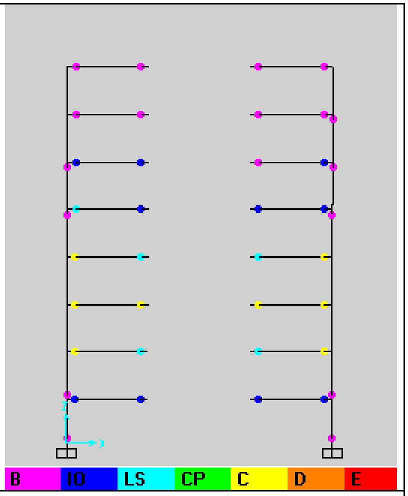

@Y=8.90m

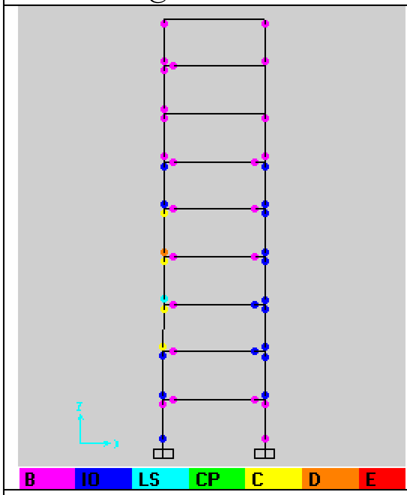

@Y=11.00m

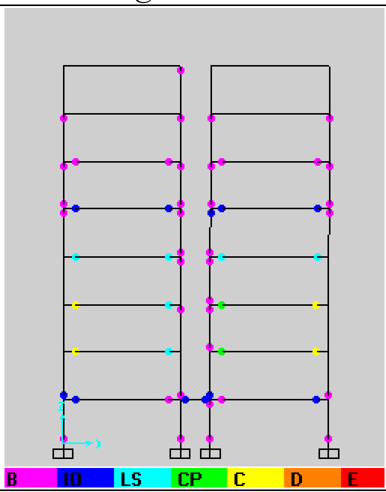

@Y=16.00m

Record: TCU102-090

Max abs $Ux_{,Top}$ = 0.3525 m

Estimated damage state:
EXTENSIVE

Description:

- Failure at some beams
- Extensive column yielding
- Column failure at Y=11m

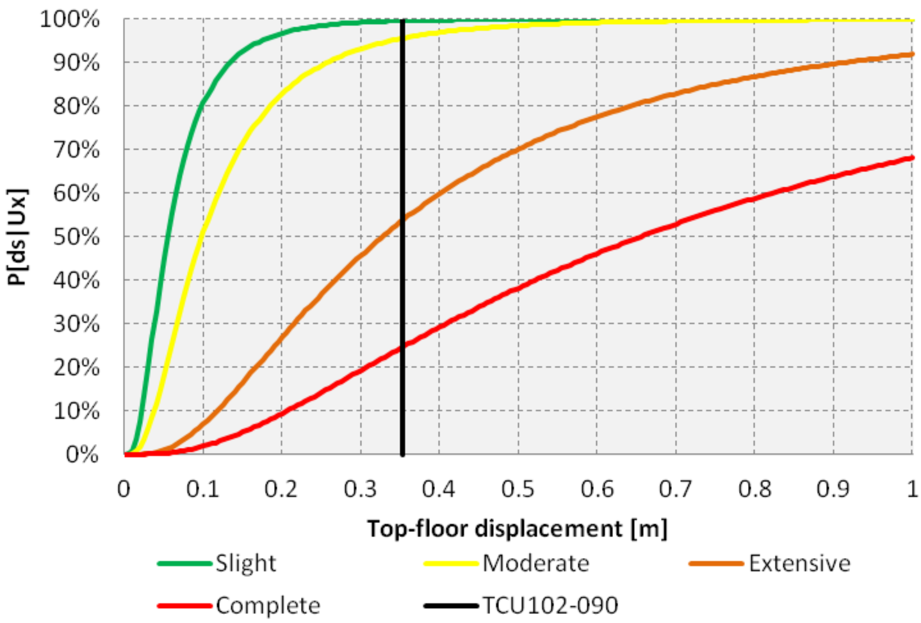

Figure 93: Damage due to the TCU102-090 component of the Chi-Chi, Taiwan (1999) earthquake

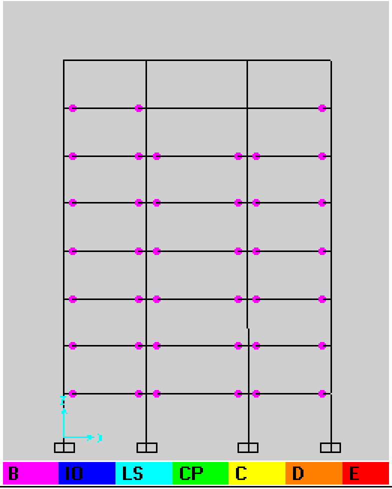

@Y=0.00m

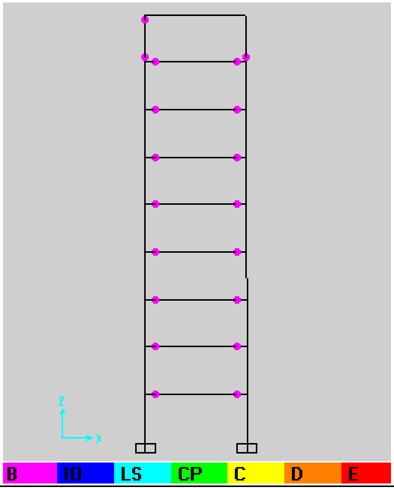

@Y=7.20m

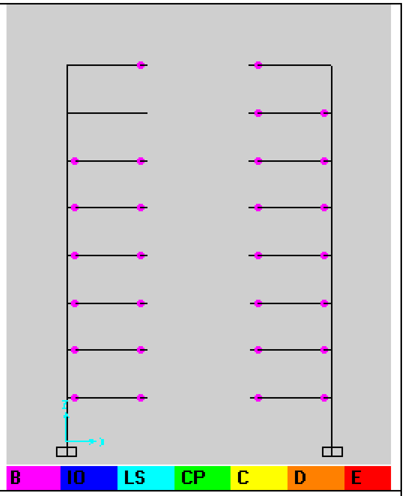

@Y=8.90m

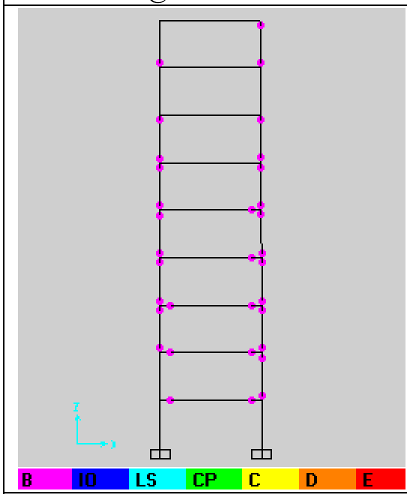

@Y=11.00m

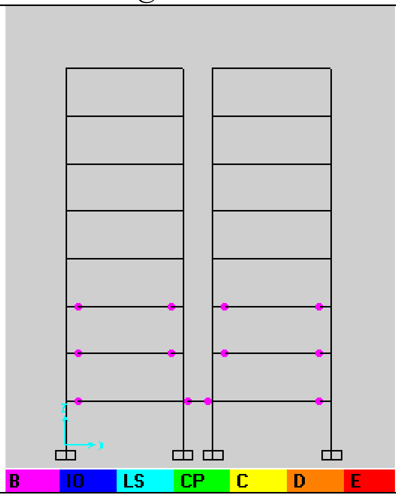

@Y=16.00m

Record: TCU103-090

Max abs $Ux_{,Top}$ = 0.08845 m

Estimated damage state:
MODERATE

Description:

- Yielding at lower & upper floors
- No failures

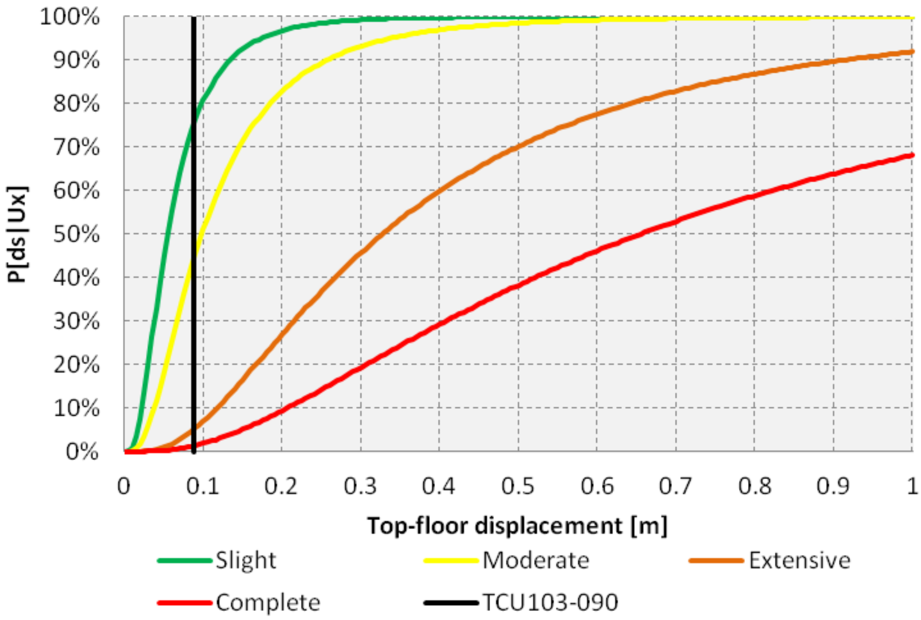

Figure 94: Damage due to the TCU103-090 component of the Chi-Chi, Taiwan (1999) earthquake

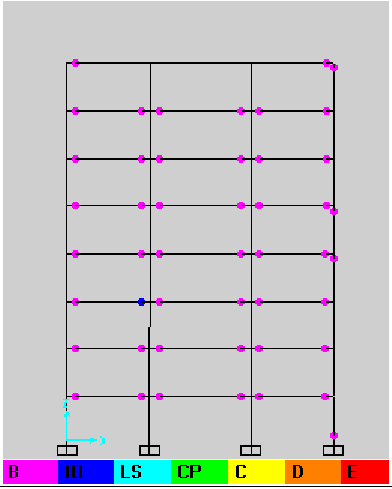

@Y=0.00m

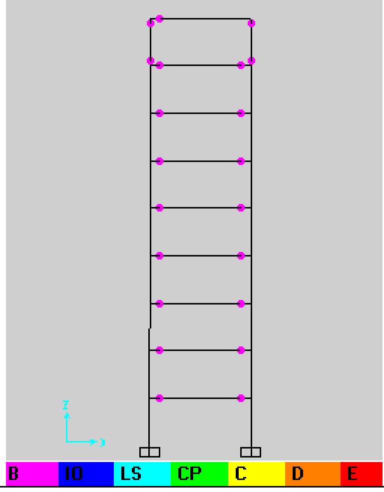

@Y=7.20m

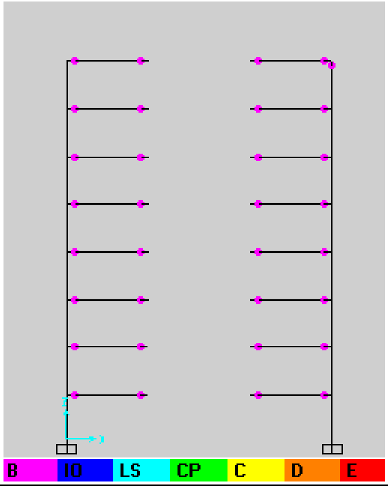

@Y=8.90m

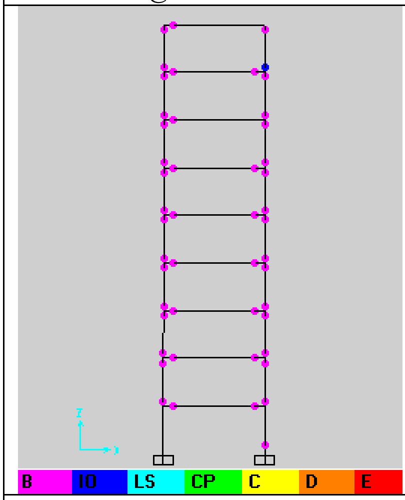

@Y=11.00m

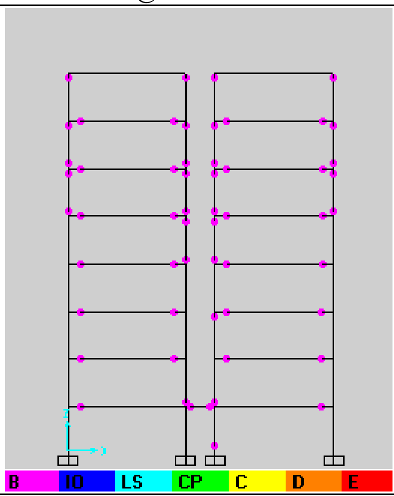

@Y=16.00m

Record: DZC-180

Max abs $Ux_{,Top}$ = 0.1316 m

Estimated damage state:
MODERATE

Description:

- Yielding at lower & upper floors
- No failures

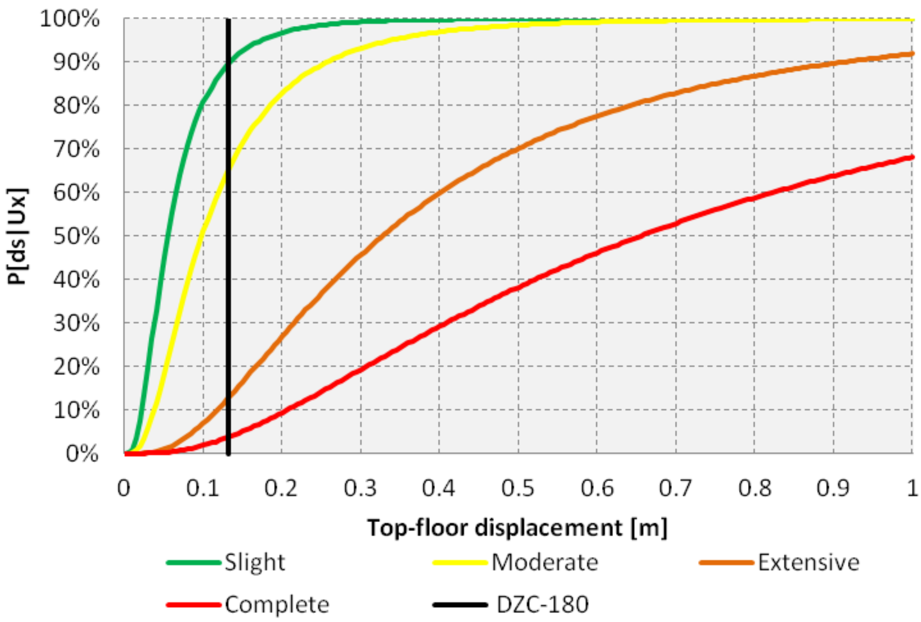

Figure 95: Damage due to the DZC-180 component of the Duzce, Turkey (1999) earthquake

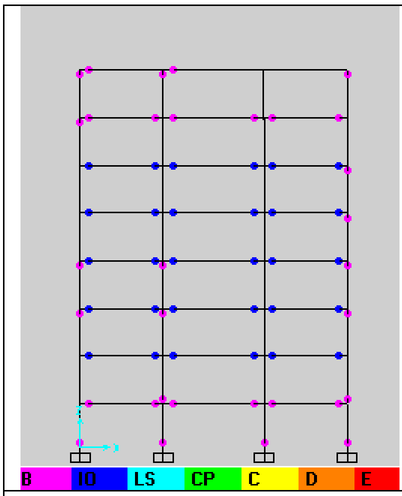

@Y=0.00m

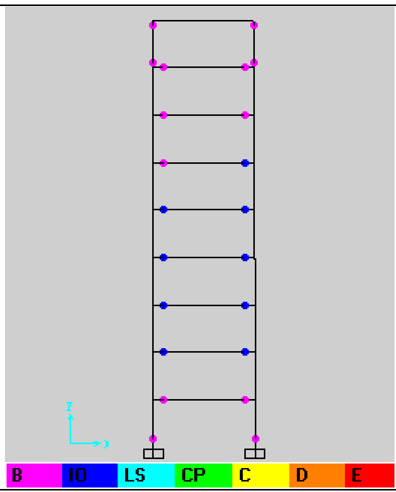

@Y=7.20m

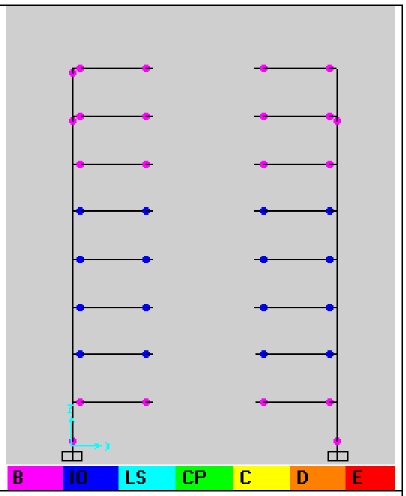

@Y=8.90m

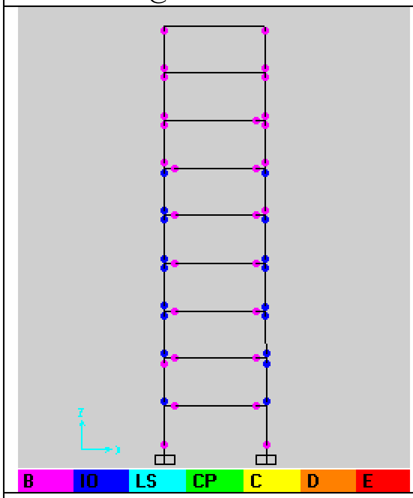

@Y=11.00m

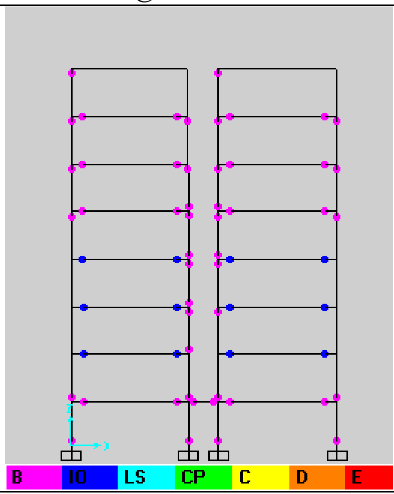

@Y=16.00m

Record: DZC-270

Max abs $Ux_{,Top}$ = 0.2386 m

Estimated damage state:
MODERATE

Description:

- Yielding at lower & upper floors
- No failures

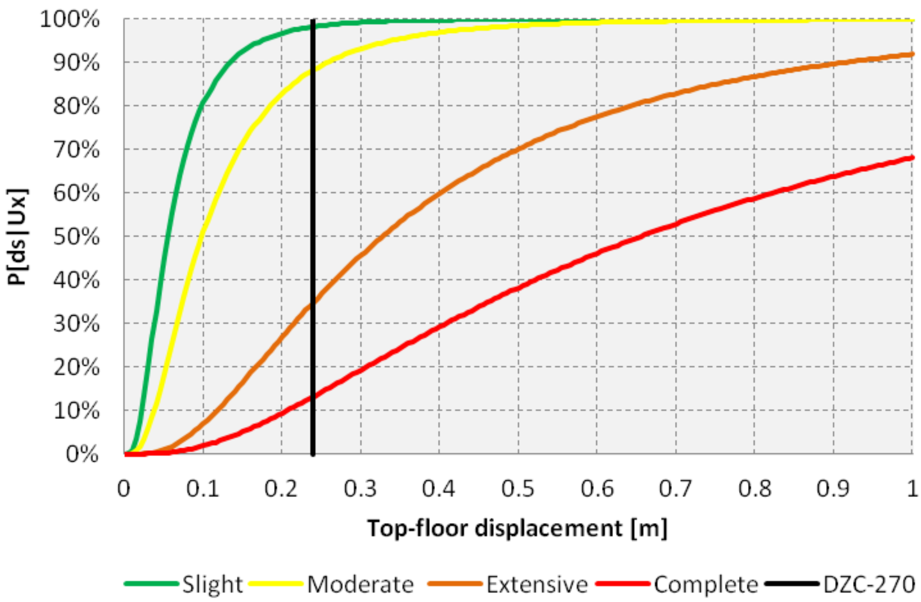

Figure 96: Damage due to the DZC-270 component of the Duzce, Turkey (1999) earthquake

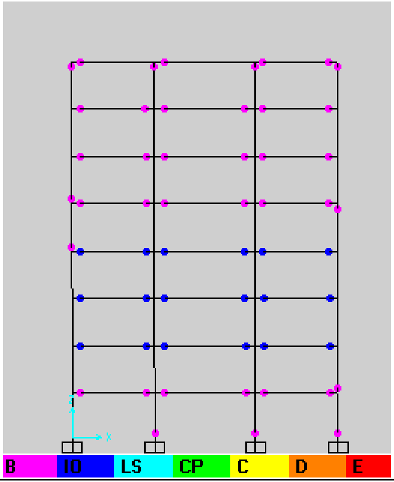

@Y=0.00m

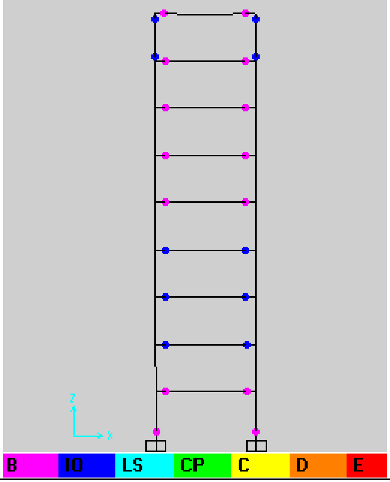

@Y=7.20m

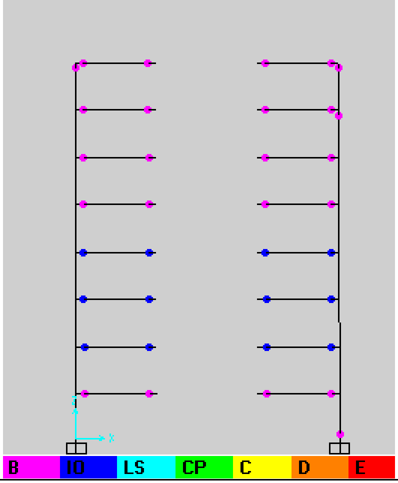

@Y=8.90m

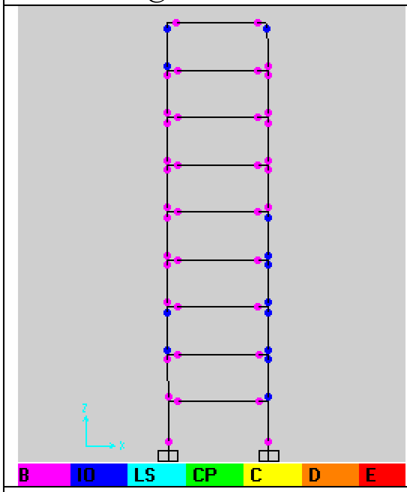

@Y=11.00m

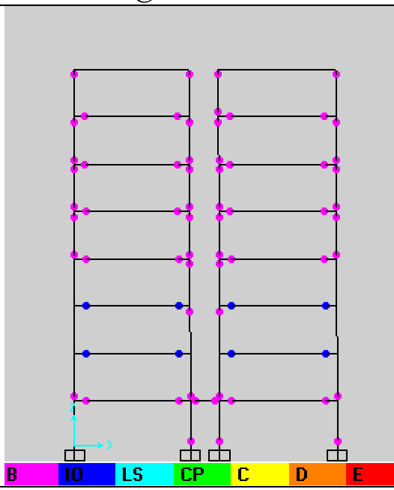

@Y=16.00m

Record: BOL-000

Max abs $Ux,_{Top}$ = 0.1835 m

Estimated damage state:
MODERATE

Description:

- Yielding at lower & upper floors
- No failures

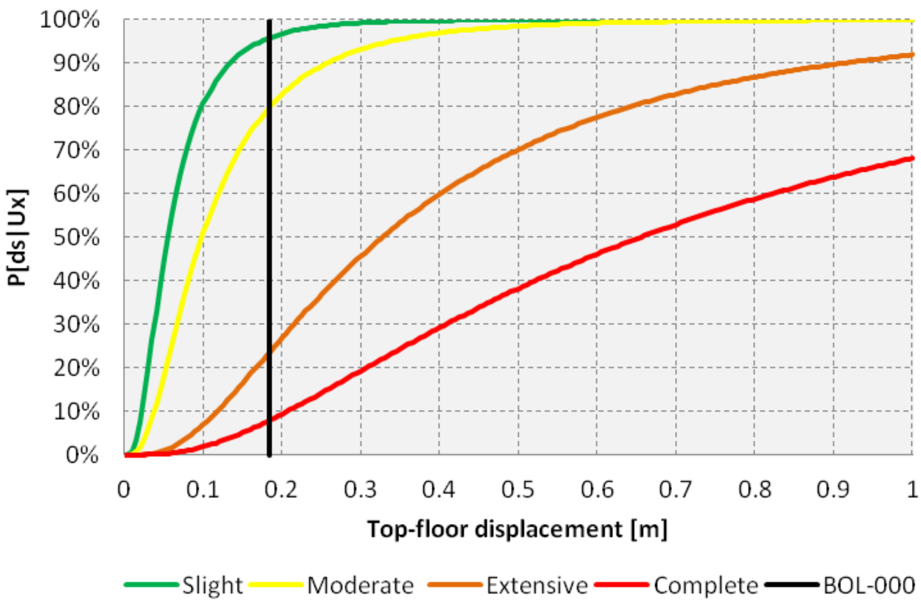

Figure 97: Damage due to the BOL-000 component of the Duzce, Turkey (1999) earthquake

6 Comparison and discussion of the results

Table 25 presents the structural damage levels for all earthquake records, which have been obtained using the “HAZUS-Umax” and “Observation” methods, respectively, as those have been described in previous. A general observation is that all seismic motions result in structural damage, while, in the majority of the cases, the damage level is either “moderate” or “extensive”, indicating the detrimental effects of near-fault ground-motions on the seismic performance of the 8-storey reinforced concrete building. Nevertheless, none of the two methods showed that the building will undergo complete damage or collapse during any of the selected seismic actions.

Moreover, it seems that the magnitude of the earthquake is not the primary factor that determines the severity of the damage of the analysed structure. It is observed that earthquakes of higher magnitude, such as the Izmit (Mw = 7.4) and Duzce (Mw = 7.1) result in lower damage levels than seismic events of lower magnitude, such as the Kobe (Mw = 6.8) and Northridge (Mw = 6.7) earthquakes. That means that other important factors and characteristics of the ground motion, in combination with the structural properties, determine the overall seismic performance of the building during an earthquake. For example, it is observed that a significant role on the severity of the damage plays the epicentral distance of the seismic recording. In particular, when observing the results in Table 25, we can see that in the case of the Chi-Chi earthquake, the ground-motions with relatively small epicentral distance (TCU065, TCU068 and TCU102) result in “extensive” damage, while the rest of the records from the same event with larger epicentral distances result in “moderate” and “slight” damage.

Furthermore, some variation is observed between the results of the two damage-assessment methods. In particular, there is a disagreement between the resulting damage level using the HAZUS-Umax method (fragility curves) and the observed damage from SAP2000 in the case of 4 ground motions (13% disagreement). The four records are TAB-344, ARC-270, TCU053-360 and TCU103-090. In order to identify the reasons of this variation, the Table 26 is constructed, which provides the possibility of damage occurrence for each damage limit state, as computed from the corresponding fragility curves (Figure 41) for the provided top-floor displacement, obtained from the time-history analysis. In the case of TAB-344, we can see that although the damage level is characterised as “moderate” according to the method, with 93% possibility of occurrence, there is a considerable possibility of 46% the damage to be characterised as “extensive”. In addition, looking at the fragility curves in Fig. 38 we can see how close we are to the case of “extensive” damage, which complies with the observation of the damage in SAP2000. Similar case is the case of ARC-270 record, where according to the HAZUS method we are in “pre-yielding” state, while some yielding occurs as it is observed from non-linear time-history analysis. The difference is small and therefore HAZUS Method can be used as reliable method.

However, Figure 85 shows that, for the specific displacement, we are very close to the limit state of slight damage. In the case of the TCU053-360 record the expected damage according to the HAZUS method is “slight”, while the observed damage in SAP2000 is characterised as “moderate”. The later characterisation was based on the yielding of beams at upper storeys. However, someone could characterise the observed damage (Figure 87) as “slight”, considering that no significant yielding occurred in columns of the frame at Y=11m, which is one of the characteristics of “moderate” damage limit state, as observed in push-over analysis (Figure 38). Finally the fourth case of TCU103-090 record, is the same case with TAB-344 ground motion, where for the occurred maximum displacement, although we are below, we are closer to the moderate damage limit state that the “slight” damage limit state (Figure 94).However the difference again is small and we can say that HAZUS Method is a reliable method.

Table 25: Damage levels of the 8-storey building for the various ground motions, which resulted from both the fragility curves in terms of top-floor displacement (HAZUS – Umax method), and the time-history analyses after observation of hinges' statuses (Observation method)

Earthquake (Magnitude)	Record	DIR/TY	C/D (Km)	$\max\lvert U_{x,Top}\rvert$	Damage State		Agree-ment
					HAZUS – Umax Method	Observed (SAP2000)	
Tabas, Iran (Mw = 7.1)	TAB-074	N	1.2	0.2618	MODERATE	MODERATE	YES
	TAB-344	N	1.2	0.3012	MODERATE	EXTENSIVE	**NO**
Imperial Valley, CA, USA (Mw = 6.4)	E04-230	F	6	0.2192	MODERATE	MODERATE	YES
	E05-140	F	2.7	0.1168	MODERATE	MODERATE	YES
	E05-230	F	2.7	0.2069	MODERATE	MODERATE	YES
	E06-230	F	0.3	0.2669	MODERATE	MODERATE	YES
	E07-230	F	1.8	0.2900	MODERATE	MODERATE	YES
	EMO-270	F	1.2	0.3714	EXTENSIVE	EXTENSIVE	YES
Northridge, CA, USA (Mw = 6.7)	JFA-022	F	5.2	0.2431	MODERATE	MODERATE	YES
	JFA-292	F	5.2	0.4952	EXTENSIVE	EXTENSIVE	YES
	SCG-052	F	5.1	0.4038	EXTENSIVE	EXTENSIVE	YES
	SCG-142	F	5.1	0.4600	EXTENSIVE	EXTENSIVE	YES
	SCH-011	F	5	0.3762	EXTENSIVE	EXTENSIVE	YES
Hanshin (Kobe), Japan (Mw = 6.8)	TAK-000	F	1.1	0.5148	EXTENSIVE	EXTENSIVE	YES
	TAK-090	F	1.1	0.3963	EXTENSIVE	EXTENSIVE	YES
	KPI-000	F	3.2	0.2666	MODERATE	MODERATE	YES
Izmit, Turkey (Mw = 7.4)	YPT-000	F	2.6	0.1838	MODERATE	MODERATE	YES
	YPT-270	F	2.6	0.1354	MODERATE	MODERATE	YES
	ARC-270	F	14	0.0427	PRE-YIELDING	SLIGHT	**NO**
Chi-Chi, Taiwan (Mw = 7.6)	CHY101-090	F	7.7	0.1202	MODERATE	MODERATE	YES
	CHY101-360	F	7.7	0.2680	MODERATE	MODERATE	YES
	TCU053-360	F	4.6	0.0674	SLIGHT	MODERATE	**NO**
	TCU065-090	F	0.1	0.2826	MODERATE	MODERATE	YES
	TCU065-360	F	0.1	0.3344	EXTENSIVE	EXTENSIVE	YES
	TCU068-090	F	0.2	0.4157	EXTENSIVE	EXTENSIVE	YES
	TCU068-360	F	0.2	0.4982	EXTENSIVE	EXTENSIVE	YES
	TCU102-090	F	0.6	0.3525	EXTENSIVE	EXTENSIVE	YES
	TCU103-090	F	4.4	0.0885	SLIGHT	MODERATE	**NO**
Duzce, Turkey (Mw = 7.1)	DZC-180	N	8.3	0.1316	MODERATE	MODERATE	YES
	DZC-270	N	8.3	0.2386	MODERATE	MODERATE	YES
	BOL-000	F	19.9	0.1835	MODERATE	MODERATE	YES

Table 26: Probability of damage occurrence for each damage state (S = Slight, M = Moderate, E = Extensive, C = Complete), resulting from the fragility curves in terms of top-floor displacement (Fig. 41) and damage states according to the "Observation method"

Earthquake	Record	DIR/TY	C/D (Km)	max$\lvert U_{x,Top} \rvert$	P[ds|Ux]				Observed damage state (SAP2000)
					S	M	E	C	
Tabas, Iran	TAB-074	N	1.2	0.2618	99%	**90%**	39%	15%	MODERATE
	TAB-344	N	1.2	0.3012	99%	**93%**	46%	19%	EXTENSIVE
Imperial Valley, CA, USA	E04-230	F	6	0.2192	98%	**86%**	31%	11%	MODERATE
	E05-140	F	2.7	0.1168	86%	**59%**	10%	3%	MODERATE
	E05-230	F	2.7	0.2069	97%	**84%**	28%	10%	MODERATE
	E06-230	F	0.3	0.2669	99%	**91%**	40%	16%	MODERATE
	E07-230	F	1.8	0.2900	99%	**93%**	44%	18%	MODERATE
	EMO-270	F	1.2	0.3714	100%	96%	**56%**	26%	EXTENSIVE
Northridge, CA, USA	JFA-022	F	5.2	0.2431	98%	89%	36%	14%	MODERATE
	JFA-292	F	5.2	0.4952	100%	98%	**70%**	38%	EXTENSIVE
	SCG-052	F	5.1	0.4038	100%	97%	**60%**	30%	EXTENSIVE
	SCG-142	F	5.1	0.4600	100%	98%	**67%**	35%	EXTENSIVE
	SCH-011	F	5	0.3762	100%	96%	**57%**	27%	EXTENSIVE
Hanshin (Kobe), Japan	TAK-000	F	1.1	0.5148	100%	99%	**71%**	40%	EXTENSIVE
	TAK-090	F	1.1	0.3963	100%	97%	**59%**	29%	EXTENSIVE
	KPI-000	F	3.2	0.2666	99%	**91%**	40%	16%	MODERATE
Izmit, Turkey	YPT-000	F	2.6	0.1838	96%	**80%**	24%	8%	MODERATE
	YPT-270	F	2.6	0.1354	90%	**67%**	14%	4%	MODERATE
	ARC-270	F	14	0.0427	36%	13%	1%	0%	SLIGHT
Chi-Chi, Taiwan	CHY101-090	F	7.7	0.1202	87%	**61%**	11%	3%	MODERATE
	CHY101-360	F	7.7	0.2680	99%	**91%**	40%	16%	MODERATE
	TCU053-360	F	4.6	0.0674	**62%**	31%	2%	1%	MODERATE
	TCU065-090	F	0.1	0.2826	99%	**92%**	43%	18%	MODERATE
	TCU065-360	F	0.1	0.3344	100%	95%	**51%**	23%	EXTENSIVE
	TCU068-090	F	0.2	0.4157	100%	97%	**62%**	31%	EXTENSIVE
	TCU068-360	F	0.2	0.4982	100%	98%	**70%**	38%	EXTENSIVE
	TCU102-090	F	0.6	0.3525	100%	96%	**54%**	25%	EXTENSIVE
	TCU103-090	F	4.4	0.0885	**76%**	45%	5%	1%	MODERATE
Duzce, Turkey	DZC-180	N	8.3	0.1316	90%	**65%**	13%	4%	MODERATE
	DZC-270	N	8.3	0.2386	98%	**88%**	35%	13%	MODERATE
	BOL-000	F	19.9	0.1835	96%	**80%**	24%	8%	MODERATE

SYNOPSIS AND CONCLUSIONS

The main aim of this master thesis was to assess the vulnerability of an 8-storey reinforced concrete building that subjected to near-field earthquakes, based on the HAZUS methodology and to establish the reliability of the results according to SAP2000 program.

Moreover, comparing the maximum top displacement of the building through the sample of near field earthquakes we can conclude the important factors that give larger displacements and larger damages.The HAZUS methodology is a set of components that attempt to estimate losses, operational (probabilistic estimation) and economic, due to an earthquake scenario.

Firstly, the building subjected in modal analysis that generated the natural frequencies of it (T1 = 1.165 sec, T2 = 1.113 sec). Then it subjected in pushover analysis with load distribution according to the first Eigenmode in order to construct the pushover curve (base shear- top-floor displacement).The aim was to construct the fragility curves that defining by HAZUS. These curves classify the structure at four levels of damage (Slight, Moderate, Extensive, Collapse) and describe the possibility to have a certain level of damage to the building.

Depending on the type of building and the vulnerability curve we wanted to build was necessary to calculate standard deviations (vds) that take into account uncertainties on the curve pushover, with levels of performativity, with the features of construction, with the pulse of directivity and territorial motion. Eventually the curves defined by following lognormal distribution.

To determine the vulnerability of the building, it used an existing sample of near field earthquakes, with range of seismic magnitudes of 6.4 to 7.6, and larger maximum spectral displacement. Earthquakes applied through accelerograms (using SAP2000) in the building and after inelastic time-history analyses, resulted the maximum displacement for each record.

Comparing the records in each earthquake we are taking the following fragility curves and conclusions separate for each earthquake. The straight lines on the fragility curves are the maximum top-floor displacement for each record.

The ultimate goal was to understand how the magnitude of the earthquake, the directivity and the distance of the fault from the recording station affecting the results that have been obtained.

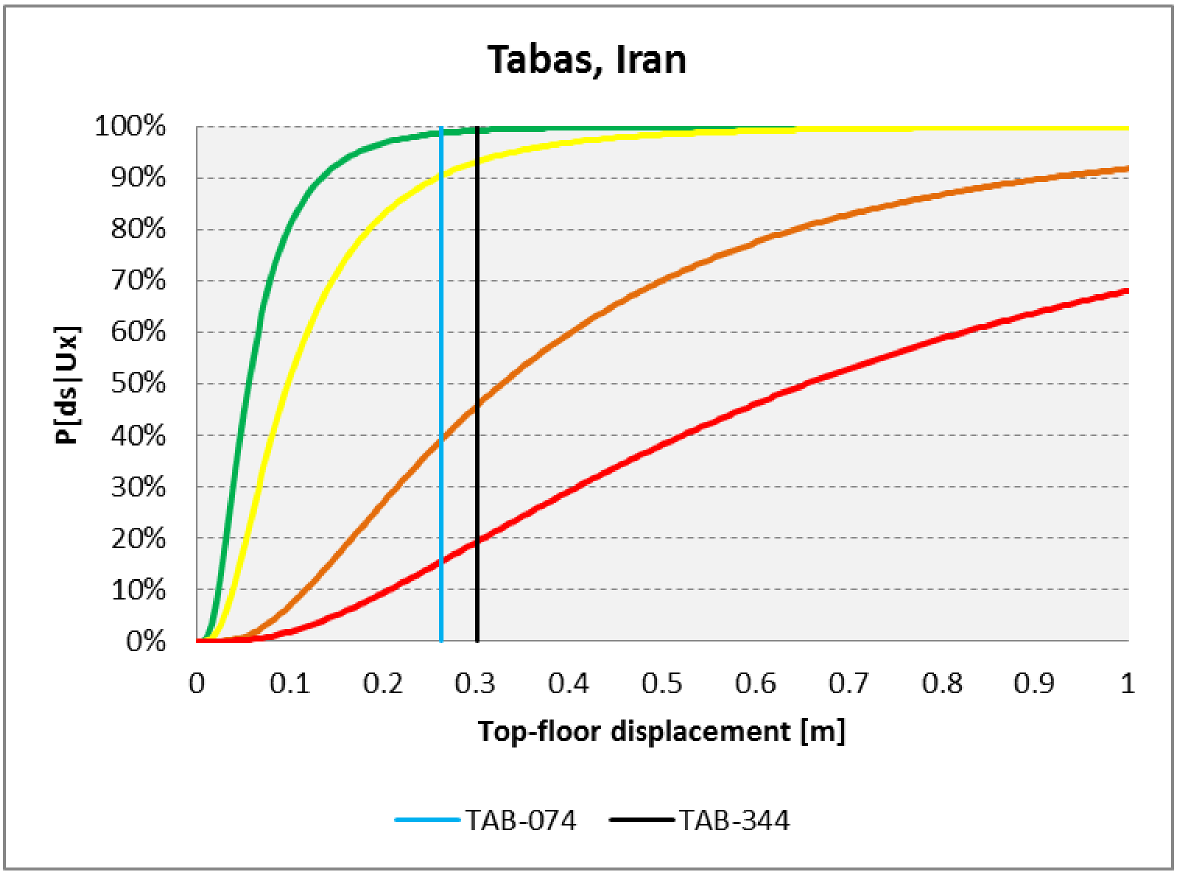

Figure 98: Comparison of fragility curves with the maximum top-floor displacement for the record stations for Tabas, Iran earthquake

Figure 98 shows that TAB-074 record gives 99% Slight damage, 90% Moderate damage, 39% Extensive damage and 15% Complete damage and TAB-344 gives 99%, 93%, 46% and 19% respectively. TAB-074 record mounts the building to Moderate damage state but for TAB-344 someone can mount the building as Extensive damage state because 46% is close to 50% and it can be Extensive damage for the site of safety but numerical is mounts as Moderate damage state. This is explaining the difference between HAZUS method and SAP2000 observed method results for damage states that table 26 shows.

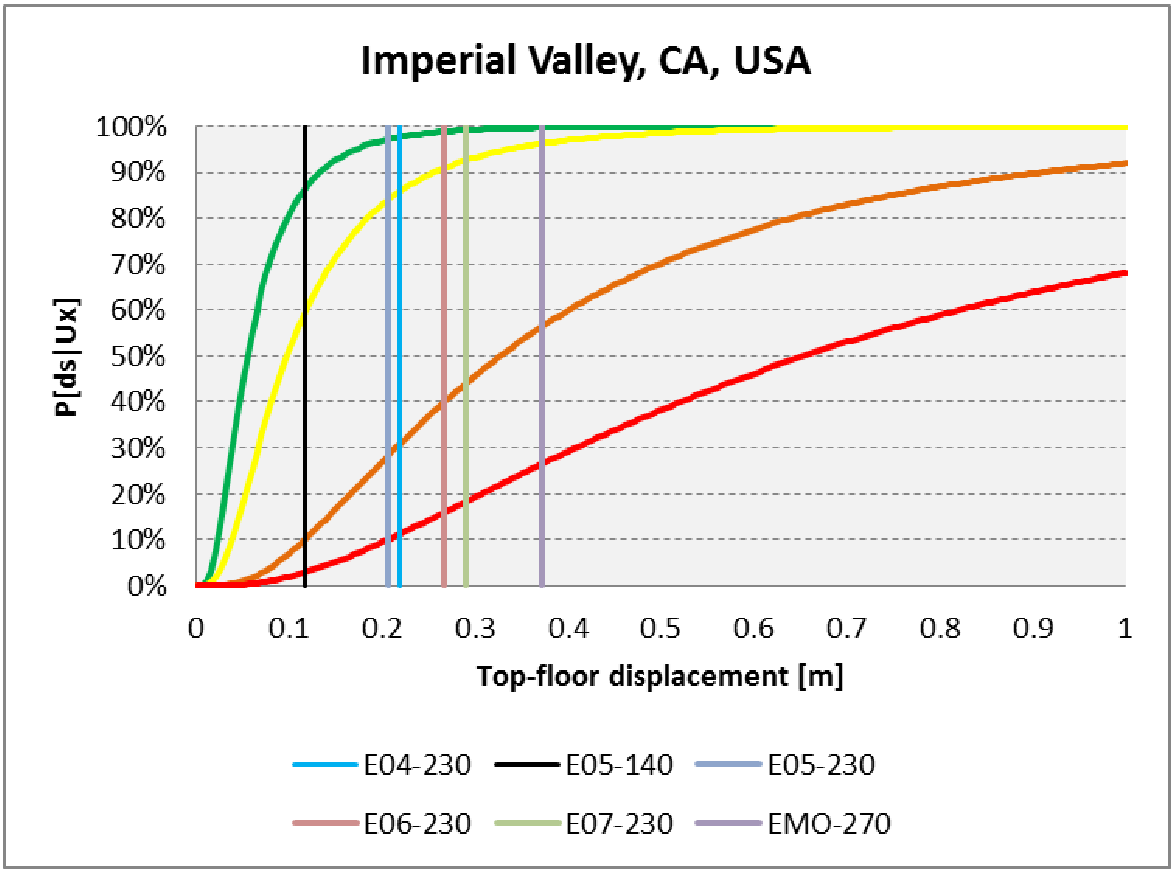

Figure 99: Comparison of fragility curves with the maximum top-floor displacement for the record stations for Imperial Valley, CA, USA earthquake

Figure 99 shows that E04-230 record gives 98% Slight damage, 86% Moderate damage, 31% Extensive damage and 11% Complete damage, E05-140 gives 86%, 59%, 10% and 3%, E05-230 gives 97%, 84%, 28% and 10%, E06-230 gives 99%, 91%, 40% and 16%, E07-230 gives 99%, 93%, 44% and 18%, EMO-270 gives 100%, 96%, 56% and 26% respectively. All the records mount the building to Moderate damage state except of EMO-270 which mount it to Extensive damage state. From the above curves we can see that EMO-270 gives the largest top-floor displacement and from Table 25 we can see that it has only 1.2 km distance from the fault. We can conclude that small distance from the fault gives larger displacement.

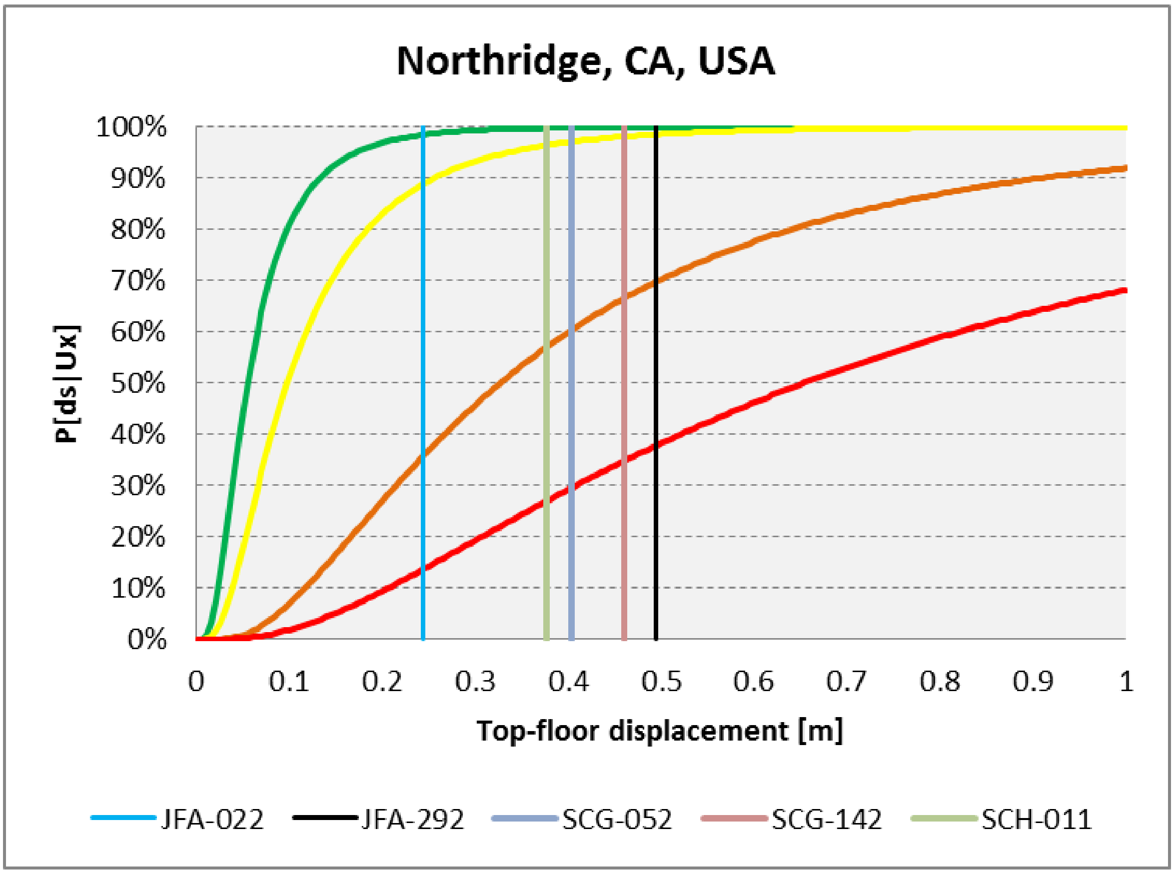

Figure 100: Comparison of fragility curves with the maximum top-floor displacement for the record stations for Northridge, CA, USA earthquake

Figure 100 shows that JFA-022 record gives 98% Slight damage, 89% Moderate damage, 36% Extensive damage and 14% Complete damage, JFA-292 gives 100%, 98%, 70% and 38%, SCG-052 gives 100%, 97%, 60% and 30%, SCG-142 gives 100%, 98%, 67% and 35%, SCH-011 gives 100%, 96%, 57% and 27% respectively. All the records mount the building to Extensive damage state except of JFA-022 which mounts it to Moderate damage state.

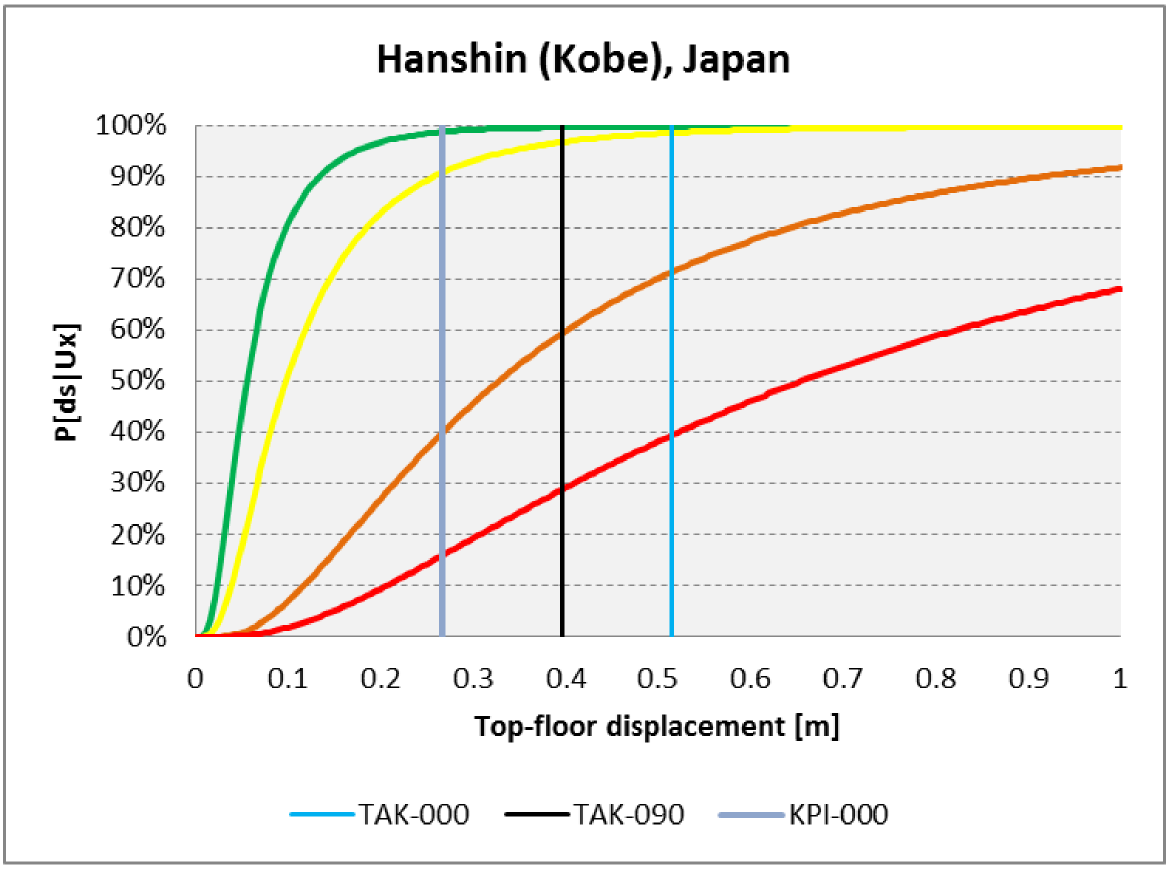

Figure 101: Comparison of fragility curves with the maximum top-floor displacement for the record stations for Hansin (Kobe), Japan earthquake

Figure 101 shows that TAK-000 record gives 100% Slight damage, 99% Moderate damage, 71% Extensive damage and 40% Complete damage, TAK-090 gives 100%, 97%, 59% and 29%, KPI-000 gives 99%, 91%, 40% and 16% respectively. All the records mount the building to Extensive damage state except of KPI-000 which mounts it to Moderate damage state. From the above curves we can see that TAK-000 gives the largest top-floor displacement and from Table 25 we can see that it has only 1.1 km distance from the fault. Moreover we can note that it gives the biggest displacement from all the records and the largest possibility for Complete damage (40%). We can conclude that small distance from the fault gives larger displacement.

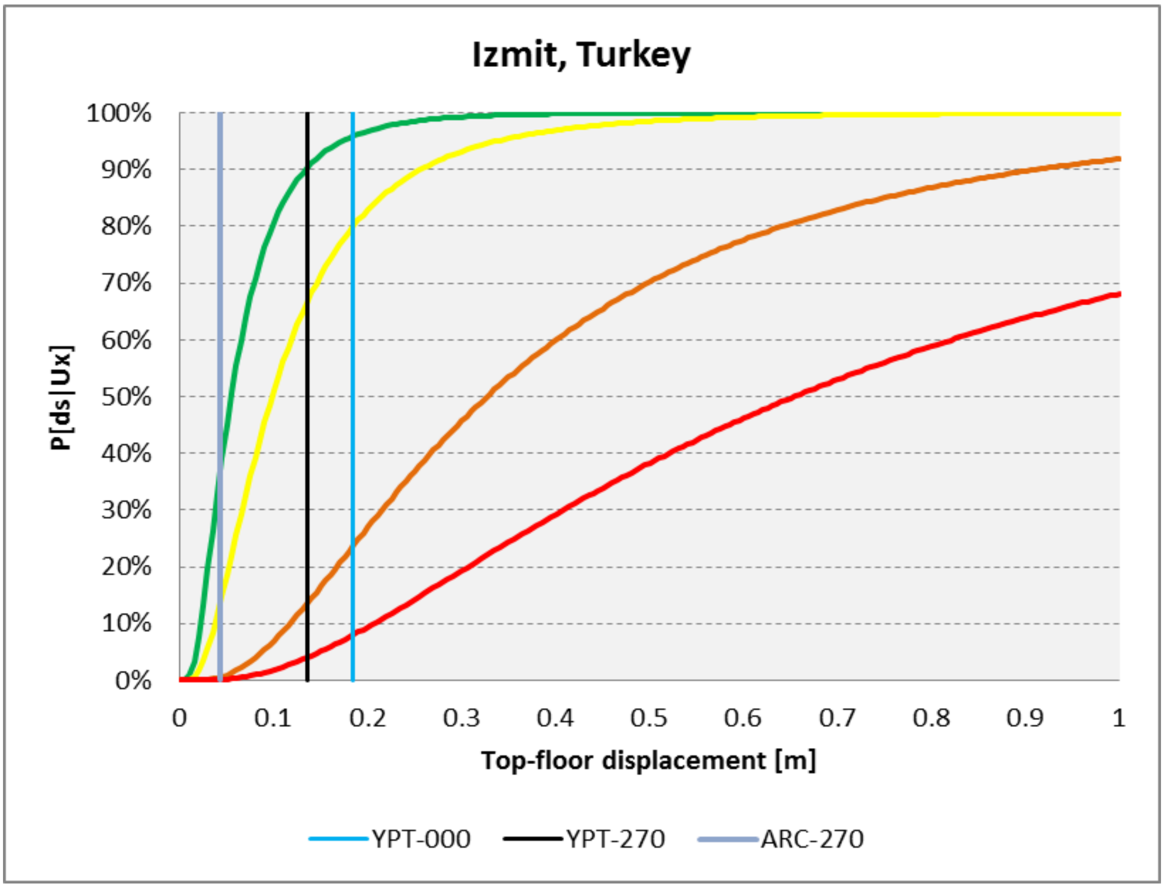

Figure 102: Comparison of fragility curves with the maximum top-floor displacement for the record stations for Izmit, Turkey earthquake

Figure 102 shows that YPT-000 record gives 96% Slight damage, 80% Moderate damage, 24% Extensive damage and 8% Complete damage, YPT-270 gives 90%, 67%, 14% and 4%, ARC-270 gives 36%, 13%, 1% and 0% respectively. All the records mount the building to Moderate damage state except of ARC-270 which mounts it to Pre-Yielding damage state. From the above curves we can see that YPT-000 gives the largest top-floor displacement and from Table 25 we can see that it has only 2.6 km distance from the fault. However, ARC-270 gives the smallest top-floor displacement and it has 14km distance from the fault. It is evident that smaller distance from the fault gives larger displacements.

Comparing the results for the damage states of HAZUS with SAP2000 we can see a difference for ARC-270 record. HAZUS mounts ARC-270 to Pre-Yielding damage and SAP2000 to Slight damage. As we can see from the above curves 36% for slight damage it is close to appears slight damage, especially if you see it from the site of safety.

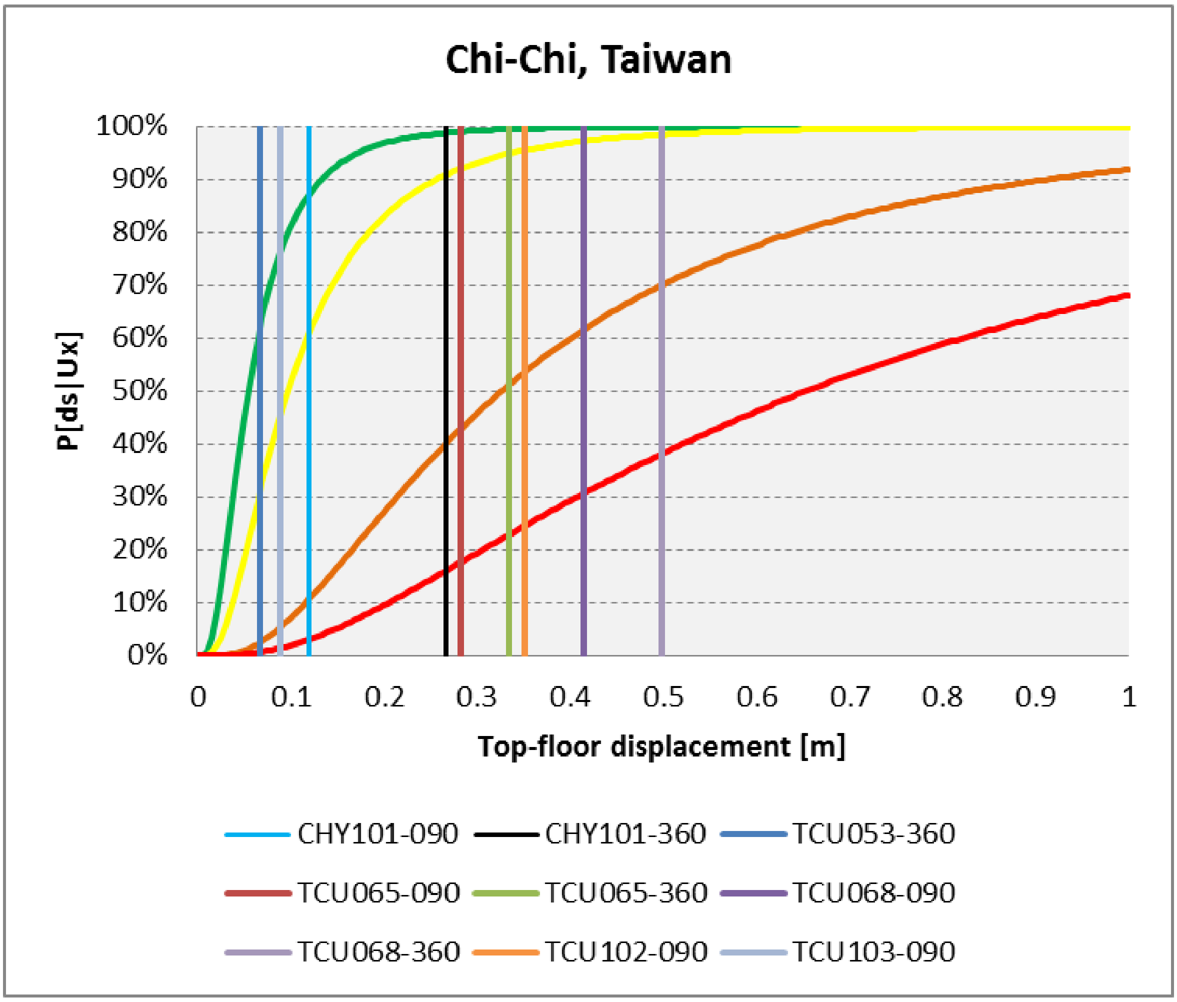

Figure 103: Comparison of fragility curves with the maximum top-floor displacement for the record stations for Chi-Chi, Taiwan earthquake

Figure 103 shows that CHY101-090 record gives 87% Slight damage, 61% Moderate damage, 11% Extensive damage and 3% Complete damage, CHY101-360 gives 99%, 91%, 40% and 16%, TCU053-360 gives 62%, 31%, 2% and 1%, TCU065-090 gives 99%, 92%, 43% and 18%, TCU065-360 gives 100%, 95%, 51% and 23%, TCU068-090 gives 100%, 97%, 62% and 31%, TCU068-360 gives 100%, 98%, 70% and 38%, TCU102-090 gives 100%, 96%, 54% and 25%, TCU103-090 gives 76%, 45%, 5% and 1% respectively. TCU065-360, TCU068-090, TCU068-360 and TCU102-090 mount the building to Extensive damage state and as we can see from Table 25 they have 0.1-0.6 distance from the fault. It is evident that smaller distance from the fault gives larger displacements.

Comparing the results for the damage states of HAZUS with SAP2000 we can see a difference for TCU053-360 and TCU103-090 records. HAZUS mounts TCU053-360 and

TCU103-090 to Slight damage and SAP2000 to Moderate damage. As we can see from the above curves 31% and 45% for slight damage it is close to appears slight damage, especially if you see it from the site of safety.

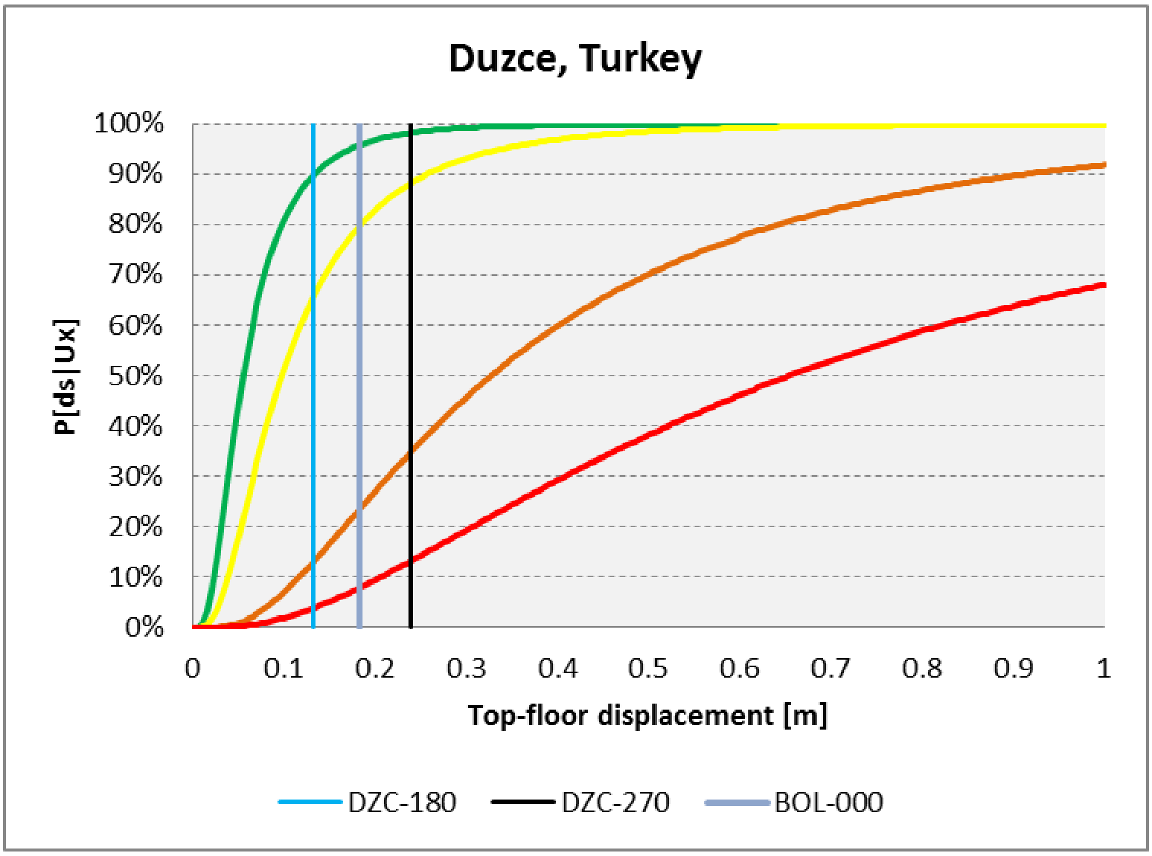

Figure 104: Comparison of fragility curves with the maximum top-floor displacement for the record stations for Duzce, Turkey earthquake

Figure 104 shows that DZC-180 record gives 90% Slight damage, 65% Moderate damage, 13% Extensive damage and 4% Complete damage, DZC-270 gives 980%, 88%, 35% and 13%, BOL-000 gives 96%, 80%, 24% and 8% respectively. All the records mount the building to Moderate damage state. As we can see from Table 25 and the above curves BOL-000 with forward directivity has 19.9 km distance from the fault and the other two records with neutral directivity have 8.3 km it gives close possibility of moderate damage as the other two. We can conclude that the forward directivity can cause larger damages.

To determine the vulnerability of the building, it used an existing sample of near field earthquakes, with range of seismic magnitudes of 6.4 to 7.6 , and larger maximum spectral displacement. Earthquakes applied through accelerograms (using SAP2000) in the building and after inelastic time-history analyses, resulted the maximum displacement for each record. Comparing the max|$U_{x,Top}$ results that analysis gave we can conclude the following:

1. **Forward directivity**: As we can see from table 26 all the earthquakes that reach the extensive damage limit had forward directivity. Earthquakes with Neutral Directivity gave moderate damage limit even if they had larger magnitudes than others with forward directivity. This gives the result that earthquakes with forward directivity can give larger displacements and larger damages.

2. **Closest distance from fault:** For the same earthquake and stations with the same directivity the displacements increase as the distance of the station from the fault is smaller. As we can see from Chi-Chi Taiwan earthquake that gave the larger displacement, the records with smaller distance from the fault gave larger displacements.

3. **Magnitude of the earthquake:** Comparing the results of Tabas (Iran), Izmit (Turkey), Chi-Chi (Taiwan) and Duzce (Turkey) with magnitude 7.1, 7.6, 7.4 and 7.1 respectively we can see that only the Chi-Chi Taiwan earthquake occurs extensive damages. It is known that as the magnitude of the earthquake is increasing the building suffers from larger top displacements and therefore stronger levels of damage. From these records we can conclude that the magnitude is not the most important factor to occur larger displacements. This may be due to the saturation of the ground motion observed in large earthquakes, ie the size grows, but does not increase ground motion. However, larger magnitude with the factors that are written above can be catastrophic.

Conclusion of all seismic excitations can conclude that the forward directivity and the closest distance from the fault resulted in large displacements in the building and larger damages. However the displacements are increasing more when seismic magnitude is increasing.
We can note that the building did not reach a complete damage despite that it was suffered by very strong earthquakes. The record that occurred largest displacement (0.51 m) was TAK-000 Hanshin Kobe), Japan with magnitude 6.8 and classified the building damages as extensive and gave the larger possibility 40% for complete damage.

BIBLIOGRAPHY

Choriki, P. (2011). "Study on inelastic behavior of twenty-story metal building in near field-earthquakes". Bsc. Ntua, Athens.

Christou, E. (2012). "Assessment of Seismic Risk of buildings in Cyprus". Bsc. Cyprus University of Technology, Limassol.

Department of Homeland Security Emergency Preparedness and Response Directorate. (2003). "HAZUS-MH MR1." FEMA, Washington, D.C.

Department of Homeland Security Emergency Preparedness and Response Directorate. (2003). "Hazus MH MR4 Technical Manual." FEMA, Washington D.C.

FEMA. (2014). "The Federal Emergency Management Agency's (FEMA's) Methodology for Estimating Potential Losses from Disasters." http://www.fema.gov/hazus 2014).

Seligson, H. (2008). "The ShakeOut Scenario, Hazus." *Rep. No. 2008-1150,* USGS, California.

S. Shahi, and Baker, J. (2012). "Pulse Classifications from NGA West2 database." http://www.stanford.edu/~bakerjw/pulse_classification_v2/Pulse-like-records.html (11/1, 2012).

Skondra, E. (2011). "Assessment of participation of higher modes in the response of eight-storey reinforced concrete frame building under the influence of near fault earthquakes". Msc. Ntua, Athens.

Technitis, G. (2007). "Assessment of seismic risk of buildings at Kifisia using Hazus software". Bsc. Harokopio University, Athens.

Vrionis, F. (2012). "Investigation of the relationship m-qy eight-storey building of reinforced concrete for earthquakes near-field using the method IDA". Bsc. NTUA, Athens.